



**Universitat Autònoma
de Barcelona**

**Development of Reagent-less Processes for Water
Decontamination. Tuning of Temperature and Redox
Parameters to Remove Toxic Oxyanions.**

LIU HE 2015

Doctoral Thesis

PhD in Chemistry



**Universitat Autònoma
de Barcelona**

**Development of Reagent-less Processes for Water
Decontamination. Tuning of Temperature and Redox
Parameters to Remove Toxic Oxyanions.**

LIU HE

Doctoral Thesis

PhD in Chemistry

Director: Manuel Valiente Malmagro

Departament de Química

Facultat de Ciències

2015



**Universitat Autònoma
de Barcelona**

Dissertation submitted for the degree of doctor

Liu HE

Supervisor

Prof Manuel Valiente Malmagro

Professor of Analytical Chemistry

Department of Chemistry. Centre GTS

Universitat Autònoma de Barcelona

Executive Director of GTS.

08193 Bellaterra (Barcelona), Spain, 28th Sep 2015

Acknowledgements

First and foremost, I wish to thank my supervisor Prof. Manuel Valiente for his guidance and support. Without his patient instruction, insightful criticism and expert guidance, the project would never matured into a typical thesis. I would also like to thank Prof. Gustavo Perez for his invaluable advice and constant encouragement. In addition, I would like to thank Prof. Olivier for providing me the short stay position in LCABIE, Pau, France, which make me to learn a lot of new techniques for analytical chemistry.

I would like to express my gratitude to Prof. Liang Jizhao (my supervisor during Master), who inspired me to do further scientific research. I would also like to take this opportunity to show my heartfelt gratitude to my uncle, Yongquan Li, who encouraged me and helped me a lot.

I would like to thank the friendly and generous staff and members of GTS for their help and guidance. My work could not have been proceeded without the assistance of several key staff members. Montserrat Lopez Mesas, Cristina Palet, Montserrat Resina Gallego, Maria dolors, Diego Morillo Martin, Fran blanco, Olga kotkowska, Maribel Restituyo Silis, Nurlin Abu Samah, Itziar, Veronica Verdugo, Shilpi Kumari, Victor Marquina Garces, Maria Angles Subirana, Albert Pell Lorante, Maria Jesus sanchez Martin.

I take this opportunity to record my sincere appreciation to my doctoral colleagues, roommates, ball friends and playmates, Guofen Ma, Shuzhen Li, Wusheng Guo, Zhiyu Jia, Helan Zhang, Muling Zeng, Meng Chen, Yuanyuan Lu, Jian Li, Siming Yu, Zhikun Xu, Min Cao, Zhen Zhan, Haijie Liu, Qin Liu, Qinyi Tan, Luyan Teng, Yangchun Xin, Shujing Ding, Ping Sun, Shuangshuang Qi, Dianfei Yuan, Yuan Zhong, for their valuable friendship. Additionally, thanks for the help of Caiyan Feng, Hongyao Yin, who are my friends in Pau, France.

I should especially acknowledge the encouragement, support and love given to me by my family, my parents and my brother and sister, without which I could have never reached this point in my life. And most of all, I would simply say to Tong Liu, who is my doctoral colleague and also my husband, “Thanks for you love, it makes everything worthwhile”. And finally, thanks for my little baby “Pedro”, who comes to my life during my PhD study period and I want to say “you are my pretty sunshine”.

Last but not least, I would like to gratefully acknowledge the financial support of Chinese scholarship council (CSC) for supporting me to pursue my stay in Spain as a PhD student. In addition, the present thesis has been developed with the financial support of Projects: CHEMSYNCRO (Ministerio de Economia y Competitividad Ref, CTM2012-30970), FP4BATIW (FP7-INCO-2013-9 R2I-ENP, project number 609550) and NANOREMOVAS (H2020-MSCA-RISE-2014, Project Number 645024).

Summary

Summary

The studies that have been carried out in the present PhD thesis project are based on the development of methods to remove water pollutants by using reagent-less processes and to provide and added value to the contaminated water treatment. In our case, the methods are related to arsenic or selenium oxyanions removal in aqueous solution. Methods are based on sorption-desorption processes for the indicated oxyanions. Nanostructured materials have been implemented as adsorption substances, being either iron or aluminum oxides the nanoparticles active constituents. Reagent-less processes were developed by using intensive thermodynamic parameters, e.g, temperature and/or redox potential of the target solution. Appropriate tuning of these parameters will allow both process selectivity and regeneration of the adsorption material. Synergic interaction of thermo-tuning with redox variation will provide such results. Thus, this reagentless method could not only provide reagent savings for recovering the adsorbent, but also the adsorbent recycling to be reused will contribute to a-cost efficient process. The results show as follows:

The adsorption capacity of arsenate/arsenite on sponge loaded with superparamagnetic iron oxide nanoparticles (SPION) is influenced by pH, contact time, initial concentration, adsorbent dosage, temperature as well as redox potential. The maximum adsorption for arsenate on sponge-SPION was obtained in an acid media (pH 3.6) in 1 hour contact time under 20°C while desorption equilibrium was achieved with 2 hours under 70°C. Equilibrium adsorption constants were determined as $\log K_{20}=4.198$ and $\log K_{70}=1.023$ under 20°C and 70°C respectively. These values correlate with the decrease of related negative ΔG° values, indicating the adsorption increase of As(V) when temperature decreases. ΔH° and ΔS° were found to be $-122.150 \text{ kJ mol}^{-1}$ and $337 \text{ J mol}^{-1} \text{ K}^{-1}$ respectively, indicating the adsorption reaction to be exothermic. The oxidation of As (III) to As(V) and the respective reduction processes were characterized to prove the concept of using redox potential as key parameter for a reagent-less process. Oxidation of As(III) to As(V) by potassium dichromate (conversion rate>91%) and reduction As(V) to As(III) by Zn powder or Sn foil (conversion rate>90%) in presence of the adsorbent, have shown the effect on the adsorption when tuning the solution redox potential, being As(V) of higher adsorption capacity than As(III).

In addition, aqueous selenate/ selenite adsorption/desorption characteristics by $\gamma\text{-Al}_2\text{O}_3$ nanospheres or SPION loaded sponge were also investigated. The maximum adsorption for selenate and selenite on $\gamma\text{-Al}_2\text{O}_3$ nanospheres was achieved at pH 2 in 6 hours under 20°C and 14 hours under 70°C, respectively. The kinetic and thermodynamic studies show that they are fitted very well to the pseudo-second order and Freundlich isotherm model. The ΔH value of Se (IV) and Se (VI) between 20°C and 70°C were $-13.955 \text{ KJ mol}^{-1}$ and $-3.927 \text{ KJ mol}^{-1}$, respectively. It shows that lower temperature favor removal of aqueous selenium. The results represent very similar adsorption phenomenon of selenate/selenite on sponge- SPION as that of arsenate/arsenite on sponge-SPION, thus, sponge-SPION has much higher adsorption capacity for arsenate or selenate than that of arsenite or selenite. The maximum adsorption for selenate and selenite on sponge loaded with SPION was achieved at pH 3.6 in 1 hour under 20°C and 6 hours under 70°C, respectively, while time for obtaining equilibrium of selenite needs 14 hours under 20°C and 24 hours under 70°C.

More importantly, the temperature dependence aspects combined with the redox potential effect for controlling the adsorption-desorption process have been studied. The column mode for treating the waste water, which contains the arsenate/ arsenite or selenate/selenite systems, confirms that toxic oxyanions could be removed by the related adsorbent, which could be regenerated and reused by controlling the temperature combined with the tuning of the reducing reagent.

Resumen

Resumen

Los estudios que se han llevado a cabo en esta tesis se basan en el desarrollo de métodos para la eliminación de contaminantes en aguas mediante procesos en los que no se utilizan reactivos, lo que proporcionan un valor añadido al tratamiento del agua contaminada. En nuestro caso, los métodos utilizados se centran en la eliminación de oxoaniones de arsénico y selenio en disoluciones acuosas mediante procesos de adsorción-desorción. Estos procesos caracterizados por la no utilización de reactivos se desarrollaron mediante el estudio de parámetros termodinámicos, como por ejemplo, la temperatura y/o el potencial redox de las disoluciones de estudio. Por tanto, estos métodos no solo nos proporcionarán un ahorro de reactivos en la recuperación del adsorbente, sino que permitirán el reciclado de dicho adsorbente y su reutilización.

La capacidad de adsorción del arsenito/arsenato en la esponja cargada con nanopartículas de óxido de hierro superparamagnéticas (SPION) está influenciada por el pH, el tiempo de contacto, la concentración inicial, cantidad de adsorbente, la temperatura y por el potencial redox. La adsorción máxima para el arsenato en el sistema esponja-SPION se ha obtenido en medio ácido (pH 3.6) tras 1 hora a 20°C, mientras que el equilibrio de desorción se alcanzó a las 2h a 70°C. Las constantes del equilibrio de adsorción se determinaron como $\log K_{20}=4,198$ y $\log K_{70}=1.023$ a 20°C y 70°C respectivamente. La disminución de estos valores se relacionan un valor de ΔG negativo, lo que indica un aumento de la adsorción de As(V) cuando la temperatura disminuye. Los valores de ΔH y ΔS calculados son $-122,150 \text{ kJ mol}^{-1}$ y $337 \text{ J mol}^{-1} \text{ K}^{-1}$ respectivamente, lo que indica que el proceso de adsorción es exotérmico. La oxidación de As(III) a As(V) y el proceso de reducción correspondiente fueron caracterizados para probar el concepto de potencial redox como parámetro clave en estos procesos. La oxidación de As(III) a As(V) mediante dicromato de potasio (tasa de conversión >91%) y la reducción de As(V) a As(III) mediante zinc en polvo o estaño laminado (tasa de conversión >90%) en presencia del adsorbente han mostrado el efecto que tiene el potencial redox en el proceso de adsorción.

Por otro lado, también se han estudiado las características del proceso de adsorción-desorción de los aniones selenito/selenato utilizando como adsorbente nanoesferas de $\gamma\text{-Al}_2\text{O}_3$ y esponja cargada con SPION. La máxima adsorción que presentan selenato y selenito sobre $\gamma\text{-Al}_2\text{O}_3$ se alcanzó a las 6 horas en un medio ácido (pH 2) a 20°C y a las 14h a 70°C, respectivamente. Los estudios cinéticos y termodinámicos muestran que los datos se ajustan a una cinética de pseudo-segundo orden y a una isoterma de Freundlich. El valor de ΔH obtenido para Se(IV) y Se(VI) entre 20°C y 70°C fue de $13,955 \text{ KJ mol}^{-1}$ y $-3,927 \text{ KJ mol}^{-1}$ respectivamente. Por tanto, el sistema esponja-SPION tiene una mayor capacidad de adsorción para arsenato y selenato que para arsenito y selenito. La máxima adsorción para selenato en el sistema esponja-SPION se alcanzó tras 1h en medio ácido (pH 3,6) a 20°C y tras 6h a 70°C respectivamente, mientras que el tiempo necesario para alcanzar el equilibrio en el caso del selenito fue de 14h a 20°C y 24h a 70°C.

En conclusión, se han estudiado el efecto que tiene sobre el proceso de adsorción-desorción la combinación de los aspectos que depende de la temperatura con el potencial redox. El modo en columna utilizado para el tratamiento de aguas residuales, que contienen arsenato/arsenito o selenato/selenito, confirma que estos oxoaniones tóxicos se pueden eliminar con estos adsorbentes, que además pueden ser regenerados y reutilizados controlando combinando la temperatura y el uso de un agente reductor.

Content

Content

1. INTRODUCTION	1
1.1. PROBLEM STATEMENT.....	1
1.1.1. Arsenic toxicity	4
1.1.2. Selenium toxicity	6
1.2. ARSENIC AND SELENIUM IN THE ENVIRONMENT	8
1.2.1. Arsenic in the environment.....	8
1.2.2. Selenium in the environment.....	9
1.2.3. Arsenic and selenium in the aquatic system.....	10
1.3. GENERAL CHEMISTRY OF ARSENIC AND SELENIUM	11
1.3.1. Arsenic chemistry	11
1.3.2. Selenium chemistry	15
1.4. DIFFERENT METHODS AND TECHNOLOGIES FOR ARSENIC AND SELENIUM OXYANIONS REMOVAL.....	18
1.4.1. Adsorption.....	20
1.5. ADSORBENTS FOR ARSENIC AND SELENIUM REMOVAL.....	22
1.5.1. Adsorbent materials for arsenic-literature review	23
1.5.2. Adsorbent materials for selenium-literature review	26
1.6. NANOTECHNOLOGY OVERVIEW	29
1.6.1. Superparamagnetic iron oxide nanoparticles(SPION)	32
1.6.2. γ -Al ₂ O ₃ alumina hollow nanospheres.....	35
1.6.3. Supporting materials for SPION–Forager sponge.....	36
1.7. KINETIC AND THERMODYNAMIC ASPECTS.....	39
1.7.1. Kinetic Model.....	39
1.7.2. Isotherm Model	42
1.7.3. Thermodynamic studies	44
1.7.4. Redox potential	48
1.8. OBJECTIVES.....	50

2. METHODOLOGY.....	55
2.1. REAGENTS AND APPARATUS.....	55
2.2. EXPERIMENT EQUIPMENT	56
2.2.1. Basic experiment equipment.....	56
2.2.2. Colorimetric technique- UV-Vis Spectrophotometer	56
2.2.3. Inductively Coupled Plasma Mass Spectrometry(ICP-MS).....	58
2.2.4. USB microscope	61
2.2.5. Scanning Electron Microscopy.....	62
2.2.6. Transmission Electron Microscopy, TEM	63
2.2.7. Energy Dispersive X-ray Spectrometer, EDS or EDX.....	64
2.3. PREPARATION OF THE ADSORBENTS	65
2.3.1. Synthesis of SPION.....	65
2.3.2. Synthesis of γ -Al ₂ O ₃ nanospheres	67
2.3.3. Forager sponge pretreatment	68
2.3.4. Loading of SPION on the sponge	69
2.4. EXPERIMENTS.....	71
2.4.1. Batch experiment	71
2.4.2. Kinetic study	73
2.4.3. pH effect on the adsorption process.....	74
2.4.4. Effect of initial concentration on adsorption process.....	74
2.4.5. Effect of temperature	75
2.4.6. Continuous adsorption-desorption experiment.....	76
2.4.7. Treatment of the real waste water sample.	78
3. RESULTS AND DISCUSSION	83
3.1. TEMPERATURE-DEPENDENCE OF ARSENIC ADSORPTION BY FORAGER SPONGE LOADED WITH SUPERPARAMAGNETIC IRON OXIDE NANOPARTICLE (SPONGE-SPION).....	84
3.1.1. Characterization of adsorbent material	85
3.1.2. Effect of contact time	90

3.1.3.	<i>Effect of initial concentration</i>	94
3.1.4.	<i>Effect of pH on Arsenic Adsorption Capacity</i>	96
3.1.5.	<i>Effect of temperature</i>	99
3.1.6.	<i>The effect of bed volume</i>	102
3.1.7.	<i>Adsorption isotherms</i>	103
3.1.8.	<i>Modeling of Arsenic Adsorption by a Ligand-Exchange Process.</i>	106
3.1.9.	<i>Thermodynamics Studies.....</i>	110
3.1.10.	<i>The dependence of separation factors on temperatures and bed volumes:</i>	111
3.2.	<i>APPLICATION OF SYNERGIC THERMO-TUNING OF REDOX POTENTIAL FOR CLEAN REMOVAL OF ARSENIC.....</i>	114
3.2.1.	<i>Experimental results of redox potential effect:</i>	115
3.2.2.	<i>Further proof of redox potential part</i>	117
3.2.3.	<i>Column Experiments.....</i>	119
3.2.4.	<i>As(III)-continuous column mode.....</i>	128
3.2.5.	<i>As(V)+As (III) adsorption-desorption on sponge loaded SPION in continuous column mode</i>	130
3.2.6.	<i>Cycled column experiment by modeling the real waste water treatment</i>	131
3.2.7.	<i>Real waste water.....</i>	136
3.3.	<i>KINETIC AND DYNAMIC ASPECTS OF SELENATE AND SELENITE ADSORPTION BY γ-Al_2O_3 NANOSPHERES</i>	139
3.3.1.	<i>Characterization of adsorbent material--SEM-EDX analysis</i>	139
3.3.2.	<i>Comparison of AlOOH, γ-Al_2O_3, modified γ-Al_2O_3 for selenium adsorption</i>	140
3.3.3.	<i>pH effect on adsorption.....</i>	141
3.3.4.	<i>Initial concentration effect on selenium adsorption.....</i>	144
3.3.5.	<i>Adsorption Isotherm modeling.....</i>	145
3.3.6.	<i>Evaluation of thermodynamic parameters.....</i>	146
3.3.7.	<i>Adsorption dynamics</i>	147
3.3.8.	<i>Adsorption kinetics</i>	148
3.3.9.	<i>Comparison of adsorption capacity between γ-Al_2O_3 nanosphere and modified γ-Al_2O_3 nanosphere</i>	152

3.4.	KINETIC AND DYNAMIC ASPECTS OF SELENATE AND SELENITE ADSORPTION BY SPONGE LOADED WITH SUPERPARAMAGNETIC IRON OXIDE NANOPARTICLES (SPION)	153
3.4.1.	<i>SEM characterization</i>	154
3.4.2.	<i>pH effect on selenate and selenite adsorption</i>	155
3.4.3.	<i>Contact time effect on selenite and selenate adsorption</i>	156
3.4.4.	<i>Adsorption kinetic study</i>	158
3.4.5.	<i>Column continuous mode</i>	160
4.	CONCLUSIONS	165
4.1.	CONCEPT OF TEMPERATURE TUNING ON ARSENIC OXYANIONS ADSORPTION-DESORPTION BY SPONGE LOADED WITH SPION	165
4.2.	APPLICATION OF SYNERGIC THERMO TUNING OF REDOX POTENTIAL FOR ARSENIC REMOVAL.....	167
4.3.	KINETIC AND DYNAMIC ASPECTS OF SELENATE AND SELENITE ADSORPTION BY Γ - Al_2O_3 NANOSPHERES.....	169
4.4.	KINETIC AND CONTINUOUS MODE ASPECTS OF SELENATE AND SELENITE ADSORPTION BY SPONGE LOADED WITH SPION	170
	FUTURE PERSPECTIVE	171
	REFERENCES	173

Annex I

Annex II

Annex III

Annex III

Chapter I

Introduction

1. INTRODUCTION

1.1. Problem statement

Arsenic and selenium are naturally-occurring, non-metallic elements with complex chemical and biological behavior in aqueous solutions. Although selenium is an essential trace nutrient for most organisms, both elements are generally considered toxic at elevated levels. Arsenic (As) and selenium (Se) are unusual metalloids as they both induce and cure cancer. They both cause carcinogenesis, pathology, cytotoxicity, and genotoxicity (Fig 1.1) in humans, with reactive oxygen species playing an important role. While As induces adverse effects by decreasing DNA methylation and affecting protein 53 expression, Se induces adverse effects by modifying thioredoxin reductase¹. A common feature is that both elements exist in multiple oxidation states in aquatic systems². Aqueous arsenic species exist in the oxidation states As(III) and As(V), while aqueous selenium species are found in the oxidation states Se(IV) and Se(VI).³.

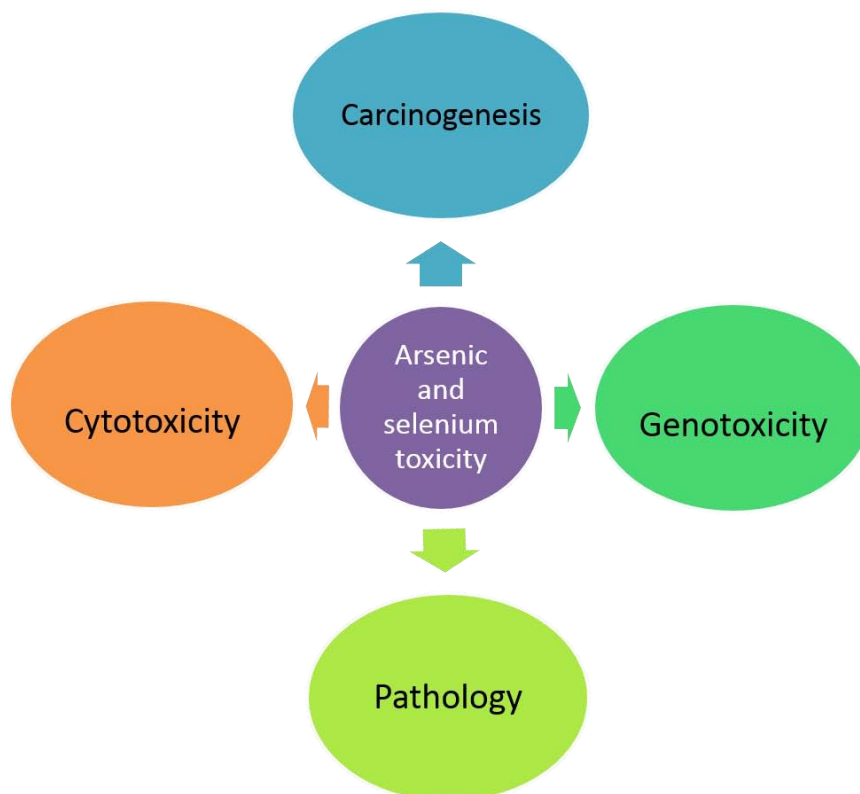


Fig 1.1 arsenic and selenium toxicity

Arsenic and selenium are among the inorganic contaminants that have become of evolving environmental concern lately⁴. Arsenic and selenium could be toxicity for human and animal if they reach dangerous concentration. Dangerous arsenic or selenium concentrations in natural water is now a worldwide problem and often referred to as a disaster⁵. Ingestion of inorganic arsenic can produce both cancer and non-cancer related health effects, such as nausea, nerve damage, cancers, and even death⁶. The USEPA has classified arsenic as a Class A carcinogen. Chronic exposure to low arsenic levels (less than 50 ppb) has been linked to health complications, including skin, kidney, lung, and bladder cancers, as well as other diseases of the skin, and the neurological and cardiovascular systems. High arsenic concentrations have been reported recently from the Bangladesh, India, USA, China, Chile, Mexico, Argentina, Poland, Canada, Hungary and Japan⁷.

Selenium is an essential nutrient for humans and animals but at higher concentrations can be harmful causing respiratory disease, mutagenic effects, reproductive failure and death⁸. Irrigation drainage and industrial wastewater often contain selenium contaminants⁸. The presence of toxic selenium in waste and surface waters at elevated levels causes a severe environmental and health problem⁹. The toxic effects of both of these metals have resulted in the U.S. government establishing drinking water limits of 10ppb for arsenic and 50 ppb for selenium.

Table 1.1 As and Se EPA water quality standard¹⁰

	As(ppb)	Se(ppb)
Drinking water	10	10
Irrigation water	100	20
Hazardous waste	5000	1000

Table 1.2 Arsenic maximum permission limits for drinking water in different countries¹¹

Countries	Maximum permission limits(ppb)
Bangladesh	50
India	10
USA	10
China	50
Chile	50
Mexico	50
Argentina	50
Hungary	-
Japan	-

1.1.1.Arsenic toxicity

Arsenic compounds can be classified into three major forms: inorganic, organic, and arsine gas¹². Inorganic arsenic may be formed with either trivalent (arsenite) or pentavalent (arsenate) arsenic. Trivalent arsenic compounds tend to be more toxic than pentavalent Arsenic compounds although pentavalent species predominate and are stable in oxygen rich Aerobic environments. Inorganic arsenic is more toxic than the organic forms although very high doses of certain organic compounds may be metabolized to inorganic arsenic and result in some of the same effects derived from an exposure to inorganic compounds. Inorganic arsenic is a naturally occurring toxic metalloid found primarily in drinking water and food ¹³, with an estimated 100 million people worldwide exposed to arsenic at levels exceeding 50 µg/L¹⁴.

Arsine gas have the highest toxicity of As compounds and it is formed by the reaction of hydrogen with arsenic, during the synthesis of organic arsenic compounds, and generated accidentally during the smelting and refining of nonferrous metals in mining processes. High levels of naturally occurring arsenic are found in soil and rocks leading to unacceptable levels of arsenic in drinking water.

The toxicity of arsenic varies widely based on the route of exposure, the form, the dose, the duration of exposure, and the time elapsed since the exposure. Ingestion and inhalation are the primary routes of both acute and chronic exposures. Arsine gas is one of the most toxic forms and is readily absorbed into the body by inhalation. Effects of acute inorganic arsenic poisoning include fever, anorexia, hepatomegaly, Melanesia, cardiac arrhythmia and eventual cardiovascular failure, upper respiratory track symptoms, peripheral neuropathies, gastrointestinal and hematopoietic effects. Dermal contact with high concentrations of inorganic arsenic compounds may result in skin irritation, redness, and swelling and high acute exposures may cause cholera like

gastrointestinal symptoms of vomiting (often times bloody) and severe diarrhea (often bloody). Ingestion of large doses of inorganic arsenic (70 to 180 mg) may be fatal.

Arsenic has been classified as a known human carcinogen by multiple agencies based on the increased prevalence of lung and skin cancer observed in human populations exposed to arsenic. Every day, lack of access to clean water and sanitation kills thousands of people, leaving others with reduced quality of life and as cities and slums grow at increasing rates, the situation worsens. Nowadays clean water is a scarce resource and arsenic removal from waters has emerged as a major concern in certain developing countries. There is a growing awareness that the toxicity of arsenic is strongly dependent on their chemical form, resulting in increasing interests in the quantitative determination of individual species. Speciation of arsenic in environmental samples is gaining increasing importance, as the toxic effects of arsenic are related to its oxidation state¹⁵. The toxicity of arsenic increases greatly when arsenic is reduced from a +5 to a +3 oxidation state. Based on the descriptions in the literature, we may conclude that As is present in the reduced form as arsenite in most instances of chronic arsenosis at low exposure levels¹⁶. Although arsenic exists in many different chemical forms in nature, it is found almost exclusively as arsenite (As(III) as H_3AsO_3) and arsenate (As(V) as H_3AsO_4) in water¹⁷. As(III) was identified as one of the most harmful substances in water to human health, and it is 60 times more toxic than As(V) or organic arsenic compounds¹⁸. Thus, As(III) is more toxic than As(V), but both As(III) and As(V) are known human carcinogen by both the inhalation and oral routes. There are several ways for arsenic to enter our body i.e. breathing, eating, or drinking the substance, or by skin contact. The degree of harmfulness of arsenic is measured by the dose, the duration of exposure, and the nature of contact with the arsenic.

The most important threat of environmental arsenic contamination is in the water, especially in drinking water due to the diversity of sources. Arsenic concentrations in

natural water are low, but elevated arsenic concentrations are common in groundwater as a result of natural conditions or anthropogenic impacts.

1.1.2. Selenium toxicity

Selenium occurs naturally in the environment and it is important in animal and human nutrition¹⁹. It is an essential micronutrient for mammals within a narrow low concentration range. Above this range, selenium can be toxic, including potentially carcinogenic, depending on dose and speciation (US EPA). It has three levels of biological activity²⁰: (1) trace concentrations are required for normal growth and development; (2) moderate concentrations can be stored and homeostatic functions maintained; and (3) elevated concentrations can result in toxic effects.

It is an essential component for plant growth, native vegetation can contain Se levels that are toxic to animals, creating animal health difficulties. In fact, there is a very narrow range between deficient and toxic levels of Se in animals. Chronic ingestion by humans at levels above 5mg/kg-day, the US EPA reference dose for selenium, can result in gastrointestinal, cardiac, skin and neurological disorders ²¹. As such, the US EPA has mandated the maximum contaminant level for selenium in drinking water at 50 ppb²¹. Anthropogenic activities such as smelting, mining, industrial production, and agricultural runoff have greatly increased the amount of selenium found in natural aquatic systems. In California, concentrations as high as 1400 ppb have been observed ²². Selenium occurs in both organic and inorganic forms, but due to the high solubility, and therefore bioavailability, of inorganic selenium in water, most remediation techniques focus on the predominant inorganic species at environmentally relevant conditions, selenite (Se(IV))and selenate (Se(VI))²⁰. Although both oxyanions are toxic, selenate is reported to be more difficult to remove due to the predominance of electrostatic dependent outer-sphere complexes it forms with many adsorbents and the

high solubility of selenate salts which makes adsorption thermodynamically unfavorable²³.

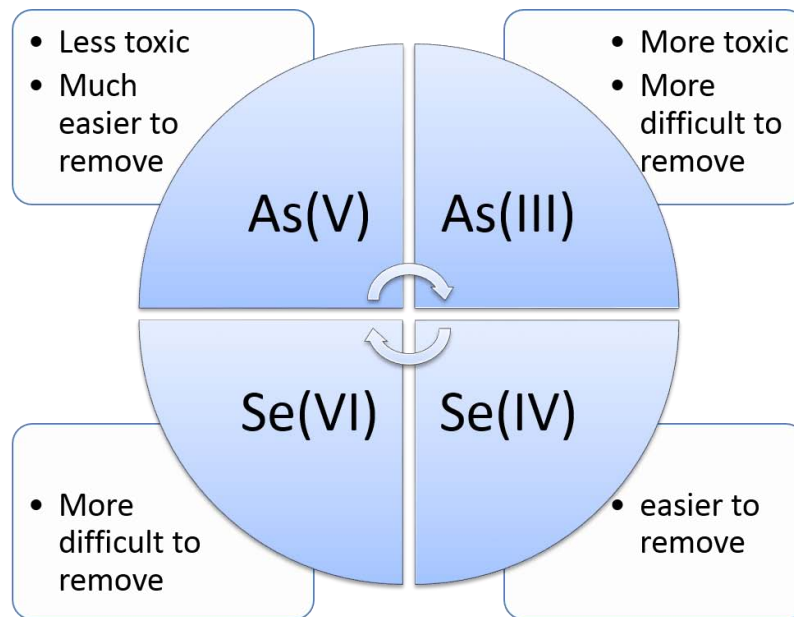


Fig 1.2 comparison of toxicity of arsenate/arsenite and selenate/ selenite

1.2. Arsenic and selenium in the environment

1.2.1. Arsenic in the environment

The arsenic is ubiquitous in the environment and occupies approximately $5 \times 10^{-5}\%$ of the earth's crust. The total amount of arsenic in the upper earth crust is estimated to be $4.1 \times 10^{16} \text{ Kg}^{24}$. In the global arsenic cycle $3.7 \times 10^8 \text{ Kt}$ occur in the oceans, another $9.97 \times 10^5 \text{ Kt}$ on earth (land), $25 \times 10^9 \text{ Kt}$ in sediments and 8.12 Kt in the atmosphere ²⁵. Arsenic is a naturally occurring in food, water, air²⁵. In sea water, the concentration of arsenic varies between $0.09 \mu\text{g/L}$ and $24 \mu\text{g/L}$ (average: $1.5 \mu\text{g/L}$) and in freshwater between $0.15 \mu\text{g/L}$ and $0.45 \mu\text{g/L}$ (maximum: 1 mg/L)²⁶. The presence of arsenic has been reported in several parts of the world, like USA, China, Bangladesh, Taiwan, Mexico, Argentina, Poland, Canada, Hungary, Japan and India. As Figure 1.3 shows. The arsenic exist in the environment not only due to the natural sources, but also from the anthropogenic sources. One important anthropogenic source of arsenic contamination of the environment was the use of arsenical fungicides, herbicides and insecticides in agriculture and wood industry²⁷. Another anthropogenic source of arsenic in the environment is the burning of fossil fuels in households and power plants.



Fig 1.3 arsenic in groundwater and the environment

1.2.2.Selenium in the environment

Selenium is a naturally occurring metal-like element (a non-metal)²⁸, it is an essential element required for the health of humans, other animals, and some plants²⁹. Specifically, it is necessary for the proper functioning of the structural proteins and cellular defences against oxidative damage. However, Se in excess and in critical chemical species in their diet can cause reproductive failures. Selenium has become a contaminant of potential concern in USA, Canada, Australia and New Zealand as a result of activities conducted by a wide variety of industrial sector, including mining and power regeneration. The large geologic extent of Se sources is connected by human activities that include power generation, oil refining, irrigation drainage, and coal, phosphate, copper, and uranium mining (Figure 1.4). Development of technologies for controlling Se pollution and predictive forecasts of ecological effects will become increasingly critical to commercial exploitation, as well as to faunal conservation.

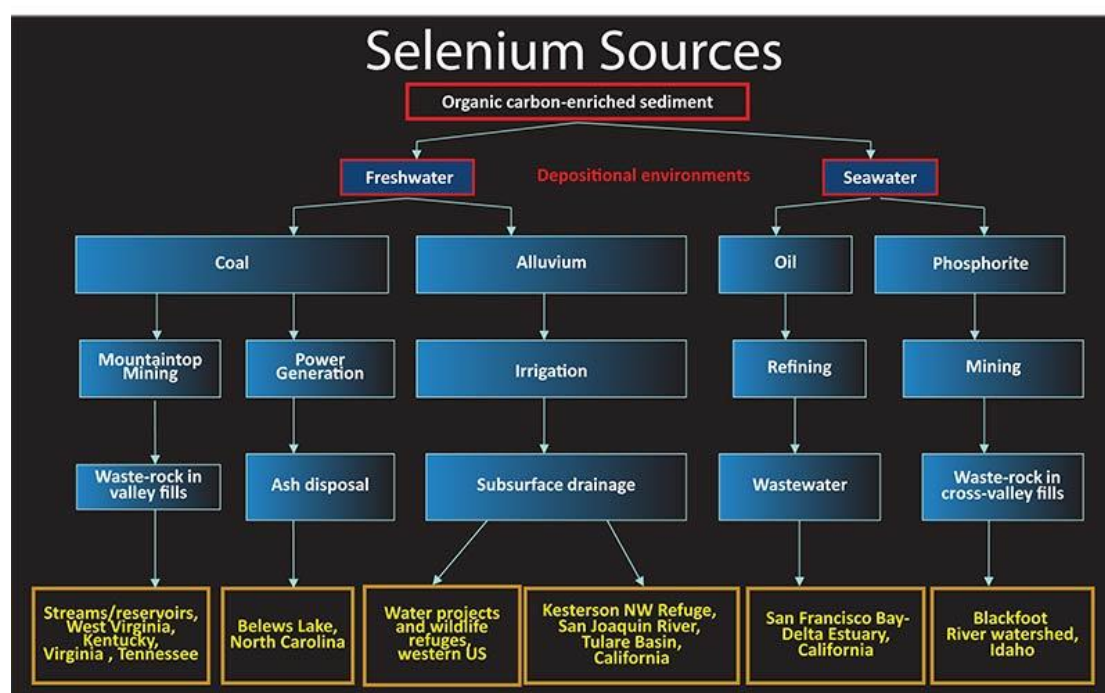


Fig 1.4 Selenium sources in the environment

1.2.3. Arsenic and selenium in the aquatic system

Widespread accumulation of arsenic and selenium has occurred most recently due to the use of arsenical pesticides, mining and processing of sulfide and uranium ores, burning of fossil fuels, and irrigation and drainage of newly developed arid and semi-acid agricultural lands³. The presence of dissolved arsenic and selenium in aquatic system, such as surface and groundwater has created significant concern on a global basis. The source of arsenic and selenium in natural water is associated with both natural and human being reasons, such as geochemical reactions and oxidative weathering, as well as uncontrolled industrial waste discharges⁷. Anthropogenic activities such as smelting, mining, industrial production, and agricultural runoff have greatly increased the amount of arsenic and selenium found in natural aquatic systems³⁰.

In water, the most prevalent species of the toxic arsenic and selenium are found as compounds of oxyanions such as arsenate [As (V)], arsenite [As (III)], selenate [Se (VI)] and selenite [Se (IV)]. The more oxidized species are more prevalent in aerobic surface waters while the more reduced species are more likely to occur in anaerobic ground waters. Their relative distributions are influenced by pH and redox conditions, at a pH between 6 and 9, it exists as oxyanions of arsenic acid [$\text{H}_2\text{AsO}_4^{4-}$ or HAsO_4^{3-}]. Under mildly reducing conditions, arsenite is thermodynamically stable and exists as a non-ionized arsenous.

It is important to note that the most effective way to overcome the adverse health effects of arsenic and selenium is to avoid the further exposure by providing safe drinking water, because there is no effective treatment to counteract arsenic or selenium toxicity. Therefore, the US Environmental Protection Agency, the World Health Organization, and the European Commission have decided to lower the maximum contaminant level of arsenic in drinking water from 50ppb to 10ppb. This stringent arsenic standard will inevitably require new better methods or consider new treatment options.

1.3. General chemistry of arsenic and selenium

1.3.1. Arsenic chemistry

Arsenic belongs to group VB (N, P, As, Sb, Bi) of the periodic table, is a nonmetallic element with the elemental electronic structure $[\text{Ar}] 3d^{10}4s^24p^3$, and is known to be toxic to plants and animals. The molecular weight of arsenic is 74.92 and an atomic number of 33. Earth's crust is the source of arsenic, and it exists as various minerals including arsenopyrite(FeAsS), orpiment(As_2S_3), realgar(AsS), and loellingite (FeAs_2).³¹ Arsenic is found both in organic and inorganic forms. Organic arsenic compounds(Fig 1.5) include CH_3AsO_2 (monomethylarsenic acid, MMA), $\text{C}_2\text{H}_5\text{AsO}_2$ (dimethylarsinic acid, DMA) and arseno-sugars, while inorganic arsenic compounds include H_3AsO_3 (arsenous acid) and H_3AsO_4 (arsenic acid).³² There are four oxidation states in which arsenic forms inorganic compounds: V, III, 0, -III. As(III) is lightly soluble in water forming arsenious acid and arsenic acid by oxidation of As(III), respectively¹⁶.

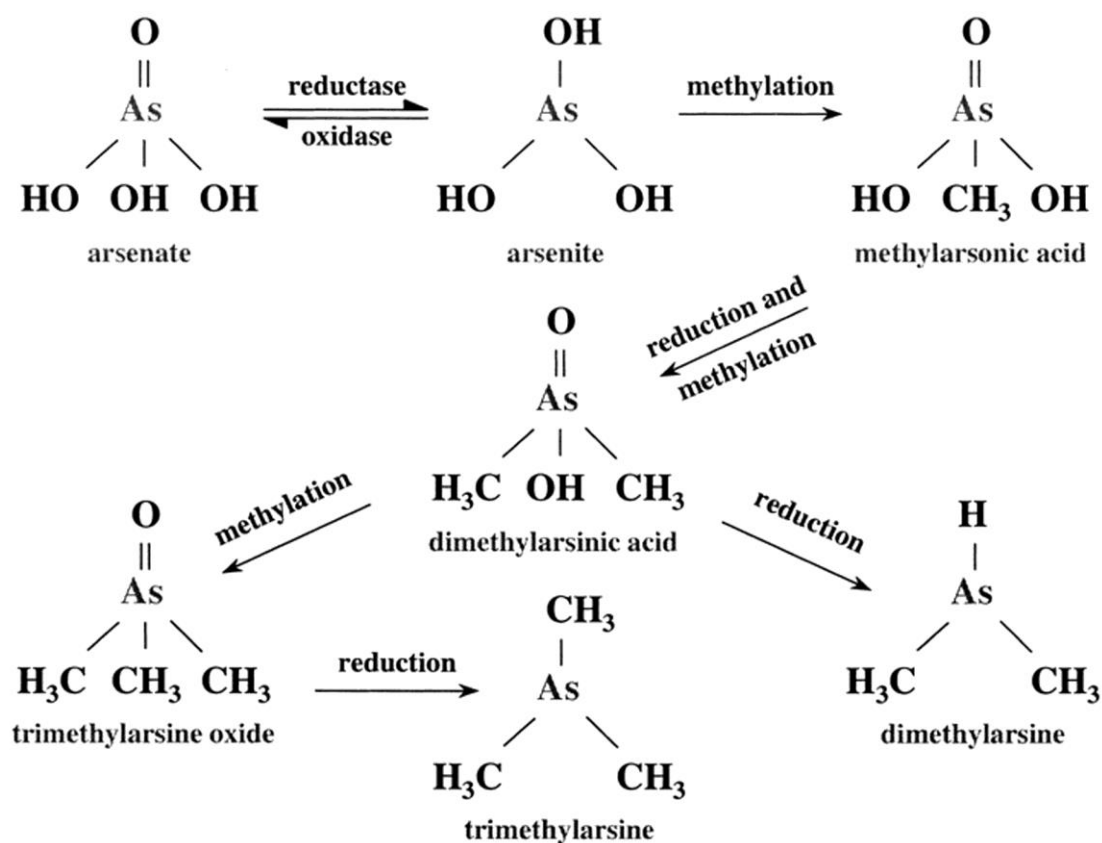


Fig 1.5 Arsenic species

The acid base equilibria and redox reactions between the oxidation states of inorganic arsenic are summarized in Table 1.3. The pE-pH diagram for inorganic arsenic is shown in Fig 1.6. As (V) is prevalent under oxidized conditions while As (III) is thermodynamically stable under reducing conditions. Arsenic acid and its ionization products are of prime importance for arsenic transport under a wide range of Eh and pH³³. The dominant arsenic species at each pH are presented in Fig 1.7a and Fig 1.7b. The primary method to remove arsenic from water is to convert As (III) to As (V) since As (V) is easier to be removed.

Table 1.3 The acid base equilibria and redox reaction of arsenic³⁴

<u>Acid-Base Equilibria</u>			
<u>Arsenic Acid - As(V)</u>			
H_3AsO_4	$\rightleftharpoons \text{H}_2\text{AsO}_4^- + \text{H}^+$	$\text{pK}_{\text{a}1} = 2.24$	
H_2AsO_4^-	$\rightleftharpoons \text{HAsO}_4^{2-} + \text{H}^+$	$\text{pK}_{\text{a}2} = 6.96$	
HAsO_4^{2-}	$\rightleftharpoons \text{AsO}_4^{3-} + \text{H}^+$	$\text{pK}_{\text{a}3} = 11.50$	
<u>Arsenious Acid - As(III)</u>			
H_3AsO_3	$\rightleftharpoons \text{H}_2\text{AsO}_3^- + \text{H}^+$	$\text{pK}_{\text{a}1} = 9.29$	
H_2AsO_3^-	$\rightleftharpoons \text{HAsO}_3^{2-} + \text{H}^+$	$\text{pK}_{\text{a}2} = 12.10$	
<u>Reduction Half Reactions</u>			
<u>As(V) - As(III)</u>	pE°	$E_{\text{H}}^\circ(\text{v})$	
$\text{H}_3\text{AsO}_4 + 2 \text{H}^+ + 2 \text{e}^- \rightleftharpoons \text{H}_3\text{AsO}_3 + \text{H}_2\text{O}$	9.85	0.58	
$\text{H}_2\text{AsO}_4^- + 3 \text{H}^+ + 2 \text{e}^- \rightleftharpoons \text{H}_3\text{AsO}_3 + \text{H}_2\text{O}$	10.85	0.64	
$\text{HAsO}_4^{2-} + 4 \text{H}^+ + 2 \text{e}^- \rightleftharpoons \text{H}_3\text{AsO}_3 + \text{H}_2\text{O}$	14.5	0.86	
$\text{HAsO}_4^{2-} + 3 \text{H}^+ + 2 \text{e}^- \rightleftharpoons \text{H}_2\text{AsO}_3^- + \text{H}_2\text{O}$	9.9	0.58	

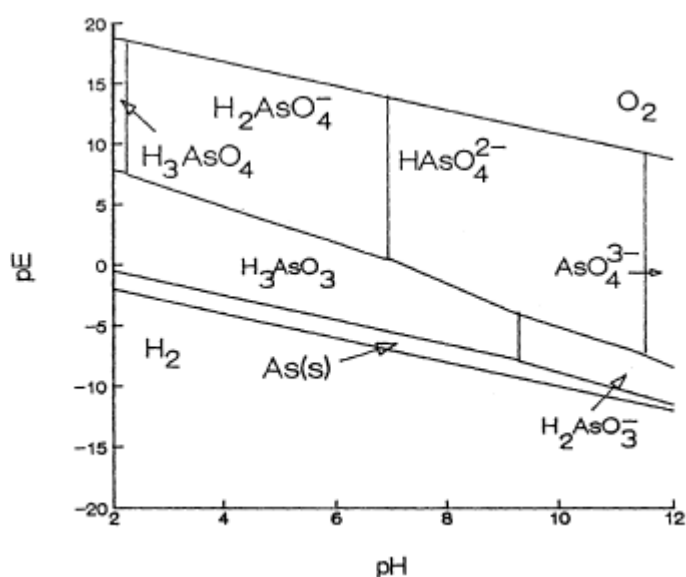


Fig 1.6 pE-pH diagram for the system As-H₂O for conditions 25°C³.

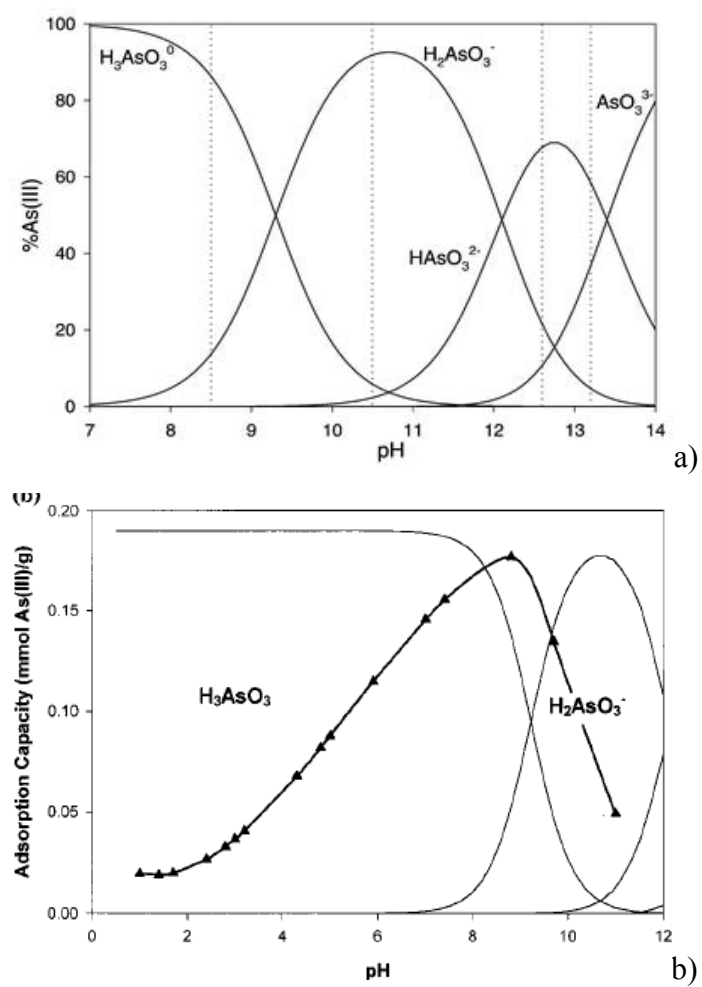


Fig 1.7 Asenic species as a pH function for (a)As(III)³⁵ and (b)As(V)³⁶

1.3.2.Selenium chemistry

Selenium belongs to group VIB (O, S, Se, Te, Po) of the periodic table and is a non-metallic element with the elemental structure $[\text{Ar}] 3d^{10}4s^24p^4$. Selenium has strong chemical similarities to sulfur, with oxidation states VI, IV, 0, and -II being important in natural systems under different redox conditions. In the environment it is present in organic and inorganic species (Fig 1.8). Inorganic selenium can exist as selenide (-II), elemental selenium (0), selenite (IV), selenate (VI); in oxic environmental matrices the main identified species are selenite (SeO_3^{2-}) and selenate (SeO_4^{2-})³⁷. The organic forms generally encountered are selenoamino acids and methylated compounds as dimethyl selenide. The aqueous chemistry of selenate is quite similar to sulfate, and researchers have observed that similar surface complexes form with both oxyanions³⁸. Another important and common form of selenium in soils and surface waters is Se (IV) which exists as the pyramidal oxyanion selenite (SeO_3^{2-}). Selenite is a weak diprotic acid that can exist as H_2SeO_3 , HSeO_3^- , or SeO_3^{2-} depending upon solution pH (pK_{a1} is 2.64 and pK_{a2} is 8.4). In soils and sediments, selenium undergoes a variety of redox reactions, and can be found in oxidation states ranging from -2 (selenide) to +6 (selenate)³⁹ with the form present in the environment being dependent upon soil redox status⁴⁰. The fully oxidized (+6) form, selenate, exists as a tetrahedral oxyanion in solution as biselenate (HSeO_4^-) or selenate (SeO_4^{2-}) with a pK_a of 1.7 for this acid dissociation. The fully protonated selenic acid is a strong acid and does not occur in water.

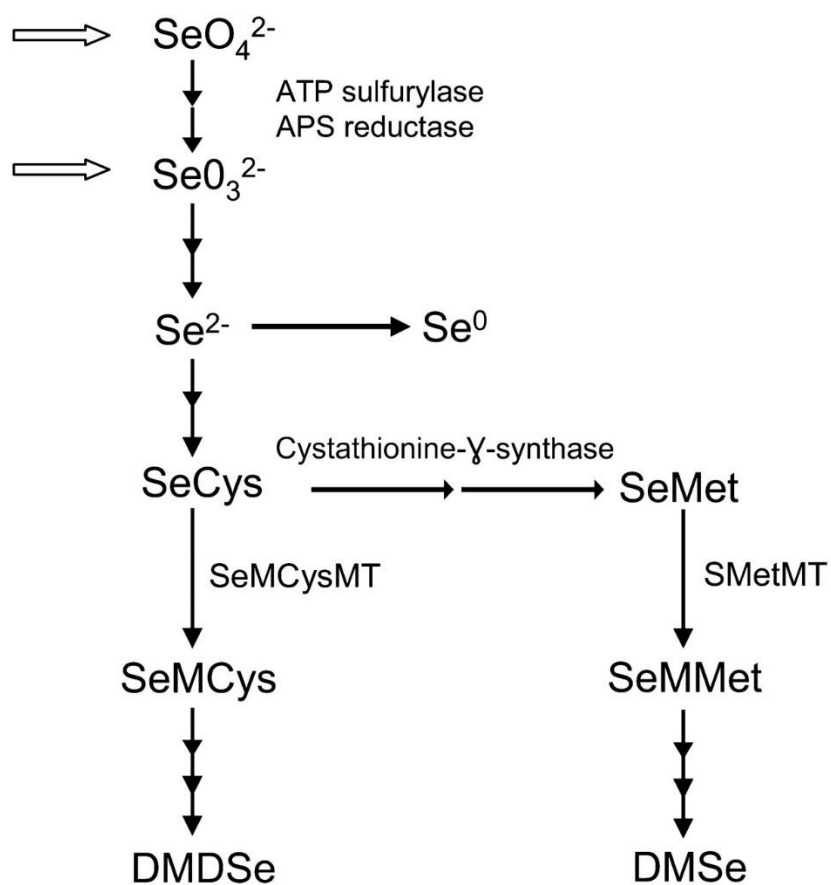


Fig 1.8 Selenium species

The acid base equilibria and redox reactions between the oxidation states of inorganic selenium are summarized in Table 1.5. Fig 1.9 is a pE-Ph diagram for inorganic selenium.

Table 1.5 The acid base equilibria and redox reaction of selenium⁴¹

Acid-Base Equilibria

Selenic Acid - Se(VI)



Selenious Acid - Se(IV)



Reduction Half Reactions

<u>Se(VI) - Se(IV)</u>	<u>pE°</u>	<u>E_H°(v)</u>
$\text{SeO}_4^{2-} + 4 \text{H}^+ + 2 \text{e}^- \rightleftharpoons \text{H}_2\text{SeO}_3 + \text{H}_2\text{O}$	19.44	1.15
$\text{SeO}_4^{2-} + 3 \text{H}^+ + 2 \text{e}^- \rightleftharpoons \text{HSeO}_3^- + \text{H}_2\text{O}$	18.24	1.08
$\text{SeO}_4^{2-} + 2 \text{H}^+ + 2 \text{e}^- \rightleftharpoons \text{SeO}_3^{2-} + \text{H}_2\text{O}$	14.54	0.86

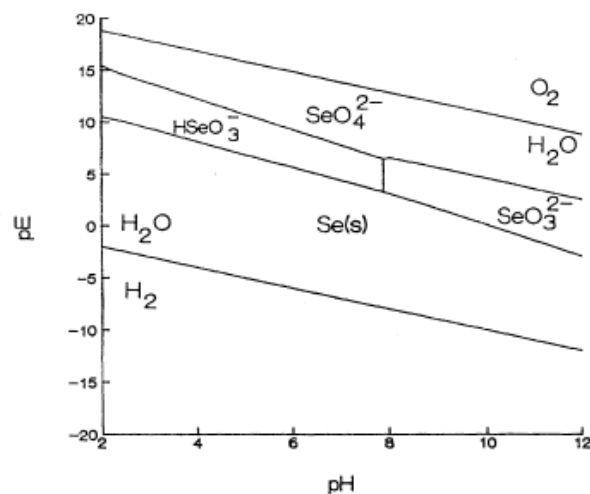


Fig 1.9 pE-pH diagram for the system Se-H₂O for conditions 25°C³.

1.4. Different Methods and technologies for Arsenic and Selenium oxyanions Removal

Treating the contaminated water which contains arsenic and selenium is thus a significant environmental issue. Several methods are available for reducing selenium and arsenic concentrations to acceptable levels in aqueous solutions⁴². There are many conventional methods for arsenic and selenium oxyanions removal, including precipitation⁴³, coagulation, ion exchange⁴⁴ and membrane filtration like reverse osmosis¹⁰ and nanofiltration, electrochemical treatment, as well as adsorption. Each of the above processes has its own advantages and disadvantages as compared in Table 1.6. The disadvantages of traditional methods are high cost (coagulation, precipitation and nanofiltration), high sludge production (coagulation, electrochemical treatment), membrane fouling (nanofiltration), and constant monitoring of the ions concentration (ion exchange). These are inherent drawbacks which make the application of these methods to be limited. Comparing all the disadvantages of above mentioned processes, adsorption is considered as one of the most popular method for arsenic, selenium oxyanions removal from aqueous solutions, and is currently considered as an efficient and economic method for water treatment. Adsorption processes are effective techniques and they have long been used in the water and wastewater industries to remove inorganic and organic pollution for its easy handling, minimal sludge production and its regeneration capability⁴⁵.

Table 1.6 Comparison of removal methods for arsenic from aqueous solution

Method	Examples	Advantage	Disadvantage
precipitation ⁴⁶	Iron precipitation Lime softening;	Simple, low cost	Disposal problems High sludge production
Coagulation		Dewatering	High sludge production; expensive, handling and disposal of contaminated coagulant sludge; requires use of large-scale facilities for implementing water treatment
Membrane filtration	Reverse osmosis; electrodialysis; nanofiltration	Very effective; Less chemical consumption	requires the use of membranes, which are expensive to maintain and replace; Membrane fouling;
Electrochemical treatment		No consumption of chemical reagents; Pure precious metal can be collected	Expensive; Sensitive operating conditions, low efficiency

Method	Examples	Advantage	Disadvantage
Ion-exchange		High regeneration of materials; ion selective	constant monitoring of the ions concentration
adsorption		Efficient and economic, easy handling, minimal sludge production and its regeneration capability	

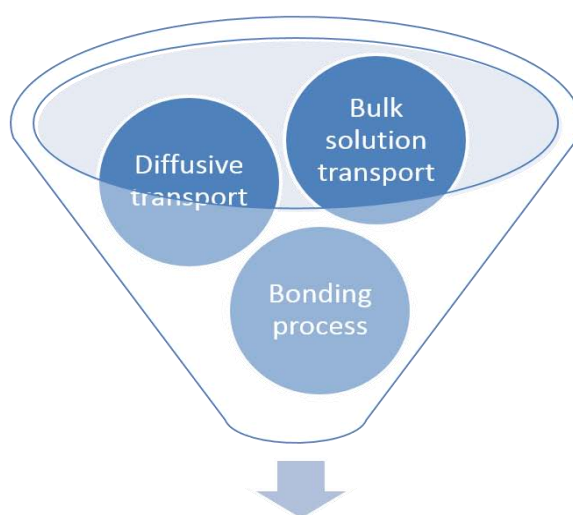
1.4.1.Adsorption

Adsorption is one of the most widely applied techniques for pollutant removal from contaminated Medias. The common adsorbents include activated carbon, molecular sieves, polymeric adsorbents, and some other low-cost materials. Adsorption is the adhesion of atoms, ions, or molecules from a gas, liquid, or dissolved solid to a surface¹¹. This process creates a film of the adsorbate on the surface of the adsorbent. It include both physical and chemical mechanisms⁴⁷. Normally, physical sorption involves the adhesion of adsorbate to the adsorbent, which is not forming a chemical bond and therefore reversible. While the chemical sorption is due to the ion complexation and chemical bond formation, which requires high energy and irreversible. As the irreversible properties of the chemical bond formation, the monolayer is expected to be formed. While the multilayer could be appeared in the physical process.

Adsorption take place in three step⁴⁸, which are bulk solution transport, diffusive transport and bonding process. Bulk solution transport is to move the adsorbate through

the bulk liquid by means of advection and dispersion, to the fixed film boundary layer surrounding the adsorbent media. While the diffusive transport is to move the adsorbate across the fixed film boundary. The bonding process is to attach the adsorbate to the surface of the adsorbent.

Adsorption is a surface phenomenon and is associated with accumulation of solute from its aqueous solution to the adsorbent surface.⁴⁹ At equilibrium the process is supposed to be at dynamic state and the rate of the forward process being equal to the rate of the backward process. The time at which the adsorption equilibrium is attained is known as equilibrium time and the corresponding concentration of solute in solution is the equilibrium concentration. Adsorption equilibrium is governed by several operational factors such as the nature of solute and adsorbent as well as the pH and temperature of the medium. Optimization of such operational parameters is the first step toward the understanding of the process. Previous investigation³³ revealed that sponge loaded with SPION, can potentially use as an effective adsorbent for the arsenate adsorption. However, the different temperature effect on adsorption equilibrium have not been studied. Therefore, here we study the thermodynamic effect on adsorption equilibrium process.



Adsorption three steps

1.10 Adsorption three steps

1.5. Adsorbents for Arsenic and Selenium Removal

Several types of adsorbents have been used for the removal of arsenic and selenium from aqueous effluents, many of them taking advantage of Fe (III) compounds affinity towards inorganic arsenic species and Al compounds for inorganic selenium species. In this regard, various methodologies for arsenic removal involve the use of Iron hydroxyoxides such as goethite (either natural or synthetic), ferrihydrite or hematite and different Fe bearing materials such as Fe (III) loaded zeolites, aluminosilicates or resins. Materials that have shown capacities for selenium sorption include activated alumina; iron media (granular ferric hydroxide, iron oxide coated sand, iron pyrites), synthetic ion exchange resins.

1.5.1. Adsorbent materials for arsenic-literature review

Several adsorbents for removing arsenic have been used as shown in Table 1.7, including: activated alumina, gibbsite⁵⁰, aluminum-loaded materials⁵¹, lanthanum compounds⁵², fly ash⁵³, natural solids⁵⁴, etc. Fe(III)-bearing materials such as goethite⁵⁵, hematite⁵⁶, ferrihydrite⁵⁷, silica that containing iron (III) oxide⁵⁸, Iron-Treated Activated Carbon and Zeolites⁵⁹, Ce(IV)-doped iron oxide⁶⁰, iron oxide-coated sand⁶¹, ferric chloride⁶², Fe(III)-doped alginate gels⁶³, Water-Dispersible Magnetite-Reduced Graphene Oxide Composites⁶⁴, and iron oxide-coated polymeric materials⁶⁵, Fe(III)-loaded resins⁶⁶, Fe(III)-loaded sponge³⁶ are used in arsenic treatment because of the Fe(III) affinity toward inorganic arsenic species and consequent selectivity of the adsorption process. While most of the Fe (III) oxides present low arsenic adsorption capacities, Fe(III)-loaded chelating resins are not economically suitable for their use in a full-scale process. Fe-loaded sponges are not suitable for the trace arsenic adsorption. Besides these drawbacks, the adsorption process is rather slow, what compromises the effectiveness of the process and thus its applicability. Therefore, in our study, we use open-celled cellulose sponge (Forager Sponge) loaded with SPION as the adsorbent since nanoparticles have the potential to eliminate the arsenic concentration from the natural water to near zero due to its inherent properties (large surface area and reactivity)⁶⁷.

Table 1.7 Comparison of adsorbent materials for arsenic adsorption

Adsorbent material	Maximum adsorption capacity (mg/g)	Maximum adsorption capacity (mmol/g SPION)	pH	Ref.
Iron chitosan composite	22.5		7.0	⁶⁸
Iron-hydroxide coated alumina	7.64		6.6-6.7	^{69, 70}
Fe-modified activated carbon	38.8		6.0	⁷¹
Commercial adsorbents (hematite)	10.0		7.3	⁵⁶
Commercial adsorbents (magnetite)	20.9		6.5	⁵⁶
Commercial adsorbents (goethite)	10.1		7.5	⁵⁶
Commercial adsorbents (activated alumina)	19.6		7.0	⁷²
Commercial adsorbents (mesoporous alumina)	47.2		7.0	⁷³
Resin (iron(III)-loaded chelating resin)	62.93		9	⁷⁴
Fe(III)-loaded cellulose sponge	18.0		9.0	³⁶

α -Fe ₂ O ₃	5.31			75
γ -Fe ₂ O ₃	4.75			76
Hydrous iron oxide		2.01	4.0	77
Flower-like iron oxides		0.07	4.0	78
Hydrous iron oxide MNPs		0.51	4.5	79
Magnetite-maghemite nanoparticles		0.05	2.0	80
Fe ₃ O ₄ @CTAB		0.31	3.0	81
SPION		0.91	3.8	82
3-MPA-coated SPION		1.92	3.6	82
Ascorbic acid-coated SPION		0.22	7.0	83
Ce(IV)-doped iron oxide	16		3-7	60
SPION		0.91		82
Ascorbic acid-coated SPION		0.22		84
3-MPA coated SPION		1.92		82

1.5.2. Adsorbent materials for selenium-literature review

Amounts of methodologies and adsorbents have been used for selenium removal from aqueous solution (as shown in Table 1.8). Such as zero-valent iron, ferric hydroxide, ferrihydrite, aluminium hydroxide, activated alumina, activated carbon, aqueous silica, biological treatment, solvent extraction and so on. But the most effective and efficient adsorbent should be aluminium or iron oxide materials. Since aluminium oxide could show complete adsorption for the selenium as well as iron oxide. Thus, in our work, the aluminium oxide and iron oxide nanostructured materials will be applied for selenium adsorption.

Table 1.8 comparison of adsorbent for selenium adsorption

material	Advantages and disadvantages
Precipitation by zero-valent iron ⁸⁵	This method is not effective for selenate removal and achieves only 87% removal efficiency
Co-precipitation by ferric hydroxide or aluminum hydroxide	This method is efficient at pH values of 7 or lower and is only effective for selenite (SeO_2^{3-}).
Adsorption by ferrihydrite	These methods are only effective for selenite (SeO_2^{3-}). It is not effective for Se (VI), The presence of other aqueous species in the solution may influence the removal of Se (VI).
Activated Alumina	
Ferric hydroxides	
Manganese hydroxides	
aluminum hydroxides	
Metal-oxide coated sand	

Ion-exchange process	This process is only effective for the removal of Se (VI). The extraction of Se (VI) is decreased by sulfate.
Biological processes.	Bacterial reduction of selenium species Se^{4+} and Se^{6+} to elemental selenium (Se^0) requires a long operating time and a large apparatus size.
Methylation/volatilization to the atmosphere	<p>This method uses bacteria, fungi and algae for methylating Se in aquatic systems.</p> <p>The rates of selenium volatilization are dependent on the Se species present, microbial activity and various environmental conditions</p>
Solvent extraction	This method is highly efficient and selective but has some disadvantages regarding the complexity of the equipment and high costs.
Electro-chemical method using dissolvable metal electrodes	The electro-chemical method has high costs affiliated with the electrolyzer construction and consumes a great deal of energy, therefore it is ineffective from an economic point of view.
Emulsion liquid membrane	It has shown that Se (VI) is extracted rapidly even in the presence of sulfate at all pH values > 2. Selenium (IV) extraction is influenced by the presence of sulfate.
Reduction process - Ferrous hydroxide	The generation of large volumes of iron sludge and the relatively high cost of reagents makes its application to mine waters questionable.
Iron	The use of iron as a reductant is based on the reduction of aqueous selenium species in the presence of copper ions. The elemental iron reduces both selenium and copper to produce a

	copper selenide on the iron surface.
Lime softening	Application of these unit operations to mine waters was not found in the literature. The achievement of selenium removal to regulated discharge concentrations by these technologies is doubtful.
Activated Carbon	Activated carbon is ineffective for adsorbing selenium from mine waters.
Alumina	Alumina-Selenium (IV) adsorption is nearly complete at pH levels between 3-8.. Selenium (VI) adsorption by alumina is poor. Selenium (VI) adsorption drops off rapidly with increasing pH and is less than 50% at pH 7.
Aqueous silica	Aqueous silica adsorbs in preference to Se (IV) at pH 7 but is no problem at pH 4

1.6. Nanotechnology overview

Nanotechnology, the engineering and art of manipulating matter at the nanoscale (1–100 nm), offers the potential of novel nanomaterials for fields such as materials, electronics, medical remediation, health, medicine, information technology, energy and environment, food⁸⁶ and agriculture⁸⁷(shown in Fig 1.11). Nanoscale science have the extraordinary impact on the current crucial issues, such as improved medical diagnosis and treatment, renewable energy, more efficient information technology, and environmental protection. It involves the production and utilization of a diverse array of nanomaterials (NMs), which include structures and devices with a size ranging from 1 to 100 nm and displays unique properties not found in bulk-sized materials. In the last decade, nanotechnology has developed to such an extent that it has become possible to fabricate, characterize and specially tailor the functional properties of nanoparticles for waste water and natural water treatment applications⁸⁸.The treatment of surface water, groundwater, and wastewater contaminated by toxic metal ions, organic and inorganic solutes, and microorganisms⁸⁹. Nanoparticles (NPs) have been recognized as promising revolution in science and technology due to their unusual properties, high surface area, well difined structure, high reactivity and easy dispersability⁹⁰. Nanotechnology (NT) nowadays is a hot topic and developing very quickly⁹¹. Nanotechnology, which is defined as control of matter at dimensions of roughly 1–100 nm, where unique phenomena enable novel applications, is making a significant impact on our everyday lives, making the today's products much lighter, stronger, smaller, faster, more durable⁹¹⁻⁹². Immense progress and improvements of nanotechnology will have tremendous impact on fields such as materials, electronics, telecommunications, manufacturing technologies, medicine, health and even environmental remediation³³. Nanoscale science and engineering are providing us with unprecedented understanding and control of matter at its most fundamental level: the atomic and molecular scales⁹³..

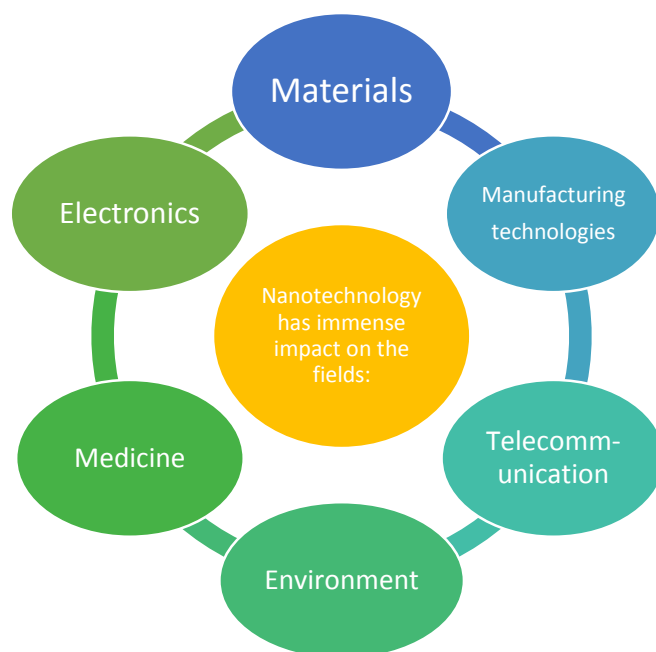


Fig 1.11 Nanotechnology impact on different fields

The sciences such as physics, chemistry, biology, engineering, medicine and energy and environment which complement each other combines and have tremendous effect on nanotechnology^{33,94}. Surface chemistry is especially of great importance concerning the properties of nanomaterials and nanoparticles in particular. The decreasing nanoparticles size causes their surface effects to become more significant due to an increase of surface atoms ration in the volume fraction⁹⁴. The properties of nanoparticles are size dependent⁹⁵. The small size (shown in Fig 1.12) often results in higher reactivity since surface atoms make a large contribution to the thermodynamic characteristics of solids⁹⁶. Such small size gives nanoparticles a high surface area-to-volume ratio^{88a}; surface tailor ability and multifunctionality open to multitude of new possibilities for a wide variety of application in different fields of the science and technology⁹⁷. In addition, chemical reactivity is enhanced by the large surface area⁹⁸, since large surface area might mean a high concentration of surface defects which facilitates interaction with several kinds of chemical species, both gaseous and aqueous. Hence, the properties and functions of nanomaterials often differ drastically from their bulk counterparts (as shown in Fig 1.13). Nanomaterials will attract more considerable

research interest in environmental engineering due to their size effect, high specific surface area and unique structural properties in recent years⁹⁹. Functional nanomaterials are especially attractive because of their improved properties, resulting from their synergistic and cooperative effects⁹⁹⁻¹⁰⁰.

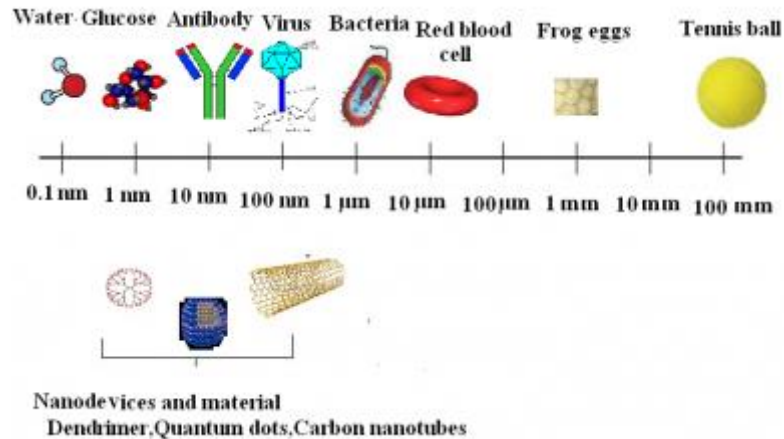


Fig 1.12 how small is nano scales

- High specific surface area and high surface area-to-volume ratio
- Enhanced chemical reactivity
- well structured
- high concentration of surface defects which facilitates interaction with several kinds of chemical species

Highlights
advantages of
nanomaterials

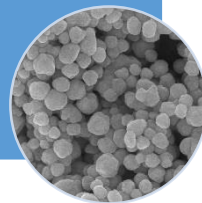


Fig 1.13 Advantages of nanomaterials

1.6.1. Superparamagnetic iron oxide nanoparticles (SPION)

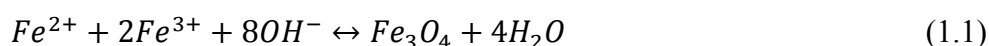
In recent years, the synthesis and utilization of iron oxide nanomaterials with novel properties and functions have been widely studied, due to their size within the nano-range, high surface area to volume ratios and superparamagnetism¹⁰¹. Regarding to wastewater treatment, selection of the best method and material for wastewater treatment is a highly complex task, which should consider a number of factors, such as the quality standards to be met, the treatment flexibility, the efficiency, environment security and friendliness as well as the cost. Iron oxide NMs are a promising material for industrial scale wastewater treatment, due to their low cost, strong adsorption capacity, easy separation and enhanced stability. Current applications of iron oxide NMs in contaminated water treatment can be divided into two groups: nanosorbent or carrier immobilization.

Generally, NMs should be stable to avoid aggregation and with a low deposition rate, in order to assure their reactivity and mobility. However, it is reported that NMs tend to aggregate in solution. One attractive potential approach is the modification of NMs, based on the fact that iron oxide NMs could react with different functional groups. The use of stabilizers, electrostatic surfactants, and steric polymers has been widely proposed for facilitating NMs with non-specific moieties, group specific or highly specific ligands.

Superparamagnetic iron oxide nanoparticles (SPION) with appropriate surface chemistry have been widely used experimentally for numerous biomedical applications such as magnetic resonance imaging contrast enhancement, tissue repair, immunoassay, detoxification of biological fluids, hyperthermia, drug delivery and in cell separation, etc^{88a}. SPIONs consist of cores made of iron oxides that can be targeted to the required area through external magnets. They show interesting properties such as superparamagnetism, high field irreversibility, high saturation field^{93, 102}. Magnetite

(Fe₃O₄), maghemite (γ-Fe₂O₃) and hematite (α-Fe₂O₃) are three main iron oxides that fall under the category of SPIONs. The three main important published routes for the synthesis of superparamagnetism iron oxide nanoparticles (SPIONs) are co-precipitation, hydrothermal reactions and high temperature decomposition. Amongst these methods, co-precipitation of Fe²⁺ and Fe³⁺ ions in a basic aqueous media (e.g. NaOH or NH₄OH solutions) is the simplest way and it is quick and has high yield, but the disadvantage is that the nanoparticles are polydispersed and easy to aggregate.

SPION can be formed by the addition of an alkali solution to an aqueous solution containing Fe³⁺ and Fe²⁺ in a molar ratio of 2, which leads to the formation of complexes with formula, Fe²⁺Fe³⁺O_x(OH) · xH₂O, from which SPION precipitates. Also, it has been suggested that the formation of SPION involves the interaction of Fe²⁺ with precipitated ferrihydrite. The equation is shown as follows:



Magnetic nanoparticles offer some attractive possibilities as shown in Fig 1.15 in water treatment. First, they have controllable sizes ranging from a few nanometres up to tens of nanometres¹⁰³. Second, the nanoparticles are magnetic, which means that they obey Coulomb's law, and can be manipulated by an external magnetic field gradient.

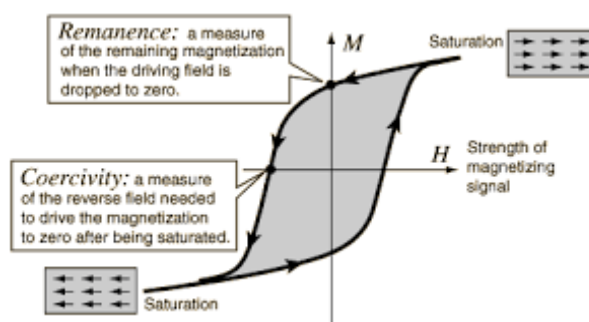


Fig1.14 Magnetization curve displaying hysteresis loop¹⁰⁴.

Once the SPION has been synthesized, the SPION show superparamagnetism property, which has no hysteresis. Superparamagnetic materials are those which behave as

ferromagnets in bulk state as shown in Fig 1.14, but below sizes of 100nm. In most of the envisaged applications, the particles perform best when the size of the nanoparticles is below a critical value, which is dependent on the material but is typically around 10–20 nm¹⁰⁵. They consist of individual magnetic domains, each nanoparticle becomes a single magnetic domain. When a ferromagnetic is sufficiently small, it acts like a single magnet spin that is subject to Brownian motion¹⁰⁶. Such individual nanoparticles have a large constant magnetic moment and behave like a giant paramagnetic atom with a fast response to applied magnetic fields with negligible remanence (residual magnetism) and coercivity (the field required to bring the magnetization to zero). In the absence of an external magnetic field, their magnetization appears to be in average zero: such materials are said to be in the superparamagnetic state. In this state, an external magnetic field is able to magnetize the nanoparticles, similarly to a paramagnet but with a higher stability¹⁰⁷. If enough energy is supplied, magnetism can be reversed along this axis, therefore no hysteresis is observed¹⁰⁸. These features make superparamagnetic nanoparticles very attractive for a broad range of biomedical applications because the risk of forming agglomerates is negligible at room temperature.

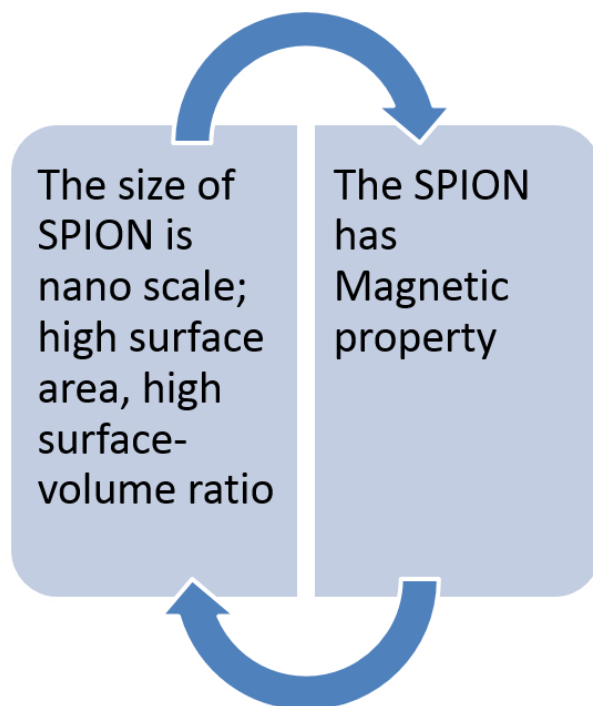


Fig 1.15 Advantages of superparamagnetic iron oxide nanoparticles (SPION)

1.6.2. γ -Al₂O₃ alumina hollow nanospheres

Porous aluminum oxides are of great interest because of their widespread applications in catalysis (as catalyst and catalyst support), adsorption, and separation. Many attempts have been made to synthesize ordered mesoporous alumina¹⁰⁹. Hollow spheres, owing to their tailored structural, optical, and surface properties, have many potential applications such as photonic crystals, delivery vehicle system, fillers, and catalysts. So far, various approaches such as templates and sonochemical, hydrothermal, and emulsion combustion methods have been developed for the preparation of hollow spheres of different materials including ceramics, semiconductors, and metals. Hollow spheres of metal oxide were recently obtained by the emulsion combustion method (ECM) using metal precursors, kerosene, and surfactant¹¹⁰. It has been shown that the structure, size, and composition of the hollow spheres can be altered in a controllable way to tailor various properties over a broad range.

AlOOH and γ -Al₂O₃ have interesting properties and are widely used in industry as adsorbents, abrasive, catalysts, catalyst supports, and ceramics¹¹¹. AlOOH is also used as a template in the preparation of nanostructured materials¹¹². So far, various morphologies of AlOOH have been prepared such as nanotubes¹¹³⁻¹¹⁴, nanowires¹¹⁵, nanobelts¹¹⁶, nanofibers¹¹⁷, nanorods¹¹⁸, whiskers¹¹⁹ and cantaloupe like¹¹³⁻¹²⁰ structures. γ -Al₂O₃ was usually prepared by dehydration of AlOOH at elevated temperatures.

Several methods for γ -Al₂O₃ alumina hollow nanospheres chemical synthesis have been described. Those commonly used are summarized in Table 1.9. Amongst these methods, microwave-assisted solvothermal method for the preparation of γ -AlOOH hierarchically nanostructured microspheres firstly and then thermal treatment of the γ -AlOOH at 600°C produced intact hollow spheres of γ -Al₂O₃ nanosphere is the simplest way.

Table 1.9 Comparison of main chemical methods for aluminum nanomaterials synthesis

Synthesis method	Properties and advantages	Ref.
High-Speed Jet Flame Combustion	The process is simple and effective. The size of nanocrystalline of 5 nm and shell thickness of 10-30 nm	¹¹⁰
Hydrothermal method	Only one step, very facile, the size of the nanorod is 2.5*1.5µm	¹¹³
Hydrothermal method	The length of the tubes is 30–70 nm and their outer diameter is 5–6 nm.	¹²¹
Microwave-assisted	The process is rapid, the morphology is well preserved during the thermal transformation process	¹¹¹

1.6.3. Supporting materials for SPION–Forager sponge

SPION and γ -Al₂O₃ nanospheres, which have been widely applied in the areas of environment protection¹²² and adsorbents¹²³ have the disadvantages which is easy to aggregate into large particles *via* the interparticle dipolar force,¹²⁴ leading to the loss of size effect and the decrease of specific surface area. In order to avoid the agglomeration,

many materials, such as carbon nanotubes¹²⁵, reduced graphene oxide¹²⁶, silica microspheres¹²⁷, bacterial cellulose¹²⁸ and layered double hydroxides¹²⁹, have been used as the template to disperse the magnetic nanoparticles. Among these matrix materials, cellulose has been considered to be an ideal candidate for the dispersion of these nanoparticles owing to the fact that cellulose is one of the most abundant and renewable biopolymers on earth. Therefore, composites of cellulose and magnetic nanomaterials are very promising in many applications.

Forager™ sponge (shown in Fig 1.16) is a high porosity and economic ion exchange material with selective affinity for dissolved heavy metals in both cationic and anionic states. Such material is able to promote high rates of adsorption and flexibility which enables their compressibility into an extremely small volume to facilitate disposal once the capacity of the material has been exhausted. Forager is an open celled cellulose sponge which contains a water insoluble polyamide chelating polymer formed by the reaction of polyethyleneimine and nitrilotriacetic acid. This material is claimed to contain free available ethyleneamine and iminodiacetate groups to interact with heavy metals ions by chelation and ion exchange. In this sense, it has selective affinity for dissolved heavy metals in both cationic and anionic states. Forager sponge and other adsorbent sponges have been successfully used in the treatment of heavy metals solutions.



Fig 1.16 Forager sponge

Several advantages of the sponge material were identified. The first was its open celled nature that allows relatively high flow rates; the second was cost effectiveness; and the

third was the material's low affinity for sodium, potassium, and calcium, three common naturally occurring groundwater ions that can interfere with the effectiveness of typical ion exchange systems for treating specific priority pollutant metals. The selective affinity of the polymer enables the Forager™ Sponge to bind toxic heavy metals over benign monovalent and divalent cations such as calcium, magnesium, potassium and sodium. In addition, prior studies have shown that the sponge material is effective over a wide range of pH. The pH at the site was determined to range from 4 to 5 standard units. Another advantage was that a simple treatment system could be designed and installed similar to a typical carbon adsorption system. It is an open celled cellulose housing iminodiacetic acid groups which chelate transition metal cations by cation exchange processes in the following affinity sequence: $\text{Cd}^{2+} > \text{Cu}^{2+} > \text{Hg}^{2+} > \text{Pb}^{2+} > \text{Au}^{3+} > \text{Zn}^{2+} > \text{Fe}^{3+} > \text{Ni}^{2+} > \text{Co}^{2+} > \text{Al}^{3+}$. The sponge polymer also contains tertiary amine salt groups that can bind anionic contaminants, such as the chromate, arsenic, selenium and uranium oxide species. It can be designed for site specific needs to contain a cation that forms a highly insoluble solid with the anion of interest. Another advantage is its high porosity and flexibility which allows its compressibility into an extremely small volume to facilitate disposal.

1.7. Kinetic and Thermodynamic Aspects

1.7.1. Kinetic Model

Adsorption equilibrium studies are necessarily and significant for determining the efficiency of adsorption process. Predicting the rate at which adsorption takes place for a given system is probably the most important factor in adsorption system design, with adsorbate residence time and the reactor dimensions controlled by the system's kinetics¹³⁰. Moreover, it is important to identify the adsorption mechanism and the potential rate controlling steps such as mass transport and chemical reaction process in such systems. General models which describe the kinetics of adsorption onto solid surfaces in liquid-solid phase adsorption system include: pseudo-first order equation, pseudo-second order equation and the Weber-Morris intraparticle diffusion. A number of adsorption processes for pollutants have been studied in an attempt to find a suitable explanation for the mechanisms and kinetics for sorting out environment solutions. Therefore, adsorption onto solid adsorbent has great environment significance.

When adsorption is concerned, kinetic and thermodynamic aspects should be involved to know more details about its performance and mechanisms. Especially for adsorption capacity, kinetic performance of a given adsorbent is also of great significance for the pilot application. From the kinetic analysis, the solute uptake rate, which determines the residence time required for completion of adsorption reaction, may be established. Also, one can know the scale of an adsorption apparatus based on the kinetic information. Generally speaking, adsorption kinetics is the base to determine the performance of fixed-bed or any other flow-through.¹³¹

1.7.1.1. Pseudo-first order equation

Lagergren (1898) presented a first-order rate equation to describe the kinetic process of liquid-solid phase adsorption of oxalic acid and malonic acid onto charcoal, which is believed to be the earliest model pertaining to the adsorption rate based on the

adsorption capacity.¹³¹ The pseudo-first order has been most widely used for the adsorption of an adsorbate from aqueous solution, such as for heavy metal ions, organic compounds.¹³² This model based on the solid capacity considers that the rate of occupation of adsorption sites is proportional to the number of unoccupied sites.¹³³ The best-fit model was selected based on both linear regression correlation coefficient (R^2) and the calculated q_e values. The pseudo-first order rate equation is generally expressed as follows:

$$\frac{dq}{dt} = k_1(q_e - q_t) \dots \dots \dots (1.2)$$

where q_e and q_t (mg/g) are the adsorption capacities (concentration of adsorbed arsenic or selenium anion per unit of adsorbent mass, mmol/g) at equilibrium and time t (min), respectively. k_1 (min^{-1}) is the pseudo-first-order rate constant for the kinetic model. Integrating Eq.(1.2) with the boundary conditions of $q_t=0$ at $t=0$ and $q_t=q_t$ at $t=t$, yields

$$\ln \left(\frac{q_e}{q_e - q_t} \right) = k_1 t \dots \dots \dots (1.3)$$

Which can be arranged to:

$$\log(q_e - q_t) = \log q_e - \frac{k_1}{2.303} t \dots \dots \dots (1.4)$$

Where q_e and q_t are the amount of selenium adsorbed (mg.g^{-1}) at equilibrium and at time t , respectively. K_f (min^{-1}) is the rate constant of pseudo-first order adsorption reaction. A plot of $\log (q_e - q_t)$ vs. t is expected to yield a straight line and the rate constant K_f can be evaluated from the slope.

To distinguish kinetic equations based on adsorption capacity from solution concentration, Lagergren's first order rate equation has been called pseudo-first-order.¹³⁴ In recent years, it has been widely used to describe the adsorption of pollutants from wastewater in different fields.¹³⁰

1.7.1.2. Pseudo-second order equation

The main assumptions for the pseudo second-order model for the adsorption is: the rate of occupation of adsorption sites is proportional to the square of the number of unoccupied sites. The rate limiting step may be chemical adsorption involving valent forces through sharing or the exchange of electrons between the reactions. In addition, the adsorption follows the Langmuir equation.¹³⁵ It can be expressed as follows:

$$\frac{dq}{dt} = k_2(q_e - q_t)^2 \dots\dots\dots(1.5)$$

where k_2 is the rate constant of sorption, ($\text{g mmol}^{-1} \text{min}^{-1}$), q_e is the amount of adsorbed arsenic or selenium anions per unit of mass adsorbent at equilibrium, (mmol/g), q_t is amount of adsorbed arsenic or selenium anions on the surface of the adsorbent at any time, t , (mmol/g). Separating the variables in Eq. (1.5) gives:

$$\frac{dq_t}{(q_e - q_t)^2} = k dt \dots\dots\dots(1.6)$$

Integrating this for the boundary conditions $t=0$ to $t=t$ and $q_t=0$ to $q_t=q_t$, gives:

$$\frac{1}{(q_e - q_t)} = \frac{1}{q_e} + kt \dots\dots\dots(1.7)$$

Which is the integrated rate law for a pseudo-second order reaction.

$$q_t = \frac{t}{\frac{1}{kq_e^2} + \frac{t}{q_e}} \dots\dots\dots(1.8)$$

Which has a linear form

$$\frac{t}{q_t} = \frac{1}{kq_e^2} + \frac{t}{q_e} \dots\dots\dots(1.9)$$

The plot of t/q_e versus t should give a straight line if second order kinetics are applicable, and q_e and k_2 can be determined by the slope and intercept of the plot,

respectively. It is important to notice that for the application of this model the experimental estimation of q_e is not necessary. The pseudo-second order equation can predicts the behavior over the whole range of time studied, and is in agreement with chemical adsorption as the rate controlling step.

1.7.2. Isotherm Model

The most commonly used isotherm equations for the equilibrium modeling of adsorption are, the Freundlich and Langmuir isotherms.¹³⁶ Both represent the equilibrium amount of toxic element ions removed (q_e , mmol/g) as a function of the equilibrium concentration (C_e , mmol/L) of toxic element ions in the solution, corresponding to the equilibrium distribution of ions between aqueous and solid phases as the initial concentration increases.

1.7.2.1. Langmuir Isotherm

Langmuir isotherm is based on the assumption that enthalpy of adsorption is independent of the amount adsorbed¹³⁷. A basic of assumption of the Langmuir theory is that sorption takes place at specific homogenous sites within the sorbent, no further sorption can take place at that sites¹³⁸. The Langmuir equation is valid for monolayer sorption onto a surface with a finite number of identical sites. It incorporates two easily interpretable constants: q_{\max} , which corresponds to the highest possible adsorbate uptake; and coefficient b , which is related to the affinity between the adsorbent and adsorbate. The empirical Freundlich equation, based on the multilayer adsorption on heterogeneous surface. The Freundlich isotherm describing the non-ideal and reversible adsorption, not restricted to the formation of monolayer. This empirical model can be applied to multilayer adsorption, with non-uniform distribution of adsorption heat and affinities over the heterogeneous surface¹³⁸. It can be derived assuming a logarithmic decrease in the enthalpy of adsorption with the increase in the fraction of occupied sites.

The Langmuir equation assumes that (i) the solid surface presents a finite number of identical sites which are energetically uniform; (ii) there is no interactions between adsorbed species, meaning that the amount adsorbed has no influence on the rate of adsorption; (iii) a monolayer is formed when the solid surface reaches saturation.¹³⁶ It assumes the form:

$$q_e = \frac{Q_0 K_L C_e}{1 + K_L C_e} \dots\dots\dots(1.10)$$

where Q_0 (mg/g) is the maximum amount of arsenic or selenium anion per unit weight of adsorbent to form a complete monolayer on the surface and K_L is the equilibrium adsorption constant which is related to the affinity of the binding sites. Q_0 represents a practical limiting adsorption capacity when the surface is fully covered with arsenic or selenium anions and allows the comparison of adsorption performance, particularly in the cases where the adsorbent did not reach its full saturation in experiments.¹³⁹ The Langmuir equation can be described by its linearized form:

$$\frac{C_e}{q_e} = \frac{C_e}{Q_0} + \frac{1}{Q_0 K_L} \dots\dots\dots(1.11)$$

A plot of C_e/q_e versus C_e gives a straight line with the slope equal to $1/Q_0$, the intercept equal to $\frac{1}{Q_0 K_L}$. while Langmuir isotherm assumes that enthalpy of adsorption is independent of the amount adsorbed.

1.7.2.2. Freundlich isotherm model

The empirical Freundlich isotherm, based on the multilayer adsorption on heterogeneous surface, describe the relationship between equilibrium liquid and solid phase capacity. It can be derived assuming a logarithmic decrease in the enthalpy of adsorption with the increase in the fraction of occupied sites.¹³⁶ It also assumes that the stronger adsorption sites are occupied first and the binding strength decreases with the increasing degree of site occupation, and is given by:

$$q_e = k_F C_e^{1/n} \dots\dots\dots(1.12)$$

where K_F and n are the Freundlich constants characteristics of the system, indicating the adsorption capacity and adsorption intensity, respectively. C_e is the equilibrium concentration of the ion in the residual solution (mmol/L), q_e is the equilibrium concentration of the adsorbed per unit of mass of sorbent (mol/g). Eq. (1.12) can be linearized in logarithmic form (1.13) and the Freundlich constants can be determined:

$$\log q_e = \log k_F + \frac{1}{n} \log C_e \dots\dots\dots (1.13)$$

If the value of n is greater than unity, this is an indication of a favorable adsorption. A plot of $\log q_e$ versus $\log C_e$ will give a straight line of slope $1/n$ and intercept k_F , when the liquid-solid system follows this model.

1.7.3. Thermodynamic studies

1.7.3.1. Thermodynamic parameters

The thermodynamic feasibility of adsorbent–anion interaction was studied by variation of temperature of the medium in a temperature range. Thermodynamic parameters such as ΔG^0 , ΔS^0 , ΔH^0 were calculated using Van't Hoff equation:¹⁴⁰

$$\Delta G^0 = -RT \ln K_a \dots\dots\dots(1.14)$$

and

$$\Delta G^0 = \Delta H^0 - T \Delta S^0 \dots\dots\dots(1.15)$$

where R is the universal gas constant ($8.314 \text{ J mol}^{-1} \text{ K}^{-1}$), T is the temperature (K), K_a is the Langmuir equilibrium affinity coefficient shown in equation (1.9), ΔG^0 is the change in free energy. Further, the relationship between K_a vs. standard enthalpy (ΔH^0) and standard entropy (ΔS^0) factors can be represented using the following equation:

$$\ln K_a = \frac{\Delta S^0}{R} - \frac{\Delta H^0}{RT} \dots\dots\dots(1.16)$$

Here ΔH^0 and ΔS^0 parameters can be calculated, respectively, from the slope and intercept of plot of $\ln K_a$ vs. $1/T$.

1.7.3.2. Thermodynamic studies for arsenic removal-literature review

Previous research has investigated adsorption kinetic as the removal mechanisms of metals or oxyanions by nanomaterials, comparatively little research has investigated the detailed adsorption characteristics and thermodynamics of metal or oxyanions removal by nanomaterials. Table 1.10 shows the Equilibrium, thermodynamic investigations for arsenic removal from aqueous solution in recent years.

Table 1.10 Equilibrium and thermodynamic studies for arsenic removal-literature review

Isotherm	adsorbent	Temp. (°C)	As(V) /As(III)	ΔG^0 (KJ/mol)	ΔH^0 (KJ/mol)	ΔS^0 (J/molK)	ref
Freundlich	Granular ferric hydroxide (GFH)	20	As(V)	-11.368	45.940		141
		30		-13.376			
		40		-15.276			
		20	As(III)	-9.033	68.367		
		30		-11.401			
		40		-14.330			
Langmuir/ D-R	Algea	20	As(III)	-18.39	-26.69	-38.42	70
		30		-18.21			
		40		-17.70			
		50		-17.24			
D-R	Activated aluminum	20	As(III)	-33.12	-6.096	-91	142
		30		-34.15			
		40		-34.96			
		50		-35.87			
	Dolomite	20	As(V)	80.57	-3.67	-287.35	143
		45		87.75			
		65		93.5			
		80		97.81			
Langmuir	Activated red mud	25	As(III)	-27.75		69.9	144
		40		-29.06		70.8	
		55		-30.00		70.3	
		70		-30.90		69.9	
Langmuir		25	As(V)	-30.36		125.6	
		40		-32.67		126.9	
		55		-34.16		125.6	
		70		-36.88		128.1	

1.7.3.3. Thermodynamic study of selenium removal- literature review

Just a few research investigations have been reported in the literature related to the thermodynamic study of selenium adsorption (shown in Table.1.11). From the previous report, the thermodynamic parameters for the sorption of Se (VI) and Se (IV) indicate exothermic or endothermic behavior. Exothermic behavior could make the tuning of

the lower temperature to favor the adsorption while higher temperature could help the desorption process to occur. Endothermic behave in an opposite way. That means, the adsorption of Se (VI) and Se (IV) could be done by tuning of the higher temperature and desorption can be realize by tuning of the lower temperature. Lei Zhang¹⁴⁵ studied that removal of selenium ions from aqueous by using nano-TiO₂. The mean energy of adsorption (14.46 kJ mol⁻¹) was calculated from the Dubinin–Radushkevich (D-R) adsorption isotherm at room temperature. The thermodynamic parameters for the sorption were also determined, and the negative ΔH_0 and ΔG_0 values indicate exothermic behavior. Mustafa Tuzen¹⁴⁶ studied the selenium biosorption from aqueous solution by green algae, the calculated thermodynamic parameters, ΔG_0 (between -18.39 and -16.08 kJ/mol at 20–50°C) and ΔH_0 (-45.96 kJ/mol) showed that the biosorption of Se(IV) onto *C. hutchinsiae* biomass was feasible, spontaneous and exothermic, respectively. Ramakrishnan Kamaraj¹⁴⁷ has studied selenate removal from aqueous solution by oxidized multi-walled carbon nanotubes. It has demonstrated that the calculated values of enthalpy change (ΔH) and entropy change (ΔS) are 19.474 kJ/mol and 69.9058 J/mol K respectively. Further, these studies revealed that the adsorption reaction was spontaneous and endothermic process (the ΔH is positive) .

Table 1.11 Thermodynamic studies for selenium removal-literature review

isotherm	adsorbent	Temp. (K)	Se(IV) / Se(VI)	$\Delta G^0 (KJ/mol)$	ΔH^0 ($KJmol^{-1}$)	ΔS^0 ($J mol^{-1}K^{-1}$)	ref
Langmuir	Cladophora hutchinsiade	293	Se(IV)	-18.93	-45.96	-70.92	146
		303		-18.12			
		313		-17.70			
		323		-16.08			
Langmuir	nano-TiO ₂	273	Se(IV)	-4.44	-11.2	-24.76	145
		293		-3.71		-25.56	
		313		-3.12		-25.83	
Langmuir	oxidized multiwalled carbon nanotubes (MWCNT)	303	Se(VI)	-0.657	19.479	69.9058	147
		313		-1.297			
		323		-1.972			
		333		-2.428			

1.7.4.Redox potential

Redox potential (also known as reduction potential, oxidation / reduction potential, pE or E_h) is a measure of the tendency of a chemical species to acquire electrons and thereby be reduced⁴⁷. Redox potential is measured in volts (V), or millivolts (mV). Each species has its own intrinsic redox potential; the more positive the potential, the greater the species' affinity for electrons and tendency to be reduced. pE is a common measurement for water quality.

In the field of environmental chemistry, the redox potential is used to determine if oxidizing or reducing conditions are prevalent in water or soil, and to predict the states of different chemical species in the water, such as dissolved metals¹⁴⁸. pE values in water range from -12 to 25; the levels where the water itself becomes reduced or oxidized, respectively.

The reduction potentials in natural systems often lie comparatively near one of the boundaries of the stability region of water. Aerated surface water, rivers, lakes, oceans, rainwater and acid mine water, usually have oxidizing conditions (positive potentials). In places with limitations in air supply, such as submerged soils, swamps and marine sediments, reducing conditions (negative potentials) are the norm. Intermediate values are rare and usually a temporary condition found in systems moving to higher or lower pE values.

1.8. Objectives

From the literature review, the Arsenic and Selenium oxyanions removal will be paid by more attention due to their toxicity properties and their existence in environment, especially in aquatic system. Compared with other removal methods, the adsorption method will be really amazing for both oxyanions removal since it has high efficiency and capacity. The nanostructured materials, either iron nanoparticles or aluminum Nanosphere will be applied for such kind of oxyanions removal by taking advantage of their remarkable properties. The Forager sponge will be used for supporting the nanomaterial in order to avoid aggregation thus improve the adsorption capacity and efficiency. The kinetic, equilibrium and thermodynamic studies will be investigated, which could provide information for understanding the adsorption mechanism and thus control the adsorption process by modifying the thermodynamic parameters, such as temperature and redox potential, in order to realize the desorption process.

Desorption and sorbent regeneration is a critical step contributing to increase process costs. Once the sorbent becomes exhausted, then, either the Arsenic or Selenium oxyanions must be recovered, the adsorbent regenerated or disposed in a controlled dumping site for toxic substances that use to be expensive. A successful desorption process must restore the sorbent close to its initial properties for effective reuse. In most of the published arsenic sorption studies (some discussed earlier), desorption/regeneration was not included. Very few desorption studies are detailed in literature. Few attempts have been made to address the handling of concentrated arsenic wastes. Tuutijärvi T¹⁴⁹ has tried five different alkaline solutions: NaOH, Na₂CO₃, Na₂HPO₄, NaHCO₃ and NaAc for arsenate batch desorption and regeneration. But this process also need to spend a lot of alkaline solution which is very expensive and is not feasible for industrial sense. Thus, in the thesis work, reagent-less processes has been developed --Arsenic and Selenium desorption and sorbent regeneration with no

reagents added by taking advantage of the thermodynamic properties of the adsorption system.

The main purpose of the work presented in this PhD thesis is focused on Arsenic adsorption-desorption by adsorbent systems based on superparamagnetic iron oxide nanoparticles (SPION) loaded sponge, Selenium adsorption-desorption by γ - Al_2O_3 nanospheres for waste water treatment application. In addition, in order to overcome the weakness of using reagents to regenerate the adsorbents, this study finds a reagent-less way to remove the oxyanions. Specifically, this work investigates the thermodynamic aspects of the adsorbent systems and redox potential effect on the Arsenic and Selenium oxyanions removal. In overall, the major scientific and technical objectives of the PhD thesis involve:

1. To optimize the synthesis of Superparamagnetic Iron Oxide Nanoparticles (SPION). To develop a procedure to load SPION on treated Forager sponge by nebulizer in order to decrease the SPION aggregation. Characterization of nanostructured adsorbent by SEM and TEM will help on the process optimization
2. To study the parameters which maximize the adsorption capacity of arsenate on SPION loaded sponge, including pH, contact time, target oxyanions initial concentration, temperature, redox potential.
3. To study the temperature and redox parameters tuning effect on arsenic oxyanions removal. To determine the thermodynamic values which have influence on arsenate adsorption-desorption, including Gibb's free energy, enthalpy, entropy as well as redox potential.
4. To develop the continuous column mode for arsenic oxyanions removal, arsenate, arsenite and arsenate/arsenite mixture. To study the adsorption-desorption recycled process therefore develop the reagent-less process for water decontamination. Tuning of Temperature and redox parameters for toxic arsenic oxyanions removal.

5. To optimize the synthesis of γ - Al_2O_3 nanospheres by microwave assistant process. To modified the γ - Al_2O_3 nanospheres by diethylammonium N,N-diethyldithiocarbamate(DDC). To characterize the γ - Al_2O_3 nanospheres by Scanning Electron Microscopy (SEM) and X Ray Diffraction (XRD).
6. To determine the effect of parameters including pH, contact time, temperature, initial concentration and oxidation state on the Selenooxynions adsorption on γ - Al_2O_3 nanospheres . In addition, to evaluate the dynamics of the adsorption process
7. To determine the adsorption parameters such as contact time, pH effect, concentration effect, both in batch and column continuous mode on the Selenooxynions adsorption on SPION loaded sponge.
8. To develop reagent-less processes for Arsenic and Selenium oxynions adsorption-desorption and sorbent regeneration with no reagents added by tuning of thermo and redox potential parameters.

Chapter II

Methodology

2. Methodology

2.1. Reagents and Apparatus

All the chemicals used were of analytical reagent grade. Stock solutions of separate oxyanions, such as As (V), As (III), Se (IV), Se (VI) were prepared by dissolving their sodium salts. The As (V) and As (III) source was sodium arsenate ($\text{Na}_2\text{HAsO}_4 \cdot 7\text{H}_2\text{O}$) and sodium arsenite (NaAsO_2), ACS reagent from Aldrich (Milwaukee, USA). The Se (VI) and Se (IV) source was sodium selenate and sodium selenite, Na_2SeO_4 , Na_2SeO_3 , ACS reagent from Aldrich (Milwaukee, USA). A 1000 ppm stock solutions of each oxyanion were first prepared, which were then diluted to the aqueous feed initial oxyanion concentration for each experiment. Sodium acetate trihydrate (>99%, ACS reagent from Aldrich, USA) and Acetic acid (>99%, ACS reagent from Aldrich) were used for the preparing the buffer in order to adjust the pH of the feed initial aqueous solution.

$\text{KAl}(\text{SO}_4) \cdot 12\text{H}_2\text{O}$, Urea, NaAc and HAc were ACS reagents from Panreac S.A. (Barcelona, Spain) Iron chloride ($\text{FeCl}_3 \cdot 6\text{H}_2\text{O}$) and Ferrous chloride ($\text{FeCl}_2 \cdot 4\text{H}_2\text{O}$) were ACS reagent from Aldrich (Milwaukee, USA), HCl were ACS reagents from Panreac S.A. (Barcelona, Spain).

Forager Sponge, an open-celled cellulose sponge which contains a water-insoluble polyamide chelating polymer. (Formed by reaction of polyethyleneimine and nitrilotriacetic acid), was kindly supplied by Dynaphore Inc. (Richmond, VA, U.S.A.). This material is claimed to contain free available ethyleneamine and iminodiacetate groups to interact with heavy metals ions by chelation and ion exchange.

All of the aqueous solution were prepared by deionized water which was purified with a milli-Q Gradient system from Millipore Corporation. pH standard buffer solutions were used to calibrate an Omega 300 pH meter (Crison instruments, S.A., Spain) for the measurement of the initial and final aqueous pH values in all the experiment.

2.2. Experiment Equipment

2.2.1. Basic experiment equipment

The experiment performed and developed for this thesis work should be used amount of basic experiment equipment, such as the balance for weighting the adsorbent, chemical reagent, the pH-meter for analyzing and confirming the aqueous solution pH, the centrifuge to separate the adsorbent and suspension, the agitator, the oven for doing the experiment under high temperature, as well as the micropipettes of different volumes. Different glass material, such as flasks and bakers, electronic devices, like pumps, and syringes and needles have also been used.

2.2.2. Colorimetric technique- UV-Vis Spectrophotometer

UV-Vis spectrophotometer is a device in which a light coming from a continuous source pass through a monochromator, which select a narrow band of wavelengths of the incident beam¹⁵⁰. This monochromatic light go through a cuvette in which the sample is and measure the radiant power of the light that emerges. The amount of adsorbed radiation is related with the Lambert – Beer law¹⁵¹:

$$A = \varepsilon * b * C \dots\dots\dots(2.1)$$

Where A= absorbance, ε = molar attenuation coefficient, b= cuvette length, C= Concentration

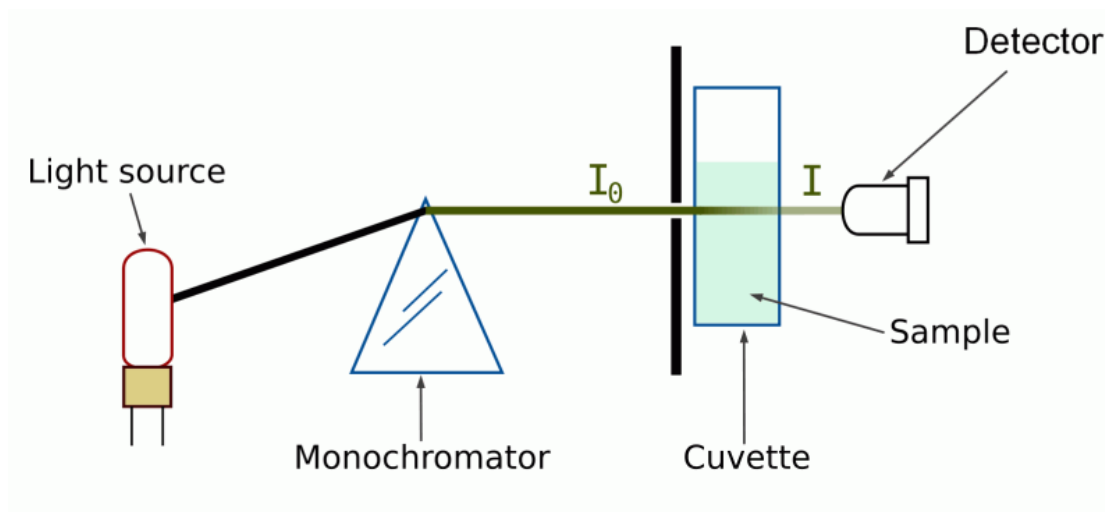


Figure 2.1 UV-Vis spectrophotometer scheme



Fig 2.2 UV-Vis Spectrometer

In a double beam spectrophotometer, the light pass through the sample cuvette and the reference cuvette alternately. Comparing a lot of times both energies, the double beam device can correct some errors associated with the intensity of the source and with the detector¹⁵².

2.2.2.1. Colour Reagent

The colour reagent used for the detection of Arsenic has clearly described elsewhere¹⁵³, a mixture of 4 different reagents. Each reagent is putted into a solution in a separated 50mL volumetric flask using miliQ water as solvent. The reagents are:

- Ammonium Molybdate (1.485g) in 50mL of miliQ water.

- L-Ascorbic Acid (5.4g) in 50mL of miliQ water.
- Antimony Potassium Tartrate (0.267g) in 50mL of miliQ water.
- Sulfuric Acid (6.71mL) 95-98% in 43.29mL of miliQ water.

The mixture of those reagents is done in the following ratio: 2:2:1:5. After the addition of Antimony Potassium Tartrate, Sulfuric Acid should be added immediately in order to avoid turbidity of the colour reagent.¹⁵⁴

Currently, the popular methods for arsenic detection are chromatography, spectroscopic and electrochemistry methods¹⁵⁵. These methods tend to be complex, expensive and time-consuming, so they are neither readily available in developing countries nor capable of on-site field detection. With the colour reagent, arsenic(V) concentration can be analysed by UV¹⁵⁶ which is very facile and quickly. since As (V) form a complex with reduced molybdate that strongly absorbs in the infrared¹⁵⁷, while As (III) need to be oxidized firstly to be As(V) and then analysed¹⁸. Doing a calibration curve using known concentrations of As (V) make possible to obtain the real unknown concentration of As (V) without the interference of phosphates present in the samples. The wavelength used to perform these analyses is 860nm.

Arsenic and iron concentrations in solution were determined by the Colorimetric technique. The wavelength used for analysis were 840 nm(As), 490 nm(Fe).

2.2.3.Inductively Coupled Plasma Mass Spectrometry(ICP-MS)

Inductively coupled plasma mass spectrometry (ICP-MS) is a fast and accurate trace element determination technique¹⁵⁸. ICP-MS is capable to carry out rapid multi-element determination at the ultra-trace level¹⁵⁹. The instrument detection limits are at or below the single ppt level for most of the periodic table element¹⁶⁰. Most analysis performed on ICP-MS instrumentation are quantitative. The device has to be placed in a white clean room to avoid contamination of the samples due to the large sensibility of the instrument. An ICP-MS consist of the following components(shown in Fig 2.3):

Sample introduction system (composed of a nebulizer and spray chamber), ICP torch and RF coil, interface, vacuum system, collision/reaction cell, ion optics, mass spectrometer, detector and data handling and system controller¹⁶¹.

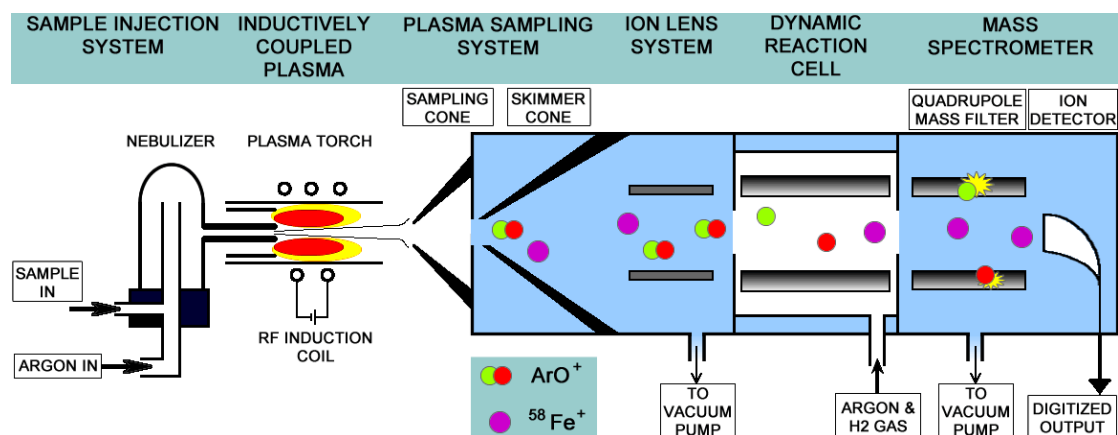


Figure 2.3 ICP-MS scheme

The sample, usually in liquid form is pumped into a nebulizer, where it is converted into a fine aerosol with argon gas. The fine droplets of the aerosol, which represent only 1-2% of the sample, are separated from larger droplets by means of a spray chamber. The fine aerosol then emerges from the exit tube of the spray chamber and is transported into the plasma torch via sample injector, where the plasma is formed by the interaction of an intense magnetic field on a tangential flow of gas (normally argon) flowing through a concentric quartz tube (torch). This has the effect of ionizing the gas and, when seeded with a source of electrons from a high-voltage spark, forms a very-high-temperature plasma discharge at the open end of the tube. The plasma torch, which is positioned horizontally, is used to generate positively charged ions. It is the production and the detection of large quantities of these ions that give ICP-MS its characteristic low ppt detection capability.

Once the ions are produced in the plasma, they are directed into the mass spectrometer via the interface region, which is maintained at a vacuum with mechanical roughing pump. This interface region consists of two metallic cones (usually nickel), called the

samples and a skimmer cone, each with a small orifice to allow the ions to pass through to the ion optics, where they are guided into the mass separation device.

The interface region is one of the most critical areas of and ICP-MS because the ions must be transported efficiently and with electrical integrity from the plasma, which is at atmospheric pressure, to the mass spectrometer analyser region at approximately 10^{-6} Torr. Once the ions have been successfully extracted from the interface region, they are directed into the main vacuum chamber by a series of electrostatic lens, called ion optics which have the function of electrostatically focus the ion beam toward the mass separation device, while stopping photons, particulates, and neutral species from reaching the detector. The operating vacuum in this region is maintained at about 10^{-3} Torr with a turbo molecular pump.

The ion beam containing all the analytes and matrix ions exits the ion optics and now passes into the heart of the mass spectrometer, the mass separation device, which is kept at an operating vacuum of approximately 10^{-6} Torr with a second turbo molecular pump. The separation device allow analyte ions of a particular mass-to-charge ratio through to the detector and to filter out all the nonanalyte, interfering and matrix ions.


The final process is to convert the ions into an electrical signal with an ion detector. This electronic signal is then processed by the data handling system and then converted into analyte concentration using ICP-MS calibration standards.

ICP-MS technique was employed to analyze the arsenic and selenium oxyanion content in the liquid phases of several adsorption parameters¹⁶². ICP-MS is the most sensitive technique for trace elements in solution¹⁶³. Typical detection limits for ICP-MS are around $0.01\text{-}1\text{ }\mu\text{g /L}$ (ppb) in solution.

When the arsenic, selenium and metal ions concentrations were very low (about ppb level), ICP-MS was employed after a previous treatment of the sample by diluting them in 2% nitric acid. Additionally, iron and alumina content was determined to control the

stability of SPION and γ -Al₂O₃ in the experimental media during the adsorption experiments and the results reveal an iron and alumina content below the detection limit of the equipment (1 ppb). This content confirms the SPION and γ -Al₂O₃ stability in all the performed experiments. The instrumental average uncertainty of metal ions determination was in all cases lower than 2 %. Equipment description is specified in Table 2.2.

Table 2.2 ICP-MS equipment description

Equipment	ICP-MS
Model	VG Plasma Quad ExCell and XSeries 2
Company and country	Thermo Scientifics, UK
Laboratory	Centre Grup de Tècniques de Separació en Química, GTS (UAB, Barcelona, Spain)
Image	

2.2.4. USB microscope

USB microscope was applied for characterize the general morphology of the blank sponge, sponge loaded with SPION, sponge loaded with SPION as adsorbent for the arsenic adsorption. The auto focus USB microscope-UM05 can observe objects by automatically or manual zoom. The auto focus can be achieved by PC software or manually press the machine buttons. The delicate UM05 applies the self-developed application software, and deliver 2M pixels live image to PC by motion JPGE mode,

the data is delivered fast without image distortion. User put UM05 over the observed object, can choose single or continuous auto focus as well as manually turning the clear focus, so that to control the observable subject. Equipment description is specified in Table 2.3


Table 2.3 USB microscope equipment description

Equipment	USB microscope
Models	UM05
Company and Country	VITINY Co. USA
Laboratory of analysis	Servei de microscopía (UAB, Barcelona, Spain).
Image	

2.2.5. Scanning Electron Microscopy

SEM technique was employed to study the morphology of the adsorbent systems surface in the case of Forager Sponge loaded SPION, γ -Al₂O₃ nanospheres. The SEM equipment (SEM ZEISS EVO® MA 10, Oberkochen, Germany) is a powerful tool which was used to analyze the morphological structure of the adsorbent materials. Equipment description is specified in Table 2.3


Table 2.3 SEM equipment description

Equipment	SEM
Models	Zeiss EVA MA 10
Company and Country	Carl Zeiss Microscopy, Germany
Laboratory of analysis	Servei de microscopía (UAB, Barcelona, Spain).
Image	

2.2.6. Transmission Electron Microscopy, TEM

TEM technique was employed to characterize the morphology of the SPION and their particle size distribution. For non-soluble nanocomposites (Forager® Sponge), samples were embedded in an epoxy resin and cross-sectioned with a Leica EM UC6 ultramicrotome using a 35°diamond knife form Diatome. Equipment description is specified in Table 2.4

Table 2.4 TEM equipment description

Equipment	TEM
Model	JEOL FEG-TEM 2100F
Company and Country	Jeol Ltd., Japan
Laboratory of analysis	Servei de microscopía (UAB, Barcelona, Spain)
Image	

We have synthesized the SPION for 5 times. And Each time, prepare three kinds of sample, including 1/100, 1/250, 1/1000(0.1mL SPION on 10mL TMAOH, 0.1mL SPION on 25mL TMAOH, 0.1mL SPION on 100mL TMAOH). We characterized the samples by TEM to see the particle size and dispersionSPION are highly dispersible in solutions. With particle sizes of from 6-20 nm, they offer a large surface area and superparamagnetic properties.

2.2.7. Energy Dispersive X-ray Spectrometer, EDS or EDX

Coupled to SEM or TEM microscopes, EDS/EDX provides the elemental chemical composition of the samples based on the X-Rays emitted by specific atoms which have been interacted with a particular electron beam. Each atom has a unique X-Ray spectrum, thus the elemental composition can be obtained by detected radiation.

2.3. Preparation of the adsorbents

2.3.1. Synthesis of SPION

The synthesis procedure of SPION has been described elsewhere.⁸² SPION are prepared in our lab (shown in Fig 2.4) by mixing iron(II) chloride and iron(III) chloride in the presence of ammonium hydroxide¹⁶⁴. First, deoxygenated the solution of NH_4OH (0.7M) by nitrogen. Second, deoxygenated the solution of 12mL HCl (0.1M) by nitrogen and mix $\text{FeCl}_3 \cdot 6\text{H}_2\text{O}$ with it. Third, heat the NH_4OH solution at 70°C . Fourth, Add the $\text{FeCl}_3 \cdot 6\text{H}_2\text{O}$ solution into the NH_4OH solution and react for 30min. Then, Add the $\text{FeCl}_2 \cdot 4\text{H}_2\text{O}$ in the previous solution with mechanic agitation of about 3000rpm and waiting for 45min, the dark precipitate will be formed, which consists of nanoparticles of magnetite. Last, wash it by MiliQ water which has been deoxygenated and centrifuged four times(3 times for 3 min and 5000rpm, 1 time for 10 min and 4500rpm) and preserve it by 50mL 0.1M TMAOH.

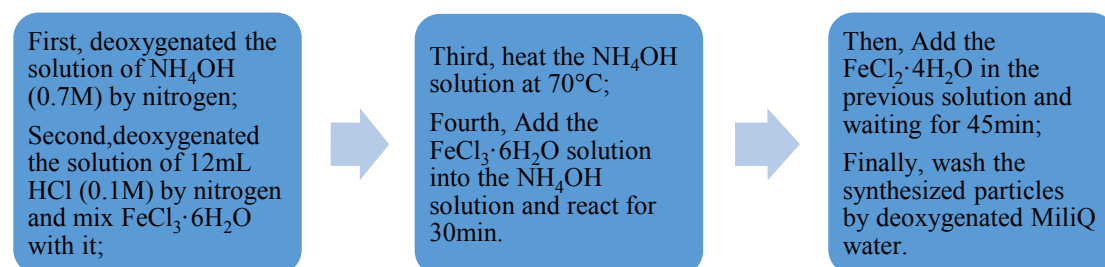


Fig 2.4 Procedure for Superparamagnetic iron oxide nanoparticles (SPION) synthesis



Fig 2.5 The synthesis of SPION procedure

The synthesis of 10 nm Superparamagnetic Iron Oxide Nanoparticles (SPION), as shows in Fig 2.4, is performed as described elsewhere with some modifications such as:

The direct addition of Fe^{2+} as salt powder and not in a mixture solution with Fe^{3+} to avoid the partial oxidation of Fe^{2+} to Fe^{3+} and a low reaction yield. A fractionated cleaning process, where the SPION synthesized is divided in different aliquots to get better cleaning.

The synthesis requires a constant bubbling of nitrogen to prevent oxidation of Fe^{2+} to Fe^{3+} and therefore, the generation of other iron oxides such as maghemite or ferrihydrite. A stock solution of Fe^{3+} in a chloride medium is prepared by dissolving $\text{FeCl}_3 \cdot 6\text{H}_2\text{O}$ in a deoxygenated HCl 0.2 M solution. A stock solution of NH_4OH 0.7 M is deoxygenated under nitrogen atmosphere and heated to 70°C . Later on, Fe^{3+} solution is added to the deoxygenated NH_4OH solution. The reaction cause a colour change in the solution and it takes brown colour. A suspension is formed (Figure 2.8). After few minutes, anhydrous FeCl_2 was added, in a ratio 1:2 of $\text{Fe}^{2+}/\text{Fe}^{3+}$, generating an immediate colour change. In this case, the suspension turns black (characteristic SPION colour, Figure 2.8b). Then, the solution is kept 45 minutes under mechanical stirring and nitrogen bubbling for the aging of nanoparticles. After sample cooling in a water bath, the

resulting suspension was centrifuged at 2000 rpm, separating the nanoparticles by a magnet and washing with deoxygenated water several times. A subsequent redispersion step of the SPION is realized.

A deoxygenated aqueous solution of tetramethylammonium hydroxide (TMAOH) 0.01 M ($\text{pH} \approx 12$) let to obtain SPION in a stable suspension for 6-8 months under deoxygenated atmosphere.

2.3.2. Synthesis of $\gamma\text{-Al}_2\text{O}_3$ nanospheres

The synthesis of nano $\gamma\text{-Al}_2\text{O}_3$ was described elsewhere.¹⁶⁵ Some details has been changed. The $\gamma\text{-Al}_2\text{O}_3$ hollow nanospheres adsorbents were readily prepared in our lab by mixing the aluminum potassium sulfate dodecahydrate ($\text{KAl}(\text{SO}_4)_2 \cdot 12\text{H}_2\text{O}$) and Urea ($\text{CO}(\text{NH}_2)_2$) in distilled water and stirred. The resulting solution was putted into a microwave vessel for heating. The pH of the resulting solution was adjusted with sodium hydroxide to 9.0. The obtained white precipitate was separated and washed by ethanol. The product was dried in the oven for 12h. Finally, the resulting form of the material synthesized ($\gamma\text{-AlOOH}$) was converted into nano- $\gamma\text{-Al}_2\text{O}_3$ by calcinating it in the muffle. We characterized the samples by scanning electron microscope (SEM ZEISS EVO@ MA 10, Oberkochen, Germany) to see the particle size and structure. The procedure for synthesis the $\gamma\text{-Al}_2\text{O}_3$ nanospheres was described as following:


1. Dissolve 4.85g of $\text{KAl}(\text{SO}_4)_2$ + 1.30g of Urea in 200mL of distilled water and stirred during 15min.
2. 35mL of the resulting solution was putted into a microwave vessel of 100mL capacity (2 vessels at the same time).
3. The solution was heated in a microwave oven during 20min at 180°C . Subsequently it was left for cooling until reaching the ambient temperature.

4. The pH of the resulting solution was adjusted with sodium hydroxide (NaOH) to 9.0. The initial pH was 7.21, and it was adjusted to a final pH of 8.99.
5. The obtained white precipitate was separated and washed (using a centrifuge) 2 times with hot water and 2 times with ethanol.
6. The product was dried in the oven for 12h at 80°C.
7. To convert the resulting form of the material synthesized (γ -AlOOH) into nano γ -Al₂O₃ the product was calcinated in the muffle at 600°C during 2 hours.

2.3.3. Forager sponge pretreatment

The Forager sponge was grinded from cubic to be small pieces by using the Coffee grinder, as shown in Table 2.5

Table 2.5 Coffee grinder description

Equipment	Coffee grinder
Model	MO-3250
Company and country	Sonifer, Murcia, Spain
Laboratory of analysis	Centre Grup de Tecniques de Separacio en Quimica, GTS(UAB, Barcelona, Spain)
Image	

The Forager sponge should be pretreated. An initial conditioning of the sponge consisting on the conversion into its acidic form by consecutive treatment with 1.0mol/L HCl, double distilled water, and HCl solution at pH 2.5 was carried out in a glass preparative column. A portion of this conditioned sponge was separated, dried during 24 h, and stored in a desiccator for its use. The procedure for treating the sponge is described as following:

1. Weight 4g of sponge(small pieces). Add 40mL MiliQ water.
2. Shake it and centrifuge it in the speed of 3500rpm for 4min.
3. Remove the water and then put 40mL 1.0M HCl and agitate it for 10min.
4. Wash with MiliQ water for 4 times(40mL water, 3500rpm, 4min) until the pH=4(use the color paper- the pH acido to see if it is pH=4).
5. When pH=4, put off the water, and put 30mL pH=2.5 HCl to add into the sponge bottle. Shake it and centrifuge it in the speed of 3500 rpm for 2 mins.
6. Remove the HCl and put 40mL miliQ water to wash the HCl and shake it, centrifuge it in 3500 rpm for 4mins.
7. Remove the water and filter it and dry it.
8. Place it in the oven under the temperature 40°C for 24h.

2.3.4. Loading of SPION on the sponge

The sponge was loaded with SPION or γ -Al₂O₃ nanospheres by using the nebulizer and peristaltic pump as shown in Fig 2.6. The SPION-loaded sponge (shown in Fig 2.7) and was dried during 24 h, and stored in a desiccator for its use. The SPION loading capacity was 0.095 ± 0.003 mmol Fe/ g sponge.



Figure 2.6 Loading of SPION into the Sponge



Figure 2.7 Sponge and SPION loaded sponge

2.4. Experiments

2.4.1. Batch experiment

2.4.1.1. Batch experiment for Arsenic removal


The batch adsorption experiments for the removal of arsenic oxyanions from aqueous solution by using sponge loaded with SPION as adsorbent were carried out under both batch operation mode and column continuous mode under both 70°C and 20°C separately. For the arsenic adsorption batch experiment, the 0.050g of adsorbent (sponge loaded with SPION) was accurately weighted in 50mL plastic extraction tubes, and 25mL of the corresponding arsenic aqueous solution was added, the As (V), As (III) and As(V)/As(III) mixture was mixing in 0.2M acetic/acetate buffer media.

2.4.1.2. Batch experiment for selenium removal

The batch adsorption experiments for the removal of selenium oxyanions from aqueous solution by using γ -Al₂O₃ nanosphere adsorbent were carried out under both 70°C and 20°C. The 0.005g of adsorbent was accurately weighted in 50mL plastic extraction tubes, and 25mL of the corresponding selenium aqueous solution was added, the As (V), As(III) and As(V)/As(III) mixture was mixing in 0.2M acetic/acetate buffer media.

The system was properly shaken on a rotary shaker (as shown in Table 2.6) at 25rpm for the proper time period. The pH of the solutions was controlled using 1.0M HNO₃ or 1.0M NaOH standardized solutions and confirmed with pH measurements (pH meter, Crison). After that, the two phases were separated firstly by centrifuge and then the supernatant was filtered through 0.22 μ m Millipore filters (Millex-GS, Millipore, Ireland). Finally, after the filtration step, the arsenic or selenium concentration in the remaining aqueous supernatant was determined by UV or ICP-MS, as indicated previously.

Table 2.6 Rotary shaker description

Equipment	Rotary shaker
Model	CE 2000 ABT-4
Company and Country	SBS Instruments SA, Barcelona, Spain
Laboratory of analysis	Centre Grup de Tècniques de Separació en Química, GTS (UAB, Barcelona, Spain)
Image	

The adsorption capacity (q , mmol/g) is determined measuring the initial (C_i , mmol/l) and final (C_f , mmol /l) arsenic or selenium concentration for each experiment and applying the following equation:

$$q(\text{mmol/g}) = \frac{(C_i - C_f) * V}{W} \dots\dots\dots(2.2)$$

This indicate the arsenic or selenium oxyanion uptake, which is the concentration of adsorbed oxyanion per unit of mass of adsorbent (in mmol/g).

Through the following sections, specific experimental conditions are going to be described for the evaluation of each parameter in order to optimize the adsorption procedure. In this study, all the experiments were carried out in duplicate and the average values are presented.

2.4.2. Kinetic study

2.4.2.1. Kinetic study of arsenic adsorption on SPION loaded sponge

In the arsenic experimental section, for the kinetic study, the experiments were carried out by mixing 25 mL of 100 ppm of As(V) with a constant amount(0.050g) of the adsorbent system, working at room temperature (20 °C) and high temperature (70°C) under pH 3.6 (after the adsorption process) with the contact time varying in the period of 2,3,5,8,12,20,40,50,70,100min and 1,2,3,4h. At each predetermined interval of time, the aqueous and the solid phases were separated by filtration (with Millipore filters) and the concentration of oxyanions in the final aqueous solution was analyzed by UV or ICP-MS, as indicated. Experiments to determine selenium adsorption in different contact time were carried out at 2-240mins in batch conditions.

2.4.2.2. Kinetic study of selenium adsorption on γ -Al₂O₃ nanosphere

The kinetic study of selenium adsorption on γ -Al₂O₃ nanospheres were carried out by mixing 25 mL of 1 ppm of Se(IV) or Se(VI) with a constant amount(0.005g) of the γ -Al₂O₃ nanospheres, working at room temperature (20 °C) and high temperature (70°C) under pH 2.0 (after the adsorption process) with the contact time varying in the period of 1,2,4,7,10,15,20,30min and 1,2,4,6,10,15,18,24,48,72h. At each predetermined interval of time, the aqueous and the solid phases were separated by filtration (with Millipore filters) and the concentration of oxyanions in the final aqueous solution was analyzed by ICP-MS, as indicated.

2.4.2.3. Kinetic study of selenium adsorption on SPION loaded sponge

Experiments to determine selenium adsorption on SPION loaded sponge in different contact time were carried out at 2, 5, 10, 12, 20, 30, 60, 120, 360, 840, 1440mins in batch conditions. The following procedures are as same as the previous ones of selenium adsorption on γ -Al₂O₃ nanospheres.

2.4.3. pH effect on the adsorption process

2.4.3.1. pH effect on arsenic adsorption

These experiments were carried out by mixing 25 mL of 100 ppm of either As (V) or As(III) with a constant amount of the adsorbent system(50mg) at both 70°C and 20°C during 1h for arsenic and 6h for selenium. A pH range 2.0-11.0 (pH values after the adsorption process) was studied in order to identify the optimum adsorption pH. The pH was adjusted by using 0.1mol/L NaOH and 0.1mol/L HNO₃ solutions, alternatively.

2.4.3.2. pH effect on selenium adsorption

These experiments were carried out by mixing 25 mL of 1ppm of either Se (IV) or Se(VI) with a constant amount of the adsorbent system(5mg) at both 70°C and 20°C during 1h for arsenic and 6h for selenium. A pH range 2.0-11.0 (pH values after the adsorption process) was studied in order to identify the optimum adsorption pH. The pH was adjusted by using 0.1mol/L NaOH and 0.1mol/L HNO₃ solutions, alternatively.

2.4.4. Effect of initial concentration on adsorption process

The successful representation of the dynamic sorption separation of solute from solution onto adsorbent depends upon a good description of equilibrium separation between two phases¹⁶⁶. Different isotherms¹⁶⁷ have been used to describe sorption equilibrium for the uptake of As (V) and Se (VI) species on the solid surface of sponge loaded with SPION and γ -Al₂O₃ nanospheres, respectively. Langmuir and Freundlich isotherms were being used for the present experimental work.

2.4.4.1. Effect of arsenic initial concentration on adsorption capacity of the SPION loaded sponge

Experiments to determine arsenic adsorption capacity in different initial concentration were carried out at 1-100ppm in batch conditions under 20°C and 70°C. While the experiments to determine selenium adsorption capacity in different initial concentration were carried out at 1, 5, 10, 25, 50, 100 ppm. The other parameters are kept to be constant, such as pH (3.6), adsorbent dosage for arsenic (0.050g), contact time for arsenic (1h) and aqueous solution volume (25mL).

2.4.4.2. Effect of initial selenium concentration on adsorption capacity of γ - Al_2O_3 nanosphere

Experiments to determine selenium adsorption capacity in different initial concentration were carried out at 2-100ppm in batch conditions under 20°C and 70°C. While the experiments to determine selenium adsorption capacity in different initial concentration were carried out at 2, 4, 5, 10, 20, 40, 50, 100 ppm. The other parameters are kept to be constant, such as pH (2), adsorbent dosage for selenium (0.005g), contact time for selenium (6h) and aqueous solution volume (25mL).

2.4.5. Effect of temperature

2.4.5.1. Effect of temperature on Arsenic adsorption

Experiments to determine arsenic adsorption in different temperatures were carried out at temperature 20°C and 70°C in batch conditions by using tightly plastic tubes containing weighted amounts of SPION-loaded sponges and measured volumes of arsenate solutions in the range 1-100 ppm As (V) at a given pH. Corresponding agitation was carried out in a rotary rack shaker during 1 h (this contact time was confirmed in separate experiments). In addition, experiments were carried out at temperature 10°C, 20°C and 70°C in continuous conditions

2.4.5.2. Effect of temperature on Selenium adsorption

Experiments to determine selenium adsorption in different temperatures were carried out at temperature 20°C and 70°C in batch conditions by using tightly plastic tubes containing weighted amounts of γ - Al_2O_3 nanosphere and measured volumes of selenate and selenite solutions in the range 2-100 ppm Se(IV) and Se(VI) at a given pH 2.0. Corresponding agitation was carried out in a rotary rack shaker during 1 h (this contact time was

Experiments to determine the whether Fe was lost during As(V) adsorption process were carried out with 500ppm and 1000 ppm As(V) solutions (13.3 mmol/L) prepared in a medium containing 0.1 mL SPION under the pH=3.6 condition. Experiments were repeated for the different conditions a minimum of two times.

2.4.6. Continuous adsorption-desorption experiment

Adsorption experiments in continuous mode were performed to observe the behavior of the adsorbent system under more practical working conditions in order to assess a future application of these systems. For this reason, columns are employed.

2.4.6.1. Arsenic continuous mode experiment

Experiments in continuous mode were performed for As(V), As(III) and As(V)/As(III) mixture adsorption studies with 1g and 4g of sponge loaded with SPION. The size of the column is 20x1.5 cm. 1L of 250ppm As(V) or 250ppm As(III) or mixture solution were pumped through the column with a certain flow rate of 2.5ml/min and eluted solution was sampled periodically. The 50mL of eluted solution was collected by each plastic tubes (50mL).

After the experiment, the aliquot was centrifuged and decantation with external magnet. Arsenic and iron content in the obtained supernatant were determined by ICP-MS. The

procedure for the adsorption and desorption experiments which are performed in columns, in continuous mode by gravity was described as follows:

First of all, 1g of SPION loaded Sponge is placed into the column (as shown in Fig 2.7). For the adsorption experiment, the 250ppm As (V), 250ppm As(III) and 125ppm As(V)/125ppm As(III) mixture were passed through the column by using a peristaltic pump with a speed of 2.5mL/min. The elution samples are collected into a 50mL Falcon tube which are labelled and stored for analysis.



Figure2.7 Column continuous mode experimental set-up for As or Se adsorption

Desorption experiments were performed like the absorption processes while the working condition changed to be 70°C. The desorption process was also performed by passing solution through the column which was filled of Tin. After the desorption process, NaOH 0.05M was used to wash the column.

2.4.6.2. Selenium column experiment

Experiments in continuous mode were performed for selenate mixture adsorption studies with 1g of SPION loaded sponge. The size of the column is 20x1.5 cm. 1L of 250ppm Se(VI) was pumped through the column with a certain flow rate of 2.5ml/min

and eluted solution was sampled periodically. The 50mL of eluted solution was collected by each plastic tubes (50mL). The following procedure was the same as those of arsenic analysis by ICP-MS.

2.4.7. Treatment of the real waste water sample.

2.4.7.1. Pre-treatment of the real waste water sample

The real waste water sample is from a river called “Rio Tinto” from Huelva, Andalucia (Spain) and was proporcioned by AGQ Mining and Bioenergy, a Spanish company.

The pretreatment of the sample is bubbled with air for 4 hours, oxidizing the Fe^{2+} to Fe^{3+} , the pH of the real waste water (originally 2.45), is changed to be 3.6 by adding NaOH. The precipitation is removed by using a filter, obtaining “iron-free” wastewater. But at the same time, the arsenic is also precipitated by iron precipitation. So the “iron-free” wastewater was doping by 60ppm arsenate solution, therefore the obtained real wastewater using for our study is wastewater simulation, which contains 60ppm arsenate, meanwhile has other ions interferences.



Fig 2.8 Procedure for pre-treatment of real waste water

After doping, the real wastewater which contains “60ppm” arsenate has been adsorbed by the resin. In fact, the initial concentration could not be 60ppm as it was doped, the

reason is that some arsenic co-precipitate with some remaining iron. After analysing by ICP-MS, the real initial concentration is 42.8ppm. The resin Lewatit S-3428 is used in the real waste water experiment with the purpose of eliminate the sulphites present in the sample, otherwise sulphites would compete with arsenic in the absorption process. The resin has to be treated before use. The pretreatment of the resin was done by consecutive treatment of HCl, double distilled water, and HCl solution at pH 4 was carried out in a glass preparative column. A portion of this conditioned resin was separated, dried during 24 h in the oven in 40°C, and stored in a desiccator for its use.

2.4.7.2. Preparation of the resin.

The resin Lewatit S-3428 was used in the real waste water experiment with the purpose of eliminate the sulphites present in the sample, otherwise sulphites would compete with arsenic in the absorption process. The resin has to be treated before use. The pretreatment of the resin was done by consecutive treatment of HCl, double distilled water, and HCl solution at pH 4 was carried out in a glass preparative column. A portion of this conditioned resin was separated, dried during 24 h in the oven under 40°C, and stored in a desiccator for its use

2.4.7.3. Absorption and desorption experiments in continuous mode for real waste water.

The same column experimental was set-up for real waste water treatment (as shown in Fig 2.8). 3g of the resin are putted into a column, real waste water sample was passed through the column with a speed of 5mL/min. All the sample is collected in the baker. After this, the sample is passed to the column containing the SPION loaded sponge in the same way as previously indicated.



Fig 2.8 Column experiment set up for real waste water treatment

Chapter III

Results and Discussion

3. Results and discussion

The current section describes the results obtained from the studies carried out in the present thesis including: 1. The removal of As(V), As(III) oxyanions from aqueous solution by using Forager sponge loaded with SPION, the adsorbent-SPION loaded sponge has been characterized by digital microscope and TEM. The parameters which have impact on the adsorption capacity including the contact time, the pH of the aqueous solution, the initial arsenic oxyanions concentration as well as temperature and redox potential were analyzed. The thermodynamic parameters, such as the equilibrium constant K , Gibb's free energy ΔG , enthalpy ΔH and entropy ΔS have been determined. The results obtained have been compared with those of Jose's work. The concept of using of temperature parameters tuning on the arsenic oxyanions adsorption-desorption has been proved. 2. Another reagent-less process which was related to redox potential adjusting for arsenic oxyanions adsorption-desorption has been developed. The combined effect which was referred to synergic thermo tuning with redox potential for arsenic oxyanions adsorption-desorption has been evaluated. The application of these reagent-less processes to the continuous column mode for the adsorption-desorption and adsorbent regeneration by taking advantage of the synergic thermo tuning of redox potential have been investigated for arsenic oxyanions removal. The treatment of real waste water by using these proved methods has been investigated. 3. The γ -Al₂O₃ nanospheres has been synthesized and characterized by SEM. The parameters which influence the adsorption capacity of selenium oxyanions including the pH, contact time and initial selenium concentration as well as temperature has been determined. The adsorption kinetics of selenium oxyanions onto the adsorbent- γ -Al₂O₃ nanospheres was modeled by using the pseudo-first order and pseudo-second order kinetic models. The equilibrium data has been correlated to the Freundlich isotherm model. The thermodynamic parameters, such as enthalpy ΔH have been calculated and compared with other results obtained in the previous literatures reported. The diethylammonium N,N-diethyldithiocarbamate (DDC) has been tried to modify the γ -Al₂O₃ nanospheres

in order to improve the adsorption capacity of the adsorbent for selenium oxyanions removal. 4. The sponge loaded with SPION has been used as adsorbent for selenium oxyanions. The sponge loaded with SPION has been characterized by SEM. The influence of pH of the aqueous solution and contact time have been examined. The adsorption kinetic studies of selenium oxyanions onto the adsorbent-sponge loaded with SPION has been done by using the pseudo-second order model. The continuous column mode for selenium oxyanions adsorption has been applied and determined.

3.1. Temperature-dependence of arsenic adsorption by Forager sponge loaded with superparamagnetic iron oxide nanoparticle (sponge-SPION)

Nowadays, there is a great concern on the study of new adsorbent materials for arsenic clean removal. However, very few studies concern with regeneration and reuse of the adsorbent. On the other hand, the present section reports the results of a new reagent-less method based on the temperature dependence of the adsorption-desorption process. Results collected are shown below and observe the following aspects:

The temperature-dependence of arsenic adsorption by sponge-SPION has been studied. The results show that under 20°C, as time goes on, the adsorption process reaches equilibrium at about 1h. Under 70°C, desorption process occurs as contact time increases, desorption equilibrium was then gradually achieved with contact time. The effect of temperature on the adsorption of As (V) was studied in the continuous column mode by evaluating the adsorption at the temperature 10°C, 20°C and 70°C. The adsorption phenomenon increases with the decrease of temperature.

The results of adsorption were fitted to the Langmuir models. Thermodynamics parameters of related ion exchange equilibrium have been evaluated including the equilibrium constant K as well as Gibbs free energy. This value shows the adsorption

process to be favorable and spontaneous. The equilibrium constant K values determined at different temperatures indicate the adsorption to increase with temperature. Accordingly, a decrease in the negative value of ΔG with the temperature increase is observed. Separation factor has very strong temperature dependence. Higher temperature leads to a lower separation. The thermodynamic affinity defined by $\log K=4.198$ and $\log K=1.023$ under 20°C and 70°C were determined, respectively. Arsenic is, thus, found to be more strongly adsorbed on the sponge -SPION under 20°C than under 70°C .

All of the experimental and theoretical studies indicate that we can use the lower temperature for adsorption and higher temperature for desorption, thereby provide a reagent-less method for recovery of the toxic element Arsenic and the regeneration of adsorbents.

3.1.1. Characterization of adsorbent material

3.1.1.1. SPION and SPION loaded sponge characterized by digital microscope

The sponge-SPION adsorbent material was characterized by digital microscope. Fig 3.1 a and Fig 3.1b show the image characterized by digital microscope, the Sponge is highly porous and elastic thereby promoting convection properties that lead to high rates for arsenic adsorption on the SPION loaded sponge. Therefore sponge is a very appropriate substrate for loading SPION and for arsenic oxyanions removal. Absorbed arsenic anions can be eluted from the Sponge by using the NaOH solution. Following elution and washing, the Sponge can be reused for the next adsorption cycle. If the regeneration is not desirable or economical, the Sponge can be compacted to a small volume to facilitate disposal.

As seen from the Fig 3.2a, b, it is clear that after loading with SPION, the sponge is saturated with SPION and the surface is very smooth. Maybe it is due to the homogenous dispersion of the nanoparticles. The porous inside the sponge are fully

filled with nanoparticles. The blank sponge can adsorb and immobilize SPION by chelation through the lone pairs of electrons on the unprotonated amine groups¹⁶⁸.

It was shown from the Fig 3.3a, b that after adsorption of Arsenic by using the sponge loaded with SPION, the sponge looks like shrinkage. In addition, the surface is not smooth anymore. Probably it's because of the anion-exchange (arsenate oxyanions occur in solution from slightly acid to basic pH) between iron oxide nanoparticles and arsenate oxyanions.

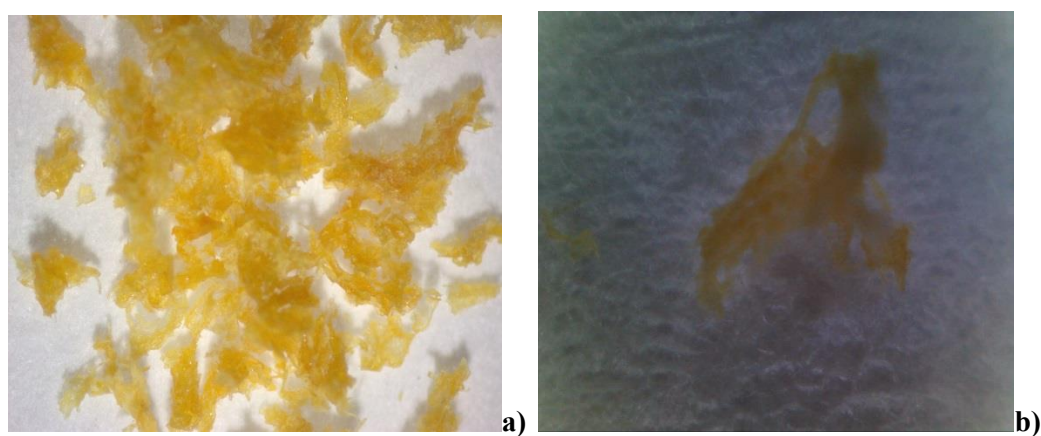


Fig 3.1 Forager sponge image by digital microscope

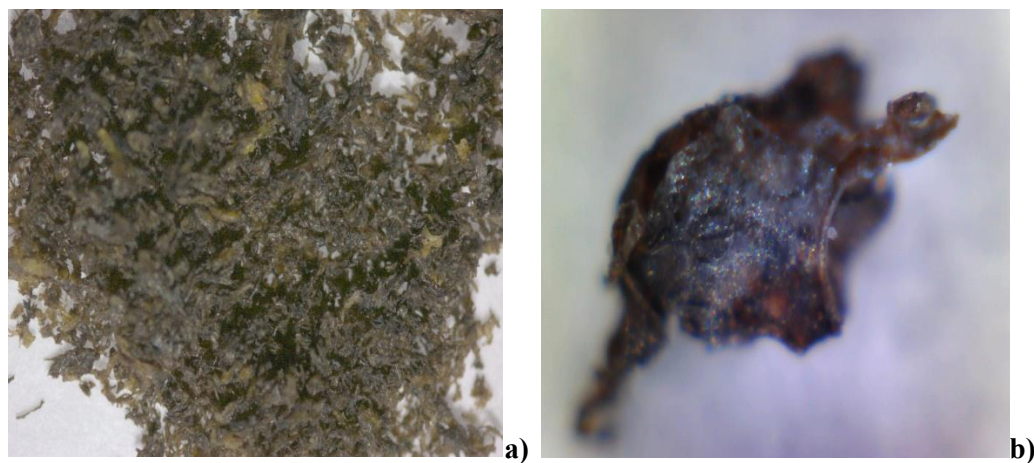


Fig 3.2 Sponge loaded with SPION (before adsorption)

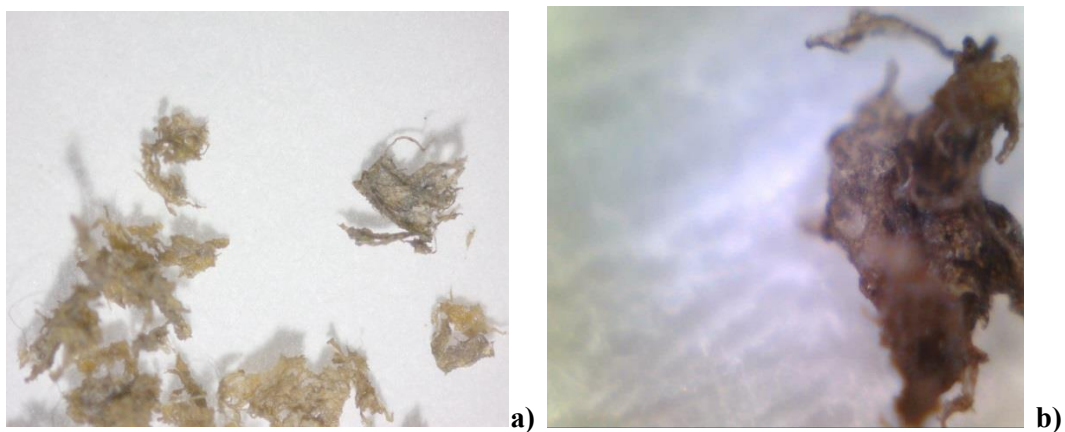


Fig 3.3 SPION Loaded sponge with arsenic (after adsorption)

3.1.1.2. SPION characterization by TEM

Before using (SPION emulsion)

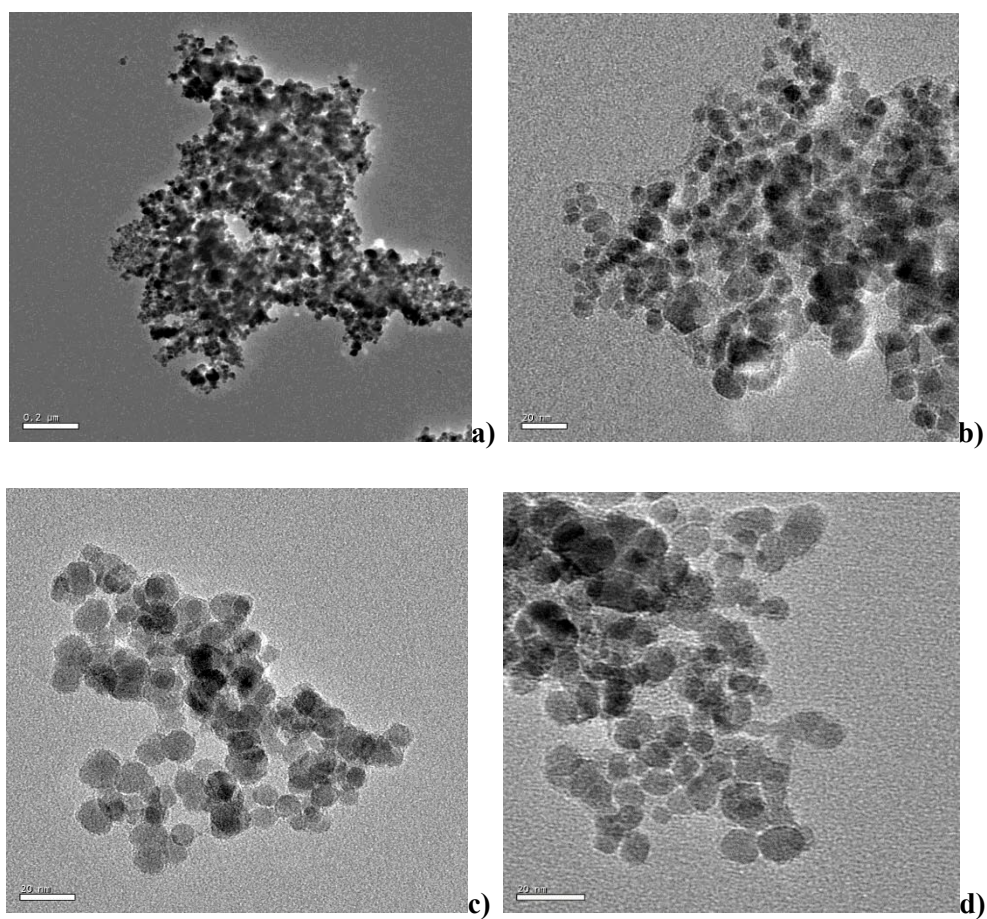


Fig 3.4 TEM micrograph of synthesized SPION

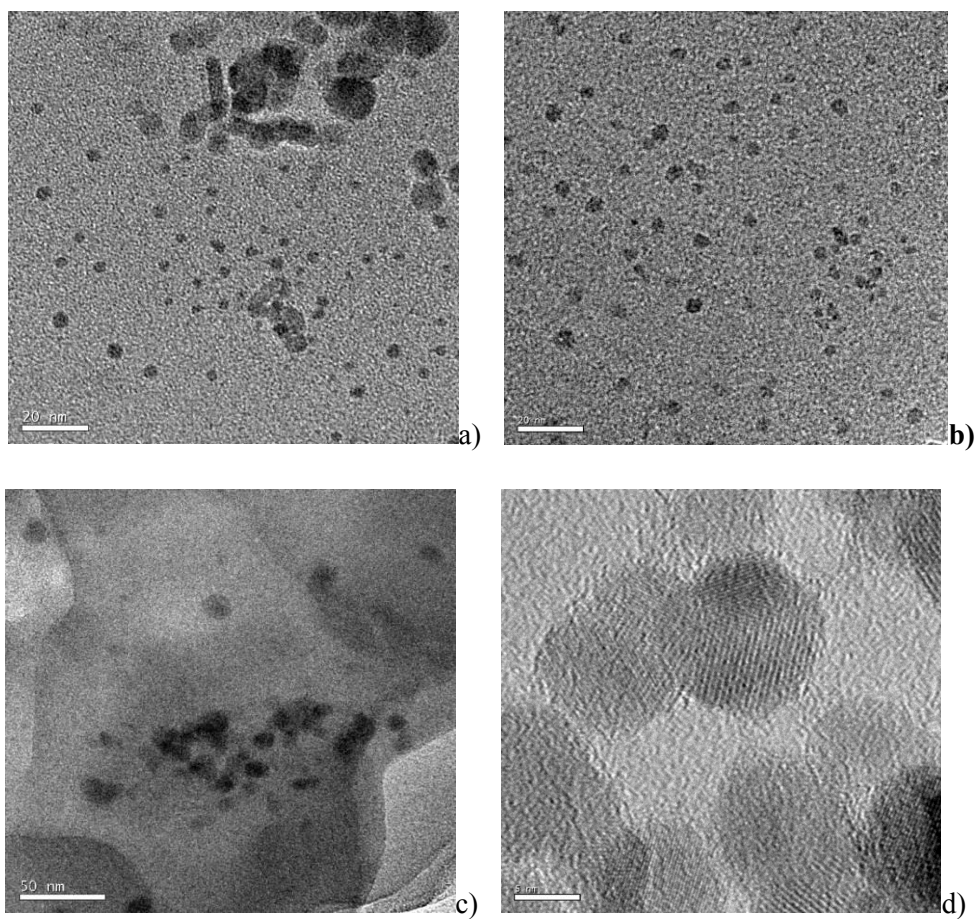
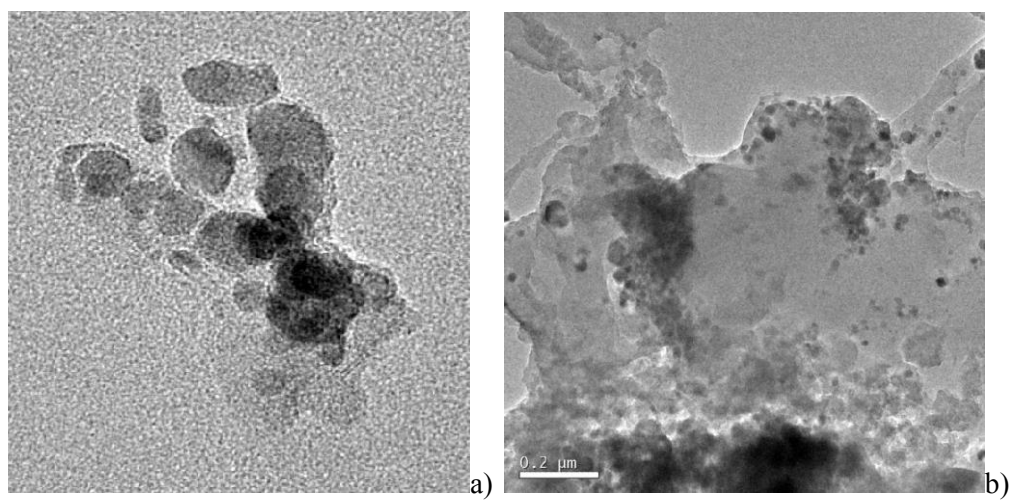


Fig 3.5 TEM image of SPION loaded on the sponge (before using)



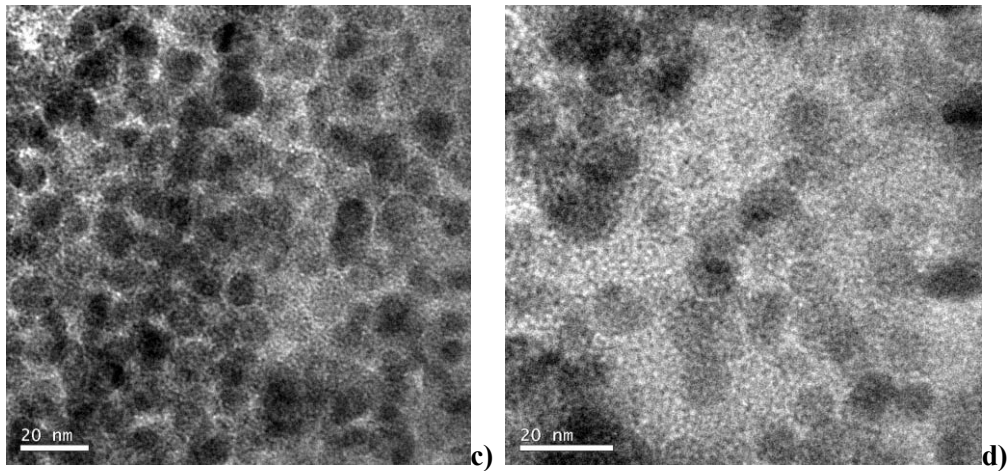


Fig 3.6 TEM image of SPION loaded on the sponge (after Arsenic adsorption)

Fig 3.4a, b, c, d show TEM images of the synthesized SPION of particles size 6-15nm. When the SPION is first synthesized and poured in the Tetramethylammonium hydroxide (TMAOH) solution and characterized by the TEM, some of the images show the nanoparticles are homogeneously distributed as single particles but other images indicate heterogeneity with agglomeration and clustering¹⁶⁹.

The using of Forager sponge³⁶ as supporting materials was undertaken to overcome the difficulties to minimize the aggregation of the SPION, the loading helps to increase the adsorption capacity. Fig 3.5a,b,c,d shows TEM images of SPION dispersed on the sponge, the particles are also ~10nm. SPION distribute on the sponge almost homogeneously, that's because during the spraying by nebulizer, there is an external force to push the nanoparticles, in addition, we use the ultra-sonication on nanoparticles suspension prior nebulization to disperse agglomerates, as it can also add an extra force to pull the liquid apart to form evacuated cavities or micro-voids.¹⁷⁰ The formation and destruction of these cavities can impose a shear force on agglomerates, capable of overcoming the van der Waals force holding them together. However, the ultrasonic applied forces are not strong enough to break the hard bonds of iron oxide molecules.

After adsorption (Fig 3.6 a, b, c, d), the SPION show a tendency to agglomerate again since the absence of external ultrasonic force for some time, makes the van der Waals force to raise affecting the distribution again.

3.1.2. Effect of contact time

The contact time with aqueous toxic element oxyanions is one of the most important parameters to be controlled for successful usage of adsorbents. The arsenic (V) aqueous system is contacted with the adsorbent (SPION loaded sponge) in the range of 2 to 100 minutes and 1 to 4 hours. The adsorption process for removing As (V) oxyanions from aqueous solution under 20°C obtain ion exchange combined with the ligand exchange equilibrium at about 1hour as shown in Fig 3.7 a, b. After that, contact time has no effect in arsenic oxyanion removal percentage. This behavior can be attributed to the effect of diffusion resistance to reach the ion exchange moieties of the adsorbent. In another hand, the most possibilities of the complexes formed in our case is, As(V) is binding to two iron nuclei as adsorbed species. Extended X-ray absorption fine structure (EXAFS)⁵⁵ and FTIR spectroscopy¹⁷¹ have shown As(V) to form bidentate inner sphere surface complexes with iron hydroxide sites as time goes on.³⁶

The effect of contact time on the desorption capacity under 70°C is shown in Fig 3.8a, b. Very high adsorption rates were achieved at the beginning because of the great number of sites available for the sorption operation. The adsorption process involves one of two types of interactions. One is anion exchange of arsenic species corresponding to the protonated amine groups present in the matrix of sponge³⁶. Another process is the ligand exchange, provided by the Fe(III) ions immobilized in the SPION as Equation 3.1 shows⁸². The adsorption process is reversible process. Suppose the reaction is exothermic process. The increase in temperature corresponds to introducing heat into the system. Le Châtelier's Principle¹⁷² states that the system will react to remove the added heat, thus the reaction must proceed in the reverse direction,

converting products back to reactants, here we see the desorption starts to occur as time goes on. Conversely if the temperature of the system were decreased, the system would react in a direction that opposed the removal of the heat. The forward reaction would thus occur to release heat in an attempt to offset the heat that was removed from the system.



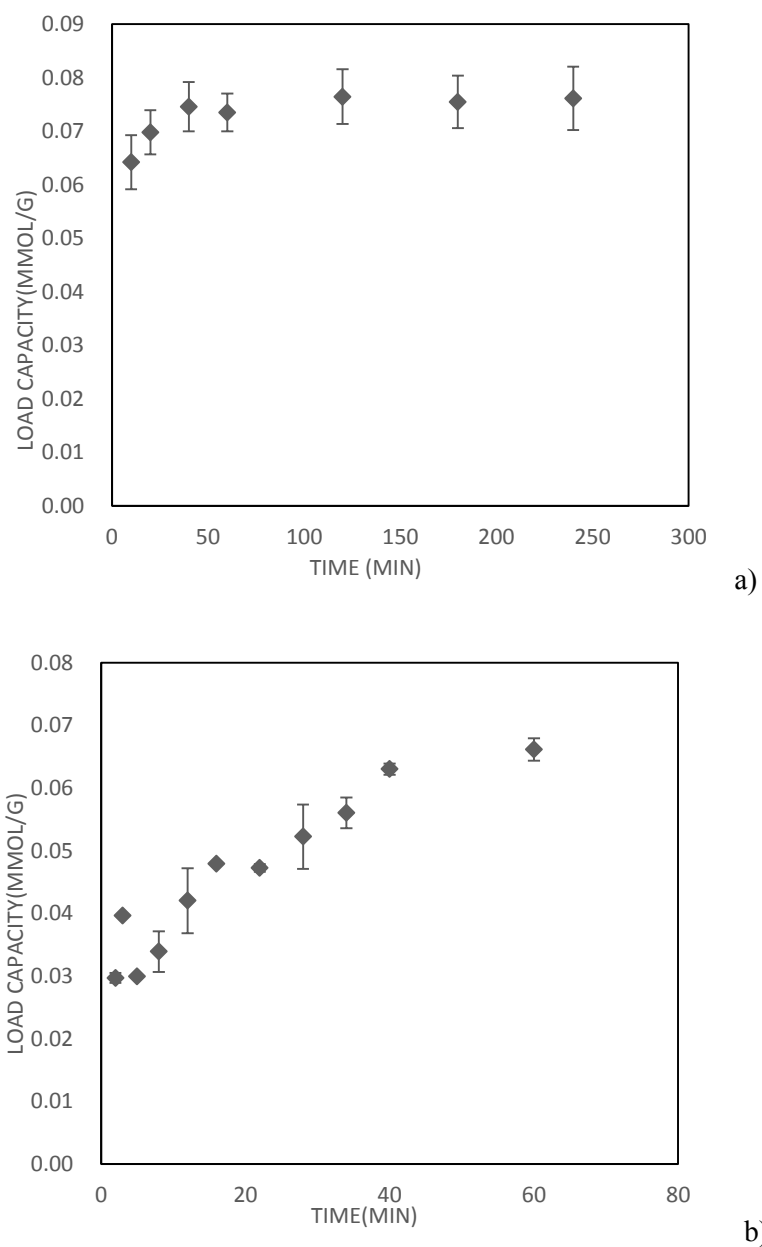
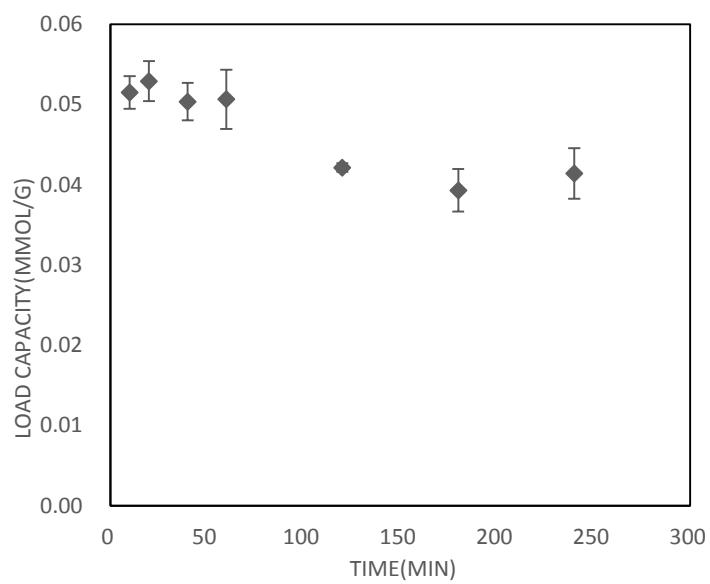
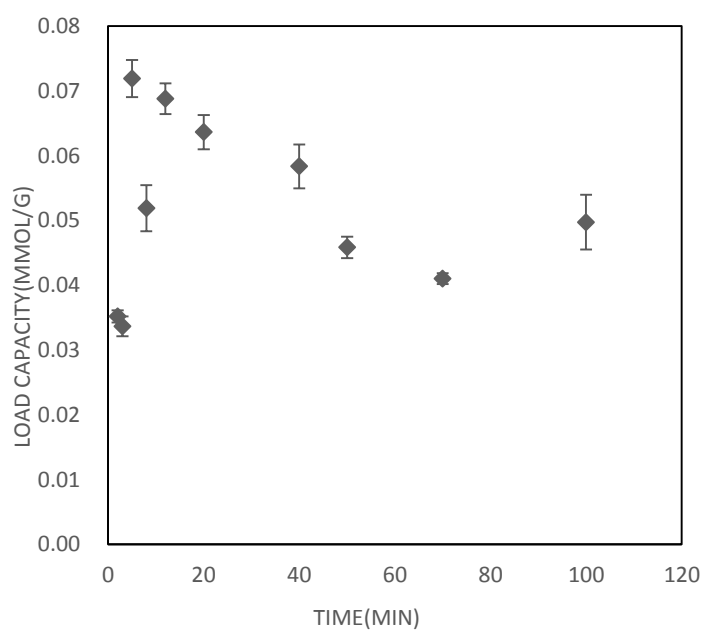


Fig 3.7. The effect of contact time on the adsorption capacity (20°C). a) from 10min to 240min, b). from 2min to 60min. The initial arsenate concentration is 50ppm, the pH is 3.6, and the adsorbent dosage is 50mg.



a)



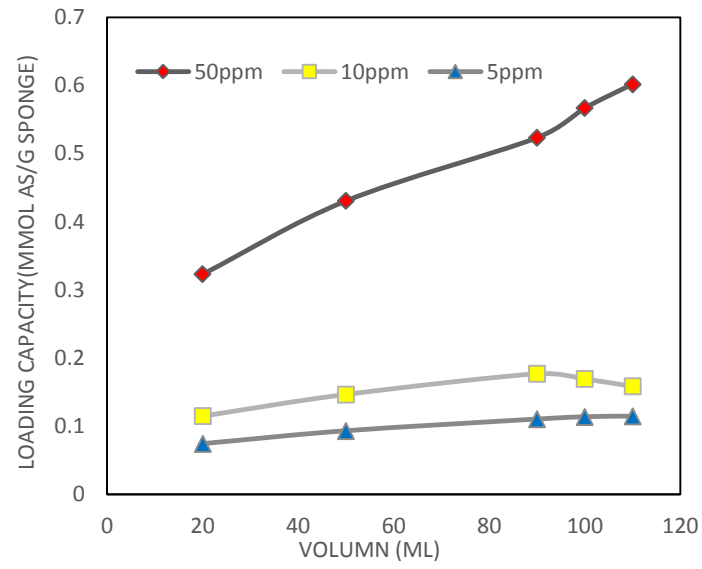
b)

Fig 3.8 The effect of contact time on the adsorption capacity (70°C). a) From 10min to 240min, b) from 2min to 60min. The initial arsenate concentration is 50ppm, the pH is 3.6, and the adsorbent dosage is 50mg.

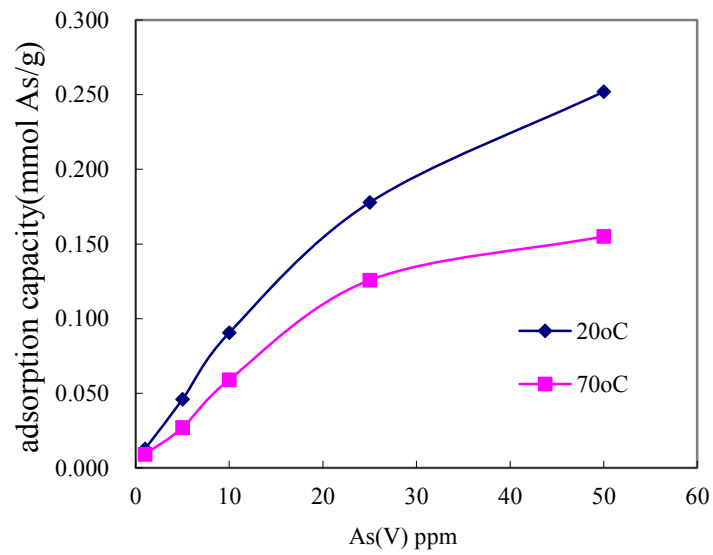
3.1.3. Effect of initial concentration

The initial arsenic oxyanion concentration in the aqueous solution is also a key parameter which affects to the driving force of the adsorption system.¹⁷³ The effects of the initial arsenic concentration (from 5ppm to 50ppm) on the adsorption capacity by the sponge loaded with SPION under 293K and 343K are shown in Fig 3.9a,b. The increase of adsorption capacity when the initial arsenic concentration increases, is due to an increase of the mass transfer driving force. Adsorption capacity limit is reached when the increase of As (V) initial concentration do not produce any further increase on the As adsorption. In this case, the surface of the sponge loaded with SPION does not have free sites for the arsenic oxyanions uptake, being fairly saturated.¹³⁶ It is probably another explanation that, as the concentration increased, a higher probability of collision between adsorbate (arsenate) and adsorbent(sponge loaded with SPION) surface happens, which could overcome the mass transfer resistance between the aqueous and the adsorbent phases.¹⁷⁴

The process of As(V) adsorption on SPION loaded sponge can occur by two different ways: one is ion-exchange on the sponge protonated amine groups, another one is As(V) are bound to iron (hydr)oxides by an inner-sphere ligand-exchange mechanism, in which the arsenic oxyanion competes with and exchanges with surface $\equiv\text{Fe}-\text{OH}$ or $\equiv\text{Fe}-\text{OH}_2^+$ groups at the iron (hydr)oxide surface.^{33, 36} The increase of adsorption with concentration is due to the diffusion process and based on the Fick first law. Normally, the ion exchange reactions are very fast compared to the diffusion of the aqueous ions to the surface moieties. When the initial concentration is higher, the arsenic oxyanions move from the solution to the surface of the adsorbent, the amount of arsenic exchanged onto the sponge and that exchanged onto the SPION increase with increasing initial As (V) concentration.



a)



b)

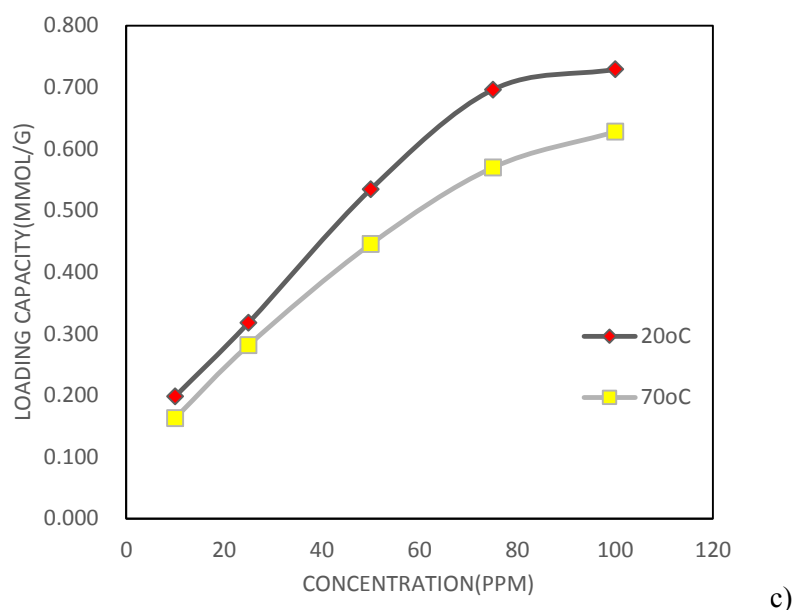


Fig 3.9 The effect of initial As(V) concentration on the adsorption capacity: a) 5ppm, 10ppm, 50ppm under 20°C, b) from 0.5ppm to 10ppm, 20°C and 70°C, c) from 10ppm to 100ppm, 20°C and 70°C

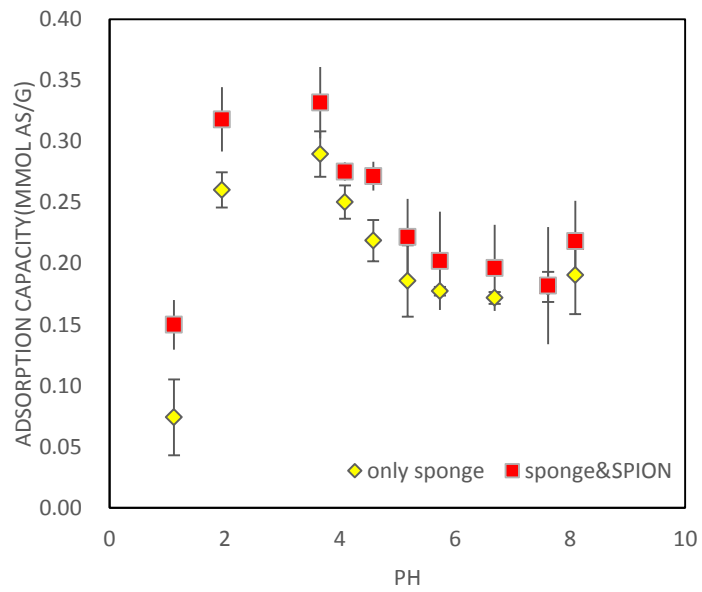
3.1.4. Effect of pH on Arsenic Adsorption Capacity

Because of the acid-base properties of arsenic oxyanions, the pH of the arsenic aqueous solution is one of the most important parameter affecting the adsorption process. The pH of the aqueous solution has both influences on the arsenic speciation and on the chemical function of the adsorbent.

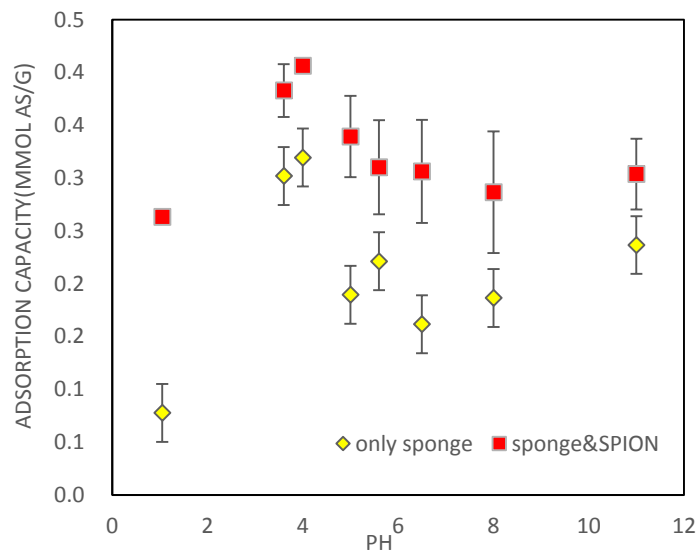
The effect of pH on the As(V) adsorption by the blank and SPION-loaded sponge under both 20°C and 70°C is shown in Fig 3.10a, b, pH ranging between 1 and 11. The results obtained revealed that the adsorption of arsenate by both blank and SPION-loaded sponge under both 20°C and 70°C are pH dependent, this can be explained by the dependence of the As (V) speciation on the pH. Comparison of the observed results of pH effect on As (V) adsorption with that of Munoz and Diego^{36, 82, 168}, it shows a similar behavior under 20°C with the adsorption of As(V) by blank sponge, Fe-loaded sponge, SPION alone and SPION-loaded sponge. The highest adsorption was observed at pH

around 3.6-4.0. Specifically, the maximum adsorption of 20°C is under pH 3.6 while the highest adsorption of 70°C is under 4.0. This similarity supports the conclusion that the arsenic species is the main reason which is responsible of the adsorption.⁸² Since the deprotonated of arsenate species ($pK_a = 2.2$) is present at pH value 3.6-4.0 in a relatively high ratio, therefore the maximum adsorption is produced at pH=3.6-4.0. For 20°C, lower pH values (1.0–2.0) and for 70°C, lower pH values (1.0-3.0), the formation of protonated arsenate species leads to a lower adsorption of arsenate species. On the other hand, for both 20°C and 70°C, at $pH > 5.0$ the observed decrease on the As (V) adsorption is due to the increase of OH^- species that compete with deprotonated arsenate for the anion exchange sites of the adsorbent.

From the Fig 3.10a, b. under both 20°C and 70°C, it confirms again that the adsorption of As (V) is enhanced by loading SPION, and supporting the indicated two ways proposed for As (V) adsorption on the SPION-loaded sponge. Thus, the ion-exchange on the protonated amine groups (present in both blank and SPION-loaded sponges) is accompanied by the additional ligand-exchange mediated by the immobilized Fe^{3+} (only present in the SPION-loaded sponge) that leads to the observed increase on the As (V) adsorption.



a)



b)

Fig 3.10 The effect of pH on the adsorption capacity, one thousand ppm As solutions and 0.10g of sponge were used in each batch experiment. a) 20°C, b) 70°C

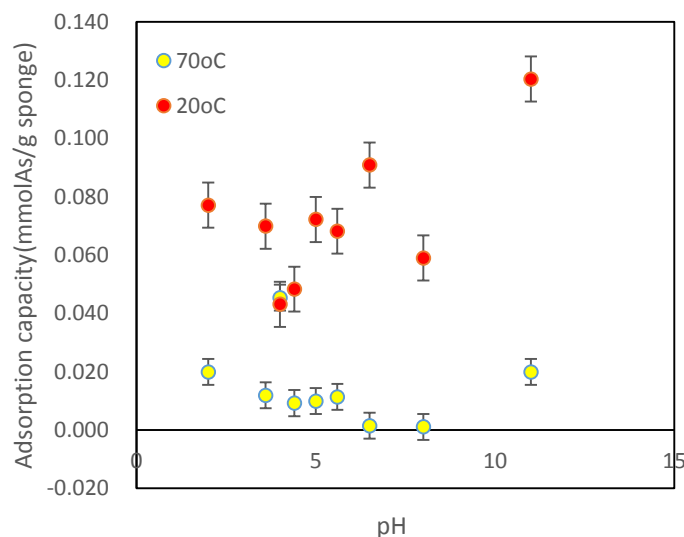


Fig 3.11. pH effect on As(III) adsorption by sponge-SPION under 20°C and 70°C

As shown in Figure 3.11, As (III) adsorption by sponge loaded with SPION at both 20°C and 70°C reveals to be independent of pH, what corresponds to the weak acidic properties of arsenious acid ($pK_{a1} = 9.2$), leading to the reduced presence of deprotonated arsenite species in the pH range of study. The higher As (III) adsorption capacity under 20°C than under 70°C may indicate the possible use of temperature to drive the adsorption/desorption process.

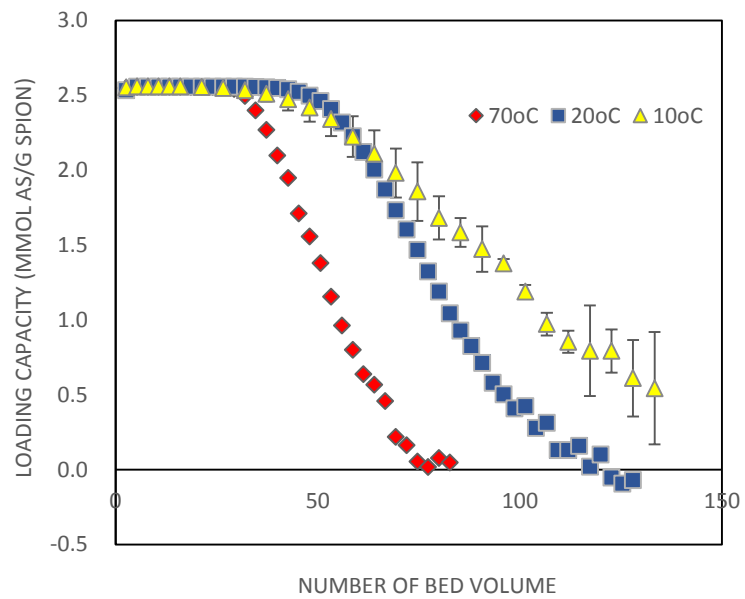
3.1.5. Effect of temperature

The effect of temperature on the adsorption of As (V) was studied in the fixed bed mode by evaluating the adsorption at the temperature 10°C, 20°C and 70°C under pH 3.6 as shown in Fig 3.12a. The observed values can be explained in terms of the thermodynamic parameters. The adsorption phenomenon is more efficient with the decrease in temperature, which indicate an exothermic process. Generally, an exothermic adsorption process signifies either physi- or chemi-sorption¹⁷⁵. The process is controlled by the adsorbate-adsorbent interaction. The breakthrough point for 10°C and 20°C is about 48 bed volume, but for 70°C, the breakthrough point is about 26 bed volume. The adsorption of arsenate onto sponge-SPION followed at three temperatures,

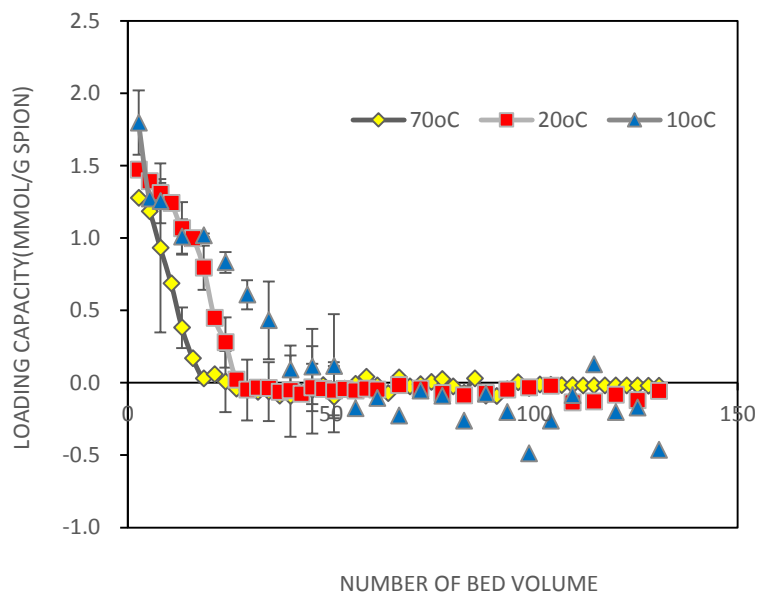
10°C, 20°C and 70°C, shows a fast arsenate uptake in all cases. The observed decrease in the adsorption capacity with an increase of the temperature from 10°C to 70°C may be due to a tendency for the arsenate oxyanions to escape from the solid phase to the bulk phase with an increase in the temperature of the solution¹⁷⁶.

The effect of temperature on the adsorption of As (V) was studied by evaluating the adsorption at the temperature 10°C, 20°C and 70°C under pH 5.6 is shown in Fig 3.12b. As indicated before, for both 20°C and 70°C, when pH is more than 5.0, the observed decrease on the As (V) adsorption is due to the increase of OH⁻ species that compete with deprotonated arsenate for the anion exchange sites of the adsorbent, which is also confirmed by the column continuous mode arsenate adsorption.

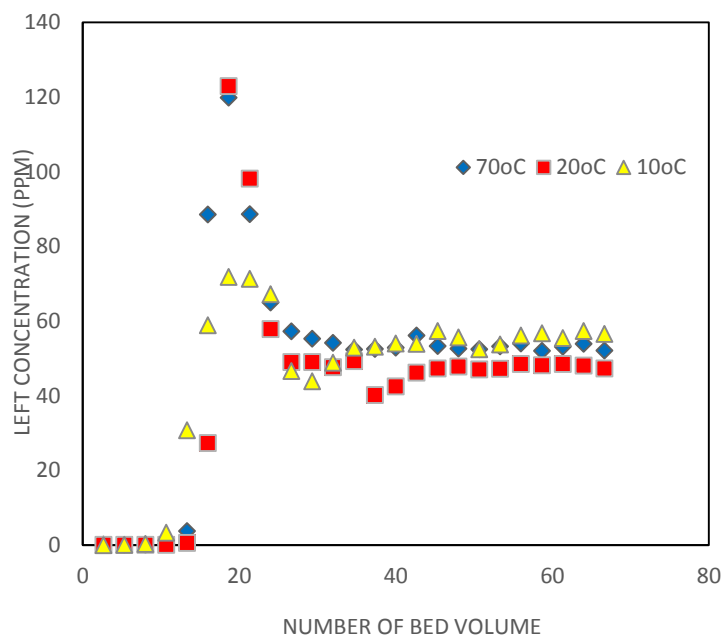
On the other hand, at pH<2.5(as shown in Fig 3.12c), iron desorbed is very significant due to protons competition, nevertheless, at pH range 3-9 iron desorption is not quite important. Thus, in this adsorption process, at the beginning of the arsenic adsorption, the iron desorbing does not have significant impact on the As (V) adsorption since the ion exchange process increases the pH value when the process begins. Then, after the continuous flow of arsenic solutions (pH 2.1) the ion exchange became saturated and then the solution in column became acidic producing iron desorption from the sponge gradually, thus leading to a decrease on the arsenic adsorption. Moreover, as the solution is under pH 2.1, the arsenic desorption occurred after previous adsorption, thus producing at the column outlet a sharp increase of arsenic concentration leading to a higher arsenic concentration than in the initial column incoming solution. The final drop of the As(V) concentration at the column outlet is due to the readsorption of part of the As(V) in column at the empty sites left by the previous As(V) release and thus will reach the value of the input solution.



a)



b)

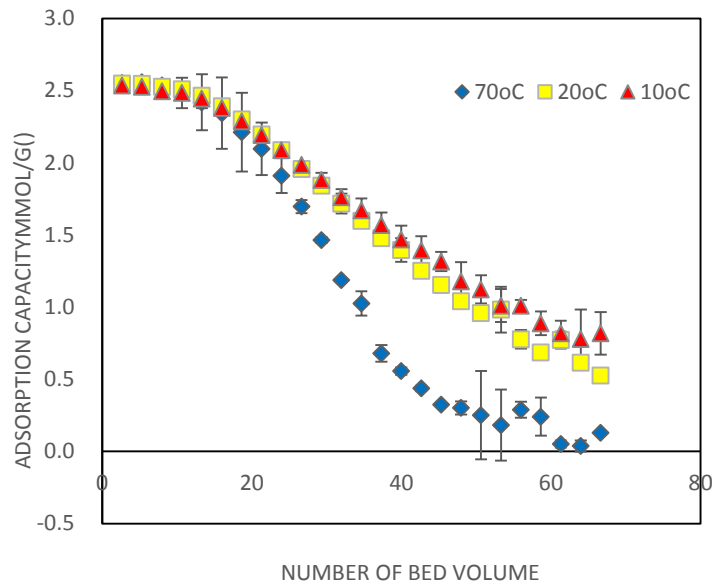


c)

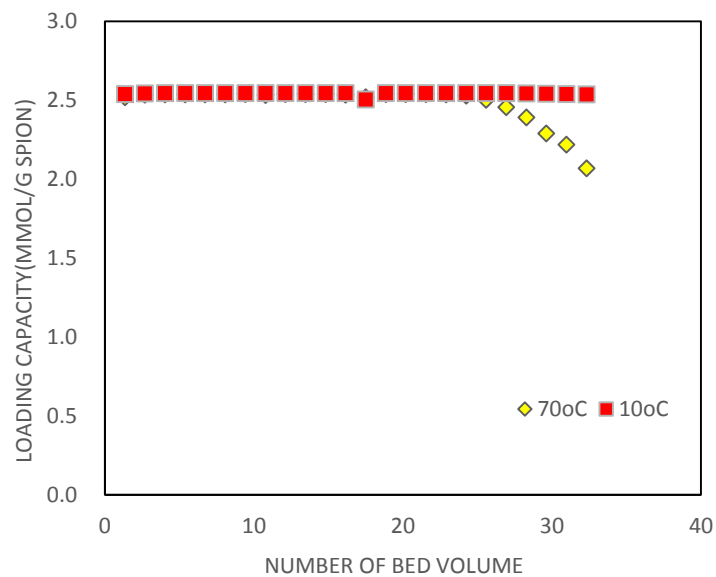
Fig 3.12 The effect of temperature on the adsorption capacity (70°C, 20°C, 10°C).a) pH=3.6, b) pH=5.6, c) pH=2.1

3.1.6.The effect of bed volume

The influences of the height of the sponge bed on the adsorption capacity are shown in Fig 3.13a, b. More adsorbent (sponge with SPION) makes the depth of bed volume to be higher. When the As(V) solution go through the column, it has longer time to contact with the adsorbent, in addition, multiple layer of the sponge with SPION can adsorb the arsenic from the top to the bottom one.



a)



b)

Fig 3.13 The effect of bed volume (70°C, 20°C, 10°C), initial arsenic concentration 50ppm, pH=3.6 a)0.5g adsorbent, b)1.5g adsorbent

3.1.7.Adsorption isotherms

3.1.7.1. Langmuir isotherm

The experimental As (V) adsorption data have been treated to fit to Langmuir isotherm showed in Fig 3.14. Langmuir isotherm equation (3.2) fitted well to the adsorption data.

$$C/C_x = 1/KC_m + C/C_m \quad (3.2)$$

-C is the concentration of sorbate in the equilibrated solution, mmol/L

-C_x is the adsorption capacity in SPION, mmol/g

-C_m is the maximum adsorption capacity

-K_L is the Langmuir coefficients

The Langmuir coefficients K_L and C_m can be determined from the intercepts and slopes of the plots C/C_x vs C, which are linear.

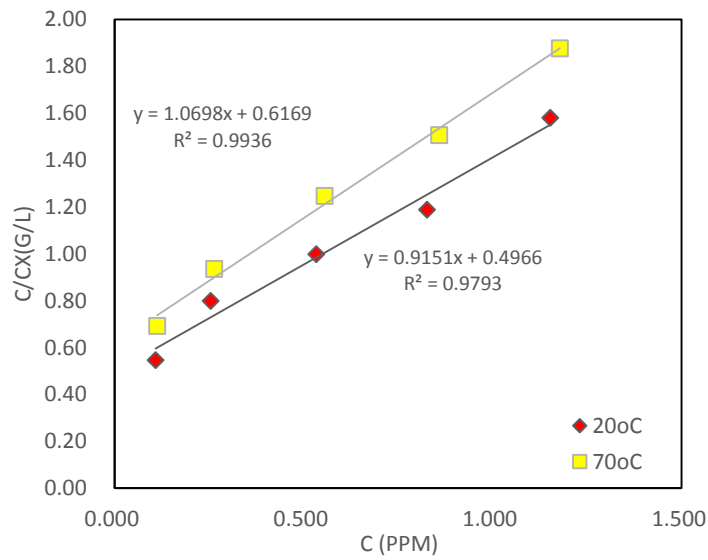


Fig 3.14 Langmuir model

The isotherm parameters for the adsorption As(V) onto the sponge with SPION at different temperatures were obtained from the Langmuir model by using the linear fitting method.

Table 3.1 The isotherm parameters for Langmuir model

T(K)	343	293
C _m (mmol/g SPION)	40.65	47.52
C _m (mmol/g sponge)	0.94	1.10
logK _L (L/mmol)	1.73	1.84
ΔG ⁰ (kJ/mol)	-9.0	-10.3
R ²	0.99	0.98

The effect of isotherm shape can be used to predict whether an adsorption system is “favourable” or “unfavourable” both in fixed-bed systems as well as in batch processes. The essential features of the Langmuir isotherm can be expressed in terms of a dimensionless constant separation factor or equilibrium parameter K, which is defined by the following relationship:

$$K = \frac{1}{1 + K_L C_0} \quad (3.3)$$

K indicate the type of isotherm, C₀ is the initial concentration (mg/L), and K_L is the Langmuir constant.

Table 3.2 Equilibrium constants

Values of K	Type of isotherm
K>1	Unfavorable
K=1	Liner
0<K<1	Favorable
K=0	Irreversible

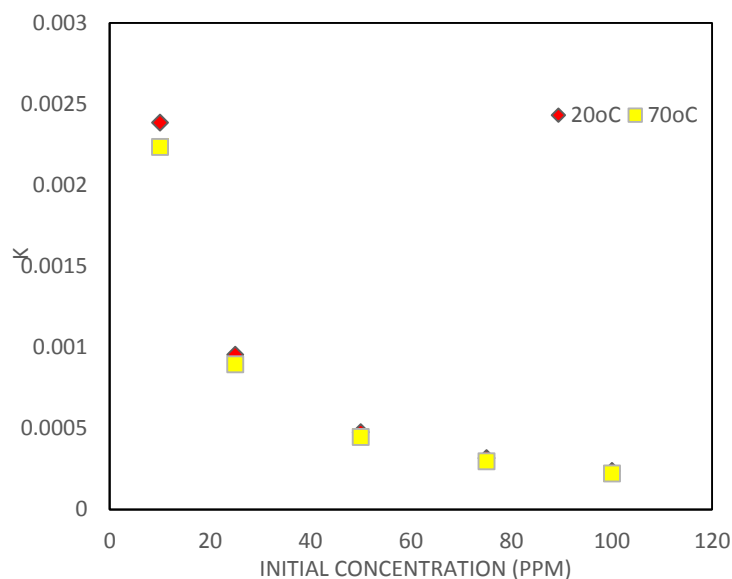
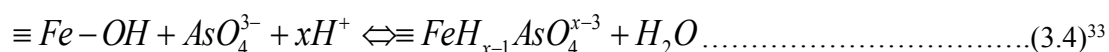


Fig 3.15 plot of K against initial arsenic concentration at two temperatures.

Fig 3.15 with a relationship between K and C_0 was presented to show the essential features of the Langmuir isotherm. The K values indicate that adsorption is more favorable for the higher initial As (V) concentration than the lower ones and also it indicate that adsorption is more favorable for the lower temperature than the higher ones.

3.1.8. Modeling of Arsenic Adsorption by a Ligand-Exchange Process.

A monodantate ligand-exchange mechanism, based on the Fe:As stoichiometry 1:1 previously discussed, is proposed for the adsorption of arsenic(V) on the SPION loaded on the sponge, as it has been considered for other iron-based materials. The corresponding reactions can be written as follows:



With an equilibrium constant

$$K = \frac{[\overline{As}]}{[\overline{Fe}][H^+]^x[As]} \dots\dots\dots(3.5)^{36}$$

Where $[\overline{As}]$ indicates the amount of arsenic species adsorbed on the SPION in the sponge (mmol/g), $[\overline{Fe}]$ indicates the amount of iron adsorbed on the sponge and not complexed with As (mmol/g), $[H^+]$ indicates the concentration of free protons in solution (mmol/g), and $[As]$ indicates the free concentrations of the corresponding AsO_4^{3-} ions in solution (mmol/g) which have been calculated from the experimental values of total arsenic concentration.

From equation, defining Y (g/mmol) as

$$Y = \frac{[\overline{As}]}{[\overline{Fe}][As]} \dots\dots\dots(3.6)$$

Then

$$\log Y = \log K - xpH \dots\dots\dots(3.7)$$

Y value at a given pH is estimated from the experimental data of arsenic adsorption by considering the formation of monodentate⁵⁵ Fe-As complexes on the sponge. $[\overline{As}]$ is calculated from the differences in adsorption capacity between the SPION loaded and the blank sponge at each pH. $[\overline{Fe}]$ is calculated by subtracting the arsenic adsorption capacity and the iron desorbed from the initial amount of Fe(III) in the SPION-loaded sponge. $[As]$ in solution is determined as indicated in the experimental part.

A plot of logY vs pH for As(V) is given in Fig 3.16. The values of x and logK obtained by the least squares fit are shown in Table 3.3. The model indicates that $H_2AsO_4^-$ are

the As(V) chemical forms adsorbed on the SPION loaded in the sponge in the pH range studied.

When reaction is expressed as a function of the adsorbed species, the stability of the complexes can be accurately evaluated:

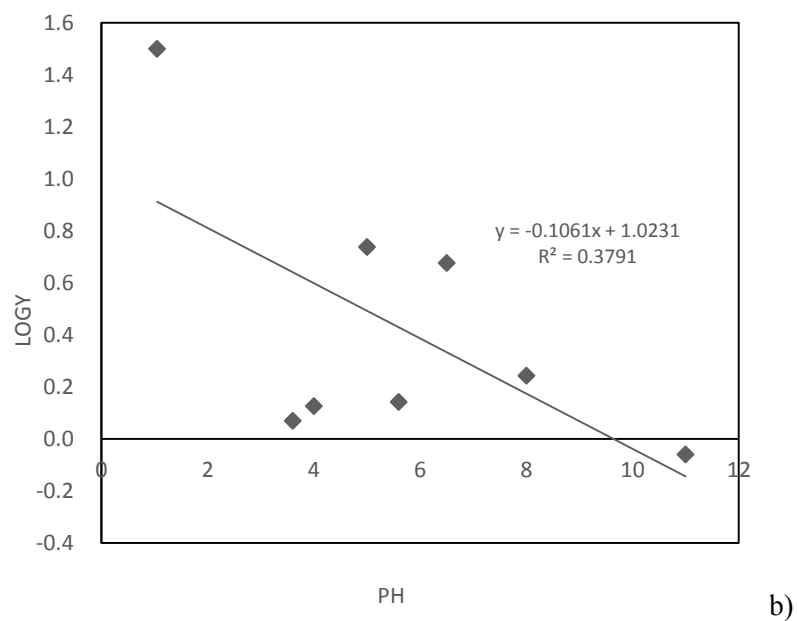
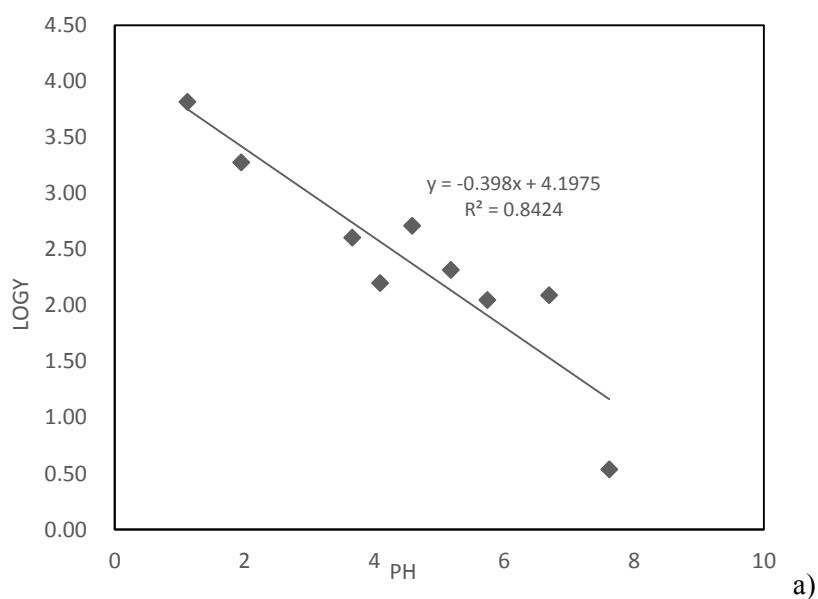
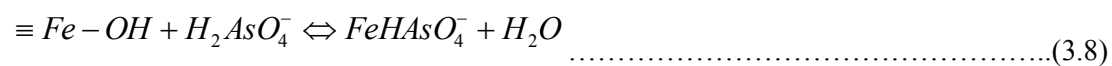


Fig 3.16 Modeling of arsenic species adsorption on the SPION-loaded in the sponge: linear relationship between log Y and pH for As (V).a) 20°C, b) 70°C

Table 3.3 Calculated Results from Fe-As Interaction Modeling Process Indicating the x and logK Values by the Least-Squares Fit¹⁷⁷

	pH range	X	logK	R ²
20°C	1-8	0.40	4.20	0.84
70°C	1-11	0.10	1.02	0.38

As would be expected, As (V) adsorption on immobilized SPION is preferred under 20°C against that the adsorption performed under 70°C. Reversibility of both process has already been proved by corresponding arsenic desorption from the SPION-loaded sponge under 70°C. It also has proved the concept that the adsorption-desorption process could be controlled by changing the temperature. The regeneration and reusing of the adsorbent-SPION loaded sponge will be possible after desorption. Alternatively, the sponge (which is an inexpensive material) could be compacted into an extremely small volume and disposed as a hazardous waste.³⁶

3.1.9. Thermodynamics Studies

The Gibb's free energy change is calculated using K_L obtained from Langmuir model and showed in Table 3.1. The equations are:

$$\Delta G^0 = -RT \ln K_L \dots \dots \dots (3.9)$$

and

$$\Delta G^0 = \Delta H^0 - T \Delta S^0 \dots \dots \dots (3.10)$$

where R is universal gas constant ($8.314 \text{ J mol}^{-1} \text{ K}^{-1}$) and T is the absolute temperature in K.

The negative values of Gibb's free energy ΔG (-9.0 kJ/mol under 70°C and -10.3 KJ/mol under 20°C) confirmed the feasibility of the process and the spontaneous nature of adsorption with a high preference of As(V) by Forager sponge with SPION. The decrease in the negative value of ΔG with a decrease in temperature indicates that the adsorption process of As (V) on adsorbent becomes more favorable at lower temperatures. The maximum adsorption capacity for SPION loaded sponge (0.933 mmol/g in 343 K , 1.094 mmol/g in 293 K) is consequence of thermodynamic characteristics of the adsorption process by the related values of the parameters ΔG .

The enthalpy change, ΔH , and the entropy change, ΔS , for the adsorption processes were obtained from the intercept and slope of Eq. (3.9) and found to be $-122.150 \text{ kJ mol}^{-1}$ and $337 \text{ J mol}^{-1} \text{ K}^{-1}$ in the temperature interval 293 K to 343 K (assume that ΔH and ΔS is not function of T, is constant in this temperature range), respectively (shown in Table 3.4). The negative value of ΔH° indicates that the adsorption reaction is exothermic. The positive value of ΔS suggests that some structural changes occur at the adsorbent surface, and the randomness at the solid/liquid interface in the adsorption system increases during the adsorption process.

Table 3.4 Thermodynamic parameters calculated

	$\Delta G(\text{kJ mol}^{-1})$	$\Delta H(\text{kJ mol}^{-1})$	$\Delta S(\text{J mol}^{-1}\text{K}^{-1})$
293K	-23.54	-122.15	337.00
343K	-6.72		

3.1.10. The dependence of separation factors on temperatures and bed volumes:

As indicated from the above equation 3.8, it was found that $\text{pK}_a < 0$ and the arsenic acid is a relatively strong acid and the removal of As(V) by anion-exchange is possible. As the anion exchange behavior, the equilibrium separation factor, α , expressed as follows.

$$\alpha_{H_2AsO_4^-}^{OH^-} = \frac{x_{OH^-} X_{H_2AsO_4^-}}{x_{H_2AsO_4^-} X_{OH^-}} \dots\dots\dots(3.11)$$

Where x and X are the equivalent fractions of ions under separation in adsorbent and solution phases, respectively.

Table 3.5 separation factors

	separation factor	
Bed volume	70°C	20°C
5	481.8	3061.2
8	545.8	11907.6
11	521.8	17861.9

13	529.6	26793.4
16	569.1	17861.9
19	560.1	107176.5
21	664.7	107176.5
24	625.8	21434.5
27	461.0	26793.4
29	141.1	8930.5
32	38.5	4121.2
35	14.9	1622.9
37	7.8	652.5
40	4.5	288.7
43	3.2	143.1
45	2.0	74.5
48	1.6	42.2
51	1.2	25.4
53	0.8	16.2
56	0.6	9.7
59	0.5	6.7
61	0.3	4.9
64	0.3	3.6
67	0.2	2.7
69	0.1	2.1

72	0.1	1.7
75	0.0	1.3
77	0.0	1.1
80	0.0	0.9
83	0.0	0.7

As can be seen from Table 3.5 that the separation factor has very strong temperature dependence. Higher temperature leads to lower separation. The capacity of anion exchange is very strongly at the beginning and meanwhile, increasing gradually as the bed volume increases until the point of 21 bed volume.

Table 3.6 Comparison of the result with Jose Munoz's work³⁶

	Fe loading capacity(mmol Fe/g sponge)	Maximum adsorption capacity(mmol As/g sponge)	maximum adsorption capacity(mmol As/mmol Fe)
Fe with sponge	0.3 ± 0.01	1.8	7.3
SPION with sponge	0.1 ± 0.003	1.1	11.5

The observed differences on Table 3.6 can be explained that the Fe (III) loaded adsorption capacity is mainly due to the acid groups in the sponge. But the better adsorption capacity of SPION loaded sponge is because of not only the acid groups but also the good properties of SPION which has a high surface-volume ratio. The nanostructure of the SPION make the adsorbent has big surface area, which has more free sites for the adsorption. The reactivity of the adsorption process are more quickly and adsorption are more efficiently.

3.2. Application of Synergic thermo-tuning of redox potential for clean removal of Arsenic

In the previous section, results including Arsenic adsorption-desorption and adsorbent regeneration by controlling the temperature have been described. Previous experimental and theoretical studies indicate that we can use the lower temperature for adsorption and higher temperature for desorption, thereby provide a new method for recovery of toxic element and regeneration of adsorbents

This section will provide results to demonstrate the concept of tuning redox potential to achieve the adsorption-desorption and adsorbent regeneration. Then the application of synergic thermo-tuning of redox potential for removal of arsenic oxyanions has been studied. The present part relates to a reagent-less recycled method for arsenic oxyanions removal from wastewater and provide and added value to the water decontamination process. Thus, the new method for Arsenic adsorption/desorption and sorbent regeneration with no reagents added by taking advantage of the synergic thermo tuning of redox potential of the adsorption-desorption system has been developed. Methods are based on sorption-desorption processes for the indicated oxyanions. Nanostructured materials have been implemented as adsorption substances, being iron oxides nanoparticles the active constituents. Reagent-less processes were developed by using intensive thermodynamic parameters, e.g, temperature and/or redox potential of the target solution. Appropriate tuning of these parameters will allow both process selectivity and regeneration of the adsorption material. Synergic interaction of thermo-tuning with redox variation will provide such results. Thus, this reagent-less method could not only provide reagent savings for recovering the adsorbent, but also the adsorbent recycling to be reused will contribute to a-cost efficient process.

After the investigation of temperature influence on adsorption-desorption, the redox potential effect on adsorption-desorption, adsorbent regeneration has been evaluated.

As indicated in the Methodology chapter, potassium dichromate has been used to oxidize the As (III) to As (V)(conversion rate>91%) and Zn powder or Sn foil have been used to reduce the As(V) to As(III)(conversion rate>90%). Since the adsorbent has big difference adsorption capacity between As (V) and As (III), the adsorption-desorption can be controlled by modifying the oxidation state. For example, the adsorbent can better adsorb the arsenic by oxidizing all of the As (III) to be As (V) and desorb the arsenic by reducing the As (V) to be As (III).

3.2.1. Experimental results of redox potential effect:

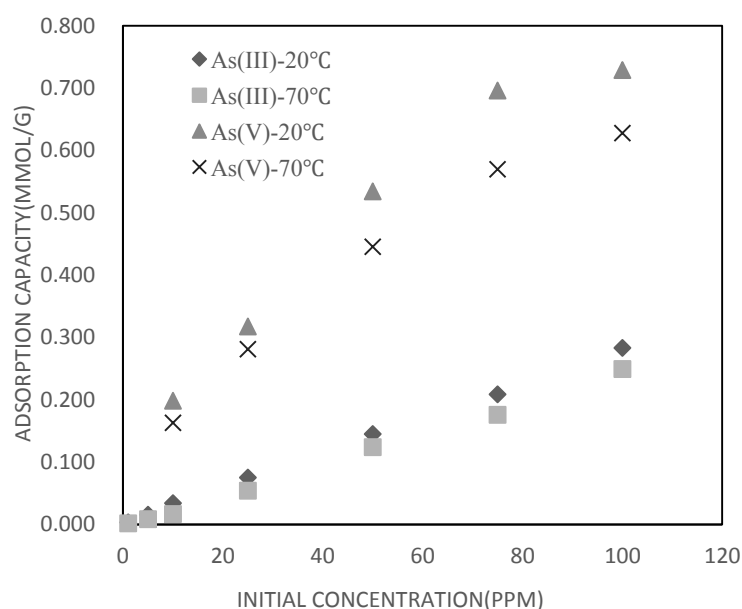


Fig 3.17 Effect of oxidation state on arsenite and arsenate adsorption, adsorbent dosage 50mg, pH=3.6, contact time 1hour, the initial concentration 1-100ppm.

Modifying the redox potential, therefore transforming between arsenite and arsenate, in order to control the adsorption-desorption is attributed to the significant difference adsorption capacity of SPION loaded sponge for As (V) and As (III), as shown in Fig 3.17. The adsorbent of SPION loaded sponge has much higher adsorption capacity for the As (V) adsorption than that for the As(III), as consequence of different acid properties of arsenate and arsenite. Many studies aiming at elucidating the structure of

arsenate complexes adsorbed on iron oxide nanoparticles have been done. Extended X-ray absorption fine structure (EXAFS)¹⁷⁸ and Fourier Transform Infrared Spectroscopy (FTIR)¹⁷¹ have shown As(V) and As(III) to form monodentate and bidentate inner sphere surface complexes with iron (hydr)oxide sites in co-precipitated and adsorbent solids.⁵⁵ In the case of As(V), the possible chemical structures which arsenate may form on the iron oxide surface upon chemical adsorption are different, such as monodentate, bidentate mononuclear, bidentate binuclear. Although there is no consensus regarding to the structure of the complex of arsenate bonding with iron oxide nanoparticles being monodentate or bidentate, Some literature reports confirmed and demonstrated that arsenic complexes were formed via the hydroxyl groups at the iron oxide surface.³³ This is a very tight bond, and once the bond is formed, removal of the arsenic is difficult. In the case of As(III) adsorption by iron (hydr)oxides, both bidentate binuclear-bridging complexes(Fe-O-As(OH)-O-Fe) and monodentate complexes have been observed.¹⁷⁹ A monodentate complex is one in which a single oxygen atom from the arsenite oxyanion coordinates a single structural Fe³⁺ at the iron (hydr)oxide surface, which is not thermodynamically stable and the bond is easy to be broken.¹⁷⁸

By changing the redox potential, the transform between As (V) and As(III) will lead the adsorption-desorption process and recycled use of the adsorbent. At the same time, the thermo tuning can help the adsorption-desorption to be much more significant and much quicker.

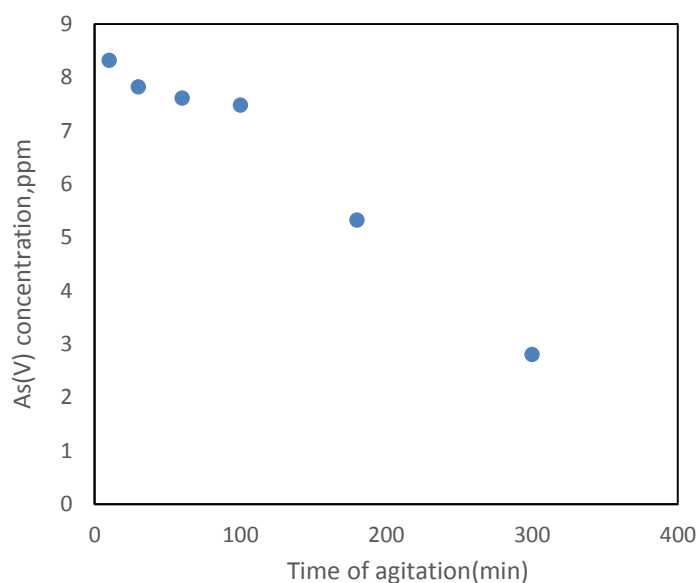


Fig 3.18 redox potential-different time-desorption

The experiment of redox potential effect on desorption has been carried under 20°C (shown in Fig 3.18). The adsorbent (sponge loaded with SPION) was used for adsorb the arsenate, which make the surface and porous of the adsorbent is full of arsenate (10.34mg arsenic/g adsorbent). Then, 50mg of Tin foil was used as the reduction reagent for desorption, and the aqueous solution pH 3.6 with the contact time from 10-300min. As time goes on, Sn could transform the arsenate to arsenite, which has weak bond to the iron oxide nanoparticles, therefore desorb from the adsorbent. That means the Tin change the redox potential, which could help to realize the desorption process. Arsenate (As(V)) react with Sn in buffered aqueous solutions to produce arsenite (As(III)).¹⁸⁰ The electron transfer reactions can be described in terms of thermodynamics through the use of standard electrode potentials.¹⁸¹

3.2.2. Further proof of redox potential part

The potassium dichromate ($K_2Cr_2O_7$) could oxidize the arsenite to arsenate by changing the solution redox potential.

Table 3.7 oxidation rate of As (III) to As(V) by potassium dichromate

Initial concentration of arsenite(ppm)	Concentration of potassium dichromate(mmol)	After oxidation, concentration of arsenate(ppm)	Conversion rate
94.9	1.3	87.2	91.9%
96.3	1.3	88.6	92.0%

Table 3.8 reduction rate of As(V) to As(III) by Zn powder

Arsenate loaded on the sponge(ppm)	After reduction, the arsenic left in the sponge(20°C)ppm	After reduction, the arsenic left in the sponge(70°C)ppm	Conversion rate
18.6	4.1	1.2	93.3%
18.9	3.8	1.8	90.4%

The oxidizing agent (potassium dichromate) could convert ~92% of arsenite to arsenate (as shown in Table 3.7). Meanwhile, the reducing reagent (Zn powder) could reduce the arsenate to arsenite (as shown in Table 3.8) by changing the redox potential, the conversion rate could be ~90%, which is very high and could help the desorption to happen. The arsenate could be much more adsorbed due to its acidity that provides high proportion of deprotonated species presents in the media at the pH of study, thus leading to a major contribution in the adsorption capacity. The sponge-SPION provide more probability to interact with arsenate and react by ligand exchange to the adsorption system. Thus arsenate has much higher adsorption rate than arsenite. By changing the redox potential, therefore transforming the arsenite to be arsenate, could help the adsorption to occur.

3.2.3. Column Experiments

Working under the optimized parameters, the maximum adsorption capacity was determined. Thus, the concept of thermodynamic effect on the adsorption-desorption process was studied in batch mode. Adsorption experiments in continuous mode were performed in order to observe the behavior of the adsorbent system in more close conditions to conventional working mode. For such purpose, a laboratory column-adsorption system, with column size of 20cmx1.5cm Ø, was implemented and employed. Aqueous solution containing arsenic oxyanions was circulated through the column and arsenic adsorption was monitored by determining its concentration at the outlet. As an example, 1L of 250ppm arsenate solution was processed through the column-adsorption system and the break-through curve was determined, yielding the sponge-SPION adsorption capacity of 0.17mmol/g sponge (21.64mmol/g SPION), almost twice the capacity found with the same sample in batch mode. As expected, in continuous mode, the efficiency of adsorption process is higher than in batch mode.

3.2.3.1. Different dosage effect on adsorption capacity

1L of 250ppm arsenate solution was processed through the filtration and column-adsorption system, yielding “zero” concentration of arsenic in the elute solution. The sponge-SPION presents an adsorption capacity of 0.167mmol/g sponge (21.64mmol/g SPION), almost twice with the same sample in batch mode. In continuous mode, the efficiency of adsorption process is higher than in batch mode. The results show that the column adsorptions are more effective than batch adsorptions. The adsorption capacity of the system is very high at the beginning.

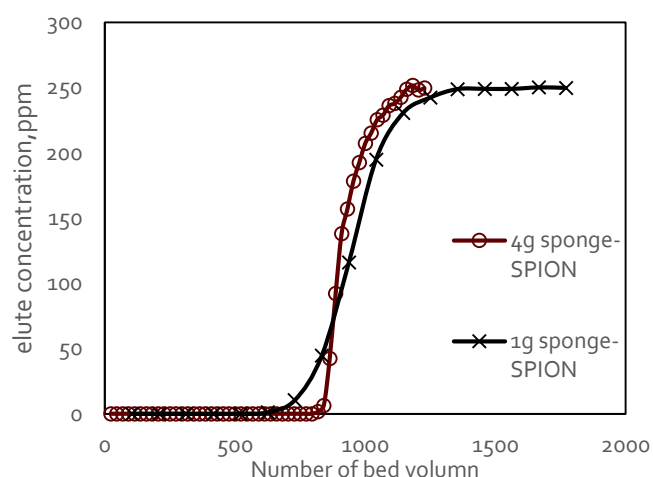


Fig 3.19 Column mode –different dosage effect on elute concentration. Initial stock solution concentration=250ppm, T=293K, 1g sponge loaded with SPION, pH=3.6.(Adsorption capacity of 4g sponge-SPION=100.06mg As/g sponge, Adsorption capacity of 1g sponge-SPION=99.14mg As/g sponge)

The observed data in Fig 3.19 shows the adsorption capacity obtained using 4g adsorbent(sponge loaded with SPION) or 1g adsorbent is the same, which indicates the homogeneity of the adsorbent prepared.

3.2.3.2. The synergic thermo tuning of redox potential-column mode:

Table 3.9 Combination of temperature effect with redox potential effect for desorption

	After adsorption		After desorption (20°C+ reduction)		After desorption (70°C+ reduction)	
	As in Sponge (ppm)	As in Sponge-SPION(ppm)	As in Sponge(ppm)	As in Sponge-SPION(ppm)	As in Sponge(ppm)	As in Sponge-SPION(ppm)
First time	18.6	21.4	3.8	9.2	1.2	7.6
repeat	18.9	21.2	3.5	9.5	1.8	7.3

Table 3.9 shows that in the column mode, both of the temperature and redox potential have significant effect on arsenic adsorption-desorption. It could be combined the temperature effect with redox potential in order to get the better and stronger desorption process without adding reagents. It shows that in the column mode, the adsorbent in the column could firstly adsorb the arsenate and then, the loaded arsenate could be eluted by the reduced hot solution. After elution, the adsorbent could be reused to adsorb the arsenic again. Which means, the adsorption-desorption recycled process could be realized and the adsorbent could be reused for several times.

3.2.3.3. Comparison of desorption by temperature-modifying and reduction-tuning methods

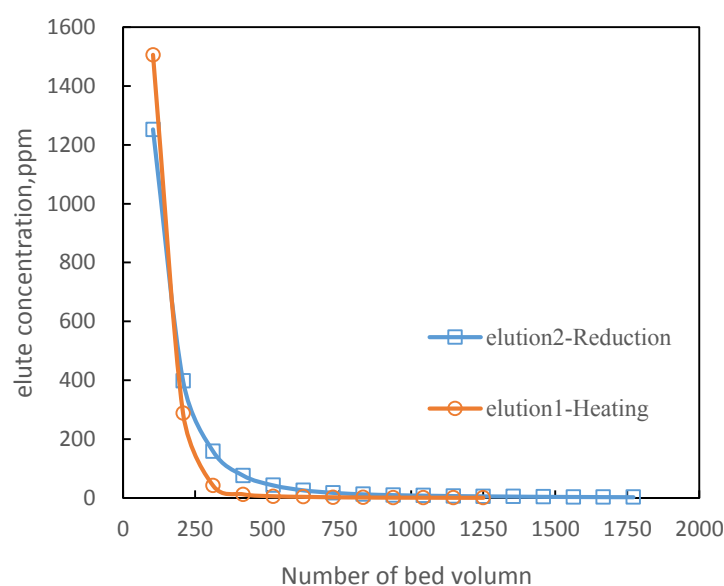


Fig 3.20 Comparison of desorption by temperature-modifying and reduction-tuning methods.

Heating: 70°C, Reduction: Sn

Table3.10 elution recovery ratio

	reduction	heating
total elute,mg	101.47	93.08
recovery, %	96.52	85.64

A comparison of the temperature-modifying and reduction-tuning methods for desorption has been shown in Fig 3.20. The desorption process can be accomplished by high temperature condition, in our case, we use 70°C hot water to thermostatic the elution solution passing through the column. Once the high temperature is stable (since we use thermometer to monitor the temperature), the desorption process occurs. Another way to realize desorption process is to use the reducing conditions. One small column (10*1.0cm) was used to be filled by reducing agent, here we use Sn, this column is connected with the big column which is used for desorption. The results reflect that both temperature-controlling and reduction-tuning method could make effective the desorption process. As the desorption efficiency of the system is very high at the beginning showing a “flash desorption”. The initial concentration of the elution shows much more than 250ppm (here is 1506ppm), this is due to the concentrate effect of the sponge-SPION during the adsorption process. The recovery efficiency of the arsenic adsorbed in the sponge-SPION is high, showing 96.52% and 85.64% for each method, respectively. Once finishing the desorption process, the adsorbent can be used again (recycling) to adsorb arsenic oxyanions under room temperature. Such process could be used in a continuous mode by applying temperature cycles. These experiments were not yet accomplished and the present results state to establish the experimental demonstration of the concept.

3.2.3.4. Comparison of different methods for desorption

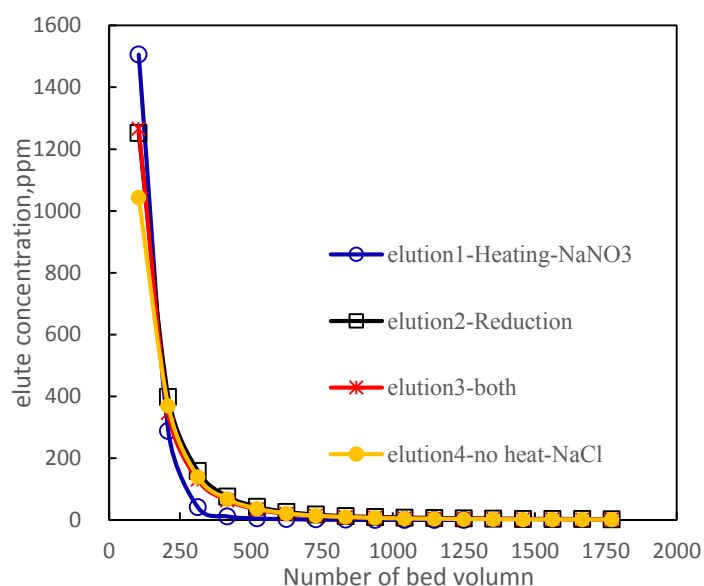


Fig 3.21 comparison of different methods for desorption

Table3.11 comparison of recovery rate by using different methods for desorption

	No heating-NaCl	Heating+Reduction	Reduction	Heating+NaNO ₃
total elute, mg	86.29	95.79	101.47	93.08
recovery, %	92.80	94.22	96.52	85.64

The comparison of different methods for desorption, the temperature with the help of NaNO₃, the reduction-tuning methods, the thermo tuning of redox potential way as well as the NaCl as desorption reagent for desorption have been evaluated as shown in Fig 3.21. In the case of NaCl at room temperature (no temperature effect and no redox conditions), the 92.80% recovery rate is due to the strong affinity of the Cl⁻ for Fe(III) present in SPION, helping thus the release of adsorbed arsenate. However, in the desorption step, the effect of the anions NO₃³⁻ or Cl⁻, which could compete with the arsenic oxyanions therefore could help the desorption process, show lower recovery rate, which is 85.64% and 92.80% than those by the redox potential tuning effect, which

is 96.52% and 94.22%, respectively. Which means that redox potential tuning has stronger impact on the desorption process.

3.2.3.5. Elution by different methods with different competing anions

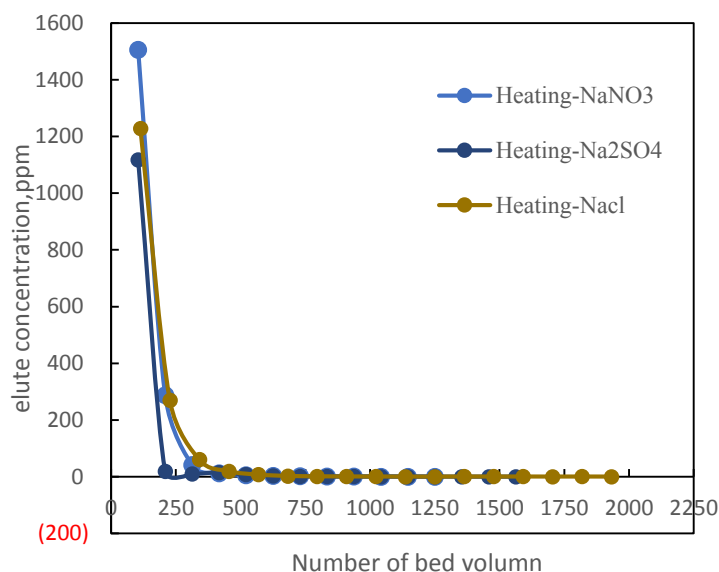


Fig 3.22 elution by different methods with different competing anions

The temperature influence has very significant effect on arsenic oxyanion desorption, which make the process to be very efficient and fast (20ml/min). The comparison of heating effect with of the help of NO_3^- , SO_4^{2-} , Cl^- have been studied (shown in Fig 3.22). The desorption is efficient and complete. The complete desorption is attributed to the thermo tuning effect combined with the function of interference anions. The recovery proportion is almost >90%.

Above all, the temperature and redox potential both have significant effect on desorption, which make the desorption to be very efficient and complete. The efficient and complete desorption process is attributed to the thermo tuning effect and to the redox potential function. Again, this complete desorption results in a “clean” sponge loaded with SPION, fully prepared for the next cycle of adsorption. The recovery proportion is almost >90%.

Table 3.12 Comparison of different methods for desorption

	Reagent-less			Reagent	
Method or stripping solution	Heating	Redox potential	Heating+ redox potential	NaOH1.0M	NaCl 1.0M
Recovery(%)	85.64	96.52	94.22	48.6	67.5

Comparing the reagent-less method with those desorption reagents (shown in Table 3.12), the reagentless method is not only much more effective, but also save the cost and environmental implication of the use of a reagent. Since our work is aimed for recycling adsorption-desorption, adsorbent regeneration and reuse, keeping the adsorbent to be the same and best pH condition for adsorption is very desirable. Thus, either the temperature-controlling or the redox potential tuning method has no effect to modify the pH. Reagent-less processes were developed by using these intensive thermodynamic parameters, e.g, temperature and/or redox potential of the target solution. Appropriate tuning of these parameters will allow both process selectivity and regeneration of the adsorption material. Synergic interaction of thermo-tuning with redox variation will be the object of future development of this process. Thus, this reagent-less method could not only provide reagent savings for recovering the adsorbent, but also the adsorbent recycling to be reused will contribute to a-cost and environmental efficient process.

3.2.3.6. Several cycles loading-reuse of the adsorbent (SPION loaded sponge)

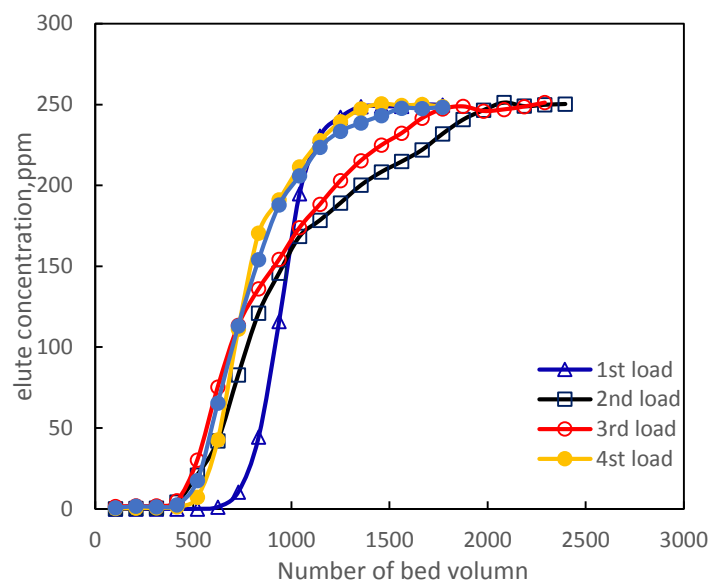
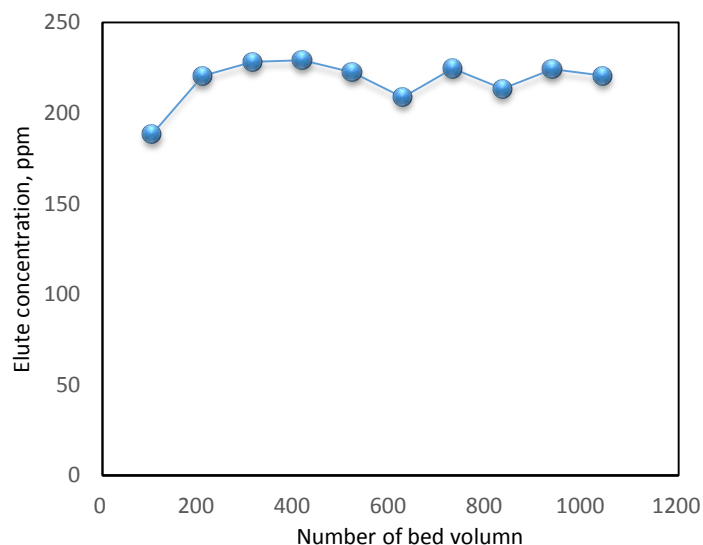


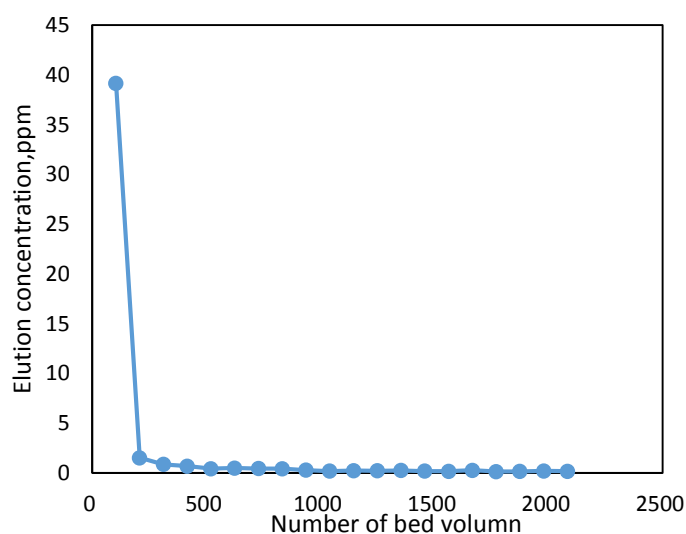
Fig 3.23 Adsorption-desorption cycles. Use of the same column in five cycles

The various adsorption-desorption cycles for arsenic in Fig 3.23. The sponge loaded with SPION as adsorbent under study reflect very good adsorption capacity that is shown to maintain in the various cycles, therefore the recycled function of the adsorbent and the reuse process are experimentally confirmed. This recycled process is not only due to the good adsorption capacity of the adsorbent (sponge-SPION), but also to the efficient elution method, which make the recovery of arsenic oxyanions to be complete and the adsorbent (sponge-SPION) to be regenerated. It demonstrate again that thermo tuning or redox potential effect on the removal of the toxic oxyanions and the adsorbent regeneration is effective and efficient.

3.2.4. As(III)-continuous column mode



3.24 As(III) adsorption on sponge loaded with SPION in continuous column mode



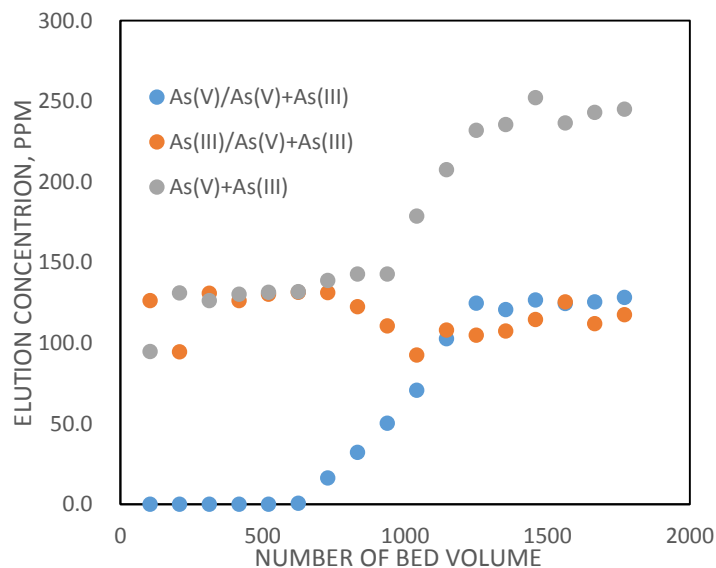
3.25 As (III) desorption on sponge loaded SPION in continuous column mode

Although arsenic adsorption/desorption behavior on iron (oxyhydr)oxides has been extensively studied¹⁸², no one study about arsenic(III) adsorption/desorption behavior using sponge-SPION system. The adsorption and desorption efficiency of As(III) in continuous column mode has been determined as shown in Fig 3.24 and Fig 3.25, respectively. For the As(III) adsorption column experiment, the initial concentration of

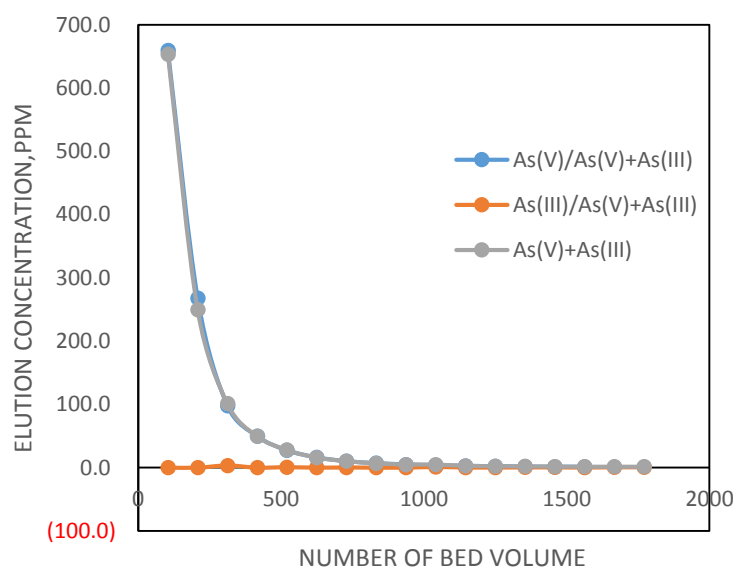
the As(III) was 250ppm. 1L of 250ppm As(III) contained solution was used to pass through the column under pH 6.5(since As(III) is not pH dependent, so we use just the MilliQ purified water instead of buffer pH 3.6 (used for As(V) adsorption) to do the adsorption/desorption experiment). The column was filled with 1g of adsorbent-SPION loaded sponge. While for the As(III) desorption process under the column continuous mode, the high temperature hot water was used to make that the desorption was undertaken in 70°C. The low adsorption and desorption capacity and efficiency of As(III), compared with As(V) adsorption on sponge loaded with SPION confirm the results obtained previously when working at room temperature¹⁶⁸. The maximum adsorption capacity of As(III) under column continuous mode is around 3.07mg As(III)/g sponge (or 0.04 mmol As(III)/g sponge). The desorption is only observed in the first elution tube(50mL) , meaning the process to be fast.

The arsenite could be much less adsorbed due to its acidity that maintain a high proportion of deprotonated species presents in the media during the adsorption process and thus leading the sponge-SPION to have less possibility to interact with arsenite, compared with that interaction and affinity to arsenate which react by anion exchange on the adsorption system. Therefore, this results supports again the concept of the redox potential as key parameter to tune the Arsenic adsorption/desorption on SPION loaded sponge system.

3.2.5. As(V)+As (III) adsorption-desorption on sponge loaded SPION in continuous column mode



3.26 As(V)+ As(III) mixture adsorption on sponge loaded with SPION in continuous column mode

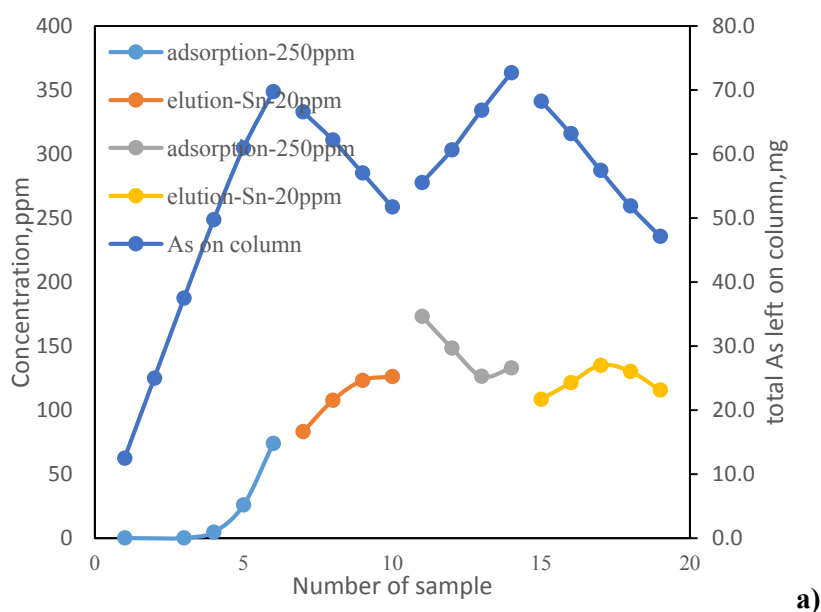


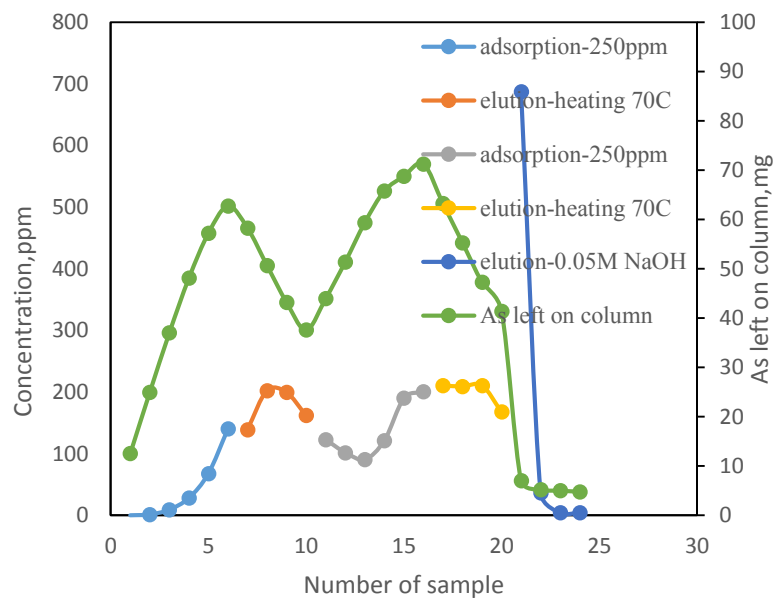
3.27 As (V)+As (III) mixture desorption on sponge loaded SPION in continuous column mode

The adsorption and desorption efficiency of As(V)+ As(III) mixture solution in continuous column mode has been determined as shown in Fig 3.26 and Fig 3.27, respectively. The results observed are due to the competitiveness between arsenate and arsenite. The column results confirmed the results studies elsewhere that, taking into account the related results for the individual species, arsenite is also adsorbed and desorbed but in much less proportion than arsenate.³³

3.2.6.Cycled column experiment by modeling the real waste water treatment

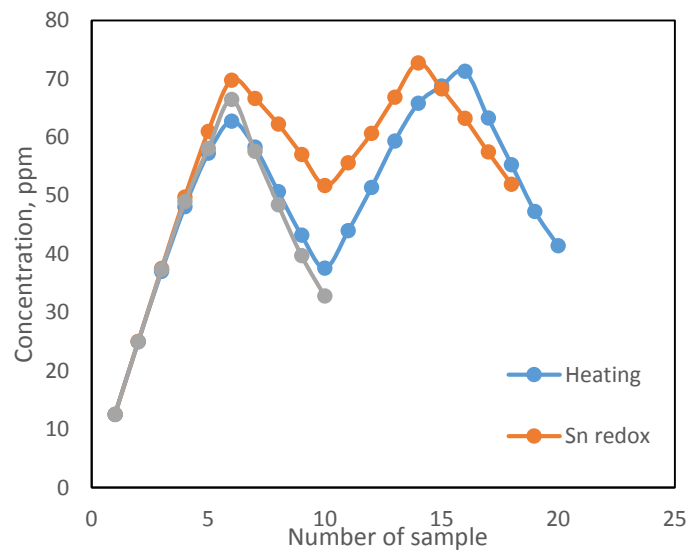
A series of adsorption/desorption experiments for modelling the real wastewater treatment process were carried out in a column continuous mode to provide the basis for a possible continuous removal of Arsenic in polluted waters.



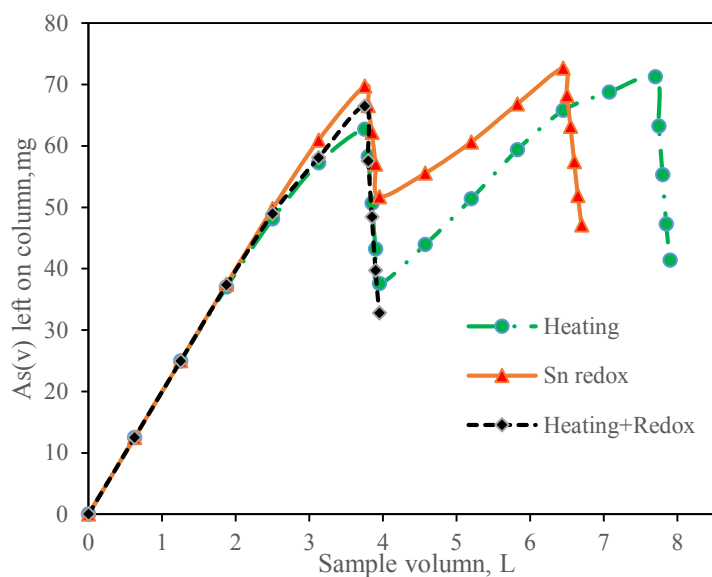


b)

3.28 Modeling of real wastewater treatment process of adsorption-desorption, a) desorption only by redox potential tuning, b) desorption by temperature and redox potential tuning



a)



b)

Fig.3.29 Adsorption/desorption cycles on a column continuous mode by using temperature or/and redox potential to tune the process, comparing of different methods, a) 20 sample, b) 8 sample

The adsorption-desorption cycling process has been characterized (shown in Fig 3.28, Fig 3.29). In these experiments, the continuous solution on column is of 50 ppm of Arsenic. In this way, we will mimic a process of polluted water treatment.

The specific experiments are described as follows:

Experiment 1, elute by heating

- 1) Loading As(v) 250ppm on the column(1g sponge-SPION), collect the elute in six 50ml tubes to assume column saturation.
- 2) Elute the column by 50ppm As(v) solution, by heating to 70°C, collect the elute in four 50ml tubes.
- 3) Repeat steps 1) and 2)

Experiment 2, elute by Sn-reduction precolumn

- 1) Load As(v) 250ppm on the column(1g sponge-SPION), collect the elute in six 50ml tubes to assure column saturation.
- 2) Elute the column by 20ppm As(v) solution, by passing the Sn-redox column(80g),collect the elute in four 50ml tubes.

3) Repeat steps 1) and 2)

Experiment 3, Heating+Redox : In this case, the continuous flowing solution is heated and passed by the solid Sn precolumn

- 1) Load As(v) 250ppm on the column(1g sponge-SPION), collect the elute in six 50ml tubes to assure column saturation.
- 2) Elute the column by 20ppm As(v) solution, passing the heated solution at 70°C by the Sn-redox pre-column(80g), and collect the eluate in four 50ml tubes.

Heating+Redox > Heating > Sn-redox

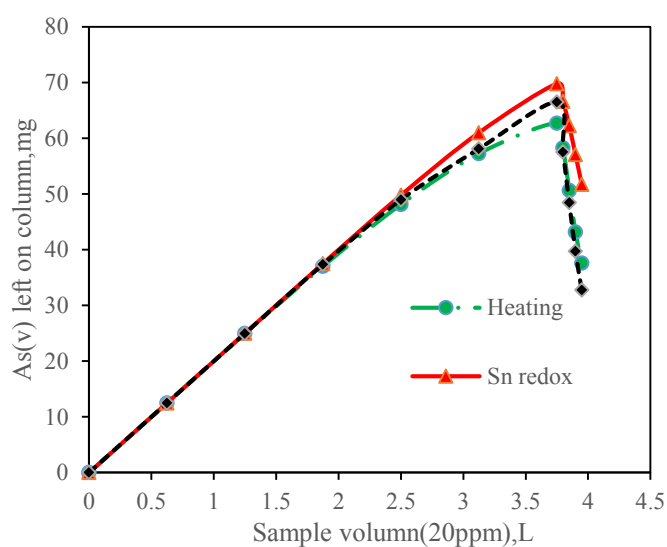


Fig.3.30 Comparative results of different methods for desorption concentration

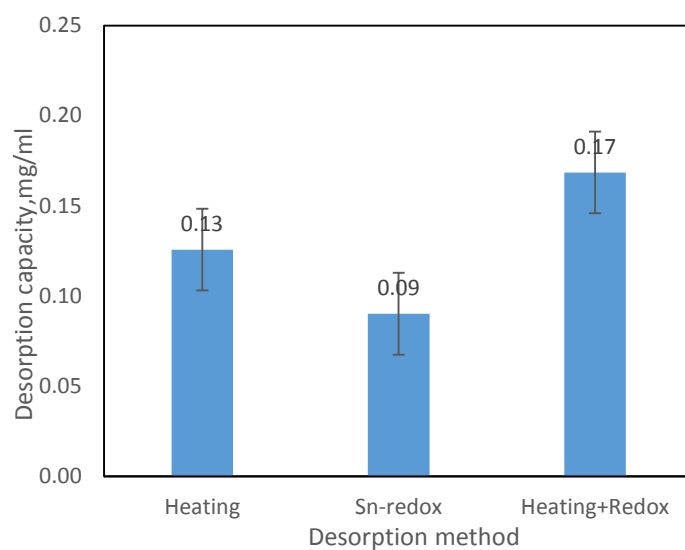


Fig.3.31 Comparative results of different methods for desorption capacity

It is observed that by tuning the thermodynamic parameters, such as the temperature, the redox potential as well as the combining thermo tuning of redox potential, the desorption is produced.

The comparison of heating, redox as well as the heating combined with redox effect on desorption process have been performed and studied as shown in Fig 3.30 and Fig 3.31. Results indicate the positive synergism between temperature and redox potential.

3.2.7.Real waste water

The real waste water sample has a high concentration of iron, which has to be eliminated before arsenic removal.

Table 3.13: Original concentrations of different elements in real waste water

	ppm
Fe	979
Al27	773.5
Mg 26	715.5
Zn	198.5
Cu	194.8
Mn 55	74.2
Ca 44	39.9
Si 28	34.7
Na 23	14.1
Co 59	7.0
As	3.1
Li 7	2.8
Ni	2.2
Cd 114	2.1
Sr 88	1.8
Ba 138	1.5
Ti 47	1.4

Cr 52	1.3
V 51	1.3
Sb 123	1.3
Mo 95	1.3
Ag 107	1.0
Se 82	0.4
Pb	0.2

The real waste water sample is from Rio Tinto river from Huelva province, Andalucia (Spain) and was provided by the Spanish company AGQ Mining and Bioenergy. Waste water sample was analysed by ICP-MS and we can observe a high concentration of iron to be eliminated before arsenic removal.

A sample pretreatment by bubbling air for 4 hours, to oxidize the Fe^{2+} to Fe^{3+} . In addition, the pH of the real waste water (originally 2.45), is changed to be 3.6 by adding NaOH. The precipitate is removed by using a filter, obtaining “iron-free” wastewater. But at the same time, the arsenic is also partially removed since it is adsorbed on the precipitated iron hydroxide. For this reason and to observe the influence of the waste water matrix, we proceeded to doping with 60ppm arsenate the waste water “iron-free” solution (WW). The resulting WW was treated with sponge-SPION adsorbent

After treating the wastewater, the arsenic is adsorbed and the results are shown below in the Table 3.14 and the comparison the results with that represent the data previously obtained for the synthetic As(V) solution was shown in Figure 3.32 . As expected, The first sample demonstrate that the method performs well because almost all the arsenic present in the first 50mL has been adsorbed in the SPION loaded sponge despite other elements presented in the sample can be adsorbed too (ICP show that interfering elements such as Zinc or Copper are present in a higher concentration than arsenic), the

removal efficiency is very good at the beginning (97.82% removal). However, if passing more volume of the real waste water, the removal percentage of the arsenic species is sharpening down since the interference ions, which compete with the arsenic oxyanions to be adsorbed. Therefore, the removal of the interference ions before adsorbing the arsenic species is very necessary and important. The method will perform better if instead of one column is used creating a system of columns interconnected.

Table 3.14: Real waste water absorption results(initial concentration 45.29ppm)

sample	1	2	3	4	5	6	7	8	9
Real Concentration(ppm)	0.99	22.7	36.1	39.4	39.6	44.3	43.3	44.0	43.8
Removal percent(%)	97.8	36.1	20.4	13.1	12.5	2.3	4.5	2.9	3.3

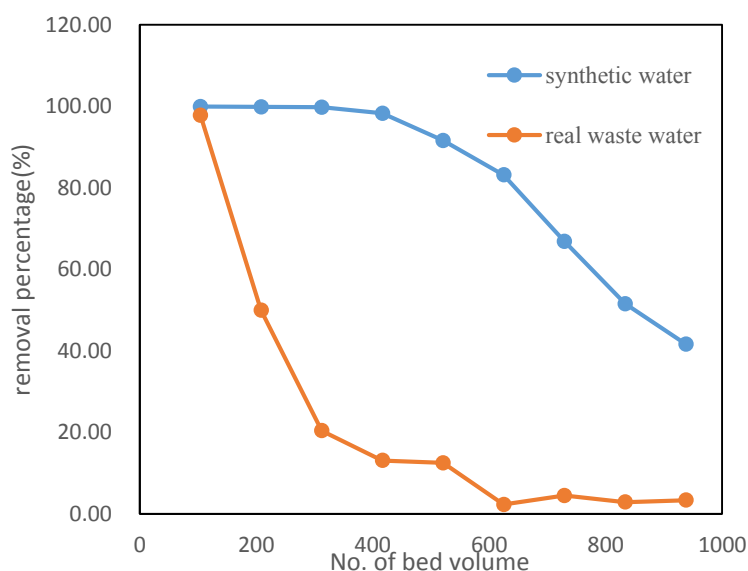
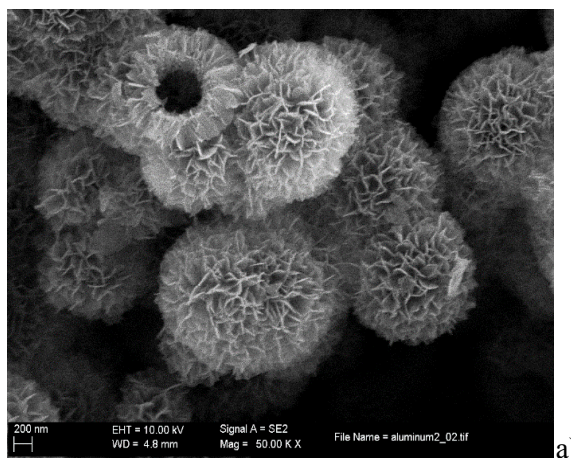


Figure 3.32 Comparison the results of arsenic removal efficiency with that represent the data previously obtained for the synthetic As(V) solution

3.3. Kinetic and Dynamic Aspects of Selenate and selenite adsorption by γ -Al₂O₃ nanospheres

3.3.1. Characterization of adsorbent material--SEM-EDX analysis

Adsorbent (i.e. γ -Al₂O₃ nanosphere) shape and size impact the adsorption capacity of the adsorbent. SEM images of fresh γ -Al₂O₃ nanospheres indicate that the material is composed of individual, hollow-spherical particles ranging in size from 200 to 400nm that form aggregates and chains (Fig3.33a). This small γ -Al₂O₃ nanospheres provides a large surface area for contaminant adsorption. Energy Dispersive X-ray (EDX) analysis data (Fig3.33b) show that the main compositions of the sample are Al and O, which confirms the nanosphere composition. The SEM images of γ -Al₂O₃ nanospheres after adsorption for the selenium was shown in Fig 3.33c. The adsorption of selenium on the γ -Al₂O₃ nanospheres did not influence the structure of the nanoparticles.



a)

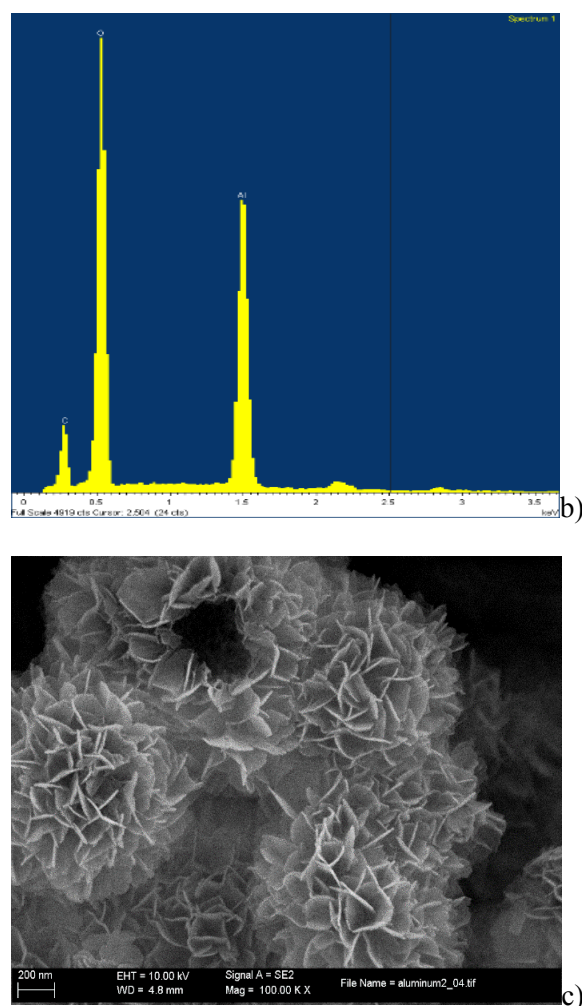


Fig 3.33 SEM image of γ - Al_2O_3 nanospheres a) before adsorption of selenium b) EDX analysis c) after adsorption of selenium

3.3.2. Comparison of AlOOH , γ - Al_2O_3 , modified γ - Al_2O_3 for selenium adsorption

AlOOH hierarchically nanostructured hollow microspheres¹⁶⁵ with nanoflake-like porous surface textures was fabricated in our lab by chemically induced self-transformation of metastable solid particles of amorphous aluminum oxyhydroxide produced in situ within hydrothermal reaction mixtures containing aluminum sulfate and urea.¹¹¹ The hollow structured γ - AlOOH microsphere has first been used for selenium adsorption to see how it behaves and how much the adsorption capacity of the

γ -AlOOH microsphere is. AlOOH hierarchically nanostructured microspheres are used as the precursor and template for the preparation of γ -Al₂O₃ hierarchically nanostructured nanospheres by thermal transformation of AlOOH at 600°C in microwave, and the morphology is well preserved during the thermal transformation process. This process produce intact hollow spheres of γ -Al₂O₃. The comparison between the adsorption of selenate and selenite by γ -AlOOH microsphere and γ -Al₂O₃ nanospheres has been studied and the results are shown in Fig 3.34. The γ -Al₂O₃ nanospheres has much higher adsorption capacity for adsorbing selenate and selenite than that of γ -AlOOH microsphere. Therefore, in the following work, we use γ -Al₂O₃ nanospheres as the adsorbent for selenate and selenite adsorption.

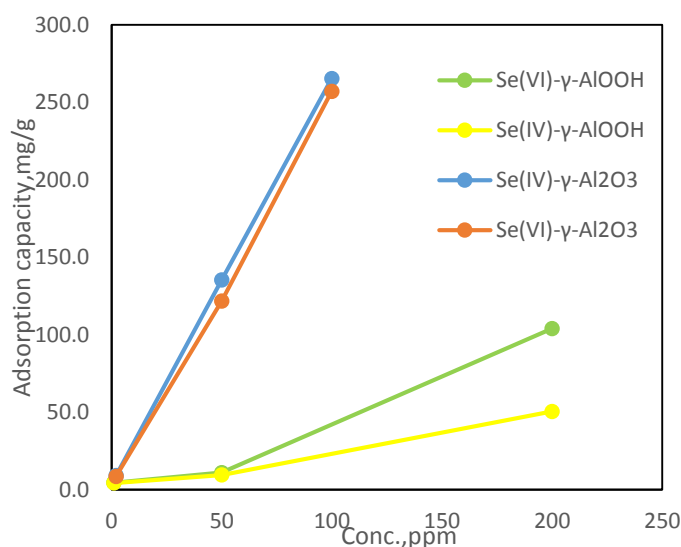


Fig 3.34 Comparison of Selenium adsorption by either AlOOH or γ -Al₂O₃

3.3.3.pH effect on adsorption.

The pH level of the aqueous solution is an important variable for the selenium adsorption process, due to the speciation of the chemical functional groups present on the adsorbent surface. So, the effect of the aqueous solution pH on the removal efficiency of the aluminum nanoparticles for selenium was studied between pH 2.0 and 11.0 (acetic/acetate media) under temperature 20°C and 70°C, respectively (Fig 3.36a,

b). Either under 20°C or 70°C, the results obtained reveal that the adsorption of both Se (IV) and Se (VI) are pH dependent. The observed pH effect revealed the adsorption of Se (IV) and Se (VI) is maximum at pH 2. The adsorption of selenium is occurring through a hydrogen bridge formation and it is coherent with the behavior against the pH, decreasing at more alkaline pH values. In the case of Se (VI) the sorption decreases as the percentage of the aqueous species HSeO_4^- decreases. For sorption edge coincides with the predominance of HSeO_3^- .

Selenate adsorption primarily occurs under acidic conditions, as shown in Figure 3.36. In the pH range studied, the dominant selenium species is SeO_4^{2-} , since the pK_{a2} for Selenic acid is 2¹⁸³. With an increase in pH, SeO_4^{2-} adsorption rapidly decreased. At pH 3.6, the total percent of adsorption was 91%. When pH was higher than 8.0, very little adsorption was observed. This effect can be interpreted as the Se(VI) adsorption taking place by the formation of a hydrogen bridge between the $\gamma\text{-Al}_2\text{O}_3$ and the Selenate oxyanion, thus a certain acidity is needed to maintain such hydrogen bridge, this would explain the decrease of the adsorption of Se(VI) by increasing pH. Se (IV) species in aqueous solution include selenious acid (H_2SeO_3 , $\text{pK}_{a1}=2.6$), biselenite (HSeO_3^- , $\text{pK}_{a2}=8.3$) and selenite (SeO_3^{2-}). Thus, between pH 3.5 and 9.0, the biselenite ion is the predominant ion in water. Above pH 9.0 selenite species dominate, and as the pH decreases below pH 2.6, selenious acid dominates. Se(IV) sorption decreases at alkaline pH due to the decrease of the fraction of aqueous species of HSeO_3^- that provides the hydrogen bonding interaction with the $\gamma\text{-Al}_2\text{O}_3$.¹⁸⁴

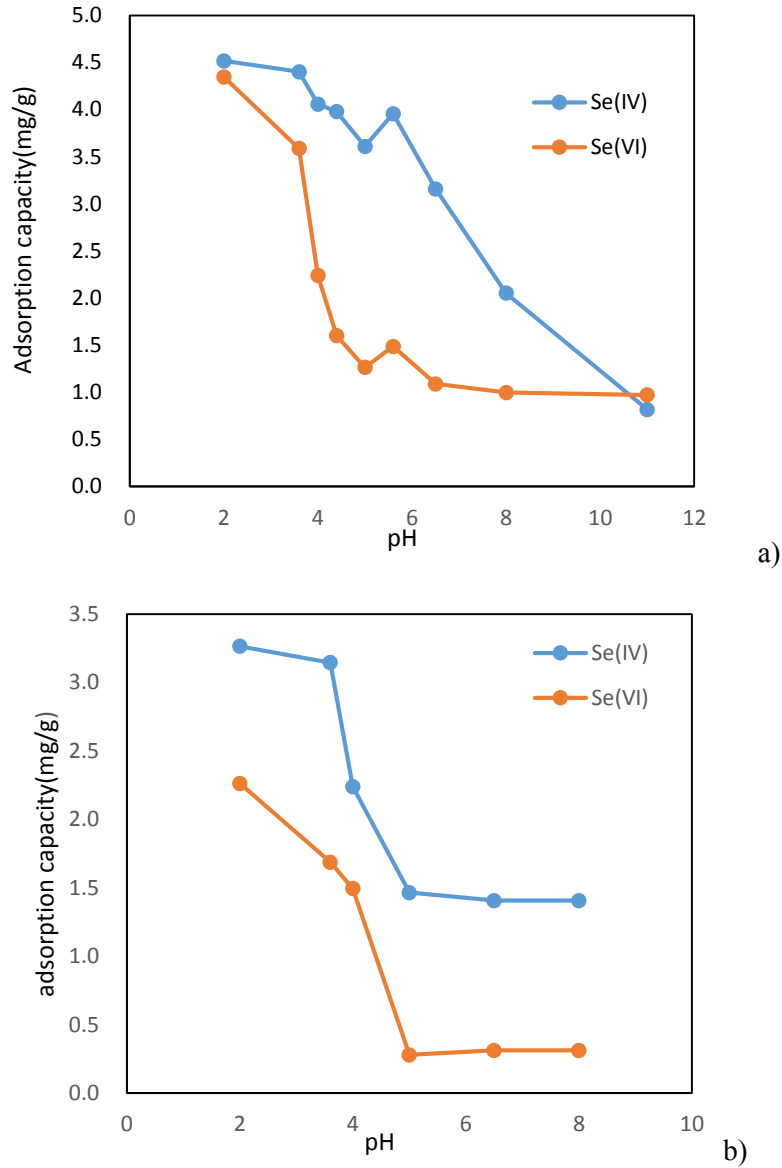


Fig3.36. pH effect on selenium adsorption, initial concentration: 1ppm, using 0.005g aluminum nanosphere as adsorbent. 25mL, contact time is 18h. a) 20°C b) 70°C

The observed differences on adsorption behavior between Se (IV) and Se(VI) are due to the differences on acidity of the corresponding oxyanions that need the formation of corresponding hydrogen bonding with the corresponding γ - Al_2O_3 .

3.3.4. Initial concentration effect on selenium adsorption

These experiments are planned to assess the effect of the initial selenate and selenite concentration on the sorption process and estimate the maximum aluminum nanosphere adsorption capacity for both species. The adsorption of selenium oxyanions by γ - Al_2O_3 nanospheres is determined in a proper initial selenium concentration range at pH 2. The effects of the initial selenium concentration (from 2ppm to 100ppm) on the adsorption capacity by the γ - Al_2O_3 nanosphere are shown in Fig 3.36. The increase of adsorption capacity when the initial selenium concentration increases can be explained in terms of diffusion resistance. Adsorption capacity equilibrium is reached when the surface of γ - Al_2O_3 nanosphere does not have free sites for the selenium oxyanions uptake, being saturated.¹³⁶ It is probably another explanation that, as mentioned before, a higher probability of collision between adsorbate (arsenate) and adsorbent(sponge loaded with SPION) surface happens as initial concentration increases, which could overcome the mass transfer resistance between the aqueous and the adsorbent phases.¹⁷⁴

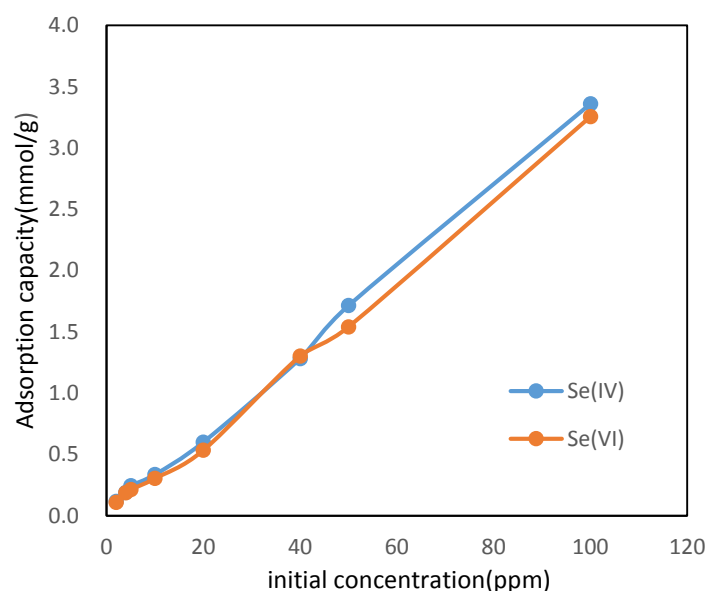


Fig3.36. Se (VI) and Se(VI) initial concentration effect on selenium adsorption, initial concentration: 1ppm, using 0.005g aluminum nanoparticle as adsorbent. 25mL, contact time is 18h.

3.3.5. Adsorption Isotherm modeling.

In these experiments the effect of the initial Se (IV) and Se (VI) concentration on the sorption of Se (IV) and Se (VI) was studied in order to estimate the maximum loading capacity of γ - Al_2O_3 nanoparticles. The obtained results are not fitted to Langmuir isotherm, fitted to the well-known Freundlich isotherm model, as shown in Fig3.38. The experimental observation are in good agreement with the Freundlich model¹⁸⁵

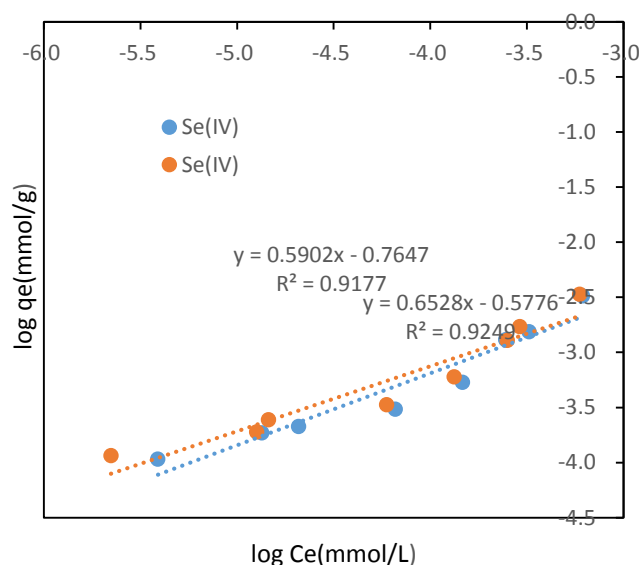


Fig3.37 Freundlich isotherm model for the adsorption of Se (VI) and Se(IV) by γ - Al_2O_3 nanosphere

Table 3.15 Freundlich parameters

	$\log k_f$	$1/n$	R^2
Se(IV)	-0.76	0.59	0.92
Se(VI)	-0.58	0.65	0.92

Regarding the corresponding correlation coefficient values obtained, the Freundlich isotherm fits the data showing that the adsorption process not rely on a specific sites adsorption mechanism but in the multilayer of the surface not occupying specific sites on the adsorbent. The adsorbent (here is γ -Al₂O₃ nanospheres) is not homogeneous but it is heterogeneous.

3.3.6.Evaluation of thermodynamic parameters

The influence of the temperature on the equilibrium constant k can be described by the following relationship:

$$\ln\left(\frac{k_1}{k_2}\right) = \frac{\Delta H}{R} * \left(\frac{1}{T_1} - \frac{1}{T_2}\right) \dots\dots\dots 3.11$$

And K can be calculated by the equation:

$$k = q_e/C_e \dots\dots\dots 3.12$$

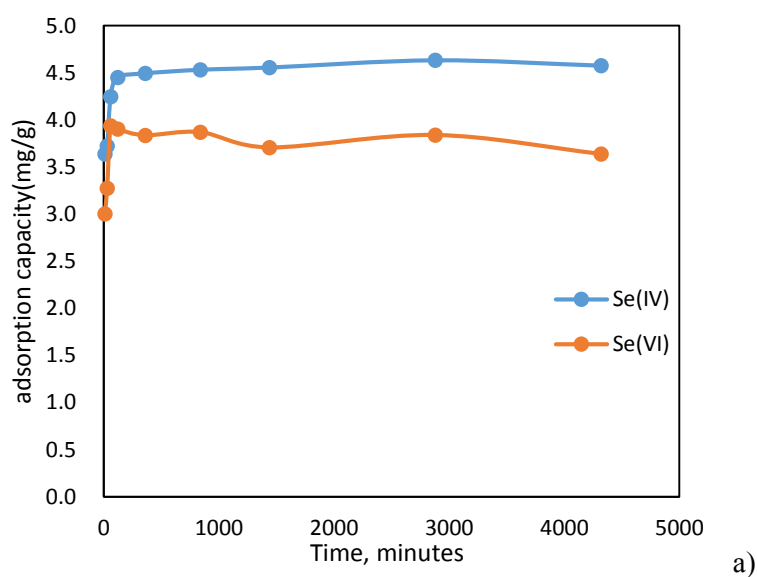
Table3.16 Differential enthalpies of complexation for hypothetical nanoparticles with selectivity dependent on temperatures

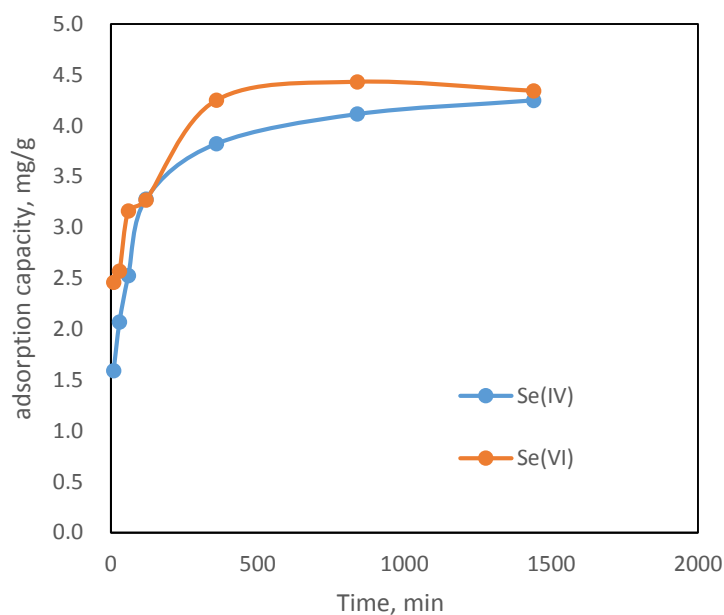
343K-293K	K(T2)/K(T1)	Ln(K2/K1)	ΔH , KJ/mol	LogKf	1/n
Se(IV)	0.43	-0.84	-13.96	-0.77	0.59
Se(VI)	0.79	-0.24	-3.93	-5.78	0.65

It was observed from Table 3.16 the ΔH value shows that lower temperature favor removal of selenium within the defined range of study. The reaction could be attributed to the fact that the adsorption of selenium oxyanions onto the surface of the γ -Al₂O₃ nanosphere could be favored by elimination of water molecule previously bonded to the surface of the adsorbent favoring the increase of entropy value. The negative value of ΔH confirms the exothermic nature of the adsorption process. The ΔH value of Se (IV) and Se (VI) between 20°C and 70°C were -14.0 KJ mol⁻¹ and -3.9 KJ mol⁻¹ shows that lower temperature favor removal of selenium.

3.3.7. Adsorption dynamics

The variation of contact time is one of the most important parameters in determining the adsorption potential of an adsorbent material, the adsorption dynamics. Adsorption of selenium by aluminum nanospheres was studied within a time period of 2-4320min (2min to 72h). As shown in Fig 3.38, the equilibrium adsorption of selenium can be obtained in 6h under 20°C at pH 2, the adsorption of selenium presents an anion exchange behavior. The reason could be attributed to the availability of high surface area as well as porous structural features facilitating easy removal of selenium. Apart from this, surface hydrophilicity could be a factor responsible for anion-surface functional group interaction which is entropically favorable. On the other hand, for 70°C, the maximum adsorption was attained in 14 hours.





b)

Fig3.38 Variation of contact time period, pH=3.6, conc. of Se(IV) or Se(VI): 1ppm; adsorbent dose:5mg.a)20°C, b) 70°C

3.3.8.Adsorption kinetics

Adsorption of selenium oxyanions on γ -Al₂O₃ nanospheres is a complex process. The adsorption mechanism during the present adsorption process involve the potential rate controlling steps such as mass transport, pore diffusion and chemical reaction processes. Indeed, the speed of adsorption is strongly influenced by several parameters such as the status of the solid matrix that has generally heterogeneous reactive sites, and the physical-chemical conditions under which the adsorption take place.¹⁸⁶

In order to understand kinetics process and predict the mechanism involved during the present adsorption process, the adsorption data were analyzed and two kinetic models were used to fit the experimental data, namely, pseudo first-order (shown in Fig 3.39) and pseudo-second-order (shown in Fig 3.40). The pseudo first order kinetic model was based on the capacity of the solid adsorbent by considering that the rate of occupation of adsorption sites is proportional to the number of unoccupied sites. The best-fit model was selected based on both linear regression correlation coefficient (R^2) and the

calculated q_e values. The correlation coefficients for Lagergren irreversible first-order model obtained were low. Therefore, the reaction involved in the present adsorption system is not of the first-order. The calculated q_e by this model differs significantly from those measured during the experiment. The kinetic studies show that they are fitted very well to the pseudo-second order, which showed the best fit to the experimental data with the highest squared correlation coefficients ($R^2 = 0.999$) and the theoretical Q_e give acceptable values when compared to the experimental ones. This suggests that selenium oxyanions were adsorbed onto the aluminum nanosphere surface via chemical interaction, which is probably involving valency forces through sharing or exchange of electrons between sorbent and sorbate, and provides the best correlation of the data.

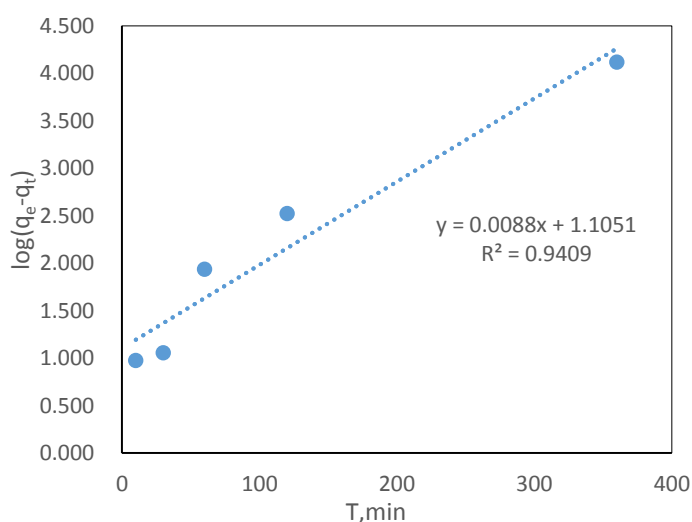
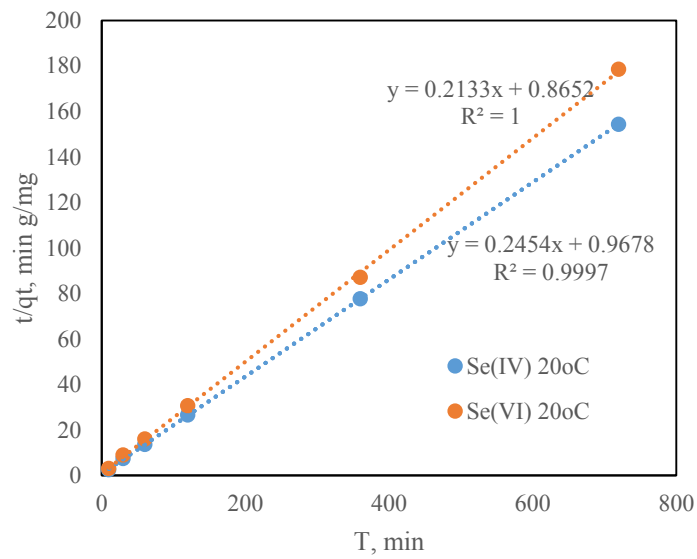
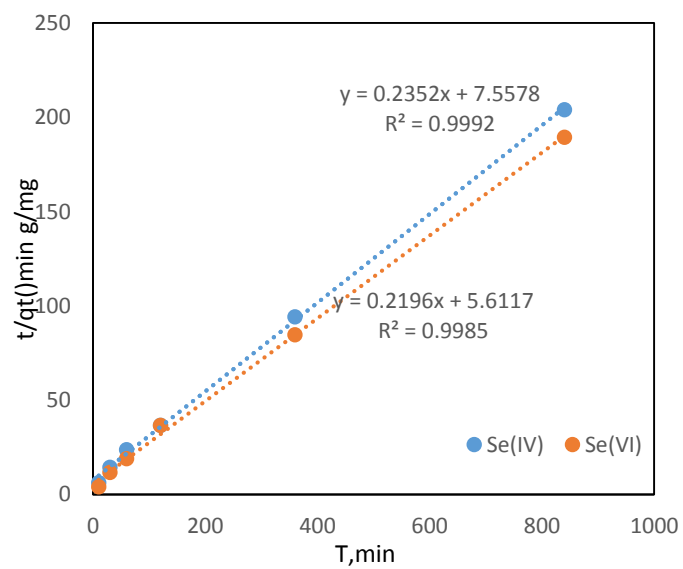


Fig3.39 Pseudo-first order adsorption kinetics plots for the adsorption of selenite by γ - Al_2O_3 nanosphere. The initial concentration of Se (IV) was 1ppm, the adsorbent dosage of γ - Al_2O_3 nanosphere was 5mg, and the volume of the adsorption aqueous system is 25mL. The experiment was undertaken under 20°C.



a)



b)

Fig 3.40. The plot of t/q_{t-1} vs. t showing the linear nature of second-order kinetic model for aluminum nanoparticle, adsorbent dose, 5mg, pH 3.6. a. Se(IV) and Se(VI), 20°C; b Se(VI) and Se(VI), 70°C

Table 3.17 Pseudo-second order kinetic constants for the adsorption of selenium oxyanions on γ -Al₂O₃ nanospheres

	K ₂ (g/mg min)	Q _e (mg/g)	R ²
Se(IV) 20°C	0.054	4.29	0.9999
Se(VI) 20°C	0.058	4.16	0.9998
Se(IV) 70°C	0.053	4.33	0.9996
Se(VI) 70°C	0.048	4.55	0.9985

Pseudo second-order adsorption parameters q_e and K_2 were determined by plotting t/q_t versus t ., the analysis of tabular data (shown in Table 3.17) reveals that values of both $q_{e, \text{exp}}$ and $q_{e, \text{cal}}$ for pseudo second order kinetic model are close to each other with relatively higher correlation coefficient (R^2) value. Given the good agreement between model fit and experimentally observed equilibrium adsorption capacity, this suggests that selenium ions were adsorbed onto the aluminum nanoparticle surface via chemical interaction. The adsorption kinetics can be conveniently represented by the pseudo second order model.

3.3.9. Comparison of adsorption capacity between γ -Al₂O₃ nanosphere and modified γ -Al₂O₃ nanosphere

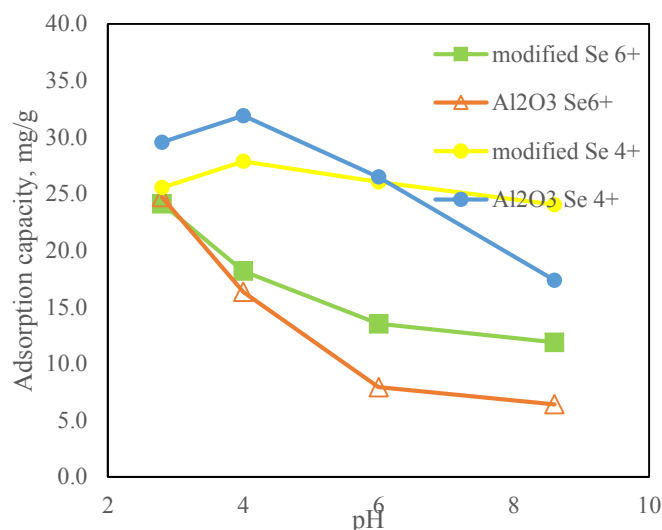


Fig 3.41 comparison of adsorption capacity between γ -Al₂O₃ and Modification of γ -Al₂O₃

Some studies on 3-mercaptopropionic acid (3-MPA) coated SPION have been done in order to modify the change the aggregation properties of SPION and link the thiol groups to SPION surface in order to improve the adsorption capacity and selectivity of SPION⁸². In our case, the γ -Al₂O₃ nanosphere has been modified by diethylammonium N,N-diethyldithiocarbamate (DDC)¹⁸⁷, since this organic reagent has the thiol group¹⁸⁸, which also could bond with γ -Al₂O₃ nanosphere¹⁸⁹, therefore make the nanospheres to be less aggregated and increase the surface area. Thus, it should improve the adsorption capacity of γ -Al₂O₃ nanosphere for selenium adsorption. The results of comparison of adsorption capacity between γ -Al₂O₃ nanosphere and DDC modified γ -Al₂O₃ nanosphere has shown in Fig 3.41. It has demonstrated that DDC modified γ -Al₂O₃ nanosphere has higher adsorption capacity for selenate. However, in the pH range of 2.8-6.0, the γ -Al₂O₃ nanosphere has higher adsorption capacity for selenite than corresponding to DDC modified γ -Al₂O₃ nanosphere for selenite. When pH > 6.0, the phenomenon is opposite. This could be interpreted as a change on the type of adsorption

interaction between the adsorbent and target Se oxyanions. In the DDC modified surface, the role of the thiol group much less acidic will provide the needed hydrogen bond interaction.

3.4. Kinetic and Dynamic Aspects of Selenate and selenite adsorption by sponge loaded with superparamagnetic iron oxide nanoparticles (SPION)

From the previous part, it was found that the γ - Al_2O_3 nanospheres can be used as potential nano-adsorbents for the removal of Se (IV) and Se (VI) oxyanions, especially Se (IV) species since it showed higher adsorption capacity for Se (IV) than that for Se (VI), mostly due to the difference on acidity of the related oxyanions. In this part, the sponge loaded with SPION is introduced again for the adsorption of selenium oxyanions. The results show that sponge loaded with SPION has much better adsorption capacity for selenate than that for selenite.

The results show that when sponge loaded with SPION as the adsorbent for selenium adsorption, the adsorption capacity of SPION-sponge for selenate is much higher than that for selenite. The maximum adsorption for selenate and selenite on sponge loaded with SPION was achieved at pH 3.6 in 1 hour under 20°C and 6 hours under 70°C, respectively, while time for obtaining equilibrium of selenite needs 14 hours under 20°C and 24 hours under 70°C.

On the other hand, a comparison of these results with those obtained for Arsenic adsorption, it is observed a parallel phenomenon, thus, sponge loaded with SPION have better adsorption capacity for As(V) and Se(VI) and lower adsorption capacity for As(III) and Se(IV). Such similarities support the suggested chemical interactions between SPION constituents and target oxyanions. Thus, in this system, the ion exchange reaction is taking place for both elements and this is why the relatively

stronger acids corresponding to oxyanions of As(V) and Se(VI) have higher adsorption and at lower pH value, since these oxyanions have higher concentrations under such conditions. On the other hand, the acids corresponding to oxyanions of As(III) and Se(IV) are much weaker acids, so their ionization take place at high pH values where the competition with hydroxyl anions hinder their possibilities for adsorption on SPION based adsorbent.

Moreover, by using sponge-SPION as adsorbent, the selenium continuous column mode experiment show very similar adsorption-desorption properties as observed for Arsenic oxyanions adsorption/desorption processes.

Therefore, it can be concluded that selenium adsorption by γ -Al₂O₃ nanosphere represent a very different adsorption system behavior than that of SPION based adsorption even if the thermodynamics show similar trend on the associated ΔH , so, same temperature-dependence effect on adsorption process while the selenate/selenite adsorption by sponge-SPION gives the same temperature impact and redox potential effect as those with arsenate/arsenite adsorption properties by sponge-SPION.

3.4.1.SEM characterization

The surface morphology of sponge and sponge loaded with SPION were characterized by SEM techniques. Figure 3.42 shows the SEM micrographs of the (a) Forager sponge and (b) sponge loaded with SPION. It is observed that the sponge is porous and the SPION is impregnated to penetrate inside of the sponge pores providing a complete SPION layer on the sponge surface,³³ which could be confirmed by the TEM results reflected in the first part. In addition, these figures reveal the surface texture and porosity of the blank and loaded adsorbent¹⁸⁴. It can be seen from these figures that the surface texture of the blank adsorbents changes drastically after the loading of SPION.

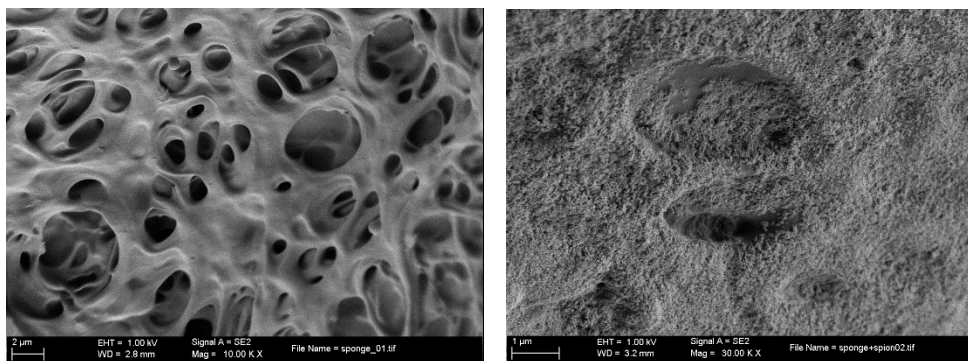


Fig3.42 Scanning electron microscopy(SEM) micrographs of sponge:(a) sponge;(b) sponge loaded with SPION

3.4.2. pH effect on selenate and selenite adsorption

Once using the sponge loaded with SPION to adsorb the selenate and selenite, the pH influence on selenate and selenite adsorption capacity has been studied between pH 2.0 and 11.0 (acetic/acetate media)(Fig 3.43a,b). The results obtained revealed that the adsorption of both Se (IV) and Se (VI) are pH dependent. The observed pH effect revealed the adsorption of Se (IV) is maximum at pH 2, while for Se (VI), the maximum adsorption is at pH 3.6. The adsorption of selenium presents an anionic behavior, decreasing at more alkaline pH values because of the competition of the hydroxyl groups. In the case of Se(VI) the adsorption decreases as the percentage of the aqueous species HSeO_4^- decreases. For sorption edge coincides with the predominance of HSeO_3^- .

A comparison of the observed pH effect with those obtained on previous As (V) adsorbent studies, e.g sponge loaded with SPION, revealed similar behavior with a maximum adsorption at pH 3.6. This similarity supports that arsenic and selenium species responsible of the adsorption are of the same type. The arsenic and selenium oxyanions both show the ion-exchange with amine groups of the sponge and ligand exchange with the SPION. The arsenate and selenate probably interact with the R-Fe-OH by forming related ion pair.

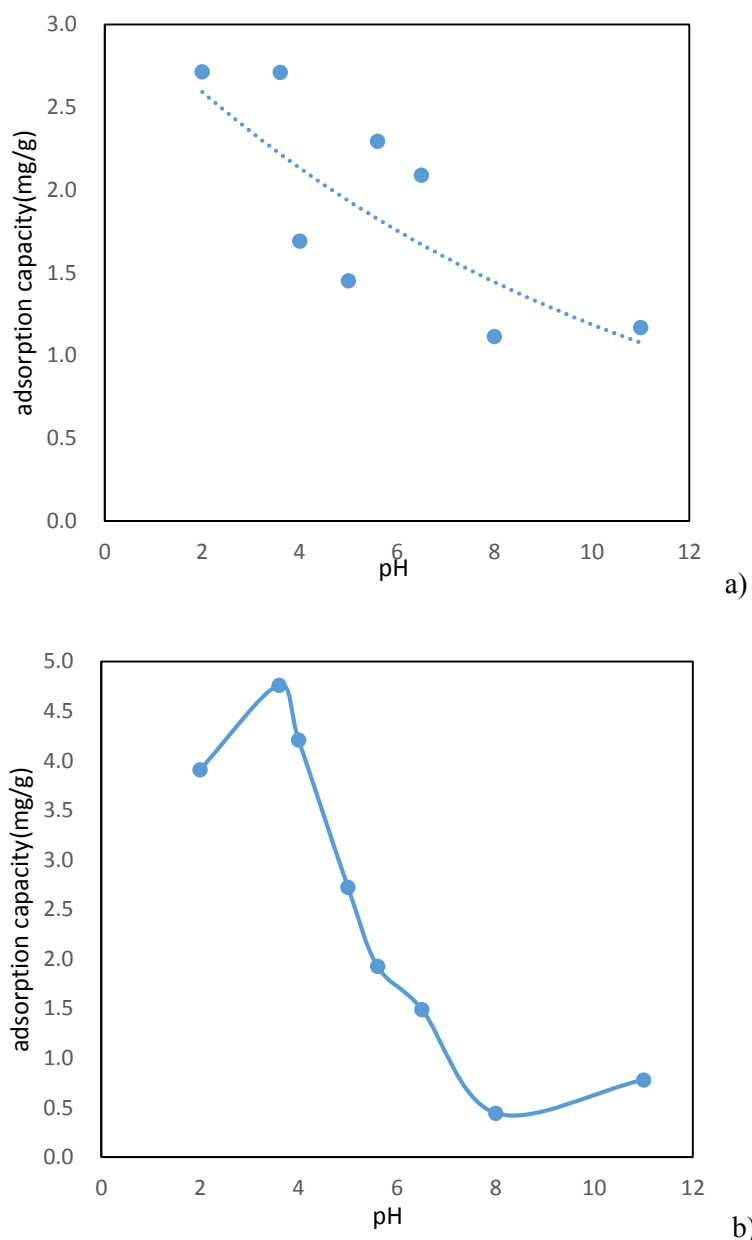
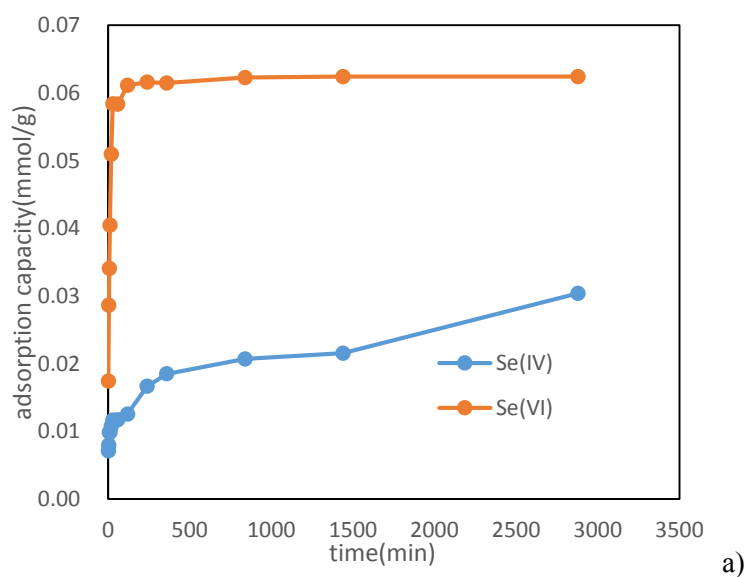


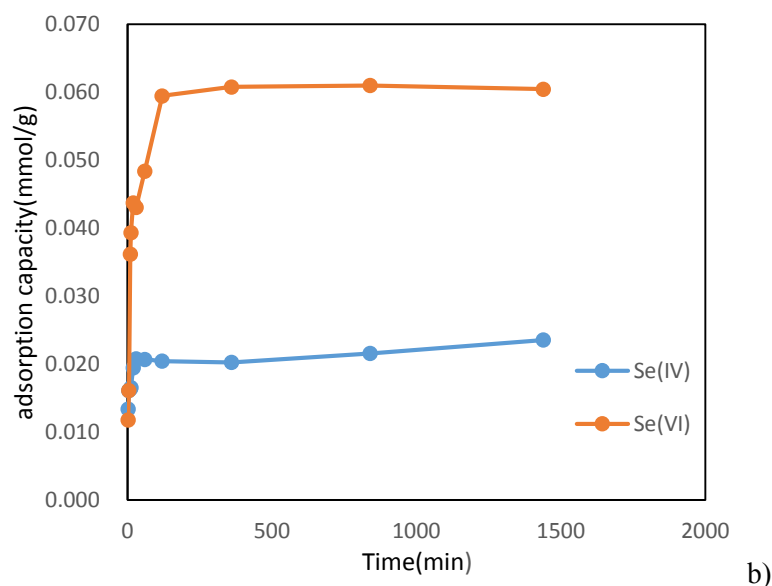
Fig 3.43 pH effect on selenite adsorption capacity, adsorbent dosage=0.005g, contact time=6h, the initial concentration of selenite is 1ppm.a) Se(IV), b) Se(VI)

3.4.3. Contact time effect on selenite and selenate adsorption

The results (shown in Fig 3.44) show that when sponge loaded with SPION as selenium adsorbent, the adsorption capacity of SPION-sponge for selenate is much higher than that for selenite. This can be interpreted as the anion exchange is more favorable to the more free anion Selenate against the Selenite less ionized. The maximum adsorption for

selenate on sponge loaded with SPION was achieved at pH 3.6 in 1 hour under 20°C and 6 hours under 70°C, respectively, while time for obtaining equilibrium of selenite on sponge loaded with SPION needs 14 hours under 20°C and 24 hours under 70°C. This result show very similar adsorption phenomenon, therefore sponge loaded with SPION have better adsorption capacity for As(V) and Se(VI) and lower adsorption capacity for As(III) and Se(IV) as a results of the different strength of related acids. The thermodynamic parameters for the sorption of Se (VI) and Se (IV) indicate exothermic behavior¹⁴⁷. Which represents the similar thermodynamic properties as those of As(V) and As(III). That means, the adsorption-desorption of Se(VI) and Se(IV) could be done by tuning of the redox potential. Since the sponge loaded SPION has much higher adsorption capacity for Se(VI) than that for Se(IV), therefore the transformation of selenite to selenate could help the adsorption happen and reduction of selenate to selenite could make the desorption to realize.





3.44 Contact time effect on selenium adsorption capacity, adsorbent dosage=0.005g, pH=2, the initial concentration of selenium is 1 ppm: a) 20°C, b) 70°C

3.4.4. Adsorption kinetic study

Pseudo second order equation was fitted to the experimental data using a non-linear regression method. This was accomplished by minimizing the respective coefficient of determination between the experimental data and predicted values¹⁸⁴. The best fit values of q_e and k_2 , along with the correlation coefficients R^2 for the selenium adsorbed by sponge loaded with SPION systems and the optimum values of the kinetic parameters are given in Table .From the linear test regression presented in Figure 3.45, it can be concluded that the experimental data fitted well the pseudo-second order kinetics. The calculated correlation coefficients were also closer to unity for pseudo second order kinetics, which indicated that chemical sorption is the rate controlling step, as expected. Therefore, the sorption can be approximated more appropriately by the pseudo second order kinetic model for the adsorption of Se (IV) and Se (VI) onto sponge loaded with SPION. The equilibrium adsorption capacity of the sponge loaded with SPION for selenate and selenite under 20oC were 0.96,1.16mg/g, respectively.

While under 70°C, the equilibrium adsorption capacity of adsorbent for selenate and selenite were 1.61, 4.94mg/g, respectively.

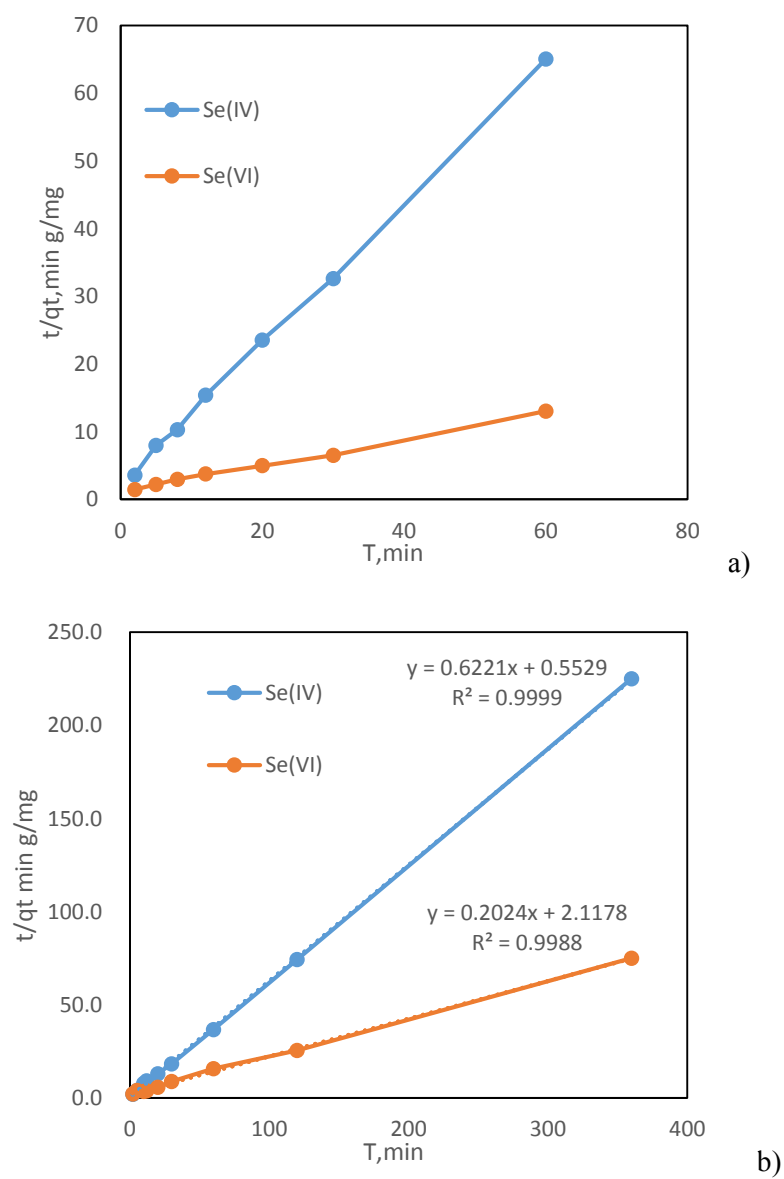


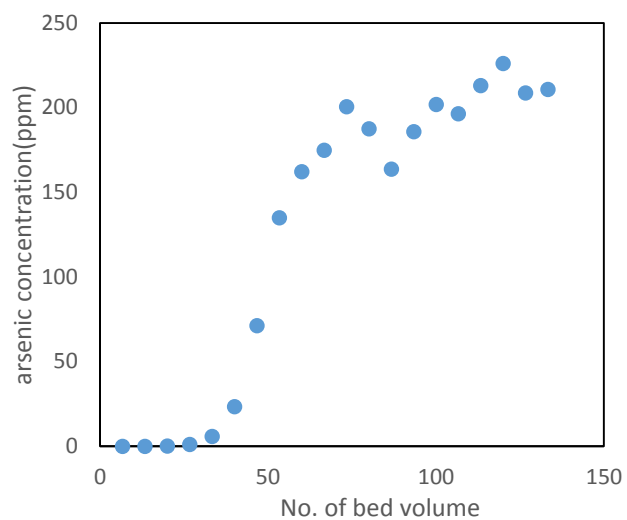
Fig3.45 The pseudo second order adsorption kinetics for the selenium adsorption by sponge loaded with SPION under (a) 20°C (b) 70°C.

Table 3.18 Pseudo-second order kinetic constants for the adsorption of selenium oxyanions on sponge loaded with SPION

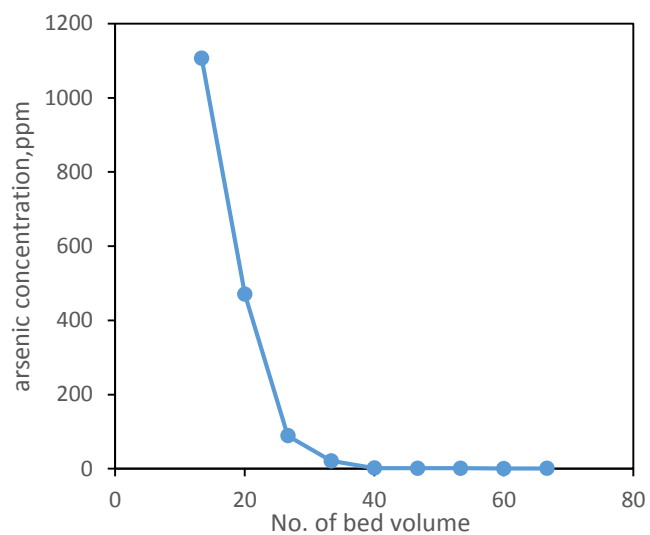
	$K_2(\text{g/mg min})$	$Q_e (\text{mg/g})$	R^2
Se(IV) 20°C	0.50	1.0	0.9991
Se(VI) 20°C	0.03	5.2	0.9954
Se(IV) 70°C	0.70	1.6	0.9999
Se(VI) 70°C	0.02	4,9	0.9988

3.4.5. Column continuous mode

The column continuous mode of Se (VI) adsorption-desorption is shown in Fig 3.46 and Fig 3.47. The adsorption-desorption behavior of Se(VI) on sponge loaded with SPION is very similar to that of As(V) on this adsorbent. The adsorption of the system is very efficient. At the beginning, the Se (VI) concentration of elute solution is about “zero”, under the detection limit of ICP-MS, which means the concentration for sure will be lower than “10ppb”. The treated water is having Se level as low as the drinking water, since it requires the standards of drinking water. After loading, the sponge loaded with SPION may be saturated of Se (VI). Under this condition, the adsorbent could be desorbed by tuning temperature or redox potential, as the same procedure as the one used before for As (V) adsorption-desorption. The desorption shows the similar behavior as those of sponge loaded with SPION for As (V) too. The desorption process was performed under high temperature condition, in our case, we use 70°C hot water for passing through the column. Once the high temperature atmosphere is stable (since we use thermometer to monitor the temperature), the desorption experiment took place.



3.46 column continuous mode study, Se (VI) adsorption in column



3.47 Column continuous mode study, Se (VI) desorption in column

Chapter IV

Conclusions

4. Conclusions

The results obtained in this work involve the development of methods to recover water contaminants by adsorption processes and to regenerate and reuse the adsorbent. Specifically, these methods are related to reagent-less processes for target pollutants removal, providing thus and added value to the contaminated water treatment. In our case, the methods concern with arsenic and selenium oxyanions removal in aqueous solution. Methods are based on sorption-desorption processes for the indicated oxyanions. Nanostructured materials have been implemented as adsorbent materials, being either iron oxide nanoparticles or aluminum oxide nanospheres the active adsorption substances. Influence of intensive thermodynamic parameters such as aqueous solution Temperature and Redox potential have been investigated. Reagent-less processes were developed, which allow the adsorption-desorption, adsorbent regeneration, are based on thermodynamic parameters tuning. Synergic interaction of thermo-tuning with redox variation will provide such results. It can be concluded that the method of synergic thermo tuning of redox potential could save amount of reagent for regenerating the adsorbent, therefore adsorbent recycling to be reused will contribute to a cost efficient process.

4.1. Concept of temperature tuning on Arsenic oxyanions adsorption-desorption by sponge loaded with SPION

4.1.1 Digital microscope has been used to observe the morphology of both the blank sponge, sponge loaded with SPION before and after adsorption of target pollutant. TEM characterization has been carried out to check the nanoparticle size and dispersion. Superparamagnetic iron oxide nanoparticles are very easy to aggregate leading to a non homogeneous distribution. After loading on the sponge, they observe homogenous dispersion on the surface of the sponge that has porous structure. SPION particle size are between 6-20nm.

4.1.2. The adsorption performance of SPION loaded sponge for arsenic oxyanions have been evaluated by using both batch and column continuous mode. It can be concluded that the sponge loaded with SPION has shown good adsorption capacity for arsenic removal. Compared with other adsorbent previously reported in the literature, they show better adsorption capacity, therefore can be considered as effective adsorbent for arsenic removal from the contaminated effluents.

4.1.3. The adsorption capacities of SPION loaded sponge for arsenate/arsenite were influenced by pH conditions of aqueous solutions, the adsorbent dosage, contact time periods, and the initial arsenic oxyanion concentration as well as temperature. The arsenic (V) oxyanion adsorption process and performance are pH dependent while arsenic (III) is not. Related anion exchange process in on the basis to this behavior, since for As(V) anionic species are present in the whole range of studied pH because of its relative strong acid properties, while for As(III) they are only present at very high pH because of the weak acid properties. In addition, the result shows that under 20°C, the maximum adsorption for arsenate on sponge-SPION was obtained in an acid media (pH 3.6) in 1 hour contact time as consequence of the arsenate acidic properties. Under 70°C, desorption process occurs as contact time increases, desorption equilibrium was then gradually achieved with 2 hours. The experimental data fitted well to the Langmuir isotherm models. The maximum adsorption capacity of SPION loaded sponge for arsenate removal by Langmuir isotherm model were 47.52mmol/g SPION on 20°C and 40.65mmol/g SPION on 70°C, respectively.

4.1.4. Thermodynamic parameters of related adsorption equilibrium have been evaluated including the equilibrium constant K_a as well as Gibbs free energy. This value shows the adsorption process to be favorable and spontaneous. The thermodynamic affinity defined by $\log K=4.198$ and $\log K=1.023$ under 20°C and 70°C were determined, respectively. Accordingly, the decrease in the negative value of ΔG° with a decrease in temperature indicates that the adsorption process of As (V) on adsorbent

becomes more favorable at lower temperatures. The enthalpy change, ΔH° , and the entropy change, ΔS° , were found to be $-122.150 \text{ kJ mol}^{-1}$ and $337 \text{ J mol}^{-1} \text{ K}^{-1}$, respectively. The negative value of ΔH° indicates that the adsorption reaction is exothermic. The positive value of ΔS° suggests that some structural changes occur on the adsorbent, and the randomness at the solid/liquid interface in the adsorption system increases during the adsorption process. Separation factor has very strong temperature dependence. Higher temperature leads to a lower separation. Arsenic is, thus, found to be more strongly adsorbed on the sponge -SPION under 20°C than that under 70°C

4.1.5. The effect of temperature on the adsorption of As (V) was also studied in the continuous column mode by evaluating the adsorption at the temperature 10°C , 20°C and 70°C . The adsorption phenomenon increases with the decrease of temperature. Compared with previous work using Fe(III) loaded sponge, SPION loaded sponge has a higher adsorption capacity for As(V) (expressed per mol of Fe on adsorbent). Thus, for SPION the maximum adsorption capacity was found to be $11.455 \text{ mmol As/ mmol Fe}$ while the Fe(III) loaded sponge the maximum adsorption capacity was of $7.32 \text{ mmol As/mmol Fe}$.

4.1.6. All of the experimental and theoretical studies indicate that we can use the lower temperature for adsorption and higher temperature for desorption, thereby it will provide a new method for recovery of toxic element and regeneration of adsorbents

4.2. Application of Synergic thermo tuning of redox potential for Arsenic removal

4.2.1. After the investigation of temperature influence on adsorption-desorption, the redox potential effect on adsorption-desorption, adsorbent regeneration has been evaluated. The potassium dichromate has been used to oxidize the As(III) to As(V)(conversion rate $>91\%$) and the Zn powder or Sn foil have been used to reduce the As(V) to As(III)(conversion rate $>90\%$). Since the adsorbent has remarkable

difference of adsorption capacity between As (V) and As (III), the adsorption-desorption can be controlled by changing the oxidation state of As. For example, the adsorbent can adsorb the arsenic by oxidizing all of the As (III) to As (V) and desorb the arsenic by reducing the As (V) to As(III).

4.2.2. The sponge-SPION provides higher probability to interact with arsenate than arsenite and react by anion exchange to the adsorption system. Thus arsenate has much higher adsorption rate than arsenite. By changing the redox potential, the transform between As(V) and As(III) will lead the adsorption-desorption process and cycling use of the adsorbent. At the same time, the thermo tuning can help the adsorption-desorption to be much more significant and much quicker.

4.2.3. Column experiments by using sponge-SPION presents an adsorption capacity of 0.167mmol/g sponge (21.64mmol/g SPION), almost twice of the obtained in batch mode using the same sample.

4.2.4. Different dosage of adsorbent have revealed the adsorbent to be homogenous.

4.2.5. The results reflect that both temperature-controlling and reduction-tuning method could make an efficient desorption process. The recovery rate of the arsenic adsorbed in the sponge-SPION is high, showing 96.52% and 85.64% for temperature tuning method and redox potential tuning method, respectively.

4.2.6. Once finishing the desorption process, the adsorbent can be used again for adsorb arsenic oxyanions under room temperature. And then desorb the arsenic oxyanions by using the reducing agent under 70°C again. The recycled method can be both technical and economically efficient.

4.2.7. The real waste water treatment process reveal that almost all the arsenic present in the first 50mL has been adsorbed in the SPION loaded sponge, although it has a lot of interference elements. The calculated sponge capacity is about 1.25mmol As (V)/ g

SPION, considerable lower than in the synthetic solutions that is due to the interfering ions present in the waste water.

4.3. Kinetic and Dynamic Aspects of Selenate and selenite adsorption by γ -Al₂O₃ nanospheres

4.3.1. SEM images of fresh γ -Al₂O₃ nanospheres indicate that the material is composed of individual, hollow-spherical particles ranging in size from 200 to 400nm that form aggregates and chains. This small γ -Al₂O₃ nanospheres provides a larger surface area for contaminant adsorption. The adsorption of selenium on the γ -Al₂O₃ nanospheres did not influence the structure of the nanospheres.

4.3.2. Under 20°C, the maximum adsorption for selenate and selenite on γ -Al₂O₃ nanospheres was achieved at pH 2 in 6 hours, the adsorption of selenium presents an hydrogen bridge forming complex, decreasing at higher pH values. In the case of Se (VI) the sorption decreases as the percentage of the aqueous species HSeO₄⁻ decreases. While for 70°C, the maximum adsorption was attained in 14 hours. The kinetic studies show that they are fitted very well to the pseudo-second order, this suggests that selenium ions were adsorbed onto the aluminum nanosphere surface via chemical interaction. The adsorption of γ -Al₂O₃ nanosphere for selenate and selenite were fitted very well to Freundlich isotherm model, which is indicated that the γ -Al₂O₃ nanosphere as adsorbent was multilayer coverage by selenium. The ΔH value of Se (IV) and Se (VI) between 20°C and 70°C were -13.955 KJ mol⁻¹ and -3.927 KJ mol⁻¹ shows that lower temperature favor removal of selenium.

4.3.3. It has demonstrated that Diethylammonium N,N-diethyldithiocarbamate DDC modified γ -Al₂O₃ nanosphere has higher adsorption capacity for selenate. However, during the pH range of 2.8-6.0, the γ -Al₂O₃ nanosphere has higher adsorption capacity for selenite than adsorption capacity of DDC modified γ -Al₂O₃ nanosphere for selenite.

When $\text{pH} > 6.0$, the phenomenon is opposite, the $\gamma\text{-Al}_2\text{O}_3$ nanosphere has lower adsorption capacity for selenite than that of DDC modified $\gamma\text{-Al}_2\text{O}_3$ nanosphere for selenite. The adsorption is occurring through a hydrogen bridge formation and it is coherent with the behavior against the pH.

4.4. Kinetic and continuous mode Aspects of selenate and selenite adsorption by sponge loaded with SPION

4.4.1. The SEM images shows that the sponge is porous and the SPION is impregnated to penetrate inside of the sponge pores providing a complete SPION layer on the sponge surface. In addition, the images reveal the surface texture and porosity of the blank and loaded sponge¹⁸⁴¹⁸⁴. It can be seen that the surface texture of the blank adsorbents changes drastically after the loading of SPION

4.4.2. The adsorption capacity of SPION-sponge for selenate is much higher than that for selenite. The maximum adsorption for selenate and selenite on sponge loaded with SPION was achieved at pH 3.6 in 1 hour under 20°C and 6 hours under 70°C, respectively, while time for obtaining equilibrium of selenite needs 14 hours under 20°C and 24 hours under 70°C. This result show very similar adsorption phenomenon, therefore sponge loaded with SPION have better adsorption capacity for Se(VI) and lower adsorption capacity for Se(IV).

4.4.3. The selenium continuous column mode experiment show very similar adsorption-desorption properties by using sponge-SPION as adsorbent for arsenic. Therefore it can be concluded that selenium adsorption by SPION loaded sponge represent the same temperature-dependence effect on adsorption process while the selenate/selenite adsorption by sponge-SPION gives the same temperature impact and redox potential effect as those with a rsenate/arsenite adsorption properties by sponge-SPION.

Future perspective

Considering the work included in the PhD thesis, the future research will be focused on arsenic removal from the real waste water, which contains a lot of interference elements. The problem should be solved in order to treat the real industrial contaminated aqueous solution. The application of synergic thermo and redox potential tuning method for recovering the metal and regenerating the adsorbent will be done under big continuous mode for industrial water treatment, such as mining industry. The pilot plant should be built up in order to analyze the adsorption-desorption processes and to confirm the thermodynamic parameters tuning for the metal recovery and adsorbent regeneration and reuse.

For the selenium adsorption, chemical modification, or combined with the formation of new functional groups will improve the adsorption capacity of γ - Al_2O_3 nanospheres, such as thiol groups. In addition, the interference ions effect on selenium removal efficiency and adsorption capacity will be investigated. The concept of temperature controlling and redox potential tuning for adsorbent regeneration will be applied to selenium adsorption. The competing adsorption capacity of arsenic and selenium from the combined aqueous solution which contain both arsenic and selenium will be studied.

The regeneration and reuse of the adsorbent should be further studied, pilot plant for the waste water treatment should be built in order to apply the temperature and redox potential tuning for toxic oxyanions removal.

The direct speciation method by using the synchrotron radiation techniques will be applied to analyze the sponge loaded SPION for $\text{As(V)}/\text{As(III)}$ and γ - Al_2O_3 nanospheres for Se(IV) and Se(VI)

References

1. Sun, H.-J.; Rathinasabapathi, B.; Wu, B.; Luo, J.; Pu, L.-P.; Ma, L. Q., Arsenic and selenium toxicity and their interactive effects in humans. *Environment international* **2014**, *69*, 148-158.
2. Yang, L.; Shahrivari, Z.; Liu, P. K.; Sahimi, M.; Tsotsis, T. T., Removal of trace levels of arsenic and selenium from aqueous solutions by calcined and uncalcined layered double hydroxides (LDH). *Industrial & Engineering Chemistry Research* **2005**, *44* (17), 6804-6815.
3. Scott, M. J., Kinetics of adsorption and redox processes on iron and manganese oxides: reactions of As (III) and Se (IV) at goethite and birnessite surfaces. **1991**.
4. Goh, K.-H.; Lim, T.-T., Geochemistry of inorganic arsenic and selenium in a tropical soil: effect of reaction time, pH, and competitive anions on arsenic and selenium adsorption. *Chemosphere* **2004**, *55* (6), 849-859.
5. Zaspalis, V.; Pagana, A.; Sklari, S., Arsenic removal from contaminated water by iron oxide sorbents and porous ceramic membranes. *Desalination* **2007**, *217* (1-3), 167-180.
6. Choong, T. S. Y.; Chuah, T. G.; Robiah, Y.; Gregory Koay, F. L.; Azni, I., Arsenic toxicity, health hazards and removal techniques from water: an overview. *Desalination* **2007**, *217* (1-3), 139-166.
7. Bissen, M.; Frimmel, F. H., Arsenic—a review. Part I: occurrence, toxicity, speciation, mobility. *Acta hydrochimica et hydrobiologica* **2003**, *31* (1), 9-18.
8. Zelmanov, G.; Semiat, R., Selenium removal from water and its recovery using iron (Fe³⁺) oxide/hydroxide-based nanoparticles sol (NanoFe) as an adsorbent. *Separation and Purification Technology* **2013**, *103*, 167-172.
9. El-Shafey, E., Sorption of Cd (II) and Se (IV) from aqueous solution using modified rice husk. *Journal of hazardous materials* **2007**, *147* (1), 546-555.
10. Clarke, S. E.; White, D.; Schaedel, A. L., Oregon, USA, ecological regions and subregions for water quality management. *Environmental Management* **1991**, *15* (6), 847-856.
11. Mohan, D.; Pittman, C. U., Arsenic removal from water/wastewater using adsorbents—a critical review. *Journal of hazardous materials* **2007**, *142* (1), 1-53.
12. Londesborough, S.; Mattusch, J.; Wennrich, R., Separation of organic and inorganic arsenic species by HPLC-ICP-MS. *Fresenius' journal of analytical chemistry* **1999**, *363* (5-6), 577-581.
13. Tchounwou, P., Development of Public Health Advisories for Arsenic in Drinking Water. *Reviews on environmental health* **1999**, *14* (4), 211-230.
14. Moon, K.; Guallar, E.; Navas-Acien, A., Arsenic exposure and cardiovascular disease: an updated systematic review. *Current atherosclerosis reports* **2012**, *14* (6), 542-555.
15. Jain, C.; Ali, I., Arsenic: occurrence, toxicity and speciation techniques. *Water research* **2000**, *34* (17), 4304-4312.
16. Ferguson, J. F.; Gavis, J., A review of the arsenic cycle in natural waters. *Water research* **1972**, *6* (11), 1259-1274.
17. Ensafi, A. A.; Ring, A. C.; Fritsch, I., Highly Sensitive Voltammetric Speciation and Determination of Inorganic Arsenic in Water and Alloy Samples Using Ammonium 2- Amino- 1- Cyclopentene- 1- Dithiocarboxylate. *Electroanalysis* **2010**, *22* (11), 1175-1185.
18. Wu, Y.; Zhan, S.; Wang, F.; He, L.; Zhi, W.; Zhou, P., Cationic polymers and aptamers mediated aggregation of gold nanoparticles for the colorimetric detection of arsenic (III) in aqueous solution. *Chemical communications* **2012**, *48* (37), 4459-4461.

19. Zhang, P.; Sparks, D. L., Kinetics of selenate and selenite adsorption/desorption at the goethite/water interface. *Environmental Science & Technology* **1990**, *24* (12), 1848-1856.
20. Rosenfeld, I.; Beath, O. A., *Selenium: geobotany, biochemistry, toxicity, and nutrition*. Academic Press: 2013.
21. Goldhaber, S. B., Trace element risk assessment: essentiality vs. toxicity. *Regulatory Toxicology and Pharmacology* **2003**, *38* (2), 232-242.
22. Min, J. H.; Hering, J. G., Removal of selenite and chromate using iron (III)-doped alginate gels. *Water environment research* **1999**, *71* (2), 169-175.
23. Sheoran, A.; Sheoran, V., Heavy metal removal mechanism of acid mine drainage in wetlands: a critical review. *Minerals engineering* **2006**, *19* (2), 105-116.
24. McLennan, S.; Taylor, S., The continental crust: its composition and evolution. *An Examination of the Geochemical Record Preserved in Sedimentary Rocks*, Oxford, Blackwell Scientific, Palo Alto, Calif **1985**.
25. Mackenzie, F. T.; Lantzy, R. J.; Paterson, V., Global trace metal cycles and predictions. *Journal of the International Association for Mathematical Geology* **1979**, *11* (2), 99-142.
26. Merian, E., *Metals and their compounds in the environment: occurrence, analysis and biological relevance*. VCH Verlagsgesellschaft mbH: 1991.
27. Košutić, K.; Furač, L.; Sipos, L.; Kunst, B., Removal of arsenic and pesticides from drinking water by nanofiltration membranes. *Separation and Purification Technology* **2005**, *42* (2), 137-144.
28. Chapman, P. M.; Adams, W. J.; Brooks, M.; Delos, C. G.; Luoma, S. N.; Maher, W. A.; Ohlendorf, H. M.; Presser, T. S.; Shaw, P., *Ecological assessment of selenium in the aquatic environment*. CRC Press: 2010.
29. Fordyce, F. M., *Selenium deficiency and toxicity in the environment*. Springer: 2013.
30. Stolz, J. F.; Basu, P.; Santini, J. M.; Oremland, R. S., Arsenic and Selenium in Microbial Metabolism*. *Annu. Rev. Microbiol.* **2006**, *60*, 107-130.
31. Nriagu, J. O., *Arsenic in the environment: Part I: Cycling and characterization*. J. Wiley: 1994.
32. Clifford, D.; Lin, C.-C. In *Ion exchange, activated alumina, and membrane processes for arsenic removal from groundwater*, Proceedings of the 45th Annual Environmental Engineering Conference, University of Kansas, 1995.
33. Morillo Martín, D.; Valiente Malmagro, M.; Pérez González, G., Superparamagnetic iron oxide nanoparticles as arsenic adsorbent. **2014**.
34. Scott, M. J.; Morgan, J. J., Reactions at oxide surfaces. 1. Oxidation of As (III) by synthetic birnessite. *Environmental Science & Technology* **1995**, *29* (8), 1898-1905.
35. Wood, S. A.; Tait, C. D.; Janecky, D. R., A Raman spectroscopic study of arsenite and thioarsenite species in aqueous solution at 25 C. *Geochemical Transactions* **2002**, *3* (4), 31.
36. Muñoz, J. A.; Gonzalo, A.; Valiente, M., Arsenic adsorption by Fe (III)-loaded open-celled cellulose sponge. Thermodynamic and selectivity aspects. *Environmental science & technology* **2002**, *36* (15), 3405-3411.
37. Elleouet, C.; Quentel, F.; Madec, C., Determination of inorganic and organic selenium species in natural waters by cathodic stripping voltammetry. *Water research* **1996**, *30* (4), 909-914.
38. Peak, D.; Sparks, D., Mechanisms of selenate adsorption on iron oxides and hydroxides. *Environmental science & technology* **2002**, *36* (7), 1460-1466.
39. Shriver, D. F.; Atkins, P. W.; Langford, C. H., *Química inorgánica. II*. Reverté: 1998; Vol. 2.

40. Peak, D., Adsorption mechanisms of selenium oxyanions at the aluminum oxide/water interface. *Journal of colloid and interface science* **2006**, *303* (2), 337-345.
41. Blaylock, M. J.; James, B. R., Redox transformations and plant uptake of selenium resulting from root-soil interactions. *Plant and soil* **1994**, *158* (1), 1-12.
42. Misra, M.; Nayak, D. C., Process for removal of selenium and arsenic from aqueous streams. Google Patents: 1997.
43. Misra, M.; Nanor, J.; Priyadarshan, G., Process for removal and stabilization of arsenic and selenium from aqueous streams and slurries. Google Patents: 2001.
44. O'Neill, G. A.; Novak, J. W.; Martin, E. S., Method for removing arsenic or selenium from an aqueous solution containing a substantial background of another contaminant. Google Patents: 1990.
45. Jeon, C. S.; Baek, K.; Park, J. K.; Oh, Y. K.; Lee, S. D., Adsorption characteristics of As(V) on iron-coated zeolite. *Journal of hazardous materials* **2009**, *163* (2-3), 804-8.
46. Kartinen, E. O.; Martin, C. J., An overview of arsenic removal processes. *Desalination* **1995**, *103* (1), 79-88.
47. Masscheleyn, P. H.; Delaune, R. D.; Patrick Jr, W. H., Effect of redox potential and pH on arsenic speciation and solubility in a contaminated soil. *Environmental Science & Technology* **1991**, *25* (8), 1414-1419.
48. Ruthven, D. M., *Principles of adsorption and adsorption processes*. John Wiley & Sons: 1984.
49. Mills, G.; Jónsson, H., Quantum and thermal effects in H₂ dissociative adsorption: Evaluation of free energy barriers in multidimensional quantum systems. *Physical review letters* **1994**, *72* (7), 1124.
50. Manning, B. A.; Goldberg, S., Modeling competitive adsorption of arsenate with phosphate and molybdate on oxide minerals. *Soil Science Society of America Journal* **1996**, *60* (1), 121-131.
51. Xu, Y.-h.; Nakajima, T.; Ohki, A., Adsorption and removal of arsenic (V) from drinking water by aluminum-loaded Shirasu-zeolite. *Journal of hazardous materials* **2002**, *92* (3), 275-287.
52. Tokunaga, S.; Wasay, S. A.; Park, S.-W., Removal of arsenic (V) ion from aqueous solutions by lanthanum compounds. *Water Science and Technology* **1997**, *35* (7), 71-78.
53. Diamadopoulos, E.; Ioannidis, S.; Sakellariopoulos, G. P., As (V) removal from aqueous solutions by fly ash. *Water research* **1993**, *27* (12), 1773-1777.
54. Elizalde-González, M.; Mattusch, J.; Einicke, W.-D.; Wennrich, R., Sorption on natural solids for arsenic removal. *Chemical Engineering Journal* **2001**, *81* (1), 187-195.
55. Fendorf, S.; Eick, M. J.; Grossl, P.; Sparks, D. L., Arsenate and chromate retention mechanisms on goethite. 1. Surface structure. *Environmental science & technology* **1997**, *31* (2), 315-320.
56. Giménez, J.; Martínez, M.; de Pablo, J.; Rovira, M.; Duro, L., Arsenic sorption onto natural hematite, magnetite, and goethite. *Journal of hazardous materials* **2007**, *141* (3), 575-580.
57. Richmond, W. R.; Loan, M.; Morton, J.; Parkinson, G. M., Arsenic removal from aqueous solution via ferrihydrite crystallization control. *Environmental science & technology* **2004**, *38* (8), 2368-2372.
58. Zeng, L., A method for preparing silica-containing iron (III) oxide adsorbents for arsenic removal. *Water research* **2003**, *37* (18), 4351-4358.
59. Payne, K. B.; Abdel-Fattah, T. M., Adsorption of arsenate and arsenite by iron-treated activated carbon and zeolites: effects of pH, temperature, and ionic strength. *Journal of Environmental Science and Health* **2005**, *40* (4), 723-749.
60. Zhang, Y.; Yang, M.; Huang, X., Arsenic (V) removal with a Ce (IV)-doped iron oxide adsorbent. *Chemosphere* **2003**, *51* (9), 945-952.

61. Joshi, A.; Chaudhuri, M., Removal of arsenic from ground water by iron oxide-coated sand. *Journal of environmental engineering* **1996**, *122* (8), 769-771.
62. Meng, X.; Bang, S.; Korfiatis, G. P., Effects of silicate, sulfate, and carbonate on arsenic removal by ferric chloride. *Water research* **2000**, *34* (4), 1255-1261.
63. Min, J. H.; Hering, J. G., Arsenate sorption by Fe (III)-doped alginate gels. *Water research* **1998**, *32* (5), 1544-1552.
64. Chandra, V.; Park, J.; Chun, Y.; Lee, J. W.; Hwang, I.-C.; Kim, K. S., Water-dispersible magnetite-reduced graphene oxide composites for arsenic removal. *ACS nano* **2010**, *4* (7), 3979-3986.
65. Katsoyiannis, I. A.; Zouboulis, A. I., Removal of arsenic from contaminated water sources by sorption onto iron-oxide-coated polymeric materials. *Water research* **2002**, *36* (20), 5141-5155.
66. Rau, I.; Gonzalo, A.; Valiente, M., Arsenic (V) removal from aqueous solutions by iron (III) loaded chelating resin. *Journal of Radioanalytical and Nuclear Chemistry* **2000**, *246* (3), 597-600.
67. Saiz, J.; Bringas, E.; Ortiz, I., Functionalized magnetic nanoparticles as new adsorption materials for arsenic removal from polluted waters. *Journal of Chemical Technology and Biotechnology* **2014**, *89* (6), 909-918.
68. Gupta, A.; Chauhan, V. S.; Sankararamakrishnan, N., Preparation and evaluation of iron–chitosan composites for removal of As (III) and As (V) from arsenic contaminated real life groundwater. *Water research* **2009**, *43* (15), 3862-3870.
69. Hlavay, J.; Polyák, K., Determination of surface properties of iron hydroxide-coated alumina adsorbent prepared for removal of arsenic from drinking water. *Journal of colloid and interface science* **2005**, *284* (1), 71-77.
70. Sari, A.; Uluozlü, Ö. D.; Tüzen, M., Equilibrium, thermodynamic and kinetic investigations on biosorption of arsenic from aqueous solution by algae (*Maugeotia genuflexa*) biomass. *Chemical Engineering Journal* **2011**, *167* (1), 155-161.
71. Chen, W.; Parette, R.; Zou, J.; Cannon, F. S.; Dempsey, B. A., Arsenic removal by iron-modified activated carbon. *Water research* **2007**, *41* (9), 1851-1858.
72. Maliyekkal, S. M.; Philip, L.; Pradeep, T., As (III) removal from drinking water using manganese oxide-coated-alumina: performance evaluation and mechanistic details of surface binding. *Chemical Engineering Journal* **2009**, *153* (1), 101-107.
73. Kim, Y.; Kim, C.; Choi, I.; Rengaraj, S.; Yi, J., Arsenic removal using mesoporous alumina prepared via a templating method. *Environmental science & technology* **2004**, *38* (3), 924-931.
74. Matsunaga, H.; Yokoyama, T.; Eldridge, R. J.; Bolto, B. A., Adsorption characteristics of arsenic (III) and arsenic (V) on iron (III)-loaded chelating resin having lysine-N α , N α -diacetic acid moiety. *Reactive and functional polymers* **1996**, *29* (3), 167-174.
75. Cao, C.-Y.; Qu, J.; Yan, W.-S.; Zhu, J.-F.; Wu, Z.-Y.; Song, W.-G., Low-cost synthesis of flowerlike α -Fe₂O₃ nanostructures for heavy metal ion removal: adsorption property and mechanism. *Langmuir : the ACS journal of surfaces and colloids* **2012**, *28* (9), 4573-4579.
76. Tuutijärvi, T.; Lu, J.; Sillanpää, M.; Chen, G., As (V) adsorption on maghemite nanoparticles. *Journal of hazardous materials* **2009**, *166* (2), 1415-1420.
77. Hsia, T.-H.; Lo, S.-L.; Lin, C.-F.; Lee, D.-Y., Characterization of arsenate adsorption on hydrous iron oxide using chemical and physical methods. *Colloids and Surfaces A: Physicochemical and Engineering Aspects* **1994**, *85* (1), 1-7.

78. Sun, Y.-P.; Li, X.-Q.; Zhang, W.-X.; Wang, H. P., A method for the preparation of stable dispersion of zero-valent iron nanoparticles. *Colloids and Surfaces A: Physicochemical and Engineering Aspects* **2007**, *308* (1), 60-66.
79. Pradeep, T., Noble metal nanoparticles for water purification: a critical review. *Thin solid films* **2009**, *517* (24), 6441-6478.
80. Chowdhury, S. R.; Yanful, E. K., Arsenic and chromium removal by mixed magnetite–maghemite nanoparticles and the effect of phosphate on removal. *Journal of environmental management* **2010**, *91* (11), 2238-2247.
81. Cao, C.-Y.; Qu, J.; Wei, F.; Liu, H.; Song, W.-G., Superb adsorption capacity and mechanism of flowerlike magnesium oxide nanostructures for lead and cadmium ions. *ACS applied materials & interfaces* **2012**, *4* (8), 4283-4287.
82. Morillo, D.; Uheida, A.; Pérez, G.; Muhammed, M.; Valiente, M., Arsenate removal with 3-mercaptopropanoic acid-coated superparamagnetic iron oxide nanoparticles. *Journal of colloid and interface science* **2015**, *438*, 227-234.
83. Xu, P.; Zeng, G. M.; Huang, D. L.; Feng, C. L.; Hu, S.; Zhao, M. H.; Lai, C.; Wei, Z.; Huang, C.; Xie, G. X., Use of iron oxide nanomaterials in wastewater treatment: a review. *Science of the Total Environment* **2012**, *424*, 1-10.
84. Feng, L.; Cao, M.; Ma, X.; Zhu, Y.; Hu, C., Corrigendum to “Superparamagnetic high-surface-area Fe₃O₄ nanoparticles as adsorbents for arsenic removal”[*J. Hazard. Mater.* 217–218 (2012) 439–446]. *Journal of hazardous materials* **2012**, (227-228), 484.
85. Mondal, K.; Jegadeesan, G.; Lalvani, S. B., Removal of selenate by Fe and NiFe nanosized particles. *Industrial & engineering chemistry research* **2004**, *43* (16), 4922-4934.
86. Sanguansri, P.; Augustin, M. A., Nanoscale materials development—a food industry perspective. *Trends in Food Science & Technology* **2006**, *17* (10), 547-556.
87. Salamanca-Buentello, F.; Persad, D. L.; Court, E. B.; Martin, D. K.; Daar, A. S.; Singer, P. A., Nanotechnology and the developing world. *PLoS Medicine* **2005**, *2* (5), 383.
88. (a) Gupta, A. K.; Gupta, M., Synthesis and surface engineering of iron oxide nanoparticles for biomedical applications. *Biomaterials* **2005**, *26* (18), 3995-4021; (b) Moghimi, S. M.; Hunter, A. C.; Murray, J. C., Long-circulating and target-specific nanoparticles: theory to practice. *Pharmacological reviews* **2001**, *53* (2), 283-318.
89. Theron, J.; Walker, J. A.; Cloete, T. E., Nanotechnology and water treatment: applications and emerging opportunities. *Critical reviews in microbiology* **2008**, *34* (1), 43-69.
90. Mahmoudi, M.; Laurent, S.; Shokrgozar, M. A.; Hosseinkhani, M., Toxicity evaluations of superparamagnetic iron oxide nanoparticles: cell “vision” versus physicochemical properties of nanoparticles. *ACS nano* **2011**, *5* (9), 7263-7276.
91. Martin, C. R.; Mitchell, D. T., Peer reviewed: nanomaterials in analytical chemistry. *Analytical chemistry* **1998**, *70* (9), 322A-327A.
92. Hristovski, K.; Baumgardner, A.; Westerhoff, P., Selecting metal oxide nanomaterials for arsenic removal in fixed bed columns: from nanopowders to aggregated nanoparticle media. *Journal of hazardous materials* **2007**, *147* (1), 265-274.
93. Mahmoudi, M.; Sant, S.; Wang, B.; Laurent, S.; Sen, T., Superparamagnetic iron oxide nanoparticles (SPIONs): development, surface modification and applications in chemotherapy. *Advanced drug delivery reviews* **2011**, *63* (1), 24-46.

94. Alonso González, A.; Muñoz Tapia, M.; Muraviev, D., Development of polymeric nanocomposites with enhanced distribution of catalytically active or bactericide nanoparticles. **2012**.
95. Spanier, J. E.; Robinson, R. D.; Zhang, F.; Chan, S.-W.; Herman, I. P., Size-dependent properties of CeO₂-y nanoparticles as studied by Raman scattering. *Physical Review B* **2001**, *64* (24), 245407.
96. Auffan, M.; Rose, J.; Bottero, J.-Y.; Lowry, G. V.; Jolivet, J.-P.; Wiesner, M. R., Towards a definition of inorganic nanoparticles from an environmental, health and safety perspective. *Nature nanotechnology* **2009**, *4* (10), 634-641.
97. Salata, O. V., Applications of nanoparticles in biology and medicine. *Journal of nanobiotechnology* **2004**, *2* (1), 3.
98. Carnes, C. L.; Klabunde, K. J., Synthesis, isolation, and chemical reactivity studies of nanocrystalline zinc oxide. *Langmuir : the ACS journal of surfaces and colloids* **2000**, *16* (8), 3764-3772.
99. Nata, I. F.; Sureshkumar, M.; Lee, C.-K., One-pot preparation of amine-rich magnetite/bacterial cellulose nanocomposite and its application for arsenate removal. *RSC Advances* **2011**, *1* (4), 625-631.
100. Yu, X.; Tong, S.; Ge, M.; Zuo, J.; Cao, C.; Song, W., One-step synthesis of magnetic composites of cellulose@ iron oxide nanoparticles for arsenic removal. *Journal of Materials Chemistry A* **2013**, *1* (3), 959-965.
101. Afkhami, A.; Saber-Tehrani, M.; Bagheri, H., Modified maghemite nanoparticles as an efficient adsorbent for removing some cationic dyes from aqueous solution. *Desalination* **2010**, *263* (1), 240-248.
102. Kodama, R., Magnetic nanoparticles. *Journal of magnetism and magnetic materials* **1999**, *200* (1), 359-372.
103. Pankhurst, Q. A.; Connolly, J.; Jones, S.; Dobson, J., Applications of magnetic nanoparticles in biomedicine. *Journal of physics D: Applied physics* **2003**, *36* (13), R167.
104. hysteresis loop of a ferromagnetic material. <http://what-when-how.com/electronic-properties-of-materials/magnetic-phenomena-and-their-interpretationclassical-approach-magnetic-properties-of-materials-part-1/>.
105. Lu, A. H.; Salabas, E. e. L.; Schüth, F., Magnetic nanoparticles: synthesis, protection, functionalization, and application. *Angewandte Chemie International Edition* **2007**, *46* (8), 1222-1244.
106. Mishima, N.; Petrosky, T. Y.; Minowa, H.; Goto, S., Model experiment of two- dimensional Brownian motion by microcomputer. *American Journal of Physics* **1980**, *48* (12), 1050-1055.
107. Shen, T.; Weissleder, R.; Papisov, M.; Bogdanov, A.; Brady, T. J., Monocrystalline iron oxide nanocompounds (MION): physicochemical properties. *Magnetic Resonance in Medicine* **1993**, *29* (5), 599-604.
108. Gittleman, J.; Abeles, B.; Bozowski, S., Superparamagnetism and relaxation effects in granular Ni-Si O₂ and Ni-Al₂ O₃ films. *Physical review B* **1974**, *9* (9), 3891.
109. Ren, T.-Z.; Yuan, Z.-Y.; Su, B.-L., Microwave-assisted preparation of hierarchical mesoporous-macroporous boehmite AlOOH and γ -Al₂O₃. *Langmuir : the ACS journal of surfaces and colloids* **2004**, *20* (4), 1531-1534.
110. Hu, Y.; Li, C.; Gu, F.; Ma, J., Preparation and formation mechanism of alumina hollow nanospheres via high-speed jet flame combustion. *Industrial & Engineering Chemistry Research* **2007**, *46* (24), 8004-8008.
111. Zhang, L.; Zhu, Y.-J., Microwave-assisted solvothermal synthesis of AlOOH hierarchically nanostructured microspheres and their transformation to γ -Al₂O₃ with similar morphologies. *The Journal of Physical Chemistry C* **2008**, *112* (43), 16764-16768.

112. Van Bruggen, M., Preparation and properties of colloidal core-shell rods with adjustable aspect ratios. *Langmuir : the ACS journal of surfaces and colloids* **1998**, *14* (9), 2245-2255.
113. Feng, Y.; Lu, W.; Zhang, L.; Bao, X.; Yue, B.; Lv, Y.; Shang, X., One-step synthesis of hierarchical cantaloupe-like ALOOH superstructures via a hydrothermal route. *Crystal Growth and Design* **2008**, *8* (4), 1426-1429.
114. Lu, C.; Lv, J.; Xu, L.; Guo, X.; Hou, W.; Hu, Y.; Huang, H., Crystalline nanotubes of γ -AlOOH and γ -Al₂O₃: hydrothermal synthesis, formation mechanism and catalytic performance. *Nanotechnology* **2009**, *20* (21), 215604.
115. Tang, B.; Ge, J.; Zhuo, L.; Wang, G.; Niu, J.; Shi, Z.; Dong, Y., A Facile and Controllable Synthesis of γ -Al₂O₃ Nanostructures without a Surfactant. *European journal of inorganic chemistry* **2005**, *2005* (21), 4366-4369.
116. Zhang, M.; Lu, Y.; Chen, J.-F.; Zhang, T.-K.; Liu, Y.-Y.; Yang, Y.; Yao, W.-T.; Yu, S.-H., Selective Synthesis of Zn_{1-x}Mn_xSe Nanobelts and Nanotubes from [Zn_{1-x}Mn_xSe](DETA) 0.5 Nanobelts in Solution (x= 0– 0.15) and Their EPR and Optical Properties. *Langmuir : the ACS journal of surfaces and colloids* **2010**, *26* (15), 12882-12889.
117. Zhu, H. Y.; Riches, J. D.; Barry, J. C., γ -alumina nanofibers prepared from aluminum hydrate with poly (ethylene oxide) surfactant. *Chemistry of Materials* **2002**, *14* (5), 2086-2093.
118. Ma, D.; Zhang, J.; Hu, X.; Zhou, H.; Qian, Y., Surfactant-assisted hydrothermal route to organometallic tris (8-hydroxyquinoline) aluminum nanorod bundles. *Chemistry Letters* **2007**, *36* (5), 630-631.
119. Hazama, K.; Nakamura, Y.; Nittono, O., Growth of aluminum whiskers below the melting point of aluminum. *Japanese journal of applied physics* **1988**, *27* (7R), 1142.
120. Zhang, H.; Zhang, L.; Han, L.; Shen, S.; Lu, W., Synthesis, Characterization and Growth Mechanism of Hierarchical Cantaloupe-Like ALOOH Superstructures by a Simple Hydrothermal Process. *Integrated Ferroelectrics* **2011**, *129* (1), 111-121.
121. Kuang, D.; Fang, Y.; Liu, H.; Frommen, C.; Fenske, D., Fabrication of boehmite ALOOH and γ -Al₂O₃ nanotubes via a soft solution route. *Journal of Materials Chemistry* **2003**, *13* (4), 660-662.
122. Rong, C.-b.; Li, D.; Nandwana, V.; Poudyal, N.; Ding, Y.; Wang, Z. L.; Zeng, H.; Liu, J. P., Size-dependent chemical and magnetic ordering in L10-FePt nanoparticles. *Advanced Materials* **2006**, *18* (22), 2984-2988.
123. Luther, S.; Borgfeld, N.; Kim, J.; Parsons, J., Removal of arsenic from aqueous solution: a study of the effects of pH and interfering ions using iron oxide nanomaterials. *Microchemical Journal* **2012**, *101*, 30-36.
124. Wu, Z.; Li, W.; Webley, P. A.; Zhao, D., General and controllable synthesis of novel mesoporous magnetic iron oxide@ carbon encapsulates for efficient arsenic removal. *Advanced Materials* **2012**, *24* (4), 485-491.
125. Jin, Z.; Pramoda, K.; Xu, G.; Goh, S. H., Dynamic mechanical behavior of melt-processed multi-walled carbon nanotube/poly (methyl methacrylate) composites. *Chemical Physics Letters* **2001**, *337* (1), 43-47.
126. Stankovich, S.; Dikin, D. A.; Piner, R. D.; Kohlhaas, K. A.; Kleinhammes, A.; Jia, Y.; Wu, Y.; Nguyen, S. T.; Ruoff, R. S., Synthesis of graphene-based nanosheets via chemical reduction of exfoliated graphite oxide. *Carbon* **2007**, *45* (7), 1558-1565.

127. Hua, Z.; Zhou, S.; Zhao, M., Fabrication of a surface imprinted hydrogel shell over silica microspheres using bovine serum albumin as a model protein template. *Biosensors and Bioelectronics* **2009**, *25* (3), 615-622.
128. Olsson, R. T.; Kraemer, R.; Lopez-Rubio, A.; Torres-Giner, S.; Ocio, M. J.; Lagarón, J. M., Extraction of microfibrils from bacterial cellulose networks for electrospinning of anisotropic biohybrid fiber yarns. *Macromolecules* **2010**, *43* (9), 4201-4209.
129. Zhao, Y.; Li, F.; Zhang, R.; Evans, D. G.; Duan, X., Preparation of layered double-hydroxide nanomaterials with a uniform crystallite size using a new method involving separate nucleation and aging steps. *Chemistry of Materials* **2002**, *14* (10), 4286-4291.
130. Ho, Y.-S., Review of second-order models for adsorption systems. *Journal of hazardous materials* **2006**, *136* (3), 681-689.
131. Qiu, H.; Lv, L.; Pan, B.-c.; Zhang, Q.-j.; Zhang, W.-m.; Zhang, Q.-x., Critical review in adsorption kinetic models. *Journal of Zhejiang University Science A* **2009**, *10* (5), 716-724.
132. Yuh-Shan, H., Citation review of Lagergren kinetic rate equation on adsorption reactions. *Scientometrics* **2004**, *59* (1), 171-177.
133. Boparai, H. K.; Joseph, M.; O'Carroll, D. M., Kinetics and thermodynamics of cadmium ion removal by adsorption onto nano zerovalent iron particles. *Journal of hazardous materials* **2011**, *186* (1), 458-465.
134. Saiers, J. E.; Hornberger, G. M.; Liang, L., First- and second- order kinetics approaches for modeling the transport of colloidal particles in porous media. *Water Resources Research* **1994**, *30* (9), 2499-2506.
135. Ho, Y.-S.; McKay, G., The kinetics of sorption of divalent metal ions onto sphagnum moss peat. *Water research* **2000**, *34* (3), 735-742.
136. Cruz, C. C.; da Costa, A. C. A.; Henriques, C. A.; Luna, A. S., Kinetic modeling and equilibrium studies during cadmium biosorption by dead *Sargassum* sp. biomass. *Bioresource technology* **2004**, *91* (3), 249-257.
137. Limousin, G.; Gaudet, J.-P.; Charlet, L.; Szenknect, S.; Barthes, V.; Krimissa, M., Sorption isotherms: a review on physical bases, modeling and measurement. *Applied Geochemistry* **2007**, *22* (2), 249-275.
138. Foo, K.; Hameed, B., Insights into the modeling of adsorption isotherm systems. *Chemical Engineering Journal* **2010**, *156* (1), 2-10.
139. Aksu, Z., Equilibrium and kinetic modelling of cadmium (II) biosorption by *C. vulgaris* in a batch system: effect of temperature. *Separation and Purification Technology* **2001**, *21* (3), 285-294.
140. Swain, S. K.; Patnaik, T.; Singh, V. K.; Jha, U.; Patel, R. K.; Dey, R. K., Kinetics, equilibrium and thermodynamic aspects of removal of fluoride from drinking water using meso-structured zirconium phosphate. *Chemical Engineering Journal* **2011**, *171* (3), 1218-1226.
141. Banerjee, K.; Amy, G. L.; Prevost, M.; Nour, S.; Jekel, M.; Gallagher, P. M.; Blumenschein, C. D., Kinetic and thermodynamic aspects of adsorption of arsenic onto granular ferric hydroxide (GFH). *Water research* **2008**, *42* (13), 3371-3378.
142. Singh, T. S.; Pant, K., Equilibrium, kinetics and thermodynamic studies for adsorption of As (III) on activated alumina. *Separation and Purification Technology* **2004**, *36* (2), 139-147.

143. Salameh, Y.; Al-Lagtah, N.; Ahmad, M.; Allen, S.; Walker, G., Kinetic and thermodynamic investigations on arsenic adsorption onto dolomitic sorbents. *Chemical Engineering Journal* **2010**, *160* (2), 440-446.
144. Altundoğan, H. S.; Altundoğan, S.; Tümen, F.; Bildik, M., Arsenic adsorption from aqueous solutions by activated red mud. *Waste Management* **2002**, *22* (3), 357-363.
145. Zhang, L.; Liu, N.; Yang, L.; Lin, Q., Sorption behavior of nano-TiO₂ for the removal of selenium ions from aqueous solution. *Journal of hazardous materials* **2009**, *170* (2), 1197-1203.
146. Tuzen, M.; Sarı, A., Biosorption of selenium from aqueous solution by green algae (*Cladophora hutchinsiae*) biomass: equilibrium, thermodynamic and kinetic studies. *Chemical Engineering Journal* **2010**, *158* (2), 200-206.
147. Kamaraj, R.; Vasudevan, S., Decontamination of selenate from aqueous solution by oxidized multi-walled carbon nanotubes. *Powder Technology* **2015**, *274*, 268-275.
148. Calmano, W.; Hong, J.; Förstner, U., *Binding and mobilization of heavy metals in contaminated sediments affected by pH and redox potential*. 1993.
149. Tuutijärvi, T.; Vahala, R.; Sillanpää, M.; Chen, G., Maghemite nanoparticles for As (V) removal: desorption characteristics and adsorbent recovery. *Environmental technology* **2012**, *33* (16), 1927-1936.
150. Haiss, W.; Thanh, N. T.; Aveyard, J.; Fernig, D. G., Determination of size and concentration of gold nanoparticles from UV-vis spectra. *Analytical chemistry* **2007**, *79* (11), 4215-4221.
151. Volkamer, R.; Spietz, P.; Burrows, J.; Platt, U., High-resolution absorption cross-section of glyoxal in the UV-vis and IR spectral ranges. *Journal of Photochemistry and Photobiology A: Chemistry* **2005**, *172* (1), 35-46.
152. Culbertson, C. T.; Jorgenson, J. W., Lowering the UV absorbance detection limit in capillary zone electrophoresis using a single linear photodiode array detector. *Analytical chemistry* **1998**, *70* (13), 2629-2638.
153. Dhar, R. K.; Zheng, Y.; Rubenstone, J.; van Geen, A., A rapid colorimetric method for measuring arsenic concentrations in groundwater. *Analytica chimica acta* **2004**, *526* (2), 203-209.
154. <As(V) Color.pdf>.
155. Mays, D. E.; Hussam, A., Voltammetric methods for determination and speciation of inorganic arsenic in the environment—a review. *Analytica chimica acta* **2009**, *646* (1), 6-16.
156. Dhar, R.; Zheng, Y.; Rubenstone, J.; Van Geen, A., A rapid colorimetric method for measuring arsenic concentrations in groundwater. *Analytica chimica acta* **2004**, *526* (2), 203-209.
157. Stratton, G.; Whitehead, H. C., Colorimetric determination of arsenic in water with silver diethyldithiocarbamate. *Journal (American Water Works Association)* **1962**, 861-864.
158. Jenner, G.; Longerich, H.; Jackson, S.; Fryer, B., ICP-MS—a powerful tool for high-precision trace-element analysis in earth sciences: evidence from analysis of selected USGS reference samples. *Chemical Geology* **1990**, *83* (1), 133-148.
159. Field, M. P.; Sherrell, R. M., Direct determination of ultra-trace levels of metals in fresh water using desolvating micronebulization and HR-ICP-MS: application to Lake Superior waters. *Journal of Analytical Atomic Spectrometry* **2003**, *18* (3), 254-259.
160. Stetzenbach, K. J.; Amano, M.; Kremer, D. K.; Hodge, V. F., Testing the Limits of ICP- MS: Determination of Trace Elements in Ground Water at the Part- Per- Trillion Level. *Groundwater* **1994**, *32* (6), 976-985.
161. Elmer, P., The 30-minute Guide to ICP-MS. *Perkin Elmer, Shelton CT* **2001**.

162. Larsen, E. H.; Stürup, S., Carbon-enhanced inductively coupled plasma mass spectrometric detection of arsenic and selenium and its application to arsenic speciation. *Journal of Analytical Atomic Spectrometry* **1994**, *9* (10), 1099-1105.
163. Thomas, R., *Practical guide to ICP-MS: a tutorial for beginners*. CRC press: 2013.
164. Mahmoudi, M.; Sant, S.; Wang, B.; Laurent, S.; Sen, T., Superparamagnetic iron oxide nanoparticles (SPIONs): development, surface modification and applications in chemotherapy. *Advanced drug delivery reviews* **2011**, *63* (1-2), 24-46.
165. Cai, W.; Yu, J.; Mann, S., Template-free hydrothermal fabrication of hierarchically organized γ -AlOOH hollow microspheres. *Microporous and Mesoporous Materials* **2009**, *122* (1), 42-47.
166. Kamsonlian, S.; Suresh, S.; Ramanaiah, V.; Majumder, C.; Chand, S.; Kumar, A., Biosorptive behaviour of mango leaf powder and rice husk for arsenic (III) from aqueous solutions. *International Journal of Environmental Science and Technology* **2012**, *9* (3), 565-578.
167. Kamsonlian, S.; Suresh, S.; Majumder, C.; Chand, S., Biosorption of arsenic from contaminated water onto solid Psidium guajava leaf surface: equilibrium, kinetics, thermodynamics, and desorption study. *Bioremediation Journal* **2012**, *16* (2), 97-112.
168. Morillo, D.; Pérez, G.; Valiente, M., Efficient arsenic (V) and arsenic (III) removal from acidic solutions with Novel Forager Sponge-loaded superparamagnetic iron oxide nanoparticles. *Journal of colloid and interface science* **2015**, *453*, 132-141.
169. Narayanan, T.; Mary, A. R.; Shaijumon, M.; Ci, L.; Ajayan, P.; Anantharaman, M., On the synthesis and magnetic properties of multiwall carbon nanotube–superparamagnetic iron oxide nanoparticle nanocomposites. *Nanotechnology* **2009**, *20* (5), 055607.
170. Jiang, J.; Oberdörster, G.; Biswas, P., Characterization of size, surface charge, and agglomeration state of nanoparticle dispersions for toxicological studies. *Journal of Nanoparticle Research* **2009**, *11* (1), 77-89.
171. Sun, X.; Doner, H. E., An investigation of arsenate and arsenite bonding structures on goethite by FTIR. *Soil Science* **1996**, *161* (12), 865-872.
172. Melott, A. L., Le Châtelier's principle. *Journal of Chemical Education* **1968**, *45* (6), A519.
173. Malkoc, E.; Nuhoglu, Y., Investigations of nickel (II) removal from aqueous solutions using tea factory waste. *Journal of hazardous materials* **2005**, *127* (1), 120-128.
174. Ozsoy, H. D.; Kumbur, H., Adsorption of Cu (II) ions on cotton boll. *Journal of hazardous materials* **2006**, *136* (3), 911-916.
175. Martinez, S.; Stern, I., Thermodynamic characterization of metal dissolution and inhibitor adsorption processes in the low carbon steel/mimosa tannin/sulfuric acid system. *Applied Surface Science* **2002**, *199* (1), 83-89.
176. Xu, X.; Gao, B.; Wang, W.; Yue, Q.; Wang, Y.; Ni, S., Adsorption of phosphate from aqueous solutions onto modified wheat residue: characteristics, kinetic and column studies. *Colloids and Surfaces B: Biointerfaces* **2009**, *70* (1), 46-52.
177. Weisstein, E. W., Least squares fitting. **2002**.
178. Lafferty, B. J.; Loeppert, R., Methyl arsenic adsorption and desorption behavior on iron oxides. *Environmental science & technology* **2005**, *39* (7), 2120-2127.
179. Manning, B. A.; Fendorf, S. E.; Goldberg, S., Surface structures and stability of arsenic (III) on goethite: spectroscopic evidence for inner-sphere complexes. *Environmental Science & Technology* **1998**, *32* (16), 2383-2388.

180. Cullen, W. R.; Reimer, K. J., Arsenic speciation in the environment. *Chemical reviews* **1989**, *89* (4), 713-764.
181. Carter, D. E., Oxidation-reduction reactions of metal ions. *Environmental health perspectives* **1995**, *103* (Suppl 1), 17.
182. Masue, Y.; Loeppert, R. H.; Kramer, T. A., Arsenate and arsenite adsorption and desorption behavior on coprecipitated aluminum: iron hydroxides. *Environmental science & technology* **2007**, *41* (3), 837-842.
183. Afkhami, A.; Madrakian, T., Kinetic–spectrophotometric determination of selenium in natural water after preconcentration of elemental selenium on activated carbon. *Talanta* **2002**, *58* (2), 311-317.
184. Wasewar, K. L.; Prasad, B.; Gulipalli, S., Adsorption of selenium using bagasse fly ash. *CLEAN–Soil, Air, Water* **2009**, *37* (7), 534-543.
185. Quiñones, I.; Guiochon, G., Derivation and application of a Jovanovic–Freundlich isotherm model for single-component adsorption on heterogeneous surfaces. *Journal of colloid and interface science* **1996**, *183* (1), 57-67.
186. Wahab, M. A.; Jellali, S.; Jedidi, N., Ammonium biosorption onto sawdust: FTIR analysis, kinetics and adsorption isotherms modeling. *Bioresource technology* **2010**, *101* (14), 5070-5075.
187. Hocquellet, P.; Candillier, M.-P., Evaluation of microwave digestion and solvent extraction for the determination of trace amounts of selenium in feeds and plant and animal tissues by electrothermal atomic absorption spectrometry. *Analyst* **1991**, *116* (5), 505-509.
188. Rausch, H.; Salamon, A., Activation analysis for selenium and tellurium trace impurities in gallium, arsenic and gallium arsenide. *Talanta* **1968**, *15* (9), 975-978.
189. Hani, N.; Wai, C.; Willmes, H., Dithiocarbamate extraction of trace amounts of selenium from biological samples for neutron activation analysis. *Journal of radioanalytical and nuclear chemistry* **1986**, *104* (1), 19-28.

ANNEX I

Temperature-dependence of arsenic adsorption-desorption, reagent-less process for regeneration and reuse of the adsorbent-Forager sponge loaded with superparamagnetic iron oxide nanoparticle (sponge-SPION)

Liu HE^a, Tong Liu^a, Manuel Valiente^{*}

Department de Quimica, Quimica Analitica, Universidad Autonoma de Barcelona, 08193 Bellaterra, Barcelona, Spain

Corresponding author footnote

Centre Grup de Techniques de Separacio en Quimica.

Tel. +34-935812903

Fax. +34-945811985

Email. Manuel.Valiente@uab.cat

Abstract:

Nowadays, there is a great concern on the study of new adsorbent materials for arsenic clean removal. However, very few studies concern about regeneration and reuse the adsorbent. This article describes a new reagent-less method which could regenerate the adsorbent by controlling the temperature.

The temperature-dependence of arsenic adsorption by sponge-SPION has been studied. It has demonstrated that low-temperature could help to realize the adsorption process and high-temperature can lead the desorption process to happen. The result shows that under 20°C, as time goes on, the adsorption process reaches equilibrium at about 1h. Under 70°C, desorption process occurs as contact time increases, desorption equilibrium was then gradually achieved with contact time. The effect of temperature on the adsorption of As (V) was studied in the continuous column mode by evaluating the adsorption at the temperature 10°C, 20°C and 70°C. The adsorption phenomenon increases with the decrease of temperature. The adsorption results were fitted to the Langmuir models. Thermodynamic parameters of related ion exchange equilibrium have been evaluated including the equilibrium constant K_a as well as Gibbs free energy. This value shows the adsorption process to be favorable and spontaneous. The equilibrium constant K_L values determined at different temperatures indicate the adsorption to increase with the temperature rising. Accordingly, a decrease in the negative value of ΔG° with the temperature increase is observed. Separation factor has very strong temperature dependence. Higher temperature leads to a lower separation. The thermodynamic affinity defined by $\log K=4.198$ and $\log K=1.023$ under 20°C and 70°C were determined, respectively. Arsenic is, thus, found to be more strongly adsorbed on the sponge -SPION under 20°C than that under 70°C.

All of the experimental and theoretical studies indicate that we can use the lower temperature for adsorption and higher temperature for desorption, thereby provide a new method for recovery of toxic element and regeneration of adsorbents.

Key words: Forager sponge, superparamagnetic iron oxide nanoparticle (SPION), arsenic, adsorption, temperature, thermodynamic, Gibb's free energy, equilibrium

constant, recovery, regeneration

1. Introduction

Arsenic is one of the most toxic elements occurring naturally in the environment [1]. Arsenic is abundant in our environment with both natural and anthropogenic sources which is considered to be one of the major problems in pollution because of their high toxicity and the consequent risks for human health [2]. Several countries have to deal with the problem of arsenic contamination of groundwater, used for drinking water, such as Bangladesh and India, China, United States, Mexico, Australia, Greece, Italy, Hungary, etc [3]. Thus, there is a growing interest in using low-cost methods and materials to remove arsenic from industrial effluents or drinking water before it may cause significant contamination [4-5].

Although many different methods such as precipitation [6], coagulation [7], oxidation [8], reverse osmosis [9], ion-exchange [10] have been used for arsenic removal, there are some drawbacks of these methods. Coagulation requires use of large-scale facilities for implementing water treatment [11]. Reverse osmosis requires the use of membranes, which are expensive to maintain and replace [12]. Coagulation, reverse osmosis, and ion exchange require the treatment of rejected stream for the ultimate disposal of arsenic contaminants [13]. Therefore, the adsorption from solution has attracted more attention due to its simple procedure that overcome most of the drawbacks of other techniques.

However, almost all of the above traditional methods have the problems on adsorbent regeneration. Once the adsorbent becomes exhausted, then, either the toxic elements must be recovered or the adsorbent regenerated or disposed in a controlled dumping site for toxic substances that use to be expensive. Desorption and adsorbent regeneration is a critical step contributing to increase process costs. A successful desorption process must restore the sorbent close to its initial properties for effective reuse. In most of the published arsenic sorption studies (some discussed earlier), desorption/regeneration was not included. Very few desorption studies are detailed in literature. Furthermore, once arsenic is recovered in the pure and concentrated form, the problem of its disposal of this concentrated arsenic product must be addressed. This is a difficult and expensive task. Few attempts have been made to address the handling of concentrated arsenic wastes. Tuutijärvi T [36] has tried five different alkaline solutions: NaOH, Na₂CO₃, Na₂HPO₄, NaHCO₃ and NaAc for arsenate batch desorption and regeneration. But this process also need to spend a lot of alkaline solution which is very expensive and is not feasible for industrial sense. Thus, in our work, we develop a new method for Arsenic desorption and sorbent regeneration with no reagents added by taking advantage of the thermodynamic properties of the adsorption system. In this paper, the influence of time, concentration, pH as well as bed volume on the adsorption rate under different temperature has been studied. More importantly, the temperature effect on the adsorption-desorption properties has been observed. In addition, the thermodynamic aspects of the adsorption have been studied. The aim of this article is to provide a reagentless method to recover the metals and regenerate the adsorbents.

2. Experiment

2.1 Reagents and Apparatus

The As(V) source was sodium arsenate ($\text{Na}_2\text{HAsO}_4 \cdot 7\text{H}_2\text{O}$), ACS reagent from Aldrich(Milwaukee, USA). Iron chloride($\text{FeCl}_3 \cdot 6\text{H}_2\text{O}$) and Ferrous chloride($\text{FeCl}_2 \cdot 4\text{H}_2\text{O}$) were ACS reagent from Aldrich(Milwaukee, USA), HCl were ACS reagents from Panreac S.A. (Barcelona, Spain).

Forager Sponge, an open-celled cellulose sponge which contains a water-insoluble polyamide chelating polymer. (formed by reaction of polyethyleneimine and nitrilotriacetic acid), was kindly supplied by Dynaphore Inc. (Richmond,VA,U.S.A.). This material is claimed to contain free available ethyleneamine and iminodiacetate groups to interact with heavy metals ions by chelation and ion exchange

Arsenic and iron concentrations in solution were determined by the Colorimetric technique. The wavelength used for analysis were 840 nm(As), 490 nm(Fe).

2.2 Preparation of the Adsorbents

2.2.1 Synthesis of adsorbent materials

The synthesis procedure of SPION has been described elsewhere[14].SPION are prepared in our lab by mixing iron(II) chloride and iron(III) chloride in the presence of ammonium hydroxide. First, deoxygenated the solution of NH_4OH (0.7M) by nitrogen. Second, deoxygenated the solution of 12mL HCl (0.1M) by nitrogen and mix $\text{FeCl}_3 \cdot 6\text{H}_2\text{O}$ with it. Third, heat the NH_4OH solution at 70°C . Fourth, Add the $\text{FeCl}_3 \cdot 6\text{H}_2\text{O}$ solution into the NH_4OH solution and react for 30min. Then, Add the $\text{FeCl}_2 \cdot 4\text{H}_2\text{O}$ in the previous solution with mechanic agitation of about 3000rpm and waiting for 45min, the dark precipitate will be formed, which consists of nanoparticles of magnetite. Last, wash it by MilliQ water which has been deoxygenated and centrifuged four times(3 times for 3 min and 5000rpm, 1 time for 10 min and 4500rpm) and preserve it by 50mL 0.1M TMAOH.

2.2.2 Clean of the Forager sponge

An initial conditioning of the sponge consisting on the conversion into its acidic form by consecutive treatment with 1.0mol/L HCl, double distilled water, and HCl solution at pH 2.5 was carried out in a glass preparative column. A portion of this conditioned sponge was separated, dried during 24 h , and stored in a desiccator for its use

2.2.3 Loading of SPION on the sponge

The sponge was loaded with iron oxide nanoparticles by using the nebulizer. The SPION-loaded sponge was dried during 24 h, and stored in a desiccator for its use. The SPION loading capacity was $0.0955 \pm 0.0029 \text{ mmol Fe/ g sponge}$

2.3 Characterization

We have synthesized the SPION for 5 times. And Each time, prepare three kinds of sample, including 1/100, 1/250, 1/1000(0.1mL SPION on 10mL TMAOH, 0.1mL SPION on 25mL TMAOH, 0.1mL SPION on 100mL TMAOH). We characterized the samples by TEM to see the particle size and dispersion SPION are highly dispersible in solutions. With particle sizes of from 6-20 nm, they offer a large surface area and superparamagnetic properties.

2.4 Arsenic adsorption and desorption experiment

Effect of contact time

Experiments to determine arsenic adsorption in different contact time were carried out at 2-240mins in batch conditions.

Effect of initial concentration

Experiments to determine arsenic adsorption capacity in different initial concentration were carried out at 0.5-100ppm in batch conditions.

Effect of temperature

Experiments to determine arsenic adsorption in different temperatures were carried out at temperature 10°C, 20°C and 70°C in batch conditions by using tightly plastic tubes containing weighted amounts of SPION-loaded sponges and measured volumes of arsenate solutions in the range 0.5-100 ppm As(V) at a given pH. Corresponding agitation was carried out in a rotary rack shaker during 1 h (this contact time was confirmed in separate experiments). Experiments to determine the interfering effect of Fe on As(V) adsorption were carried out with 500ppm and 1000 ppm As(V) solutions (13.3 mmol/L) prepared in a medium containing 0.1 mL SPION under the pH=3.6 condition. Experiments were repeated for the different conditions a minimum of two times.

3. Results and Discussion

3.1 Characterization of adsorbent material

The sponge-SPION adsorbent material was characterized by digital microscope. Fig 1 shows the image characterized by digital microscope, the Sponge is highly porous and elastic thereby promoting high rates for SPION loading and arsenic absorption. Therefore it's a very appropriate substrate for loading SPION and also for adsorbing arsenic anions. Absorbed arsenic anions can be eluted from the Sponge by using the NaOH solution. Following elution and washing, the Sponge can be used for the next absorption cycle. If the regeneration is not desirable or economical, the Sponge can be compacted to a small volume to facilitate disposal.

As seen from the Fig 2a, b, it is clear that after loading with SPION, the sponge is saturated with SPION and the surface is very smooth. Maybe it is due to the homogenous dispersion of the nanoparticles. The porous inside the sponge are fully filled with nanoparticles. The blank sponge can adsorb and immobilize SPION by chelation through the lone pairs of electrons on the unprotonated amine groups.

It was shown from the Fig 3a,b that After adsorption by using the sponge loaded with SPION, the sponge looks like shrinkage. And in addition, the surface is not smooth anymore. Probably it's because of the anion-exchange (arsenate oxyanions occur in solution from slightly acid to basic pH) between iron oxide nanoparticles and arsenate oxyanions.

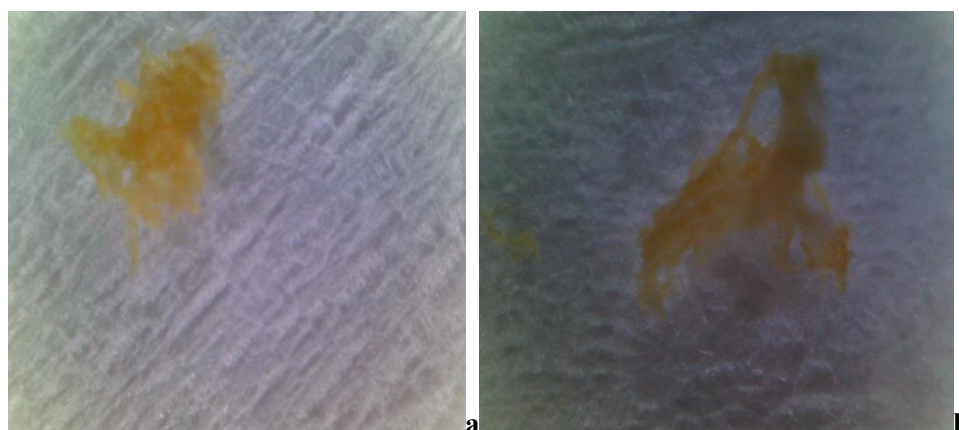


Fig 1 Forager sponge image by digital microscope

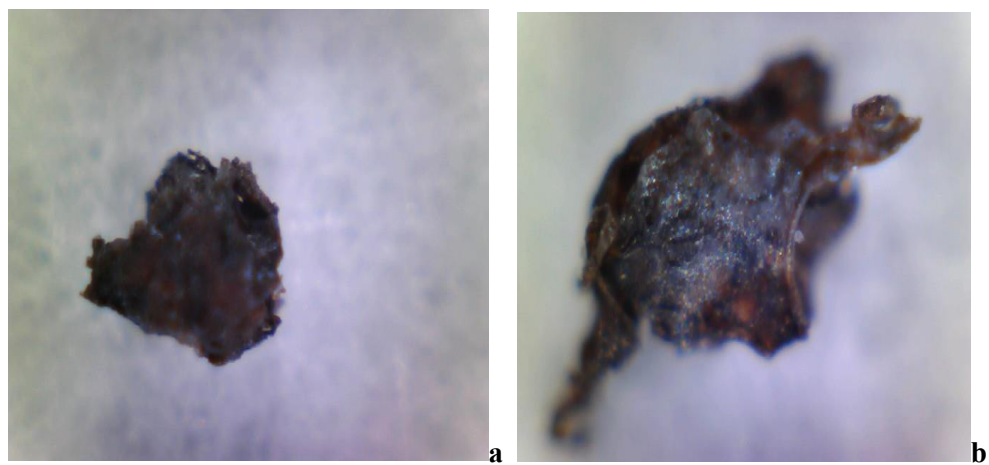


Fig 2 sponge with SPION

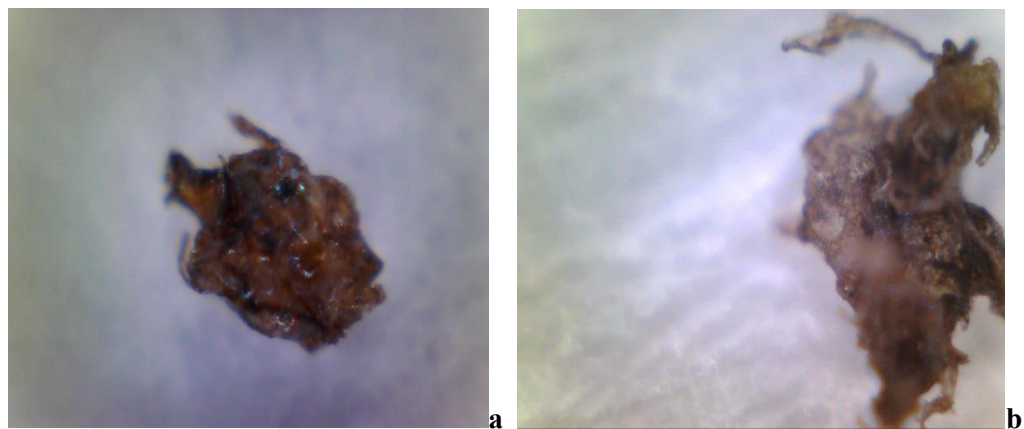
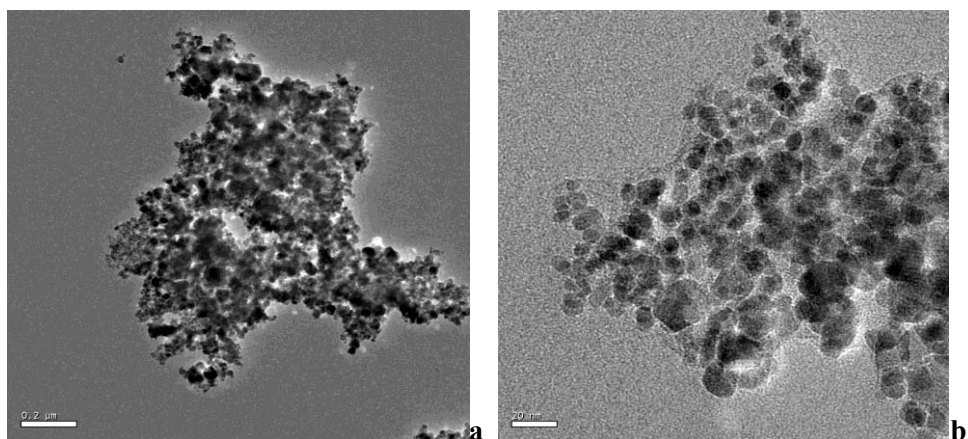


Fig 3 SPION Loaded sponge with arsenic (after adsorption)

SPION characterization by TEM
Before using (SPION emulsion)



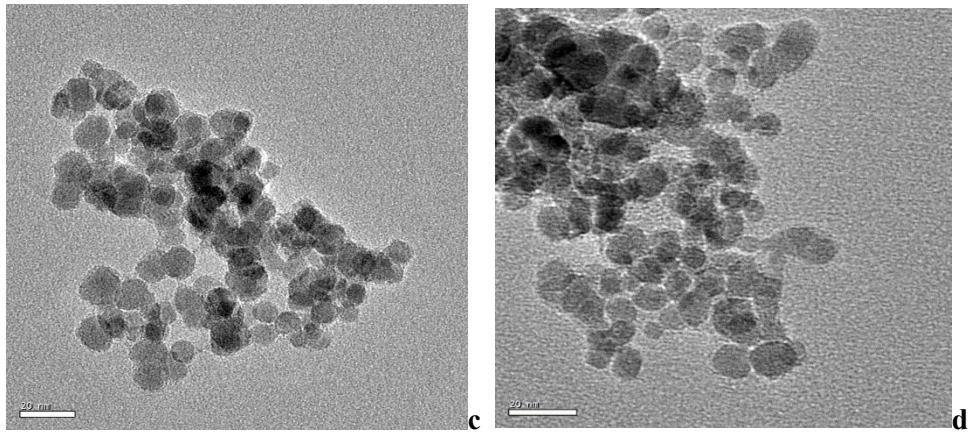


Fig 4 TEM image of SPION

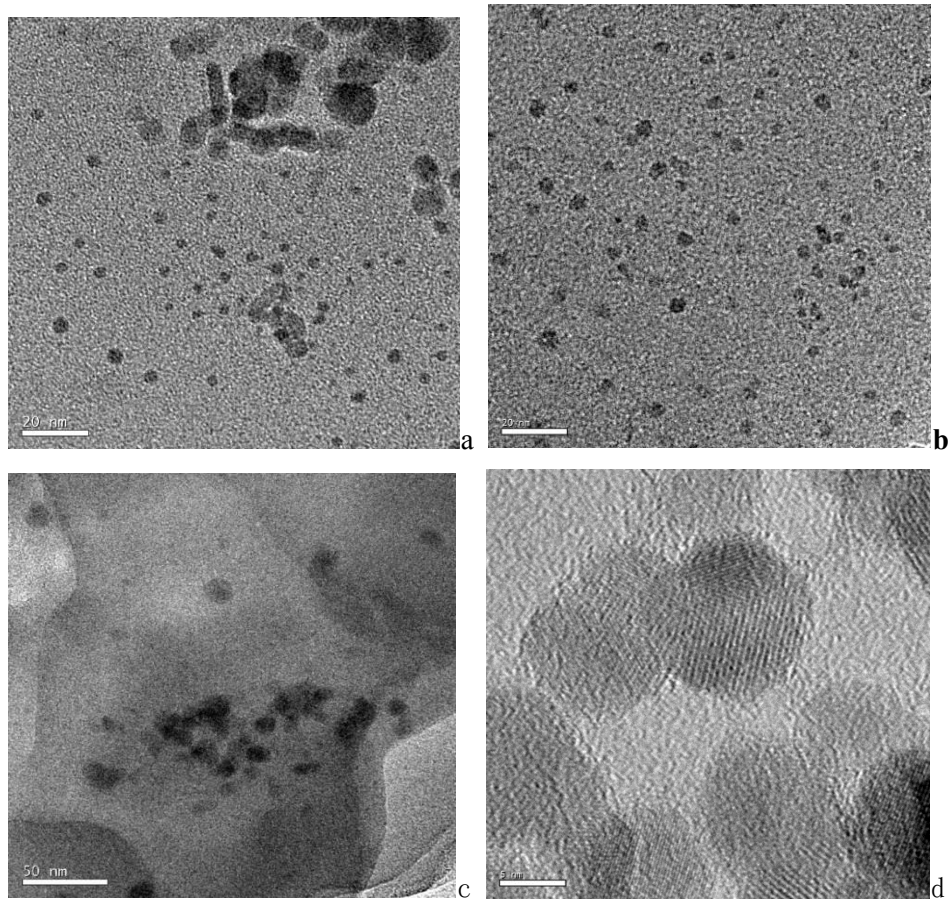


Fig 5 TEM image of SPION loaded on the sponge (before using)

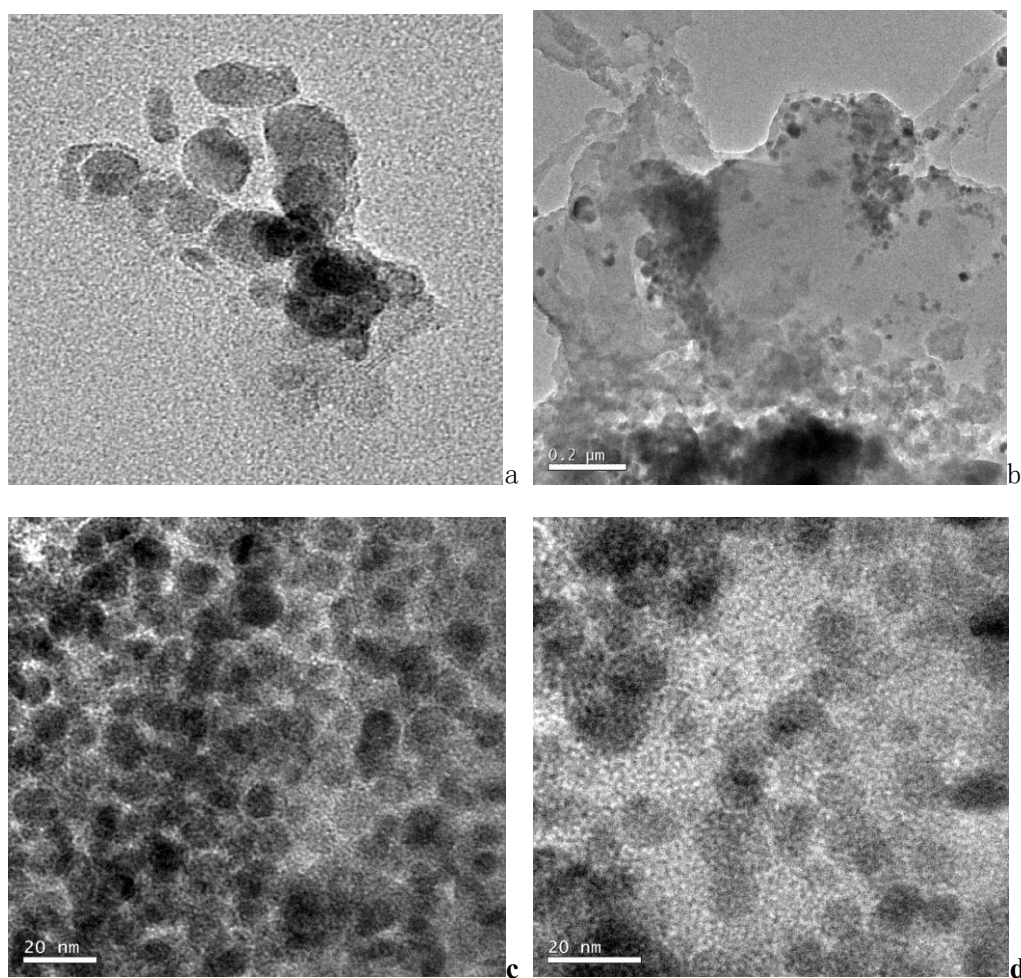


Fig 6 TEM image of SPION loaded on the sponge(after As adsorption)

Fig 4 shows TEM images of the synthesized SPION that reveals particles are 6-15nm in size. when the SPION is first synthesized and poured in the TMAOH solution and characterized by the TEM, some of the images show that the nanoparticles are homogenous but others are not dispersed very well. They are agglomerated and clustered.

Fig 5 shows TEM images of SPION dispersed on the sponge, the particles are also ~10nm. SPION distribute on the sponge almost homogeneously, that's because during the spraying by nebulizer and nitrogen, there is an external force to push the nanoparticles, and in addition, we use the ultrasonication on nanoparticles suspension prior nebulization to disperse agglomerates, as it can also add an extra force to pull the liquid apart to form evacuated cavities or microvoids.¹ The formation and destruction of these cavities can impose a shear force on agglomerates, capable of overcoming the van der Waals force holding them together. However, the ultrasonic applied forces are not strong enough to break the hard bonds of iron oxide molecules.

After adsorption (Fig 6), the SPION show a tendency to agglomerated again since the absence of external ultrasonic force for some time, makes the van der Waals force to raise affecting the distribution again.

Effect of contact time

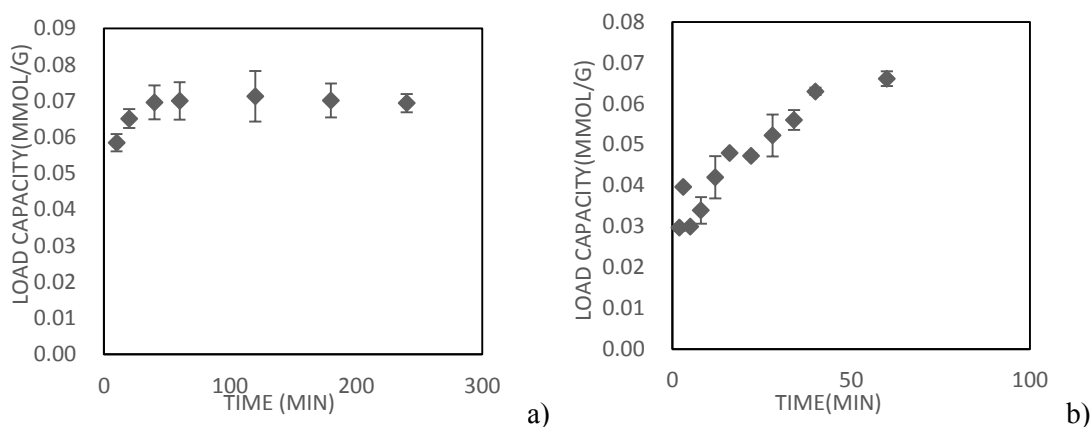


Fig 7 The effect of contact time on the adsorption capacity (20°C), a). from 10min to 240min, b). from 2min to 60min

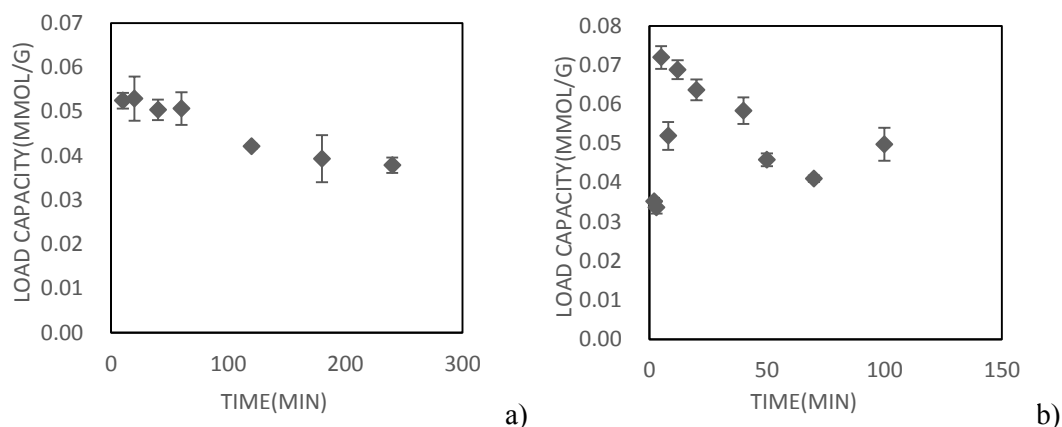


Fig 8 The effect of contact time on the adsorption capacity (70°C), a). from 10min to 240min, b). from 2min to 60min

The contact time with aqueous toxic element oxyanions is one of the most important parameters to be controlled for successful usage of adsorbents. The arsenic (V) aqueous system is contacted with the adsorbent (SPION loaded sponge) in the range of 2 to 100 minutes and 1 to 4 hours. The adsorption process for removing As (V) oxyanions from aqueous solution under 20°C obtain ion exchange combined with the ligand exchange equilibrium at about 1 hour as shown in Fig 7 a, b. After that, contact time has no effect in arsenic oxyanion removal percentage. This behavior can be attributed to the effect of diffusion resistance to reach the ion exchange moieties of the adsorbent. In another hand, the most possibilities of the complexes formed in our case is, As(V) is binding to two iron nuclei as adsorbed species. Extended X-ray absorption fine structure (EXAFS)² and FTIR spectroscopy³ have shown As(V) to form bidentate inner sphere surface complexes with iron hydroxide sites as time goes on.⁴

The effect of contact time on the desorption capacity under 70°C is shown in Fig 8a, b. Very high adsorption rates were achieved at the beginning because of the great number of sites available for the sorption operation. The adsorption process involves one of two types of

interactions. One is anion exchange of arsenic species corresponding to the protonated amine groups present in the matrix of sponge⁴. Another process is the ligand exchange, provided by the Fe(III) ions immobilized in the SPION as Equation 1 shows⁵. The adsorption process is reversible process. Suppose the reaction is exothermic process. The increase in temperature corresponds to introducing heat into the system. Le Châtelier's Principle⁶ states that the system will react to remove the added heat, thus the reaction must proceed in the reverse direction, converting products back to reactants, here we see the desorption starts to occur as time goes on. Conversely if the temperature of the system were decreased, the system would react in a direction that opposed the removal of the heat. The forward reaction would thus occur to release heat in an attempt to offset the heat that was removed from the system.



Effect of initial concentration

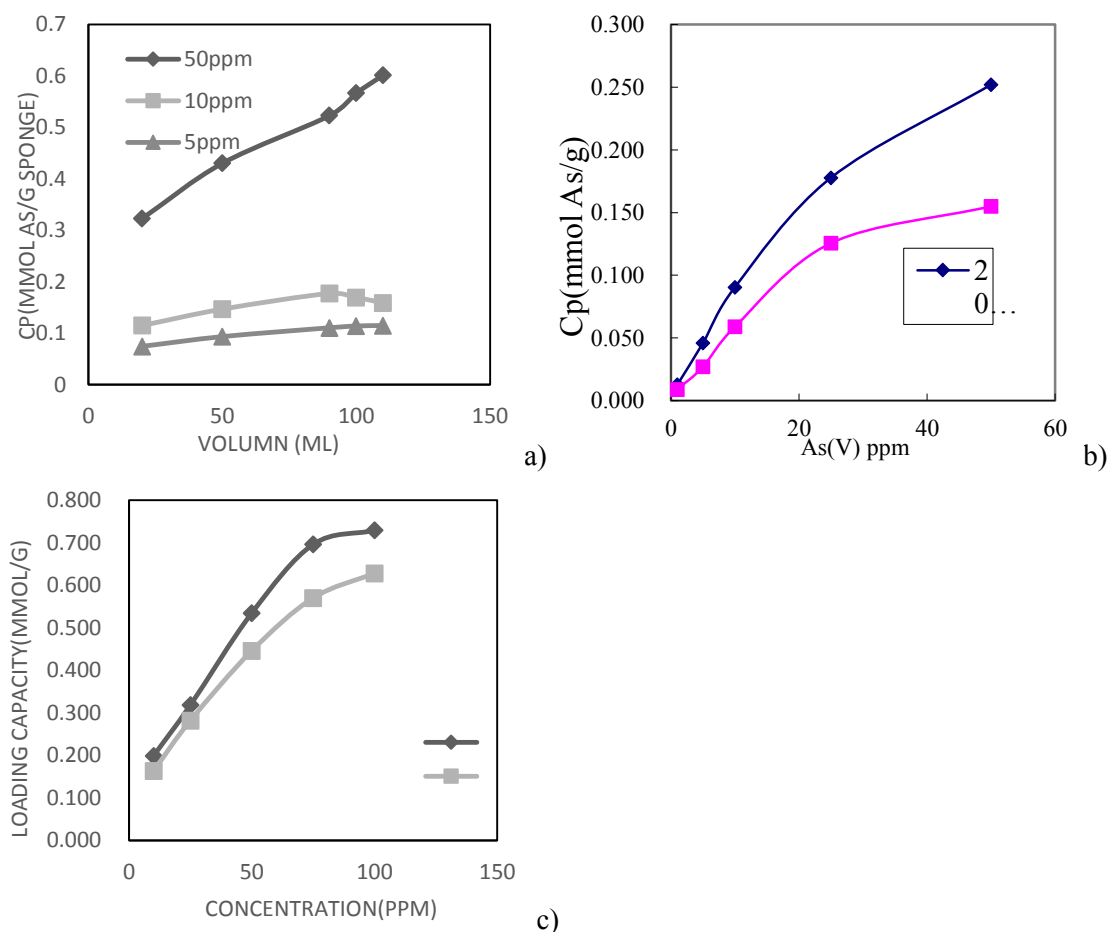


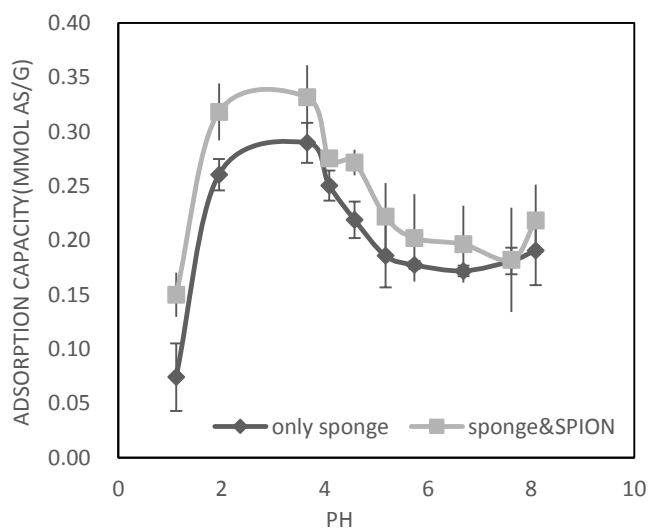
Fig 9 The effect of initial As(V) concentration on the adsorption capacity: a) 5ppm, 10ppm, 50ppm under 20°C, b) from 0.5ppm to 10ppm, 20°C and 70°C, c) from 10ppm to 100ppm, 20°C and 70°C

The initial arsenic oxyanion concentration in the aqueous solution is also a key parameter which affects to the driving force of the adsorption system.⁷ The effects of the initial arsenic concentration (from 5ppm to 50ppm) on the adsorption capacity by the sponge loaded with

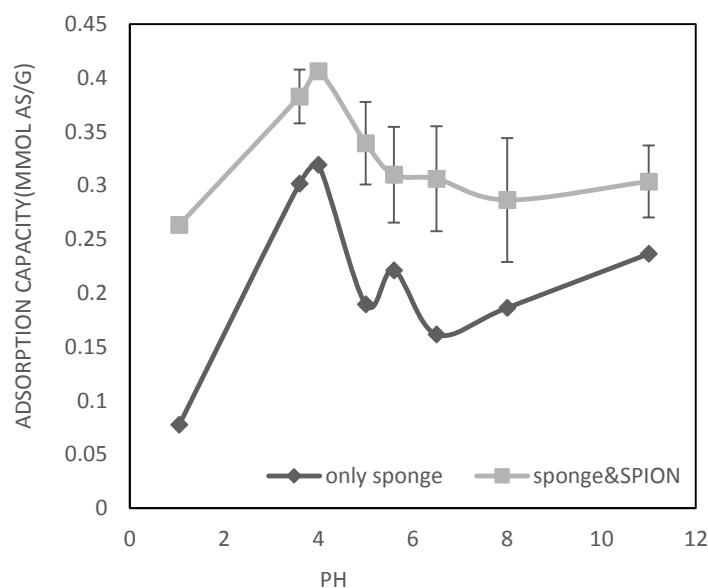
SPION under 293K and 343K are shown in Fig 9a,b. The increase of adsorption capacity when the initial arsenic concentration increases, is due to an increase of the mass transfer driving force. Adsorption capacity limit is reached when the increase of As (V) initial concentration do not produce any further increase on the As adsorption. In this case, the surface of the sponge loaded with SPION does not have free sites for the arsenic oxyanions uptake, being fairly saturated.⁸ It is probably another explanation that, as the concentration increased, a higher probability of collision between adsorbate (arsenate) and adsorbent(sponge loaded with SPION) surface happens, which could overcome the mass transfer resistance between the aqueous and the adsorbent phases.⁹

The process of As(V) adsorption on SPION loaded sponge can occur by two different ways: one is ion-exchange on the sponge protonated amine groups, another one is As(V) are bound to iron (hydr)oxides by an inner-sphere ligand-exchange mechanism, in which the arsenic oxyanion competes with and exchanges with surface $\equiv\text{Fe-OH}$ or $\equiv\text{Fe-OH}_2^+$ groups at the iron (hydr)oxide surface.^{4, 10} The increase of adsorption with concentration is due to the diffusion process and based on the Fick first law. Normally, the ion exchange reactions are very fast compared to the diffusion of the aqueous ions to the surface moieties. When the initial concentration is higher, the arsenic oxyanions move from the solution to the surface of the adsorbent, the amount of arsenic exchanged onto the sponge and that exchanged onto the SPION increase with increasing initial As (V) concentration.

Effect of pH on Arsenic Adsorption Capacity



a)



b)

Fig 10 The effect of pH on the adsorption capacity, 1000 ppm As solutions and 0.10g of sponge were used in each batch experiment. a). 20°C, b). 70°C

The effect of pH on the As(V) adsorption by the blank and SPION-loaded sponge under both 20°C and 70°C is shown in Figure 10 a, b, pH ranging between 1 and 11. The results obtained revealed that the adsorption of arsenate by both blank and SPION-loaded sponge under both 20°C and 70°C are pH dependent, this can be explained by the dependence of the As(V) speciation on the pH. Compared with the observed results of pH effect on As(V) adsorption with that of Munoz and Diego^{4-5, 11}, it shows the similar behavior in both 20°C and 70°C with the adsorption of As(V) by blank sponge, Fe-loaded sponge, SPION alone and SPION-loaded sponge. The highest adsorption was observed at pH around 3.6-4.0. Specifically, the maximum adsorption of 20°C is under pH 3.6 while the highest adsorption of 70°C is under 4.0. This similarity supports the conclusion that the arsenic species is the main reason which is responsible of the adsorption.⁵ The acidity of arsenate species ($pK_a = 2.2$) can be responsible of the observed adsorption, a relatively high rate of deprotonated species are present at pH value 3.6-4.0, therefore the maximum adsorption is present at pH=3.6-4.0. For 20°C, lower pH values (1.0–2.0) and for 70°C, lower pH values (1.0-3.0), the competition of H^+ species for arsenate leads to a lower adsorption. The lower adsorption capacity at pH values below 3.6 is attributed to the high concentration of H^+ ions. In this situation, the concentration of H^+ ions far exceeds the arsenic anions concentration in the solution, which enhance the competence of H^+ , therefore the H^+ reach the adsorbent surface sites. On the other hand, for both 20°C and 70°C, at pH > 5.0 the observed decrease on the As (V) adsorption is due to the increase of OH^- species in suppressing the process.

From the Fig 10a,b. under both 20oC and 70oC, it confirmed again that the adsorption of As(V) is enhanced by loading SPION. Which demonstrate that there are two mechanism proposed

for As(V) adsorption on the SPION-loaded sponge. Not only the mechanism of ion-exchange on the protonated amine groups (present in both blank and SPION-loaded sponges) is proposed, but also the additional ligand-exchange mediated by the immobilized Fe^{3+} (only present in the SPION-loaded sponge) has big impact on the As(V) adsorption.

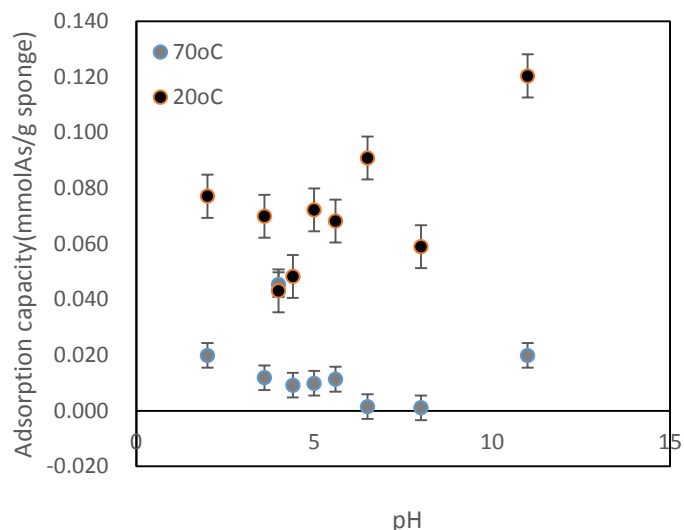
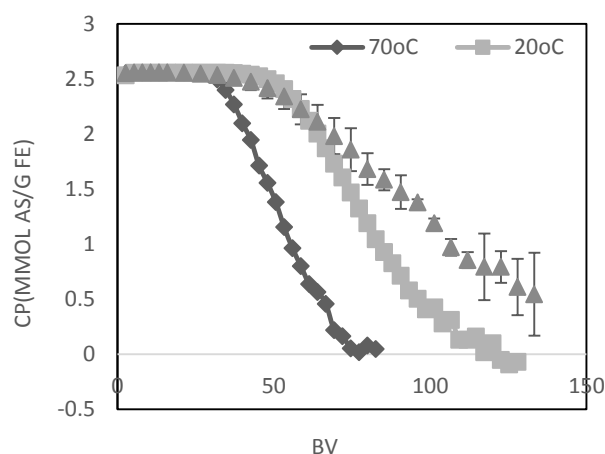


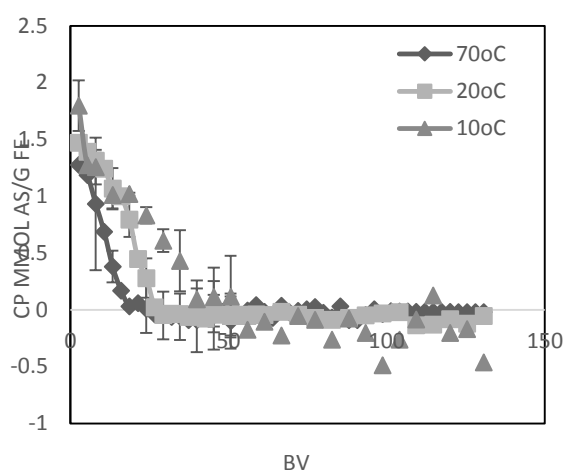
Fig 11. pH effect on As(III) adsorption by sponge-SPION under 20°C and 70°C

As shown in Figure 11, As (III) adsorption by sponge loaded with SPION at both 20°C and 70°C reveals to be independent of pH, what corresponds to the weak acidic properties of arsenious acid ($\text{pK}_{\text{a}1} = 9.2$), leading to the reduced presence of deprotonated arsenite species in the pH range of study. The higher As (III) adsorption capacity under 20°C than under 70°C may indicate the possible use of temperature to drive the adsorption/desorption process.

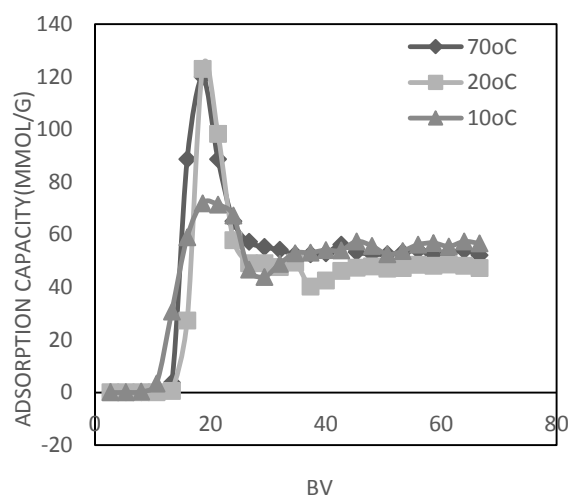
Effect of temperature



a)



b)



c)

Fig 12 The effect of temperature on the adsorption capacity (70°C, 20°C, 10°C): a). pH=3.6, b) pH=5.6, c) pH=2.1

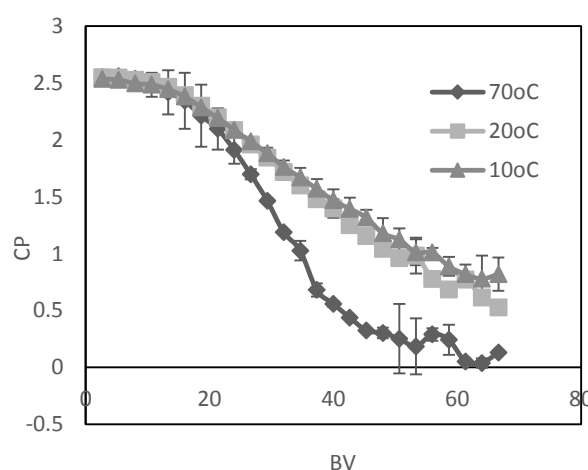
The effect of temperature on the adsorption of As (V) was studied in the fixed bed mode by evaluating the adsorption at the temperature 10°C, 20°C and 70°C under pH 3.6 as shown in Fig 12a. The observed values can be explained in terms of the thermodynamic parameters. The adsorption phenomenon is more efficient with the decrease in temperature, which indicate an exothermic process. Generally, an exothermic adsorption process signifies either physi- or chemi-sorption¹². The process is controlled by the adsorbate-adsorbent interaction. The breakthrough point for 10°C and 20°C is about 48 bed volume, but for 70°C, the breakthrough point is about 26 bed volume. The adsorption of arsenate onto sponge-SPION followed at three temperatures, 10°C, 20°C and 70°C, shows a fast arsenate uptake in all cases. The observed decrease in the adsorption capacity with an increase of the temperature from 10°C to 70°C may

be due to a tendency for the arsenate oxyanions to escape from the solid phase to the bulk phase with an increase in the temperature of the solution¹³.

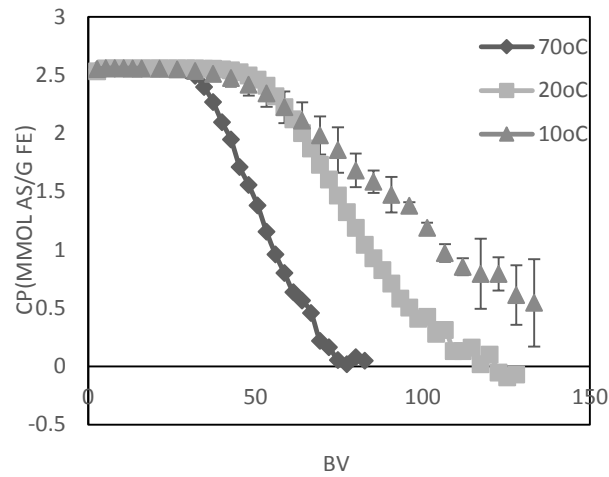
The effect of temperature on the adsorption of As (V) was studied by evaluating the adsorption at the temperature 10°C, 20°C and 70°C under pH 5.6 is shown in Fig 12b. As indicated before, for both 20°C and 70°C, when pH is more than 5.0, the observed decrease on the As (V) adsorption is due to the increase of OH⁻ species that compete with deprotonated arsenate for the anion exchange sites of the adsorbent, which is also confirmed by the column continuous mode arsenate adsorption.

On the other hand, at pH<2.5(as shown in Fig 12c), iron desorbed is very significant due to protons competition, nevertheless, at pH range 3-9 iron desorption is not quite important. Thus, in this adsorption process, at the beginning of the arsenic adsorption, the iron desorbing does not have significant impact on the As (V) adsorption since the ion exchange process increase the pH value when the process begins. Then, after the continuous flow of arsenic solutions (pH 2.1) the ion exchange became saturated and then the solution in column became acidic producing iron desorption from the sponge gradually, thus leading to a decrease on the arsenic adsorption. Moreover, as the solution is under pH 2.1, the arsenic desorption occurred after previous adsorption, thus producing at the column outlet a sharp increase of arsenic concentration leading to a higher arsenic concentration than in the initial column incoming solution. The final drop of the As(V) concentration at the column outlet is due to the readsorption of part of the As(V) in column at the empty sites left by the previous As(V) release and thus will reach the value of the input solution.

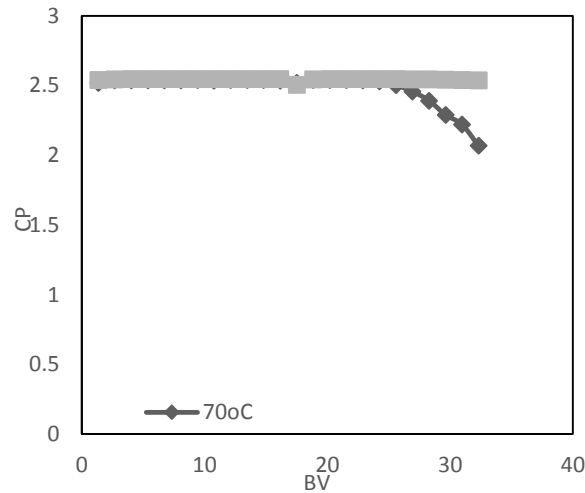
The effect of bed volume



a)



b)



c)

Fig 13 The effect of bed volume (70°C, 20°C, 10°C), pH=3.6: a) 0.5g sponge, b) 1.0g sponge, c) 1.5g sponge

The influences of the height of the sponge bed on the adsorption capacity are shown in Fig 13a, b. More adsorbent (sponge with SPION) makes the depth of bed volume to be higher. When the As(V) solution go through the column, it has longer time to contact with the adsorbent, in addition, multiple layer of the sponge with SPION can adsorb the arsenic from the top to the bottom one.

Adsorption isotherms

Langmuir isotherm

The experimental As(V) adsorption data have been subjected to Langmuir isotherm showed in Fig 14. Langmuir isotherm equation fitted well to the adsorption data.

$$C/C_x = 1/K_a C_m + C/C_m \quad (2)$$

-C is the concentration of sorbate in the equilibrated solution, mmol/L

-C_x is the adsorption capacity in SPION, mmol/g

-C_m is the maximum adsorption capacity

-K_a is the adsorption equilibrium constant

The langmuir coefficients K_a and C_m can be determined from the intercepts and slopes of the plots C/C_x vs C, which are linear.

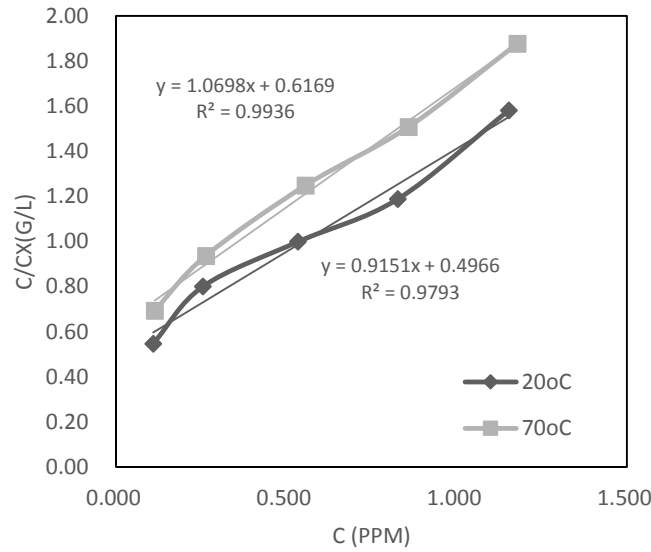


Fig 14 Langmuir model

The isotherm parameters for the adsorption As (V) onto the sponge with SPION at different temperatures were obtained from the Langmuir model by using the linear fitting method.

Table 1 The isotherm parameters for Langmuir model

T(°C)	70°C	20°C
C _m (mmol/g SPION)	40.65	47.52
C _m (mmol/g sponge)	0.935	1.093
Log K _a (L/mmol)	1.73	1.84
ΔG ⁰ (kJ/mol)	-11.463	-9.094
R ²	0.9936	0.9793

The effect of isotherm shape can be used to predict whether an adsorption system is “favourable” or “unfavourable” both in fixed-bed systems as well as in batch processes. The essential features of the Langmuir isotherm can be expressed in terms of a dimensionless constant separation factor or equilibrium parameter K_L, which is defined by the following relationship:

$$K_L = \frac{1}{1 + K_a C_0} \quad (2)$$

K_L indicate the type of isotherm, C_0 is the initial concentration (mg/L), and K_a is the Langmuir constant.

Table 2 Equilibrium constants

Values of K_L	Type of isotherm
$K_L > 1$	Unfavorable
$K_L = 1$	Liner
$0 < K_L < 1$	Favorable
$K_L = 0$	Irreversible

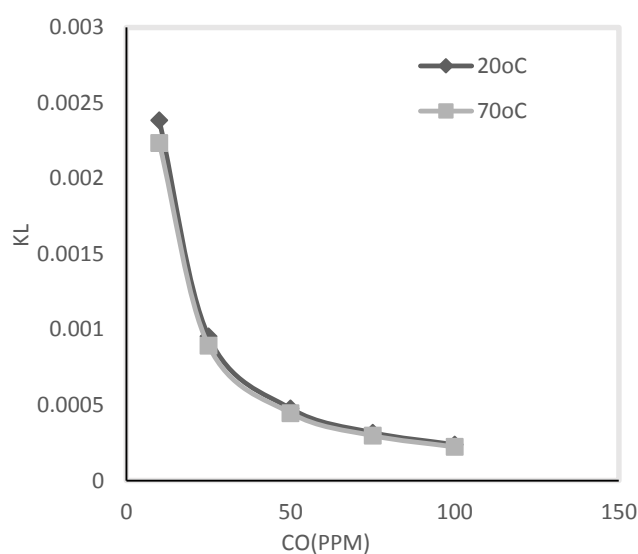


Fig 15 plot of K_L against initial arsenic concentration at two temperatures.

Fig 15 with a relationship between K_L and C_0 was presented to show the essential features of the Langmuir isotherm. The K_L values indicate that adsorption is more favorable for the higher initial As(V) concentration than the lower ones and also it indicate that adsorption is more favorable for the lower temperature than the higher ones.

Freundlich isotherm

$$\ln C_x = \ln K_f + \frac{1}{N} \ln C \quad (3)$$

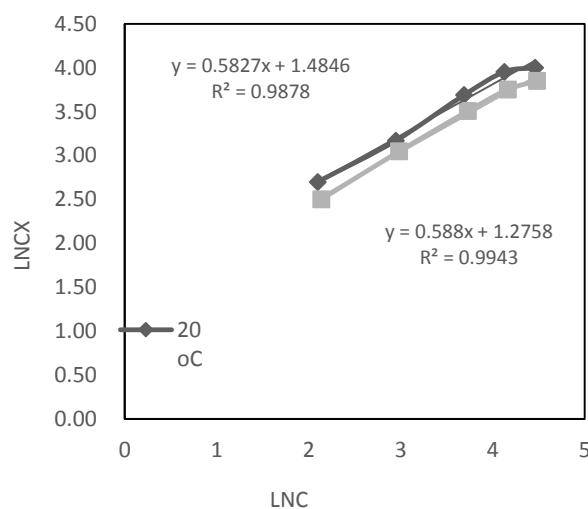


Fig 16 Freundlich model

Table 3 The isotherm parameters for Freundlich model

T(°C)	70°C	20°C
$K_f(\text{mg/g})$	3.582	4.413
$1/N$	0.588	0.583
N	1.701	1.715
R^2	0.9943	0.9878

where C_x is the mass of arsenic adsorbed (mmol/g), C is the equilibrium arsenic concentration (mg/L), and K_f and $1/N$ are constants. K_f can be used as an indicator of the adsorption capacity at a specific solution phase concentration, and $1/N$ reflects the intensity of adsorption.

The Freundlich equation predicts multilayer adsorption on heterogeneous surface, characterized by an exponential distribution of active sites. The values of the adsorption intensity obtained in nature favourable of the adsorption of As(V) ions onto sponge with SPION described by the Freundlich isotherm.

Thermodynamics Studies

The Gibb's free energy change is calculated using K_a obtained from Langmuir model and showed in table 1. The equations are:

$$\Delta G^0 = -RT \ln K_a \quad (4)$$

and

$$\Delta G^0 = \Delta H^0 - T\Delta S^0 \quad (5)$$

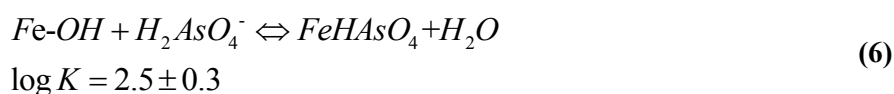
where R is universal gas constant ($8.314 \text{ J mol}^{-1}\text{K}^{-1}$) and T is the absolute temperature in K.

The negative values of Gibb's free energy confirmed the feasibility of the process and the spontaneous nature of adsorption with a high preference of As(V) by Forager sponge with iron oxide nanoparticles. The decrease in the negative value of ΔG^0 with an increase in temperature indicates that the adsorption process of As(V) on sponge becomes more favorable

at lower temperatures. But compared with the maximum adsorption capacity 0.93mmol/g in 343K, the maximum adsorption capacity in 293K is higher, 1.094mmol/g. This means under lower temperature, it can get higher maximum adsorption capacity than that under higher temperature.

The enthalpy change, ΔH° , and the entropy change, ΔS° , for the adsorption processes were obtained from the intercept and slope of Eq. (5) and found to be 0.822kJ mol⁻¹ and 0.0338 kJ mol⁻¹ K⁻¹, respectively. The positive value of ΔH° indicates that the adsorption. Reaction is exothermic. The positive value of ΔS° suggests that some structural changes occur on the adsorbent, and the randomness at the solid/liquid interface in the adsorption system increases during the adsorption process.

The dependence of separation factors on temperatures and bed volumes:



As indicated from the above equation, it was found that pK_a <0 and the arsenic acid is a relatively strong acid and the removal of As (V) by anion-exchange is possible. As the anion exchange behavior, the equilibrium separation factor, α , expressed as follows.

$$\alpha_{H_2AsO_4^-}^{OH^-} = \frac{x_{OH^-} X_{H_2AsO_4^-}}{x_{H_2AsO_4^-} X_{OH^-}} \quad (7)$$

Where x and X are the equivalent fractions of ions under separation in sponge and solution phases, respectively.

Table 4 separation factors

Bed volume	separation factor	
	70°C	20°C
5	481.8	3061.2
8	545.8	11907.6
11	521.8	17861.9
13	529.6	26793.4
16	569.1	17861.9
19	560.1	107176.5
21	664.7	107176.5
24	625.8	21434.5
27	461.0	26793.4
29	141.1	8930.5
32	38.5	4121.2
35	14.9	1622.9
37	7.8	652.5
40	4.5	288.7
43	3.2	143.1
45	2.0	74.5
48	1.6	42.2

51	1.2	25.4
53	0.8	16.2
56	0.6	9.7
59	0.5	6.7
61	0.3	4.9
64	0.3	3.6
67	0.2	2.7
69	0.1	2.1
72	0.1	1.7
75	0.0	1.3
77	0.0	1.1
80	0.0	0.9
83	0.0	0.7

As can be seen from Table 3 that the separation factor has very strong temperature dependence. Higher temperature leads to lower separation. The capacity of anion exchange is very strongly at the beginning. As the experiment goes on, with the increase of bed volume fold, the anion exchange capacity is going down sharply.

Table 4 Comparison of the result with Jose Munoz's work

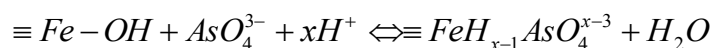
	Fe loading capacity(mmol Fe/g sponge)	Maximum adsorption capacity(mmol As/g sponge)	Maximum adsorption capacity(mmol As/mmol Fe)
Fe with sponge	0.250 ± 0.014	1.83	7.32
SPION with sponge	0.0955 ± 0.0029	1.094	11.455

After comparing the adsorption capacity of sponge loaded with SPION with that sponge loaded with Fe(III), it is found that Fe(III) load sponge has a better adsorption capability for As(V) per unit of sponge, it has a maximum adsorption capacity of 1.83mmol As/g sponge, and the SPION loaded sponge only has the maximum adsorption capacity of 1.094mmol As/g sponge. However, the SPION loaded sponge has a better adsorption capacity for As(V) per unit of Fe, it has the maximum adsorption capacity of 11.455 mmol As/ mmol Fe while the Fe(III) loaded sponge only has the maximum adsorption capacity of 7.32mmol As/mmol Fe. It is mainly because of that the Fe(III) loaded adsorption capacity is mainly due to the acid groups in the sponge. But the better adsorption capacity of SPION loaded sponge is because of not only the acid groups but also the good properties of SPION which has a high surface-volume ratio.

Modeling of Arsenic Adsorption by a Ligand-Exchange Process.

A monodantate ligand-exchange mechanism, based on the Fe:As stoichiometry 1:1 previously discussed, is proposed for the adsorption of arsenic(V) on the SPION loaded in the sponge, as it has been considered for other iron-based materials. The corresponding reactions can be

written as follows



With an equilibrium constant

$$K = \frac{[\overline{As}]}{[\overline{Fe}][H^+]^x[As]}$$

Where $[\overline{As}]$ indicates the amount of arsenic species adsorbed on the SPION in the sponge (mmol/g), $[\overline{Fe}]$ indicates the amount of iron adsorbed on the sponge and not complexed with As (mmol/g), $[H^+]$ indicates the concentration of free protons in solution (mmol/g), and $[As]$ indicates the free concentrations of the corresponding AsO_4^{3-} ions in solution (mmol/g) which have been calculated from the experimental values of total arsenic concentration and pH of the solution using the pKa values given before.

From equation , defining Y (g/mmol) as

$$Y = \frac{[\overline{As}]}{[\overline{Fe}][As]}$$

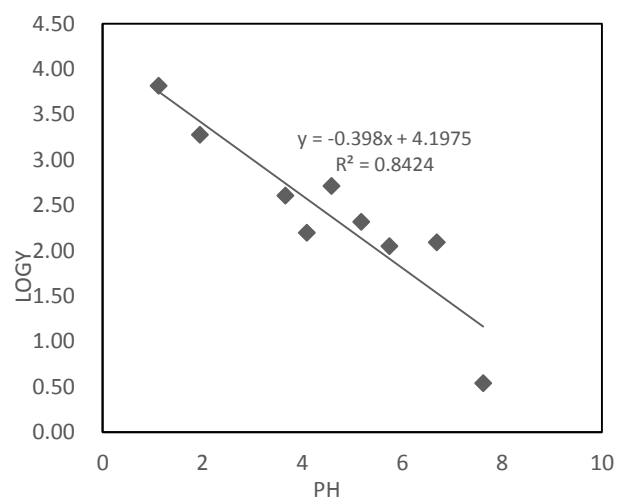
Then

$$\log Y = \log K - x pH$$

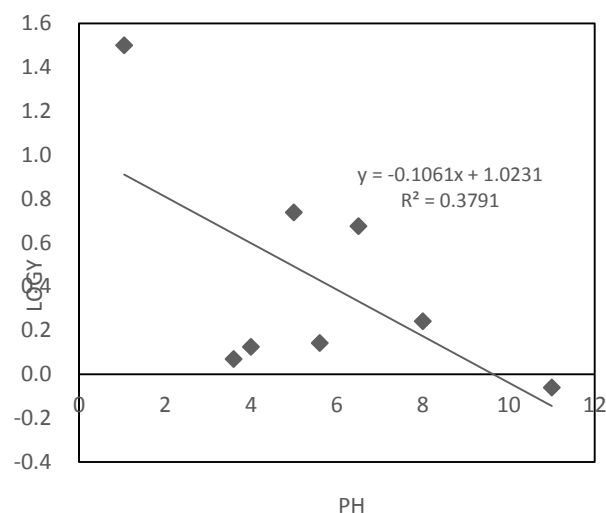
Y value at a given pH is estimated from the experimental data of arsenic adsorption by considering the formation of monodentate Fe-As complexes on the sponge. $[\overline{As}]$ is calculated from the differences in adsorption capacity between the SPION loaded and the blank sponge at each pH. $[\overline{Fe}]$ is calculated by subtracting the arsenic adsorption capacity and the iron desorbed from the initial amount of Fe(III) in the SPION-loaded sponge. $[As]$ in solution is determined as indicated in the experimental part.

A plot of logY vs pH for As(V) is given in Fig 14. The values of x and logK obtained by the least squares fit are shown in table 5. The model indicates that $H_2AsO_4^+$ are the As(V) chemical forms adsorbed on the Fe(III) loaded in the sponge in the pH range studied.

When reaction is expressed as a function of the adsorbed species, the stability of the complexes can be accurately evaluated:



a)



b)

Fig16 Modeling of arsenic species adsorption on the SPION-loaded in the sponge: linear relationship between log Y and pH for As (V).a) 20°C, b) 70°C

Table 5 Calculated Results from Fe-As Interaction Modeling Process Indicating the x and logK Values by the Least-Squares Fit

	pH range	X	logK	R
20°C	1-8	0.398	4.198	0.842
70°C	1-11	0.1061	1.023	0.379

As would be expected, As (V) adsorption on immobilized SPION is preferred under 20°C against that the adsorption performed under 70°C. Reversibility of both process has already been proved by corresponding arsenic desorption from the SPION-loaded sponge under 70°C. It also has proved the concept that the adsorption-desorption process could be controlled by changing the temperature. The regeneration and reusing of the adsorbent-SPION loaded sponge

will be possible after desorption. Alternatively, the sponge (which is an inexpensive material) could be compacted into an extremely small volume and disposed as a hazardous waste.⁴

Acknowledgement

Dynaphore Inc. (U.S.A.) is gratefully acknowledged for the samples supplied. I also should thank staffs from GTS, the Department of analytical chemistry. Thanks for their co-operation and assistance provided before and during the projects. In addition, thanks for the scholarship support of Chinese Scholar Council for the scholar-grant received.

Reference

- [1] Le Zeng, Arsenic Adsorption from Aqueous Solutions on an Fe(III)-Si Binary Oxide Adsorbent, *Water Qual. Res. J. Canada*, 2004, 39(3), 267–275
- [2] SUSHILRAJ KANEL, JEAN-MARK GRENE'CHE, AND HEECHU LCHOI, Arsenic(V) Removal from Groundwater Using Nano Scale Zero-Valent Iron as a Colloidal Reactive Barrier Material. *Environ. Sci. Technol.* **2006**, 40, 2045-2050
- [3] Dinesh Mohana, Charles U. Pittman Jr. Arsenic removal from water/wastewater using adsorbents—A critical review. *Journal of Hazardous Materials* 142 (2007) 1–53
- [4] R.S. Harisha, K.M. Hosamani, R.S. Keri, S.K. Nataraj, T.M. Aminabhavi, Arsenic removal from drinking water using thin film composite nanofiltration membrane. *Desalination* 252 (2010) 75 – 80
- [5] Vassilis Zaspalis, Adamantia Pagana, Styliani Sklari, Arsenic removal from contaminated water by iron oxide sorbents and porous ceramic membranes. *Desalination* 217 (2007) 167–180
- [6] Ernest O. Kartinen Jr., Christopher J. Martin An overview of arsenic removal processes, *Desalination* 103 (1995) 79-88
- [7] S. Song, A. Lopez-Valdivieso, D.J. Hernandez-Campos, C. Peng, M.G. Monroy-Fernandez, I. Razo-Soto, Arsenic removal from high-arsenic water by enhanced coagulation with ferric ions and coarse calcite, *WATER RESEARCH* 40 (2 0 0 6) 3 6 4 – 3 7 2
- [8] Myint Zaw, Maree T. Emett, Arsenic removal from water using advanced oxidation processes, *Toxicology Letters* 133 (2002) 113–118
- [9] Meng, X.; Bang, S.; Korfiatis, G. P. *Water Res.* **2000**, 34(4), 1255-1261.
- [10] Abrazheev, R. V.; Zorin, A. D. *J. Anal. Chem.* 1999, 54(12), 1106-1108.
- [11] Janet G. Hering, Pen-yuan Chen, etc. arsenic removal from drinking water during coagulation. *Journal of environmental engineering.* 1997, 801-807
- [12] Joan J. Waypa, Janet G. Hering. Arsenic removal by RO and NF membranes American Water Works Association. *Journal*; 1997, 89(10), 102-114
- [14] T. Burks, M. Avila, F. Akhtar.etal. *J. Colloid Interface. Sci.* 425(2014) 36-43.
- [14] Vagliasindi, G. A. F.; Henley, M.; Schultz, N.; Benjamin, M. M. *Proc. Water Qual. Technol. Conf.* 1996, Vol. Date 1995 (Pt. 2), 1829-1853.
- [15] Manning, B. A.; Goldberg, S. *Soil Sci. Soc. Am. J.* 1996, 60(1), 121-131.
- [16] Xu, Y.; Ohki, A.; Maeda, S. *Chem. Lett.* 1998, 10, 1015-1016.
- [17] Tokunaga, S.; Wasay, S. A.; Park, S. *Water Sci. Technol.* 1997, 35(7), 71-78.

- [18] Van der Hoek, E. E.; Bonouvrie, P. A.; Comans, R. N. J. *Appl. Geochem.* 1994, 9, 403-412.
- [19] Elizalde-González, M. P.; Mattusch, J.; Einicke, W. D.; Wennrich, R. *Chem. Eng. J.* 2001, 81, 187-195.
- [20] Fendorf, S.; Eick, M. J.; Grossl, P.; Sparks, D. L. *Environ. Sci. Technol.* 1997 31 (2), 315-320.
- [21] Yannick Mamindy-Pajany, Charlotte Hurel, Nicolas Marmier, Michèle Romeo, Arsenic adsorption onto hematite and goethite, *C. R. Chimie* 12 (2009) 876-881.
- [22] Jain, A.; Raven, K. P.; Loeppert, R. H. *Environ. Sci. Technol.* 1999, 33, 1179-1184.
- [23] L. Zeng, A method for preparing silica-containing iron (III) oxide adsorbents for arsenic removal, *Water Res.*, 37 (2003) 4351–4358.
- [24] Kelly B. Payne and Tarek M. Abdel-Fattah. Adsorption of Arsenate and Arsenite by Iron-Treated Activated Carbon and Zeolites: Effects of pH, Temperature, and Ionic Strength. *Journal of Environmental Science and Health*, 40:723–749, 2005
- [25] Y. Zhang, M. Yang and X. Huang, Arsenic (V) removal with a Ce(IV)-doped iron oxide adsorbent, *Chemosphere*, 51 (2003) 945–952
- [26] O.S. Thirunavakkarasu, T. Viraraghavan and K.S. Subramanian, Arsenic removal from drinking water using iron oxide-coated sand, *Water, Air, Soil Poll.*, 142 (2003) 95–111.
- [27] M.J. Haron, W.M.Z. Wan Yunus, N.L. Yong and S. Tokunaga, Sorption of arsenate and arsenite anions by iron(III)-poly(hydroxamic acid) complex, *Chemosphere*, 39 (1999) 2459–2466.
- [28] X. Meng, S. Bang and G.P. Korfiatis, Effects of silicate, sulfate, and carbonate on arsenic removal by ferric chloride, *Water Res.*, 34 (2000) 1255–1261.
- [29] J.H. Min and J.G. Hering, Arsenate sorption by Fe(III)-doped alginate gels, *Water Res.*, 32 (1998) 1544–1552.
- [30] I. Peleanu, M. Zaharescu, I. Rau, M. Crisan, A. Jitianu and A. Meghea, Nanocomposite materials for As(V) removal by magnetically intensified adsorption, *Sep. Sci. Technol.*, 37 (2002) 3693–3701.
- [31] Dmitri Muraviev, Ana Gonzalo, and Manuel Valiente. Ion Exchange on Resins with Temperature-Responsive Selectivity. I. Ion-Exchange Equilibrium of Cu^{2+} and Zn^{2+} on Iminodiacetic and Aminomethylphosphonic Resins. *Anal. Chem.* **1995**, 67, 3028-3035
- [32] Dmitri Muraviev, Ana Gonzalo, Nikolai A. Tikhonov, Manuel Valiente. Ion exchange on resins with temperature-responsive selectivity II. Thermo-induced concentration waves in ion-exchange column. *Journal of Chromatography A*, 802 (1998) 251–261
- [33] Dmitri Muraviev, Anna Gonzalo, Manuel Valiente. Ion exchange on resins with temperature-responsive selectivity III. Influence of complex formation stoichiometry on temperature dependence of resin selectivity. *Journal of Chromatography A*, 868 (2000) 143–152
- [34] Dmitri Muraviev, Ana Gonzalo, Nikolai A. Tikhonov, Maxim I. Iljin, Manuel Valiente. Ion exchange on resins with temperature-responsive selectivity IV. Influence of solution and column parameters on efficiency of reagentless separation of copper and zinc using thermo-induced concentration waves technique. *Journal of Chromatography A*, 867 (2000) 57–69
- [35] José Antonio Muñoz, Anna Gonzalo, Manuel Valiente. Kinetic and Dynamic Aspects of Arsenic Adsorption by Fe(III)-Loaded Sponge. *J Solution Chem* (2008) 37: 553–565

- [36] Abdusalam Uheida, German Salazar-Alvarez, Eva Björkman, Zhang Yu, Mamoun Muhammed, Fe_3O_4 and γ - Fe_2O_3 nanoparticles for the adsorption of Co^{2+} from aqueous solution. *Journal of Colloid and Interface Science* 298 (2006) 501–507
- [37] Abdusalam Uheida, Mònica Iglesias, Clàudia Fontàs, Manuela Hidalgo, Victòria Salvadó, Yu Zhang, Mamoun Muhammed, Sorption of palladium(II), rhodium(III), and platinum(IV) on Fe_3O_4 nanoparticles. *Journal of Colloid and Interface Science* 301 (2006) 402–408
- [38] Glenn A. Waychunas¹, Christopher S. Kim, and Jillian F. Banfield¹, Nanoparticulate iron oxide minerals in soils and sediments: unique properties and contaminant scavenging mechanisms. *Journal of Nanoparticle Research* (2005) 7: 409 – 433
- [39] J.G. Parsons, M.L. Lopez, J.R. Peralta-Videa, J.L. Gardea-Torresdey. Determination of arsenic(III) and arsenic(V) binding to microwave assisted hydrothermal synthetically prepared Fe_3O_4 , Mn_3O_4 , and MnFe_2O_4 nanoadsorbents. *Microchemical Journal* 91 (2009) 100 – 106
- [40] José Antonio Muñoz, Anna Gonzalo, Manuel Valiente. Kinetic and Dynamic Aspects of Arsenic Adsorption by Fe(III)-Loaded Sponge. *J Solution Chem* (2008) 37: 553–565
- [41] Marta A., Gustavo P., Mouhsine E., Laila M., Naaila O., Jose L. B. and Manuel V., The Open Environmental Pollution & Toxicology Journal, 2012, 3, (Suppl 1-M2) 2-12.
- [42] GUSTAVO P., MONTSERRAT L.M., MANUEL V. *Environ. Sci. Technol.* 2008, 42, 2309–2315
- [43] Ang B. C., Iskandar Idris Yaacob. *Journal of Materials Processing Technology* 191 (2007) 235–237
- [44] J.G. Parsons, M.L. Lopez, J.R. Peralta-Videa, J.L. Gardea-Torresdey. *Microchemical Journal* 91 (2009) 100–106.
- [45] Bilge Alyüz, Sevil Veli, Kinetics and equilibrium studies for the removal of nickel and zinc from aqueous solutions by ion exchange resins. *Journal of Hazardous Materials* 167 (2009) 482 – 488
- [46] JOSE ANTONIO MUNOZ ANNA GONZALO, AND MANUEL VALIENTE, Arsenic Adsorption by Fe(III)-Loaded Open-Celled Cellulose Sponge. Thermodynamic and Selectivity Aspects, *Environ. Sci. Technol.* 2002, 36, 3405-3411
- [47] Jing He, Song Hong, Liang Zhang, Fuxing Gan, and Yuh-Shan Ho. EQUILIBRIUM AND THERMODYNAMIC PARAMETERS OF ADSORPTION OF METHYLENE BLUE ONTO RECTORITE. *Fresenius Environmental Bulletin*, Volume 19 – No 11a. 2010
- [48] Chilton Ng, Jack N. Losso, Wayne E. Marshall, Ramu M. Rao. Freundlich adsorption isotherms of agricultural by-product-based powdered activated carbons in a geosmin – water system. *Bioresource Technology* 85 (2002) 131 – 135
- [49] Ming Hua, Shujuan Zhang, Bingcai Pan, Weiming Zhang, Lu Lv, Quanxing Zhang. Heavy metal removal from water/wastewater by nanosized metal oxides: A review. *Journal of Hazardous Materials* 211– 212 (2012) 317– 331
- [50] Anna Górka, Roman Bochenek, Jolanta Warchol, Krzysztof Kaczmarska, Dorota Antosa Ion exchange kinetics in removal of small ions. Effect of salt concentration on inter- and intraparticle diffusion. *Chemical Engineering Science* 63 (2008) 637 – 650
- [51] Dinesh Mohana, Charles U. Pittman Jr. Arsenic removal from water/wastewater using adsorbents—A critical review. *Journal of Hazardous Materials* 142 (2007) 1–53
- [52] Ming Hua, Shujuan Zhang, Bingcai Pan, Weiming Zhang, Lu Lv, Quanxing Zhang. Heavy

metal removal from water/wastewater by nanosized metal oxides: A review. *Journal of Hazardous Materials* 211– 212 (2012) 317– 331

[53] Jing Hu; Guohua Chen; and Irene M. C. Lo, M.ASCE, Selective Removal of Heavy Metals from Industrial Wastewater Using Maghemite Nanoparticle: Performance and Mechanisms. *J. Environ. Eng.* 2006.132:709-715.

[54] Vimlesh Chandra, Jaesung Park, Young Chun, Jung Woo Lee, In-Chul Hwang, and Kwang S. Kim, Water-Dispersible Magnetite-Reduced Graphene Oxide Composites for Arsenic Removal. *ACS NANO* 2010 VOL. 4 NO. 7 3979–3986

[55] Chang-Yan Cao, Jin Qu, Wen-Sheng Yan, Jun-Fa Zhu, Zi-Yu Wu, and Wei-Guo Song, Low-Cost Synthesis of Flowerlike α -Fe₂O₃ Nanostructures for Heavy Metal Ion Removal: Adsorption Property and Mechanism. *Langmuir* 2012, 28, 4573–4579

Annex II

Application of Synergic thermo tuning of redox potential for clean removal of Arsenic

Liu He^a, Tong Liu^a, Manuel Valiente*

Department de Química, Química Analítica, Universidad Autónoma de Barcelona, 08193
Bellaterra, Barcelona, Spain

Corresponding author footnote

Centre Grup de Tècniques de Separació en Química.

Tel. +34-935812903

Fax. +34-945811985

Email. Manuel.Valiente@uab.cat

Abstract

Development of new techniques for the clean removal of As(V) from aqueous matrixes is an important issue due to the high toxicity of this element. The present article relates to a reagentless recycled method for arsenic removal in water. In this paper, we develop a new method for Arsenic adsorption-- desorption and sorbent regeneration with no reagents added by taking advantage of the synergic thermo tuning of redox potential of the adsorption-desorption system.

Key words: Adsorption, desorption, thermo tuning, redox potential

1.Introduction

There is a growing interest in using low-cost methods and materials to remove arsenic from industrial effluents or drinking water before it may cause significant contamination. A lot of adsorbents and filters have been used for the treatment, including: ferric chloride[1], Fe(III)-doped alginate gels[2], nanocomposite adsorbent based on silica and iron(III) oxide[3], and iron oxide-coated polymeric materials[4], Fe(III)-loaded resins[5], Fe(III)-loaded sponge[6] are used in arsenic treatment because of the Fe(III) affinity toward inorganic arsenic species and consequent selectivity of the adsorption process.

In WO 2014122350A1 a filter for the treatment of liquid comprising a support made from a polymer material having at least one functional group from the group formed by carboxyl and thiol, loaded with SPION (SuperParamagnetic Iron oxide Nanoparticles)

In WO 2007/ 032860 a filter for eliminating described arsenic in water comprising a support of polyacrylonitrile (PAN) loaded with iron hydroxide nanoparticles .

The paper Morillo , D, Valiente , M., Perez , G., "Advances in adsorption Arsenic with Nanoparticles", Research Project, Master's Degree in Chemical Sciences and Technology , Universitat Autònoma de Barcelona , September 2009 , the use of a cellulose sponge as support,

in which SPION has dispersed , for removing arsenic in water.

The paper D. Morillo, A. Uheida, etcl. “Arsenate removal 3-mercaptopropionic acid-coated superparamagnetic iron oxide nanoparticles” has been described the arsenic removal by using 3-mercaptopropionic acid-coated SPION as adsorbent.

There is, however, although the filter or adsorbent has very high quality and efficiency to treat and adsorb arsenic, if they cannot be recovered and reused for several times, it is still very expensive and it is not very practical. As there are a lot of weaknesses of using reagents to recover the adsorbent or filter. Some new methods for adsorption-desorption recycled arsenic treatment and adsorbent/filter regeneration is really needed.

Almost all of the traditional methods have the problems on adsorbent/filter regeneration. Once the adsorbent/filter becomes exhausted, then, either the metals must be recovered, the sorbent/filter be regenerated or disposed in a controlled dumping site for toxic substances which use to be very expensive. Desorption and sorbent/filter regeneration is a critical step contributing to decrease process costs. A successful desorption process must restore the sorbent/filter close to its initial properties for effective reuse. In most of the published arsenic sorption studies (some discussed earlier), desorption/regeneration was not included. Very few desorption studies are detailed in literature. Furthermore, once arsenic is recovered in the pure and concentrated form, the problem of its disposal of this concentrated arsenic product must be addressed. This is a difficult and expensive task. Few attempts have been made to address the handling of concentrated arsenic wastes. (Tuutijärvi2006] has tried five different alkaline solutions: NaOH, Na₂CO₃, Na₂HPO₄, NaHCO₃ and NaAc for arsenate batch desorption and regeneration. But this process also needs to spend a lot of alkaline solution which is very expensive and is not feasible for industrial sense. Thus, in the present paper, we develop a new method for arsenic adsorption-desorption and sorbent regeneration by taking advantage of the synergic thermo tuning of redox potential for clean removal of the adsorption system.

The present work was aimed at investigating the reagentless method for arsenic (particularly As(V) and As(III)) adsorption-desorption and sorbent regeneration with no reagents added by taking advantage of the thermodynamic properties and redox potential of the adsorption system. This reagentless method could not only save a lot of reagent for recovering the sorbent, but also the adsorbent could be recycled and reused, which is low-cost and practical.

One of the objectives of the present study includes not only the new methods for arsenic adsorption-desorption by controlling the temperature or redox potential of reaction condition, but also some theoretical study which can explain the mechanism of the adsorption-desorption process. More importantly, we study effects of synergic thermo tuning and redox potential on the adsorption-desorption process. The aim of this study is to provide a totally new concept and reagentless method to recover the arsenic and regenerate the adsorbents for recycled arsenic removal treatment.

The influence of temperature and redox potential on the adsorption-desorption rate has been

studied. In addition, the thermodynamic aspects for realizing the adsorption-desorption process have been evaluated. Besides that, the application of oxidation of As(III) to As(V) and the reduction of As(V) to As(III) in order to realize the adsorption-desorption process have been characterized. More importantly, the thermodynamic aspects combined with the redox potential effect for controlling the adsorption-desorption process have been developed.

2. Experiment section

2.1 Reagents and Apparatus

$\text{Na}_2\text{HAsO}_4 \cdot 7\text{H}_2\text{O}$, $\text{FeCl}_3 \cdot 6\text{H}_2\text{O}$, $\text{FeCl}_2 \cdot 4\text{H}_2\text{O}$, were used as As(V), Fe(III), Fe(II) sources. Zinc powder and Tin foil used for the reduction purpose. Forager Sponge, supplied by Dynaphore Inc. (Richmond, VA, U.S.A.) was used as the support for the SPION. Metal concentrations in solution were determined by the Colorimetric technique. The wavelength used for analysis were 840 nm (As), 490 nm (Fe). Lewatit S-3428 resin was supplied by Purolite.

2.2 Preparation of the Adsorbents

2.2.1 Synthesis and characterization of nanoparticles

The synthesis procedure of SPION has been described elsewhere [14]. SPION are prepared in our lab by mixing iron (II) chloride and iron (III) chloride in the presence of ammonium hydroxide. First, deoxygenated the solution of NH_4OH (0.7M) by nitrogen. Second, deoxygenated the solution of 12mL HCl (0.1M) by nitrogen and mix $\text{FeCl}_3 \cdot 6\text{H}_2\text{O}$ with it. Third, heat the NH_4OH solution at 70 °C. Fourth, Add the $\text{FeCl}_3 \cdot 6\text{H}_2\text{O}$ solution into the NH_4OH solution and react for 30min. Then, Add the $\text{FeCl}_2 \cdot 4\text{H}_2\text{O}$ in the previous solution with mechanic agitation of about 3000rpm and waiting for 45min, the dark precipitate will be formed, which consists of nanoparticles of magnetite. Last, wash it by MiliQ water which has been deoxygenated and centrifuged four times(3 times for 3 min and 5000rpm, 1 time for 10 min and 4500rpm) and preserve it by 50mL 0.1M TMAOH.

2.2.2 Clean of the Forager sponge

An initial conditioning of the sponge consisting on the conversion into its acidic form by consecutive treatment with 1.0mol/L HCl , double distilled water, and HCl solution at pH 2.5 was carried out in a glass preparative column. A portion of this conditioned sponge was separated, dried during 24 h, and stored in a desiccator for its use

2.2.3 Loading of SPION on the sponge

The sponge was loaded with SPION by using the nebulizer. The SPION-loaded sponge was dried during 24 h, and stored in a desiccator for its use. The SPION loading capacity was 0.0955 ± 0.0029 mmol Fe/ g sponge

2.3 Characterization

The SPION, sponge loaded with SPION before using and after using have been characterized by TEM to see the particle size and dispersion. SPION are highly dispersible in solutions. With particle sizes of from 6-20 nm, they offer a large surface area and superparamagnetic properties.

2.4 Temperature influence

The adsorbent has been used to adsorb the arsenic in the water, the results show that the

adsorption capacity is influenced by the temperature. The adsorption capacity is decreasing as the temperature increases. That means as temperature increases, the desorption is starting to occur. Lower temperature helps the adsorbent adsorb the arsenic and higher temperature helps the adsorbent to desorb the arsenic. So, the inventor adsorbs the arsenic by using the adsorbent under room temperature and desorbs the arsenic under 70°C.

2.5 Redox potential effect on adsorption- desorption

The potassium dichromate has been used to oxidize the As(III) to As(V) and use the Zn powder or Sn foil to reduce the As(V) to As(III). Since the adsorbent has much higher adsorption capacity of As(V) than that of As(III), the adsorbent can adsorb the arsenic by oxidizing all of the As(III) to be As(V) and desorb the arsenic by reducing the As(V) to be As(III).

2.6 column continuous mode

The column continuous mode has been made in order to do the adsorption-desorption recycled processing. The adsorbent could be put inside the column. Once the wastewater which contains the arsenate and arsenite pass through the column, the arsenate and arsenite is loaded on the adsorbent and the clean water goes out. After loading, the arsenate and arsenite could be eluted by passing the hot water (70°C) or hot water combined with Sn. Therefore the adsorbent can be reused.

Above all, the desorption process can be happened by reducing with the help of higher temperature and the adsorption process can be happened by oxidizing under room temperature(if the temperature is lower, for example, 10°C, then the adsorption capacity will higher than that under room temperature, but we consider about the room temperature is normal and easy to control).

Once finishing the desorption process, the adsorbent can be used again for adsorbing arsenic under room temperature. And then desorb the arsenic by using the Zn powder under 70°C again. To repeat this adsorption-desorption process for several cycles, then the adsorbent will be useless. But the recycled method and process is really amazing since it can be saved a lot of money for reuse the adsorbent.

2.7 Adsorption-desorption

The batch mode and column mode have been used to do the adsorption-desorption process. As for the batch mode, the arsenic is adsorbed by the adsorbent in a stoppered plastic bottle with the help of agitating. The desorption process is occurred either by putting the plastic bottle in the high temperature atmosphere or with the help of Zn powder or Sn. In the column mode, the arsenic is adsorbed by adsorbent inside the column by passing the wastewater through the column. The desorption process could be realized by passing the hot water or with the help of Sn.

3 Results and discussion

3.1 The concept of redox potential part:

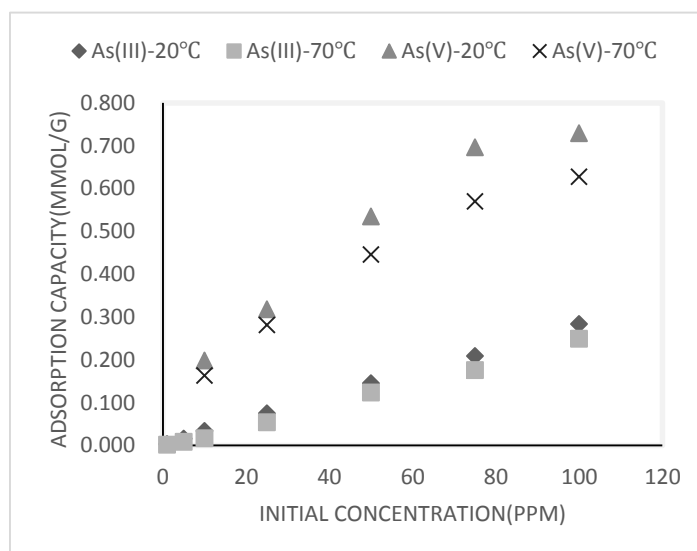


Fig 1 Effect of oxidation state on arsenite and arsenate adsorption, adsorbent dosage 50mg, pH=3.6, contact time 1hour, the initial concentration 1-100ppm.

Modifying the redox potential, therefore transforming between arsenite and arsenate, in order to control the adsorption-desorption is attributed to the significant difference adsorption capacity of SPION loaded sponge for As(V) and As(III), as shown in Fig 1. The adsorbent of SPION loaded sponge has much higher adsorption capacity for the As(V) adsorption than that for the As(III), as consequence of different acid properties of arsenate and arsenite. Many studies aiming at elucidating the structure of arsenate complexes adsorbed on iron oxide nanoparticles have been done. Extended X-ray absorption fine structure (EXAFS)¹ and Fourier Transform Infrared Spectroscopy (FTIR)² have shown As(V) and As(III) to form monodentate and bidentate inner sphere surface complexes with iron (hydr)oxide sites in co-precipitated and adsorbent solids.³ In the case of As(V), the possible chemical structures which arsenate may form on the iron oxide surface upon chemical adsorption are different, such as monodentate, bidentate mononuclear, bidentate binuclear. Although there is no consensus regarding to the structure of the complex of arsenate bonding with iron oxide nanoparticles being monodentate or bidentate, Some literature reports confirmed and demonstrated that arsenic complexes were formed via the hydroxyl groups at the iron oxide surface.⁴ This is a very tight bond, and once the bond is formed, removal of the arsenic is difficult. In the case of As(III) adsorption by iron (hydr)oxides, both bidentate binuclear-bridging complexes(Fe-O-As(OH)-O-Fe) and monodentate complexes have been observed.⁵ A monodentate complex is one in which a single oxygen atom from the arsenite oxyanion coordinates a single structural Fe³⁺ at the iron (hydr)oxide surface, which is not thermodynamically stable and the bond is easy to be broken.

By changing the redox potential, the transform between As(V) and As(III) will lead the adsorption-desorption process and recycled use of the adsorbent. At the same time, the thermo tuning can help the adsorption-desorption to be much more significant and much quicker.

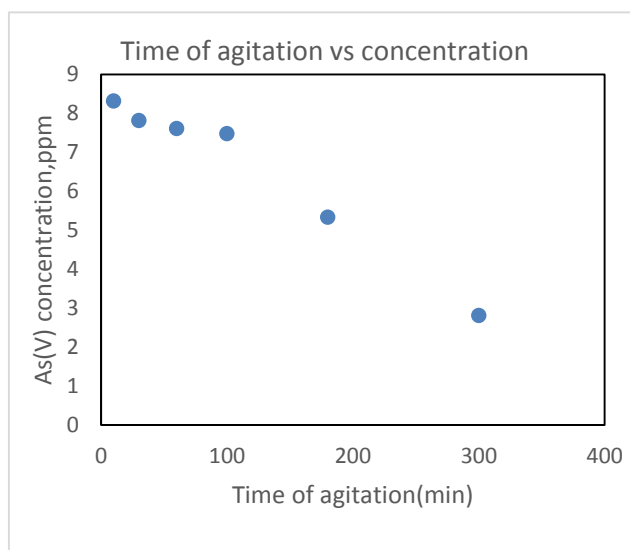


Fig 2 redox potential-different time-desorption

The experiment of redox potential effect on desorption has been carried under 20°C (shown in Fig 2). The adsorbent (sponge loaded with SPION) was used for adsorb the arsenate, which make the surface and porous of the adsorbent is full of arsenate (10.34mg arsenic/g adsorbent). Then, 50mg of Tin foil was used as the reduction reagent for desorption, and the aqueous solution pH 3.6 with the contact time from 10-300min. As time goes on, Sn could transform the arsenate to arsenite, which has weak bond to the iron oxide nanoparticles, therefore desorb from the adsorbent. That means the Tin change the redox potential, which could help to realize the desorption process. Arsenate (As(V)) react with Sn in buffered aqueous solutions to produce arsenite (As(III)).⁶ The electron transfer reactions can be described in terms of thermodynamics through the use of standard electrode potentials.⁷

3.2 Further proof of redox potential part

The potassium dichromate ($K_2Cr_2O_7$) could oxidize the arsenite to arsenate by changing the solution redox potential.

Table 1 oxidation rate of As(III) to As(V) by potassium dichromate

Initial concentration of arsenite(ppm)	Concentration of potassium dichromate(mmol)	After oxidation, concentration of arsenate(ppm)	Conversion rate
94.913	1.33	87.192	91.87%
96.317	1.33	88.615	92.00%

Table 2 reduction rate of As(V) to As(III) by Zn powder

Arsenate loaded on the	After reduction, the arsenic left in the	After reduction, the arsenic left in the	Conversion rate

sponge(ppm)	sponge(20°C)ppm	sponge(70°C)ppm	
18.569	4.119	1.239	93.33%
18.931	3.780	1.827	90.35%

The oxidizing agent (potassium dichromate) could convert ~92% of arsenite to arsenate (as shown in Table 1). Meanwhile, the reducing reagent (Zn powder) could reduce the arsenate to arsenite (as shown in Table 2) by changing the redox potential, the conversion rate could be ~90%, which is very high and could help the desorption to happen. The arsenate could be much more adsorbed due to its acidity that provides high proportion of deprotonated species presents in the media at the pH of study, thus leading to a major contribution in the adsorption capacity. The sponge-SPION provide more probability to interact with arsenate and react by ligand exchange to the adsorption system. Thus arsenate has much higher adsorption rate than arsenite. By changing the redox potential, therefore transforming the arsenite to be arsenate, could help the adsorption to occur.

3.3 The synergic thermo tuning of redox potential part:

Table3 Combination of temperature effect with redox potential effect for desorption

	After adsorption		After desorption (20°C+ reduction)		After desorption (70°C+ reduction)	
adsorbent	Sponge (ppm)	Sponge- SPION(ppm)	sponge	Sponge- SPION	sponge	Sponge- SPION
concentration	18.569	21.398	3.780	9.165	1.239	7.571
concentration	18.931	21.243	3.532	9.482	1.827	7.323

Table 3 the synergic thermo tuning of redox potential part: shows that in the bed mode, both of the temperature and redox potential have significant effect on arsenic adsorption-desorption. It could be combined the temperature effect with redox potential in order to get the better and stronger desorption process without adding reagents. It shows that in the bed mode, the adsorbent in the column could firstly adsorb the arsenic and then, the arsenic which are loaded in the adsorbent could be eluted by hot water with the help of Sn. After elution, the adsorbent could be reused to adsorb the arsenic again. Which means, the adsorption-desorption recycled process could be realized and the adsorbent could be reused for several times.

3.4 Column Experiment part

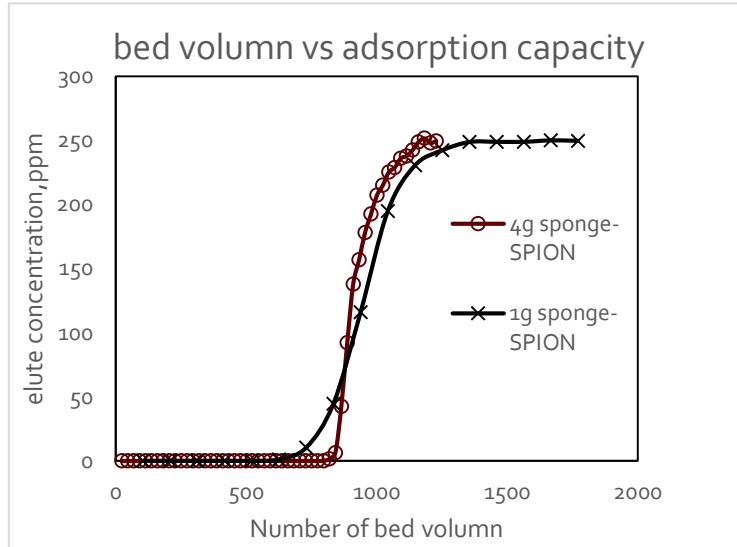


Fig 4 Column mode –different dosage effect on elute concentration. Initial stock solution concentration=250ppm, T=293K, 1g sponge loaded with SPION, pH=3.6.(Adsorption capacity of 4g sponge-SPION=100.06mg As/g sponge, Adsorption capacity of 1g sponge-SPION=99.14mg As/g sponge)

The observed data in Fig 4 shows the adsorption capacity obtained using 4g adsorbent(sponge loaded with SPION) or 1g adsorbent is the same, which indicates the homogeneity of the adsorbent prepared.

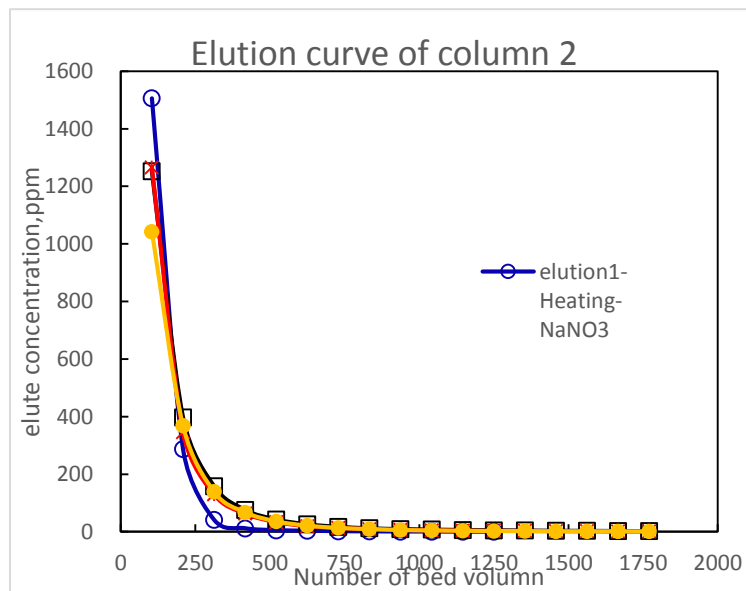


Fig 5 comparison of different methods for desorption

Table 4 comparison of recovery rate by using different methods for desorption

	No heating-NaCl	Heating+Reduction	Reduction	Heating+NaNO ₃
total elute, mg	86.29	95.79	101.47	93.08

recovery,%	92.80	94.22	96.52	85.64
------------	-------	-------	-------	-------

The comparison of different methods for desorption, the temperature with the help of NaNO_3 , the reduction-tuning methods, the thermo tuning of redox potential way as well as the NaCl as desorption reagent for desorption have been evaluated as shown in Fig 5. In the case of NaCl at room temperature (no temperature effect and no redox conditions), the 92.80% recovery rate is due to the strong affinity of the Cl^- for Fe(III) present in SPION, helping thus the release of adsorbed arsenate. However, in the desorption step, the effect of the anions NO_3^- or Cl^- , which could compete with the arsenic oxyanions therefore could help the desorption process, show lower recovery rate, which is 85.64% and 92.80% than those by the redox potential tuning effect, which is 96.52% and 94.22%, respectively. Which means that redox potential tuning has stronger impact on the desorption process.

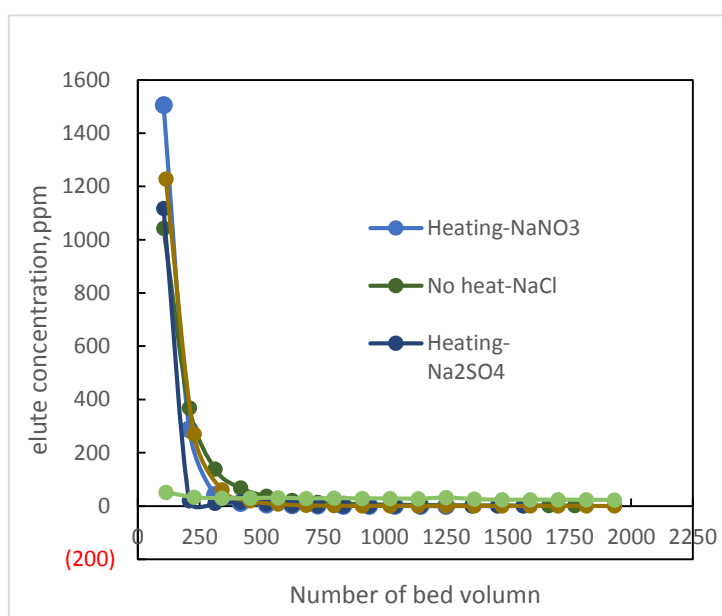


Fig 6 elution by different methods with different competing anions

Fig 5 and Fig 6 shows that the temperature and redox potential have significant effect on elution, which make the desorption to be very efficient. From the Figures, it is clear to see that the desorption is efficient and complete. The complete desorption process is attributed to the thermo tuning effect combined with the redox potential function. Furthermore, this completely desorption results in very “clean ” sponge loaded with SPION, which is fully prepared for the next cycle of adsorption. The recovery proportion is almost 100%.

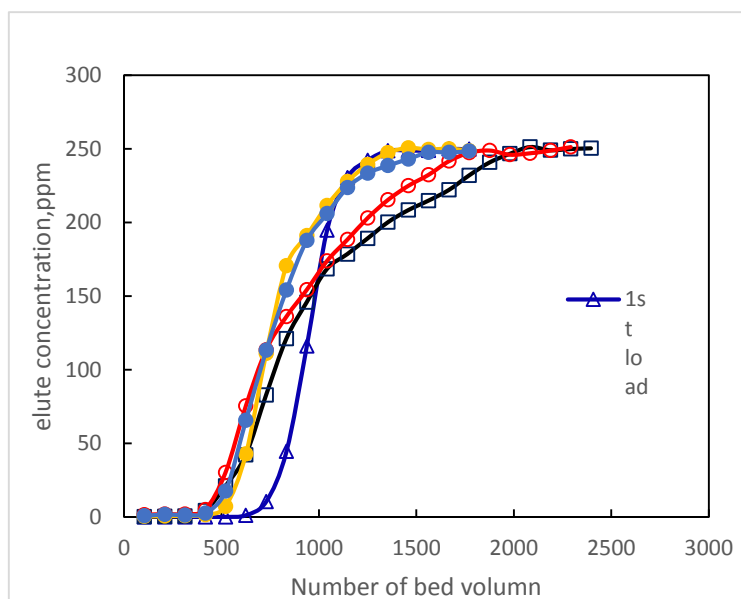


Fig 7 Different loading

The several times repeated loading of arsenic on the adsorbent are shown in Fig 7. As can be seen from the data presented in Fig 7, the sponge loaded with SPION as adsorbent under study demonstrate very good adsorption capacity, which the arsenic adsorption in the column can repeat for several cycles., therefore the recycled function of the adsorbent and the reuse processes are realized. The adsorbent regeneration and arsenic recovery is mainly due to the synergic thermo tuning of redox potential effect.

3.5 Cycled column experiment part:

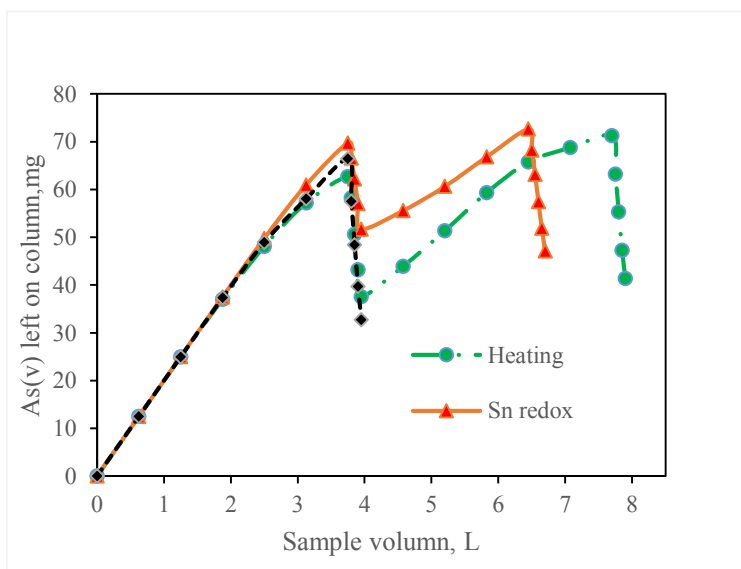


Fig.8 means that the adsorption and desorption process can repeat.

Experiment 1, elute by heating

- 1) Load As(v) 250ppm on the column(1g sponge+spion), collect the elute in six 50ml tubes.
- 2) Elute the column by 50ppm As(v) solution, by heating to 70°C, collect the elute in four

50ml tubes.

- 3) Reload As(v) 250ppm on the column, collect the elute in six 50ml tubes.
- 4) Elute the column by 50ppm As(v) solution, by heating to 70°C, collect the elute in four 50ml tubes.

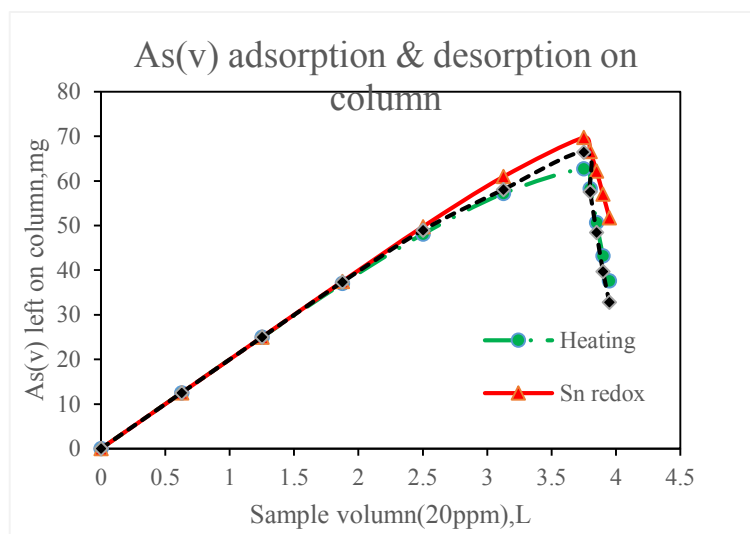


Fig.9 means that the desorption effect of the three methods

Experiment 2, elute by Sn-redox

- 1) Load As(v) 250ppm on the column(1g sponge+spion), collect the elute in six 50ml tubes.
- 2) Elute the column by 20ppm As(v) solution, by passing the Sn-redox column(80g), collect the elute in four 50ml tubes.
- 3) Reload As(v) 250ppm on the column, collect the elute in four 50ml tubes.
- 4) Elute the column by 20ppm As(v) solution, by passing the Sn-redox column, collect the elute in four 50ml tubes.

Heating+Redox > Heating > Sn-redox

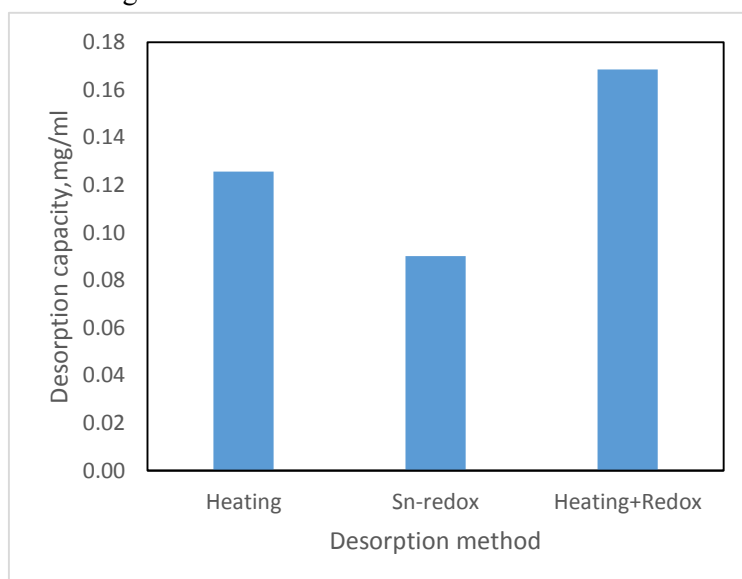


Fig.10 means that at the elution step, when we add 1 ml of As solution, we can have 0.13mg, 0.09mg, and 0.17mg of As eluted from the column material. So when we use Heating+Redox method, the elution will be better.

Experiment 3, elute by heating+Sn-redox

- 1) Load As(v) 250ppm on the column(1g sponge+spion), collect the elute in six 50ml tubes.
- 2) Elute the column by 20ppm As(v) solution, by passing the Sn-redox column(80g), and heat to 70°C, collect the elute in four 50ml tubes.

3.6 Real waste water

Table 5: The original concentration of different elements in real waste water

	ppm
Fe	979
Al27	773.5
Mg 26	715.5
Zn	198.5
Cu	194.8
Mn 55	74.2
Ca 44	39.9
Si 28	34.7
Na 23	14.1
Co 59	7.0
As	3.1
Li 7	2.8
Ni	2.2
Cd 114	2.1
Sr 88	1.8
Ba 138	1.5
Ti 47	1.4
Cr 52	1.3
V 51	1.3
Sb 123	1.3
Mo 95	1.3
Ag 107	1.0
Se 82	0.4
Pb	0.2

The real waste water sample is from a river called “Rio Tinto” from Huelva, Andalusia (Spain) and was proportioned by AGQ Mining and Bioenergy, a Spanish company. The real waste water sample has a high concentration of iron which has to be eliminated before arsenic removal.

The pretreatment of the sample is bubbled with air for 4 hours, oxidizing the Fe^{2+} to Fe^{3+} , the pH of the real waste water (originally 2.45), is changed to be 3.6 by adding NaOH. The precipitation is removed by using a filter, obtaining “iron-free” wastewater. But at the same time, the arsenic is also precipitated by iron precipitation. So the “iron-free” wastewater was doping by 60ppm arsenate solution, therefore the obtained the real wastewater using for our study is wastewater simulation, which contains inorganic arsenic species, meanwhile has other ions interferences.

After treating the wastewater, the arsenic is adsorbed and the results are shown below in the Table 6. As expected, The first sample demonstrate that the method performs well because almost all the arsenic present in the first 50mL has been adsorbed in the SPION loaded sponge despite other elements presented in the sample can be adsorbed too (ICP show that interfering elements such as Zinc or Copper are present in a higher concentration than arsenic), the removal efficiency is very good at the beginning (97.82% removal). However, if passing more volume of the real waste water, the removal percentage of the arsenic species is sharpening down since the interference ions, which compete with the arsenic oxyanions to be adsorbed. Therefore, the removal of the interference ions before adsorbing the arsenic species is very necessary and important. The method will perform better if instead of one column is used creating a system of columns interconnected.

Table 6 Real waste water absorption results

Sample	Real Concentration (ppm)	Removal percentatge (%)
Initial concentration	45,29	
After passing through the resin	44,32	
1	0,99	97,82
2	22,66	49,97
3	36,05	20,39
4	39,37	13,08
5	39,63	12,50
6	44,26	2,28
7	43,26	4,49
8	43,99	2,87
9	43,78	3,34

Acknowledgement

Dynaphore Inc. (U.S.A.) is gratefully acknowledged for the samples supplied. I also should thank staffs from GTS, the Department of analytical chemistry. Thanks for their co-operation and assistance provided before and during the projects. In addition, thanks for the scholarship support of Chinese Scholar Council for the scholar-grant received.

Reference

- [1](M.J. Haron, W.M.Z. Wan Yunus, N.L. Yong and S. Tokunaga,1999)
- [2](X. Meng, S. Bang and G.P. Korfiatis,2000)

- [3](J.H. Min and J.G. Hering,1998)
- [4](I. Peleanu, M. Zaharescu, I. Rau, M Crisan, A. Jitianu and A. Meghea,2002)
- [5](Dmitri Muraviev, Ana Gonzalo, and Manuel Valiente,1995)
- [6](José Antonio Muñoz, Anna Gonzalo, Manuel Valiente, 2008)
- [7]Dmitri Muravieva ,1, Ana Gonzaloa, Nikolai A. Tikhonovb, Manuel Valiente*,Ion exchange on resins with temperature-responsive selectivity II. Thermo-induced concentration waves in ion-exchange column. Journal of Chromatography A, 802 (1998) 251–261
- [8] I-Hsien Lee, Yu-Chung Kuan, Jia-Ming Chern, Equilibrium and kinetics of heavy metal ion exchange. Journal of the Chinese Institute of Chemical Engineers 38 (2007) 71–84
- [9] Dmitri Muraviev, Ana Gonzalo, Nikolai A. Tikhonov, Maxim I. Iljin.
Manuel Valiente. Ion exchange on resins with temperature-responsive selectivity IV. Influence of solution and column parameters on efficiency of reagentless separation of copper and zinc using thermo-induced concentration waves technique. Journal of Chromatography A, 867 (2000) 57–69
- [10] Anna Górka, Roman Bocheneka, Jolanta Warchoń, Krzysztof Kaczmarskia, Dorota Antos. Ion exchange kinetics in removal of small ions. Effect of salt concentration on inter- and intraparticle diffusion. Chemical Engineering Science 63 (2008) 637-650
- [11]Norman B. Rainer. Ion-adsorbent sponge product. US patent, patent number: 5162404
- [12] Raffaella Biesuz, Maria Pesavento, Anna Gonzalo, Manuel Valiente. Sorption of proton and heavy metal ions on a macroporous chelating resin with an iminodiacetate active group as a function of temperature. Talanta 47 (1998) 127–136
- [13] Dmitri Muraviev, Ana Gonzalo, and Manuel Valiente. Ion Exchange on Resins with Temperature-Responsive Selectivity. 1 .Ion-Exchange Equilibrium of Cu^{2+} and Zn^{2+} on Iminodiacetic and Aminomethylphosphonic Resins. Anal. Chem. 1995, 67,3028-3035.
- [14] Dmitri Muraviev* , Anna Gonzalo, Manuel Valiente. Ion exchange on resins with temperature-responsive selectivity.III. Influence of complex formation stoichiometry on temperature dependence of resin selectivity. Journal of Chromatography A, 868 (2000) 143–152.

Annex III

Kinetic and Dynamic Aspects of Selenate and selenite adsorption by γ - Al_2O_3 nanospheres

Liu He^a, Veronica Verdugo^a, Tong Liu^a, Manuel Valiente

Department de Quimica, Quimica Analitica, Universidad Autonoma de Barcelona, 08193
Bellaterra, Barcelona, Spain

Corresponding author footnote

Centre Grup de Tecniques de Separacio en Quimica.

Tel. +34-935812903

Fax. +34-945811985

Email. Manuel.Valiente@uab.cat

Abstract

Selenium is a toxic element with a relatively high mobility in the natural waters. In this work we study the kinetics of adsorption of Se(IV), and Se(VI) on γ - Al_2O_3 through batch experiments of room temperature and high temperature. Results show that under 20°C, the maximum adsorption for selenate and selenite on γ - Al_2O_3 nanospheres was achieved at pH 2 in 6 hours, the adsorption of selenium presents an anion exchange behavior, decreasing at higher pH values. In the case of Se (VI) the sorption decreases as the percentage of the aqueous species HSeO_4^- decreases. While for 70°C, the maximum adsorption was attained in 14 hours. The kinetic studies show that they are fitted very well to the pseudo-second order, this suggests that selenium ions were adsorbed onto the aluminum nanosphere surface via chemical interaction. The adsorption of γ - Al_2O_3 nanosphere for selenate and selenite were fitted very well to Freundlich isotherm model, which is indicated that the γ - Al_2O_3 nanosphere as adsorbent was multilayer coverage by selenium. The ΔH value of Se (IV) and Se (VI) between 20°C and 70°C were -13.955 KJ mol⁻¹ and -3.927 KJ mol⁻¹ shows that lower temperature favor removal of selenium.

Key words: Selenite, Selenate, kinetic, γ - Al_2O_3 nanosphere

INTRODUCTION

Selenium is a natural trace element present in the Earth's crust. It is an essential nutrient which plays an important role in biologic and physiologic body functions. However, when certain levels are attained, selenium is highly toxic and the effects depend on various factors, including the oxidation state of the element. The World Health Organisation (WHO) has recommended the maximum contaminant level (MCL) of 40 $\mu\text{g l}^{-1}$ for total selenium in drinking water³.

Selenium can exist in different oxidation states, elemental selenium (Se_0), selenite (SeO_3^{2-}), selenide (Se^{2-}) selenato (SeO_4^{2-}) and organic selenium. Selenite and selenate are found to be thermodynamically stable under the pH and redox conditions that are found in most aqueous media and are the predominant forms¹.

Although multiple methods have been reported for selenite and selenate removal, such as

precipitation⁵, ion exchange⁶, membrane filtration^{6,7}, reverse osmosis⁸, chemical reduction with iron^{9,10}, microalgae-bacterial treatment¹¹; adsorption has received more attention due to its high concentration efficiency and simple procedure that overcome most of the drawbacks of other techniques.

Numerous adsorbents have been used in selenium adsorption. The adsorbents that have been used included activated alumina^{12,13}, clays¹⁴, iron nanoparticles suspension¹⁵, goethite and hematite¹⁶ and Fe-loaded activated carbons¹⁷. Adsorption of Se by metal oxides such as iron oxides and aluminum oxide has been demonstrated and shown as promising method for selenium removal^{13,18,19}. Aluminum and iron are present in most of them, because Al- and Fe-oxides have high surface areas and point zero charge²⁰. In our study, we choose γ -Al₂O₃ which is a different type of Al-oxides because of morphological characteristics such as particle/pore size, shape and structure. It has hollow structure which provides them low density, high specific surface area, and closely packed interpenetrating networks²¹. The aim of this work is to investigate the feasibility and effectiveness of hollow-structured aluminum nanoparticles in the sorption of Se(IV) and Se(VI) ions from acidic aqueous solution. The adsorption mechanism and sorption properties were studied under static mode of operation.

2 Experimental section

2.1 Reagents and Apparatus

The Se(VI) and Se(IV) source was sodium selenate and sodium selenite, Na₂SeO₄, Na₂SeO₃, ACS reagent from Aldrich (Milwaukee, USA). KAl(SO₄).12H₂O, Urea, NaAc and HAc were ACS reagents from Panreac S.A. (Barcelona, Spain). Selenium concentration in solution was determined by the ICP-MS technique. In all the experiments, the initial and final pH was measured, pH was controlled by using a Crison pH meter micropH 2002 (Barcelona, Spain) with a combined glass electrode.

2.2 Preparation and characterization of the adsorbents

The γ -Al₂O₃ hollow nanospheres adsorbents were readily prepared in our lab by mixing the aluminium potassium sulfate dodecahydrate (KAl(SO₄).12H₂O) and Urea (CO(NH₂)₂) in distilled water and stirred. The resulting solution was put into a microwave vessel for heating. The pH of the resulting solution was adjusted with sodium hydroxide to 9.0. The obtained white precipitate was separated and washed by ethanol. The product was dried in the oven for 12h. Finally, the resulting form of the material synthesized (r-AlOOH) was converted into nano-r-Al₂O₃ by calcinating it in the muffle. We characterized the samples by scanning electron microscope (SEM ZEISS EVO@ MA 10, Oberkochen, Germany) to see the particle size and structure.

2.3 Selenium adsorption

2.3.1 Effect of contact time

Experiments to determine selenium adsorption in different contact time were carried out at 2-1440 mins in batch conditions.

2.3.2 Effect of initial concentration

Experiments to determine selenium adsorption capacity in different initial concentration were carried out at 2-100 ppm in batch conditions.

2.3.3 Effect of pH

Experiments to determine selenium adsorption in different pH were carried out at pH 2.0-11.0 in batch conditions by using stoppered polystyrene tubes. Corresponding agitation was carried out in a rotary rack shaker during 18 h (this contact time was confirmed in separate experiments). Once the equilibrium was reached, samples were taken and filtered through 0.22 μ m pore size filters. Selenium concentration in solution was determined by ICP-MS. Experiments were repeated for the different conditions a minimum of two times.

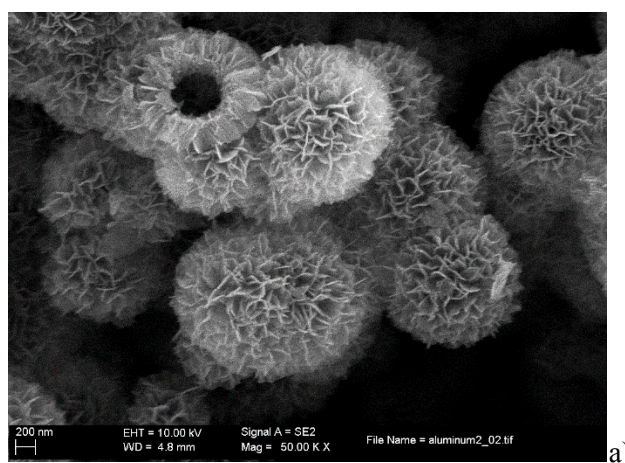
2.3 Kinetics on Se(IV) and Se(VI) Adsorption

The sorption rate was measured by shaking stoppered polystyrene tubes containing 0.005 g of the adsorbents and 25 mL of a 1 ppm selenate solution in a rotary rack shaker during different time periods. After the corresponding time, the sample was filtered and the Se(IV) and Se(VI) content measured by ICP-MS. The saturation degree is calculated by comparison with the initial Se(IV) and Se(VI) concentration in the solution to evaluate the minimum time for complete saturation of the adsorbents.

3 Results and discussion

3.1 Characterization of adsorbent material--SEM-EDX analysis

Adsorbent (i.e. γ - Al_2O_3 nanosphere) shape and size impact the adsorption capacity of the adsorbent. SEM images of fresh γ - Al_2O_3 nanospheres indicate that the material is composed of individual, hollow-spherical particles ranging in size from 200 to 400 nm that form aggregates and chains (Fig1a). This small γ - Al_2O_3 nanospheres provides a larger surface area for contaminant adsorption. Energy Dispersive X-ray (EDX) analysis data (Fig1b) show that the main compositions of the sample are Al and O, which confirms the nanosphere composition. The SEM images of γ - Al_2O_3 nanospheres after adsorption for the selenium was shown in Fig 1c. The adsorption of selenium on the γ - Al_2O_3 nanospheres did not influence the structure of the nanoparticles.



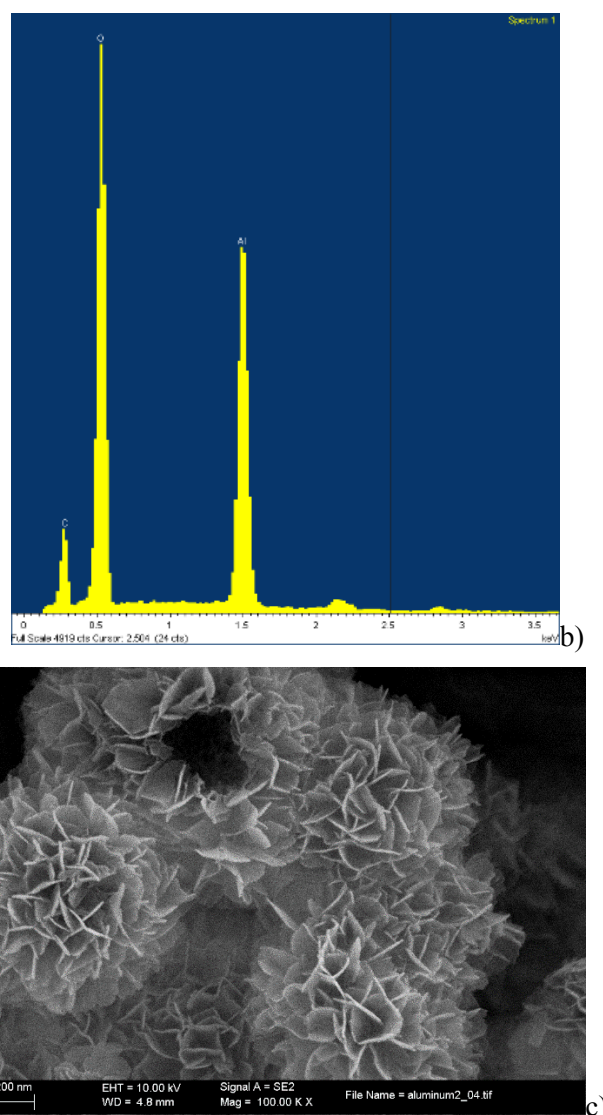


Fig 1 SEM image of γ - Al_2O_3 nanospheres a) before adsorption of selenium b) EDX analysis c) after adsorption of selenium

3.2 Comparison of AlOOH , γ - Al_2O_3 , modified γ - Al_2O_3 for selenium adsorption

AlOOH hierarchically nanostructured hollow microspheres²¹ with nanoflake-like porous surface textures was fabricated in our lab by chemically induced self-transformation of metastable solid particles of amorphous aluminum oxyhydroxide produced in situ within hydrothermal reaction mixtures containing aluminum sulfate and urea.²² The hollow structured γ - AlOOH microsphere has first been used for selenium adsorption to see how it behaves and how much the adsorption capacity of the γ - AlOOH microsphere is. AlOOH hierarchically nanostructured microspheres are used as the precursor and template for the preparation of γ - Al_2O_3 hierarchically nanostructured nanospheres by thermal transformation of AlOOH at 600°C in microwave, and the morphology is well preserved during the thermal transformation process. This process produce intact hollow sphere spheres of γ - Al_2O_3 . The comparison between the adsorption of selenate and selenite by γ - AlOOH microsphere and γ - Al_2O_3 nanospheres has been studied and the results are shown in Fig 2. The γ - Al_2O_3 nanospheres has much higher adsorption capacity for adsorbing selenate and selenite than that of γ - AlOOH

microsphere. Therefore, in the following work, we use γ - Al_2O_3 nanospheres as the adsorbent for selenate and selenite adsorption.

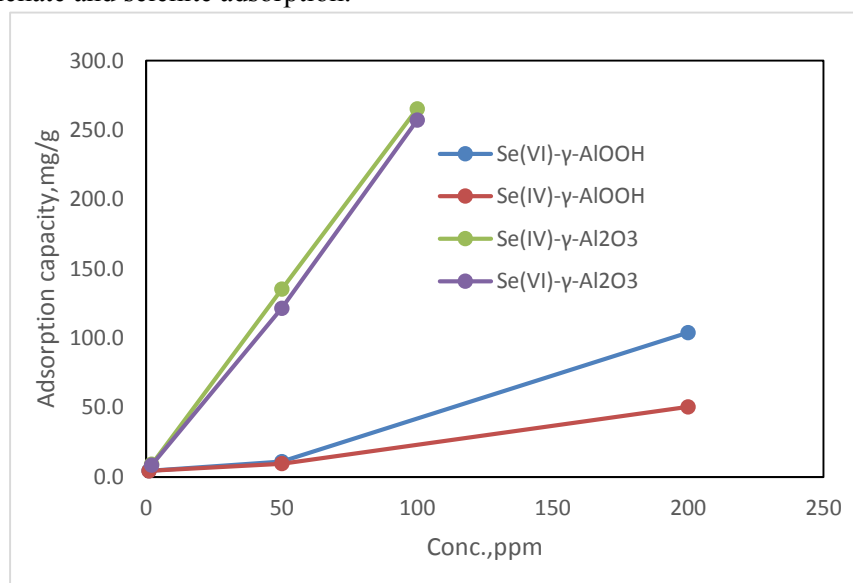


Fig 2 Comparison of Selenium adsorption by AlOOH and by γ - Al_2O_3

3.3 pH effect on adsorption.

The pH level of the aqueous solution is an important variable for the selenium adsorption process, due to the speciation of the chemical functional groups present on the adsorbent surface. So, the effect of the aqueous solution pH on the removal efficacy of the aluminum nanoparticles for selenium was studied between pH 2.0 and 11.0 (acetic/acetate media) under temperature 20°C and 70°C, respectively (Fig 36a, b). Either under 20°C or 70°C, the results obtained revealed that the adsorption of both Se (IV) and Se (VI) are pH dependent. The observed pH effect revealed the adsorption of Se (IV) and Se (VI) is maximum at pH 2. The sorption of selenium presents an anionic behavior, decreasing at more alkaline pH values. In the case of Se (VI) the sorption decreases as the percentage of the aqueous species HSeO_4^- decreases. For sorption edge coincides with the predominance of HSeO_3^{2-} .

Selenate adsorption primarily occurs under acidic conditions, as shown in Figure 3.36. In the pH range studied, the dominant selenate species is SeO_4^{2-} , since the pK_2 for selenious acid is 2²³. With an increase in pH, SeO_4^{2-} adsorption rapidly decreased. At pH 3.6, the total percent of adsorption was 91%. When pH was higher than 8.0, very little adsorption was recorded. Because too much acid was required to reduce the pH lower than 3.6 and to maintain a constant ionic strength, lower pH experiments were not conducted. Se (IV) species in aqueous solution include selenious acid (H_2SeO_3), biselenite (HSeO_3^-) and selenite (SeO_3^{2-}). Between pH 3.5 and 9.0, the biselenite ion is the predominant ion in water. Above pH 9.0 selenite species dominate, and as the pH decreases below pH 3.5, selenious acid dominates. Se(IV) sorption decreases at alkaline pH due to the decrease of the fraction of aqueous species of HSeO_3^- .²⁴

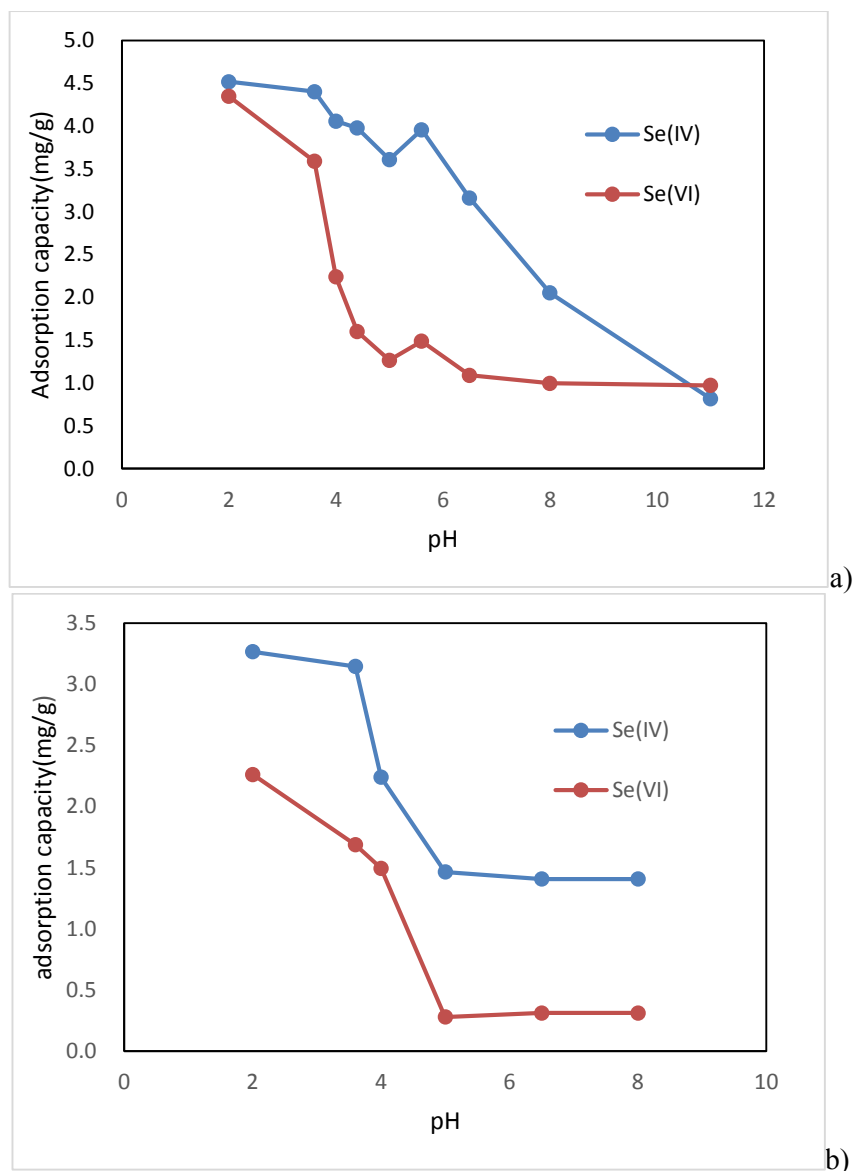


Fig3.pH effect on selenium adsorption, initial concentration: 1ppm, using 0.005g aluminum nanosphere as adsorbent. 25mL, 18h. a) 20°C b) 70°C

3.4 Initial concentration effect on selenium adsorption

These experiments are planned to assess the effect of the initial selenate and selenite concentration on the sorption process and estimate the maximum aluminum nanosphere adsorption capacity for both species. The adsorption of selenium oxyanions by γ - Al_2O_3 nanospheres is determined in a proper initial selenium concentration range at pH 2. The effects of the initial selenium concentration (from 2ppm to 100ppm) on the adsorption capacity by the γ - Al_2O_3 nanosphere are shown in Fig 4. The increase of adsorption capacity when the initial selenium concentration increases can be explained in terms of diffusion resistance. Adsorption capacity equilibrium is reached when the surface of γ - Al_2O_3 nanosphere does not have free sites for the selenium oxyanions uptake, being saturated.¹⁰ It is probably another explanation that, as mentioned before, a higher probability of collision between adsorbate (arsenate) and

adsorbent(sponge loaded with SPION) surface happens as initial concentration increases, which could overcome the mass transfer resistance between the aqueous and the adsorbent phases.¹¹

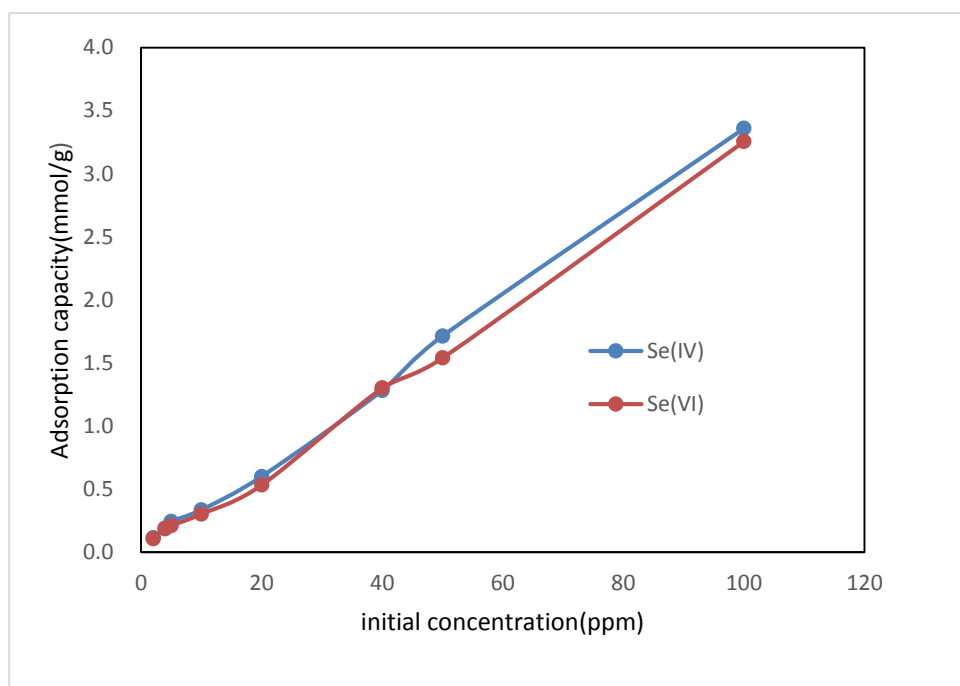


Fig4. Se (VI) and Se(VI) initial concentration effect on selenium adsorption, initial concentration: 1ppm, using 0.005g aluminum nanoparticle as adsorbent. 25mL, 18h.

3.5 Adsorption Isotherm modeling.

In these experiments the effect of the initial Se (IV) and Se (VI) concentration on the sorption of Se (IV) and Se (VI) was studied in order to estimate the maximum loading capacity of γ - Al_2O_3 nanoparticles. The obtained results are not fitted to Langmuir isotherm, fitted to the well-known Freundlich isotherm model, as shown in Fig5. The experimental observation are in good agreement with the Freundlich model²⁵

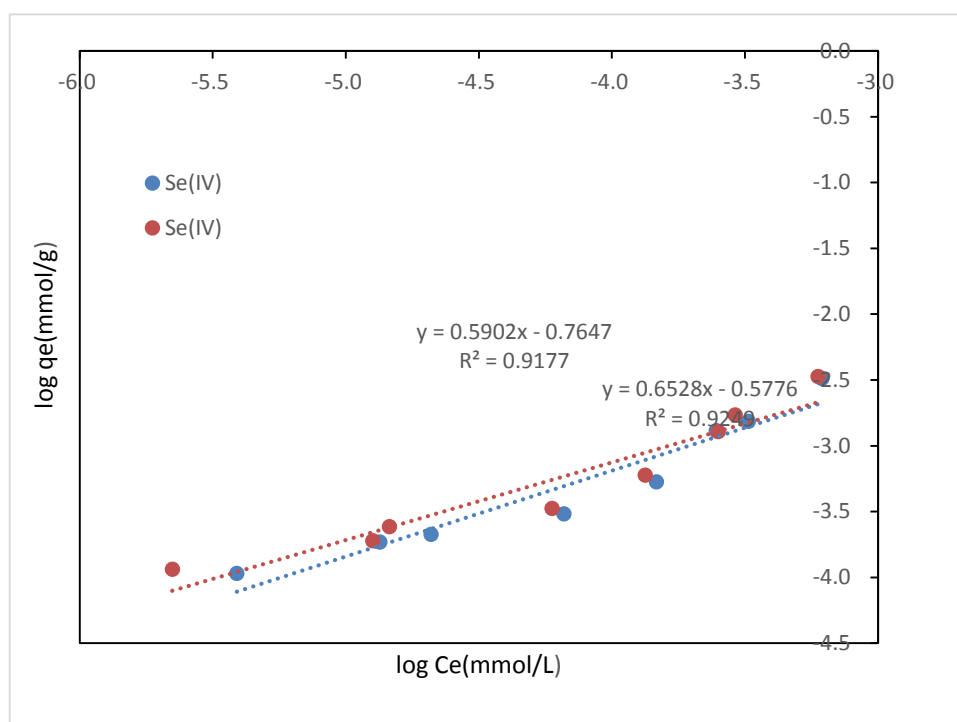


Fig5 Freundlich isotherm model for the adsorption of Se (VI) and Se(IV) by γ -Al₂O₃ nanosphere

Table 1 Freundlich parameters

	logk _f	1/n	R ²
Se(IV)	-0.76	0.59	0.9177
Se(VI)	-0.58	0.65	0.9249

Regarding the corresponding correlation coefficient values obtained, the Freundlich isotherm fits the data showing that the adsorption process not rely on a specific sites adsorption mechanism where adsorbate molecules in the multilayer of the surface not occupy specific sites on the adsorbent. The adsorbent (here is γ -Al₂O₃ nanospheres) is not homogeneous and it is heterogeneous.

3.6 Evaluation of thermodynamic parameters

The influence of the temperature on the equilibrium constant k can be described by the following relationship:

$$\ln \left(\frac{k_1}{k_2} \right) = \frac{\Delta H}{R} * \left(\frac{1}{T_1} - \frac{1}{T_2} \right) \dots \dots \dots (1)$$

And K can be calculated by the equation:

$$k = q_e / C_e \dots \dots \dots (2)$$

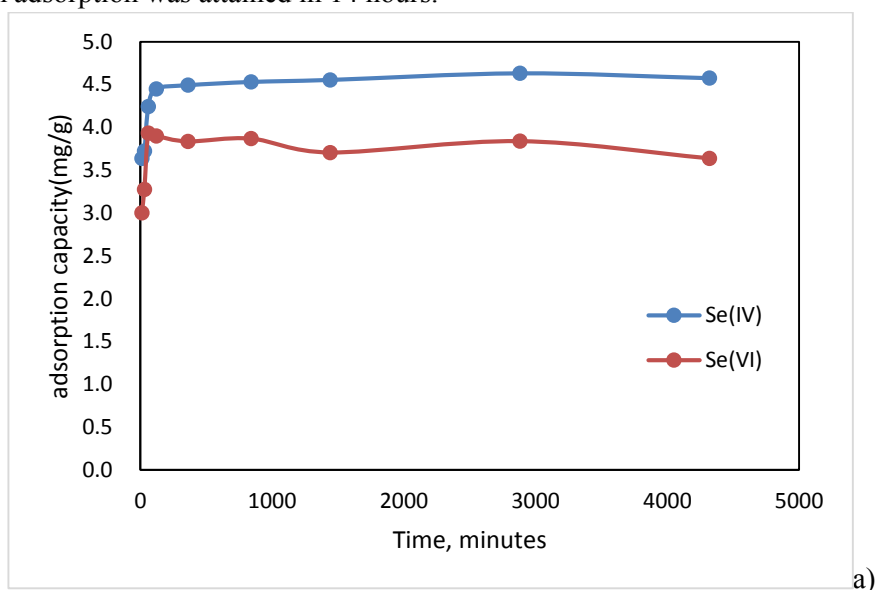
Table2 Differential enthalpies of complexation for hypothetical nanoparticles with selectivity dependent on temperatures

343K-293K	K(T2)/K(T1)	Ln(K2/K1)	ΔH, KJ/mol	LogKf	1/n
Se(IV)	0.434	-0.835	-13.955	-0.765	0.590
Se(VI)	0.791	-0.235	-3.927	-5.776	0.653

It was observed from Table 2 the ΔH value shows that lower temperature favor removal of selenium within the defined range of study. The reaction could be attributed to the fact that the adsorption of selenium oxyanions onto the surface of the γ - Al_2O_3 nanosphere could be favored by elimination of water molecule previously bonded to the surface of the adsorbent favoring increasing in entropy factor. The negative value of ΔH confirms the exothermic nature of the adsorption process. The ΔH value of Se (IV) and Se (VI) between 20°C and 70°C were -14.0 KJ mol⁻¹ and -3.9 KJ mol⁻¹ shows that lower temperature favor removal of selenium.

3.6 Variation of contact time

The variation of contact time is one of the most important parameters in determining the adsorption potential of an adsorbent material. Adsorption of selenium by aluminum nanospheres was studied within a time period of 2-4320min (2min to 72h). As shown in Fig 6, the equilibrium adsorption of selenium can be obtained in 6h under 20°C at pH 2, the adsorption of selenium presents an anion exchange behavior. The reason could be attributed to the availability of high surface area as well as porous structural features facilitating easy removal of selenium. Apart from this, surface hydrophilicity could be a factor responsible for anion-surface functional group interaction which is entropically favorable. While for 70°C, the maximum adsorption was attained in 14 hours.



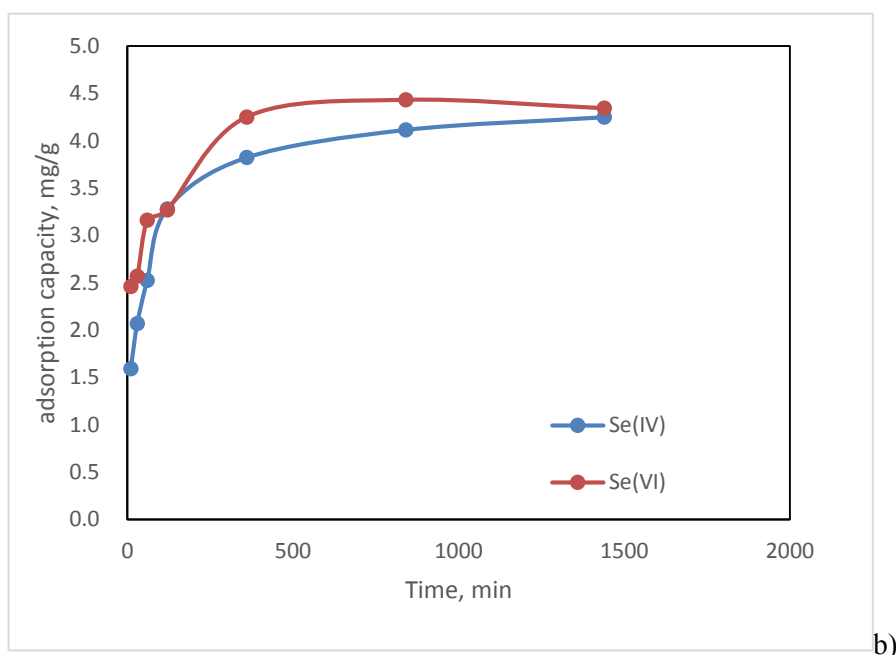


Fig6 Variation of contact time period, pH=3.6, conc. of Se(IV) or Se(VI): 1ppm; adsorbent dose:5mg.a)20°C, b) 70°C

3.7 Adsorption kinetics

Adsorption of selenium oxyanions on γ - Al_2O_3 nanospheres is a complex process. The adsorption mechanism during the present adsorption process involve the potential rate controlling steps such as mass transport, pore diffusion and chemical reaction processes. Indeed, the speed of adsorption is strongly influenced by several parameters such as the status of the solid matrix that has generally heterogeneous reactive sites, and the physical-chemical conditions under which the adsorption take place.²⁶

In order to understand kinetics process and predict the mechanism involved during the present adsorption process, the adsorption data was analyzed and two kinetic models were used to fit the experimental data, namely, pseudo first-order (shown in Fig7) and pseudo-second-order (shown in Fig 8). The correlation coefficients for Lagergren irreversible first-order model obtained were low. Therefore, the reaction involved in the present adsorption system is not of the first-order. The calculated q_e by this model differs significantly from those measured during the experiment. The kinetic studies show that they are fitted very well to the pseudo-second order, which showed the best fit to the experimental data with the highest squared correlation coefficients ($R^2 = 0.999$) and the theoretical Q_e give acceptable values when compared to the experimental ones. This suggests that selenium oxyanions were adsorbed onto the aluminum nanosphere surface via chemical interaction, which is probably involving valency forces through sharing or exchange of electrons between sorbent and sorbate, and provides the best correlation of the data.

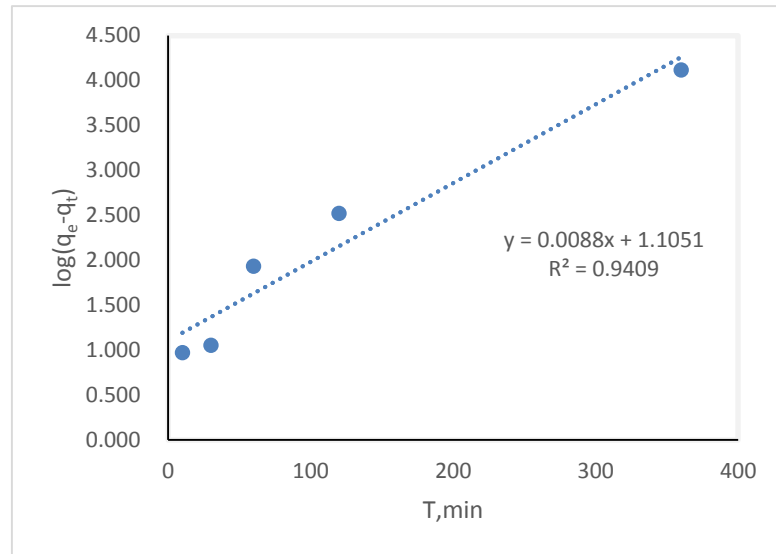
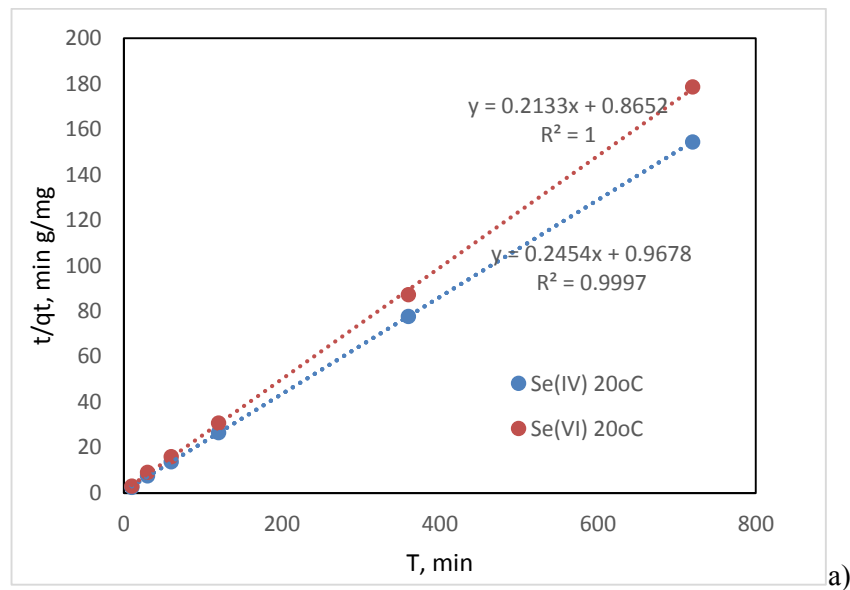


Fig7 Pseudo-first order adsorption kinetics plots for the adsorption of selenite by γ -Al₂O₃ nanosphere. The initial concentration of Se (IV) was 1ppm, the adsorbent dosage of γ -Al₂O₃ nanosphere was 5mg, the volume of the adsorption aqueous system is 25mL. The experiment was undertaken under 20°C.



a)

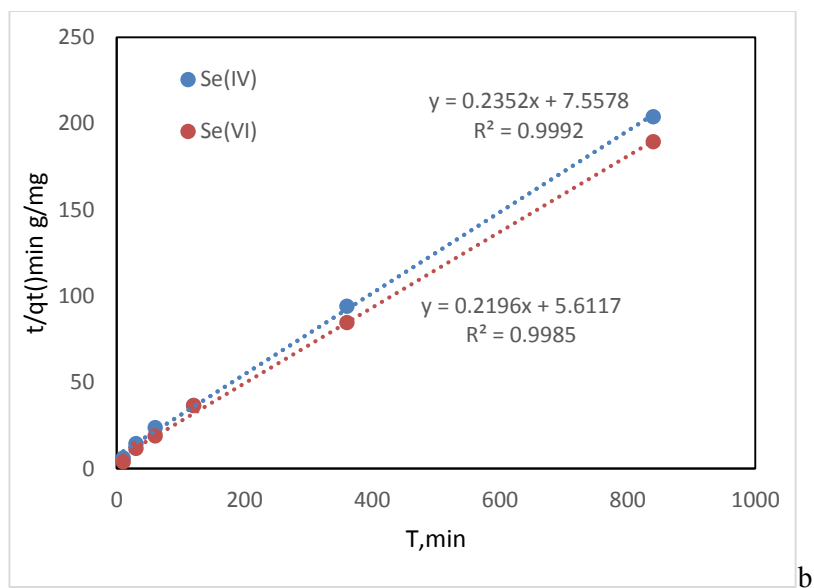


Fig 8 The plot of $t/q(t)$ vs. t showing the linear nature of second-order kinetic model for aluminum nanoparticle, adsorbent dose, 5mg, pH 3.6. a). Se(IV) and Se(VI), 20°C; b) Se(VI) and Se(VI), 70°C

Table 3 Pseudo-second order kinetic constants for the adsorption of selenium oxyanions on γ - Al_2O_3

	$K_2(\text{g/mg min})$	$Q_e (\text{mg/g})$	R^2
Se(IV) 20°C	0.054	4.29	1
Se(VI) 20°C	0.058	4.16	0.9998
Se(IV) 70°C	0.053	4.33	0.9996
Se(VI) 70°C	0.048	4.55	0.9985

The analysis of tabular data (shown in Table 3) reveals that values of both $q_{e, \text{exp}}$ and $q_{e, \text{cal}}$ for pseudo second order kinetic model are close to each other with relatively higher correlation coefficient (R^2) value. The adsorption kinetics can be conveniently represented by the pseudo second order model.

3.8 Comparison of adsorption capacity between γ - Al_2O_3 and modified γ - Al_2O_3

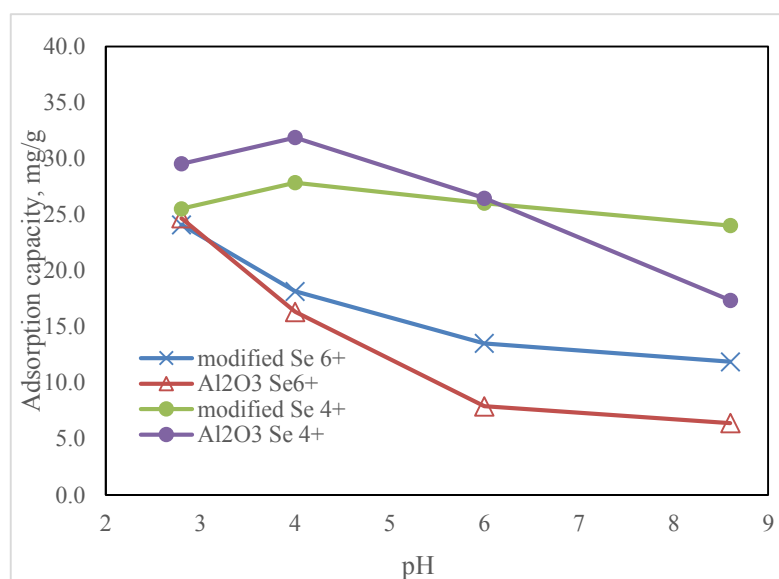


Fig 9 comparison of adsorption capacity between γ -Al₂O₃ and modified γ -Al₂O₃

Since some studies on 3-mercaptopropionic acid (3-MPA) coated SPION have been done in order to modify the change the aggregation properties of SPION and link the the thiol groups to SPION surface in order to improve the adsorption capacity of SPION. In our case, we try to modify the γ -Al₂O₃ nanosphere by using the diethylammonium N,N-diethyldithiocarbamate(DDC), since this organic reagent has the thiol group, which also could bond with γ -Al₂O₃ nanosphere, therefore make the nanospheres to be less aggregated and increase the surface area. Thus, it should improve the adsorption capacity of γ -Al₂O₃ nanosphere for selenium adsorption. The results of comparison of adsorption capacity between γ -Al₂O₃ nanosphere and DDC modified γ -Al₂O₃ nanosphere has shown in Fig 9. It has demonstrated that DDC modified γ -Al₂O₃ nanosphere has higher adsorption capacity for selenate. However, during the pH range of 2.8-6.0, the γ -Al₂O₃ nanosphere has higher adsorption capacity for selenite than adsorption capacity of DDC modified γ -Al₂O₃ nanosphere for selenite. When pH>6.0, the phenomenon is opposite, the γ -Al₂O₃ nanosphere has lower adsorption capacity for selenite than that of DDC modified γ -Al₂O₃ nanosphere for selenite.

Acknowledgement

I should thank staffs from GTS, the Department of analytical chemistry. Thanks for their co-operation and assistance provided before and during the projects. In addition, thanks for the scholarship support of Chinese Scholar Council for the scholar-grant received.

Reference

1. Zhang, N., Lin, L.-S. & Gang, D. Adsorptive selenite removal from water using iron-coated GAC adsorbents. *Water Res.* **42**, 3809–16 (2008).
2. Santos, S., Ungureanu, G., Boaventura, R. & Botelho, C. Selenium contaminated waters: An overview of analytical methods, treatment options and recent advances in sorption methods. *Sci. Total Environ.* **521-522C**, 246–260 (2015).
3. Who. Selenium in Drinking-water Background document for development of. *World Heal. Organ. Geneva* (2011). doi:WHO/HSE/WSH/10.01/14
4. Goh, K.-H. & Lim, T.-T. Geochemistry of inorganic arsenic and selenium in a tropical soil: effect of reaction time, pH, and competitive anions on arsenic and selenium adsorption. *Chemosphere* **55**, 849–59 (2004).
5. Geoffroy, N. & Demopoulos, G. P. The elimination of selenium(IV) from aqueous solution by precipitation with sodium sulfide. *J. Hazard. Mater.* **185**, 148–54 (2011).
6. Mavrov, V., Stamenov, S., Todorova, E., Chmiel, H. & Erwe, T. New hybrid electrocoagulation membrane process for removing selenium from industrial wastewater. *Desalination* **201**, 290–296 (2006).
7. Gui, M. *et al.* Engineered iron/iron oxide functionalized membranes for selenium and other toxic metal removal from power plant scrubber water. *J. Memb. Sci.* **488**, 79–91 (2015).
8. Mariñas, B. J. & Selleck, R. E. Reverse osmosis treatment of multicomponent electrolyte solutions. *J. Memb. Sci.* **72**, 211–229 (1992).
9. Puranen, A., Jonsson, M., Dähn, R. & Cui, D. Immobilization of selenate by iron in aqueous solution under anoxic conditions and the influence of uranyl. *J. Nucl. Mater.* **392**, 519–524 (2009).
10. Qiu, S. R. *et al.* Removal of contaminants from aqueous solution by reaction with iron surfaces. *Langmuir* **16**, 2230–2236 (2000).
11. Zhang, Y. & Frankenberger, W. T. Removal of selenium from river water by a microbial community enhanced with *Enterobacter taylorae* in organic carbon coated sand columns. *Sci. Total Environ.* **346**, 280–5 (2005).
12. Su, T., Guan, X., Tang, Y., Gu, G. & Wang, J. Predicting competitive adsorption behavior of major toxic anionic elements onto activated alumina: a speciation-based approach. *J. Hazard. Mater.* **176**, 466–72 (2010).

13. Yamani, J. S., Lounsbury, A. W. & Zimmerman, J. B. Adsorption of selenite and selenate by nanocrystalline aluminum oxide, neat and impregnated in chitosan beads. *Water Res.* **50**, 373–81 (2014).
14. Bleiman, N. & Mishaël, Y. G. Selenium removal from drinking water by adsorption to chitosan-clay composites and oxides: Batch and columns tests. *J. Hazard. Mater.* **183**, 590–595 (2010).
15. Olegario, J. T., Yee, N., Miller, M., Sczepaniak, J. & Manning, B. Reduction of Se(VI) to Se(-II) by zerovalent iron nanoparticle suspensions. *J. Nanoparticle Res.* **12**, 2057–2068 (2009).
16. Rovira, M. *et al.* Sorption of selenium(IV) and selenium(VI) onto natural iron oxides: goethite and hematite. *J. Hazard. Mater.* **150**, 279–84 (2008).
17. Dobrowolski, R. & Otto, M. Preparation and evaluation of Fe-loaded activated carbon for enrichment of selenium for analytical and environmental purposes. *Chemosphere* **90**, 683–690 (2013).
18. Duc, M. *et al.* Sorption of selenium anionic species on apatites and iron oxides from aqueous solutions. *J. Environ. Radioact.* **70**, 61–72 (2003).
19. Kuan, W.-H., Lo, S.-L., Wang, M. K. & Lin, C.-F. Removal of Se(IV) and Se(VI) from water by aluminum-oxide-coated sand. *Water Res.* **32**, 915–923 (1998).
20. Chan, Y. T., Kuan, W. H., Chen, T. Y. & Wang, M. K. Adsorption mechanism of selenate and selenite on the binary oxide systems. *Water Res.* **43**, 4412–4420 (2009).
21. Cai, W., Yu, J. & Mann, S. Template-free hydrothermal fabrication of hierarchically organized ??-AlOOH hollow microspheres. *Microporous Mesoporous Mater.* **122**, 42–47 (2009).

Annex IV

Synergic thermo tuning of redox potential for clean removal of toxic oxyanions

Liu HE, Tong Liu, Manuel Valiente

Department de Química, Química Analítica, Universidad Autónoma de Barcelona, 08193
Bellaterra, Barcelona, Spain

Corresponding author footnote

Centre Grup de Techniques de Separacio en Química.

Tel. +34-935812903

Fax. +34-945811985

Email. Manuel.Valiente@uab.cat

Field of the Invention

The present invention relates to a reagentless recycled method for arsenic removal in water. In our invention, we develop a new method for Arsenic adsorption-- desorption and sorbent regeneration with no reagents added by taking advantage of the synergic thermo tuning of redox potential of the adsorption-desorption system.

State of the art

Arsenic is abundant in our environment with both natural and anthropogenic sources which is considered to be one of the major problems in pollution because of their high toxicity and the consequent risks for human health(Ernest O. Kartinen Jr., Christopher J. Martin,1995; Le Zeng,2004; Sushilraj Kanel, Jean – Mark Greneche, Andheechulchoi, 2006). Several countries have to deal with the problem of arsenic contamination of groundwater, used for drinking water, such as Bangladesh and India, China, United States, Mexico, Australia, Greece, Italy, Hungary, etc.

Thus, there is a growing interest in using low-cost methods and materials to remove arsenic from industrial effluents or drinking water before it may cause significant contamination. In natural water, arsenic is primarily present in inorganic forms and the dominant arsenic species are arsenate—As(V) and arsenite-As(III)(R.S. Harisha, K.M. Hosamani , R.S. Keri, S.K. Nataraj, T.M. Aminabhavi,2010)

The adsorbents and filters have been used for the treatment, including: ferric chloride(M.J. Haron, W.M.Z. Wan Yunus, N.L. Yong and S. Tokunaga,1999), Fe(III)-doped alginate gels(X. Meng, S. Bang and G.P. Korfiatis,2000), nanocomposite adsorbent based on silica and iron(III) oxide(J.H. Min and J.G. Hering,1998), and iron oxide-coated polymeric materials(I. Peleanu, M. Zaharescu, I. Rau, M Crisan, A. Jitianu and A. Meghea,2002), Fe(III)-loaded resins(Dmitri Muraviev, Ana Gonzalo, and Manuel Valiente,1995), Fe(III)-loaded sponge(José Antonio Muñoz, Anna Gonzalo, Manuel Valiente, 2008) are used in arsenic treatment because of the Fe(III) affinity toward inorganic arsenic species and consequent selectivity of the adsorption process.

In WO 2014122350A1 a filter for the treatment of liquid comprising a support made from a polymer material having at least one functional group from the group formed by carboxyl and thiol, loaded with SPION (SuperParamagnetic Iron oxide Nanoparticles)

In WO 2007/ 032860 a filter for eliminating described arsenic in water comprising a support of polyacrylonitrile (PAN) loaded with iron hydroxide nanoparticles .

The paper Morillo , D, Valiente , M., Perez , G., "Advances in adsorption Arsenic with Nanoparticles", Research Project, Master's Degree in Chemical Sciences and Technology , Universitat Autònoma de Barcelona , September 2009 , the use of a cellulose sponge as support, in which SPION has dispersed , for removing arsenic in water.

There is, however, although the filter or adsorbent has very high quality and efficiency to treat and adsorb arsenic, if they can not be recovered and reused for several times, it is still very expensive and it is not very practical. As there are a lot of weaknesses of using reagents to recover the adsorbent or filter. Some new methods for adsorption-desorption recycled arsenic treatment and adsorbent/filter regeneration is really needed.

Almost all of the traditional methods have the problems on adsorbent/filter regeneration. Once the adsorbent/filter becomes exhausted, then, either the metals must be recovered, the sorbent/filter be regenerated or disposed in a controlled dumping site for toxic substances which use to be very expensive. Desorption and sorbent/filter regeneration is a critical step contributing to decrease process costs. A successful desorption process must restore the sorbent/filter close to its initial properties for effective reuse. In most of the published arsenic sorption studies (some discussed earlier), desorption/regeneration was not included. Very few desorption studies are detailed in literature. Furthermore, once arsenic is recovered in the pure and concentrated form, the problem of its disposal of this concentrated arsenic product must be addressed. This is a difficult and expensive task. Few attempts have been made to address the handling of concentrated arsenic wastes. Tuutijärvi T, 2006 has tried five different alkaline solutions: NaOH, Na₂CO₃, Na₂HPO₄, NaHCO₃ and NaAc for arsenate batch desorption and regeneration. But this process also needs to spend a lot of alkaline solution which is very expensive and is not feasible for industrial sense. Thus, in our invention, we develop a new method for arsenic adsorption-desorption and sorbent regeneration by taking advantage of the synergic thermo tuning of redox potential for clean removal of the adsorption system.

The present invention relates to a reagentless method for arsenic (particularly As(V) and As(III)) adsorption-desorption and sorbent regeneration with no reagents added by taking advantage of the thermodynamic properties and redox potential of the adsorption system. This reagentless method could not only save a lot of reagent for recovering the sorbent, but also the adsorbent could be recycled and reused, which is low-cost and practical.

The inventor has studied the adsorption properties of As(V) and As(III) the influence of temperature and redox potential on the desorption rate. In addition, the inventor has studied the

thermodynamic aspects for realizing the adsorption-desorption process. Besides that, the oxidation of As(III) to As(V) and the reduction of As(V) to As(III) in order to prove the concept of redox potential for adsorption-desorption have been studied. More importantly, the thermodynamic aspects combined with the redox potential effect for controlling the adsorption-desorption process have been studied.

Detailed Description of the invention

The present invention relates to a reagentless method for arsenic (particularly As(V) and As(III)) adsorption-desorption and sorbent regeneration with no reagents added by taking advantage of the thermodynamic properties and redox potential of the adsorption system.

In this work, the inventor has done the research on the effect of thermal tuning on arsenic adsorption and also studied the mechanism of thermodynamic properties of this adsorption system. Furthermore, the inventor has done some study on redox potential of As(III) oxidation and As(V) reduction.

One of the objectives of the present study includes not only the new methods for arsenic adsorption-desorption by controlling the temperature or redox potential of reaction condition, but also some theoretical study which can explain the mechanism of the adsorption-desorption process. More importantly, we study effects of synergic thermo tuning and redox potential on the adsorption-desorption process. The aim of the invention is to provide a totally new concept and reagentless method to recover the arsenic and regenerate the adsorbents for recycled arsenic removal treatment.

It is accordingly an object of the present invention to provide a highly capacity and efficiency adsorbent capable of selectively absorbing arsenic from aqueous solution.

It is another object of this invention to provide an adsorbent of the aforesaid nature in the form of an open-celled sponge loaded with controllable size of nanoparticles.

It is a further object of this invention to provide a method of capable of adsorption-desorption recycling process by taking advantages of thermo tuning effect.

It is a still further object of this invention to provide a method of capable of aforesaid adsorption-desorption recycling process by using the concept of redox potential.

It is a yet another object of the invention to provide a method of capable of aforesaid adsorption-desorption recycling process by synergic thermo tuning of redox potential.

These objects and other objects and advantages of the invention will be apparent from the following description.

The inventor use the adsorbent to adsorb the arsenic in the water, the results shows that the adsorption capacity is influenced by the temperature. The adsorption capacity is decreasing as the temperature increases. That means as temperature increases, the desorption is starting to occur. Lower temperature helps the adsorbent adsorb the arsenic and higher temperature helps the adsorbent to desorb the arsenic. So, the inventor adsorbs the arsenic by using the adsorbent under room temperature and desorbs the arsenic under 70°C.

More importantly, the inventor use the potassium dichromate to oxidize the As(III) to As(V)

and use the Zn powder or Sn to reduce the As(V) to As(III). Since the adsorbent has much higher adsorption capacity of As(V) than that of As(III), the adsorbent can adsorb the arsenic by oxidizing all of the As(III) to be As(V) and desorb the arsenic by reducing the As(V) to be As(III).

The inventor make the column mode in order to do the adsorption-desorption recycled processing. The adsorbent could be put inside the column. Once the wastewater which contains the arsenate and arsenite pass through the column, the arsenate and arsenite is loaded on the adsorbent and the clean water goes out. After loading, the arsenate and arsenite could be eluted by passing the hot water (70°C) or hot water combined with Sn. Therefore the adsorbent can be reused.

Above all, the desorption process can be happened by reducing with the help of higher temperature and the adsorption process can be happened by oxidizing under room temperature(if the temperature is lower, for example, 10°C, then the adsorption capacity will higher than that under room temperature, but we consider about the room temperature is normal and easy to control).

Once finishing the desorption process, the adsorbent can be used again for adsorb arsenic under room temperature. And then desorb the arsenic by using the Zn powder under 70°C again. To repeat this adsorption-desorption process for several cycles, then the adsorbent will be useless. But the recycled method and process is really amazing since it can be saved a lot of money for reuse the adsorbent.

In the first embodiment, the invention is directed to a method to adsorption-desorption arsenic treatment in aqueous solution. Especially inorganic arsenic species, arsenite and arsenate. Wherein the arsenate is adsorbed by the adsorbent(sponge-SPION) under the pH=3.6 condition under 20°C and the loaded arsenate is desorbed by the reducing agent under 70°C.

In the second embodiment, once the adsorbent is regenerated again(since the desorption make it clean), the adsorbent can adsorb the arsenate for the second time. The oxidant may help to change the arsenite to be arsenate, in order to be adsorbed easily.

In the third embodiment, the invention is directed to a reagentless method to adsorption-desorption recycled arsenic treatment by adjusting the temperature of the adsorption-desorption process condition.

In the fourth embodiment, the invention is directed to a reagentless method to adsorption-desorption recycled arsenic treatment by changing the redox potential of the adsorbate condition.

In the fifth embodiment, the invention is directed to a reagentless to adsorption-desorption recycled arsenic treatment by synergic thermo tuning of redox potential.

In an embodiment of the invention, the temperature could be tuned between 50°C to 950°C, the reducing reagent could be Zn or Sn and the oxidant could be potassium dichromate and potassium permanganate.

1. Methodology

1.1 Synthesis of iron oxide nanoparticles.

Magnetite nanoparticles are prepared in our lab by mixing iron(II) chloride and iron(III) chloride in the presence of ammonium hydroxide. First, deoxygenated the solution of NH_4OH (0.7M) by nitrogen. Second, deoxygenated the solution of 12mL HCl (0.1M) by nitrogen and mix $\text{FeCl}_3 \cdot 6\text{H}_2\text{O}$ with it. Third, heat the NH_4OH solution at 70 °C. Fourth, Add the $\text{FeCl}_3 \cdot 6\text{H}_2\text{O}$ solution into the NH_4OH solution and react for 30min. Then, Add the $\text{FeCl}_2 \cdot 4\text{H}_2\text{O}$ in the previous solution with mechanic agitation of about 3000rpm and waiting for 45min, the dark precipitate will be formed, which consists of nanoparticles of magnetite. Last, wash it by MilliQ water which has been deoxygenated and centrifuged four times(3 times for 3 min and 5000rpm, 1 time for 10 min and 4500rpm) and preserve it by 50mL 0.1M TMAOH.

1.2 Pre-treatment of the Forager sponge

Forager Sponge, an open-celled cellulose sponge which contains a water-insoluble polyamide chelating polymer. (formed by reaction of polyethyleneimine and nitrilotriacetic acid), was kindly supplied by Dynaphore Inc. (Richmond, VA, U.S.A.). This material is claimed to contain free available ethyleneamine and iminodiacetate groups to interact with heavy metals ions by chelation and ion exchange.

An initial conditioning of the sponge consisting on the conversion into its acidic form by consecutive treatment with 1.0mol/L HCl , double distilled water, and HCl solution at pH 2.5 was carried out in a glass preparative column. A portion of this conditioned sponge was separated, dried during 24 h , and stored in a desiccator for its use.

1.3 Loading of nanoparticle on the sponge

The sponge was loaded with iron oxide nanoparticles by using the nebulizer. The SPION-loaded sponge was dried during 24 h, and stored in a desiccator for its use. The SPION loading capacity was 0.0955 ± 0.0029 mmol Fe/ g sponge.

1.4 Characterization

We have synthesized the iron oxide nanoparticles for 5 times. And Each time, prepare three kinds of sample, including 1/100, 1/250, 1/1000(0.1mL SPION on 10mL TMAOH, 0.1mL SPION on 25mL TMAOH, 0.1mL SPION on 100mL TMAOH). We characterized the samples by TEM to see the particle size and dispersion. Iron oxide nanoparticles are highly dispersible in solutions. With particle sizes of from 6-20 nm, they offer a large surface area and superparamagnetic properties.

1.5 Adsorption-desorption

We have used the batch mode and column mode to do the adsorption-desorption process. As for the batch mode, the arsenic is adsorbed by the adsorbent in a plastic bottle with the help of agitating. The desorption process is occurred either by putting the plastic bottle in the high temperature atmosphere or with the help of Zn powder or Sn. In the column mode, the arsenic

is adsorbed by adsorbent inside the column by passing the wastewater through the column. The desorption process could be realized by passing the hot water or with the help of Sn.

Brief description of the figures.

The temperature effect part:

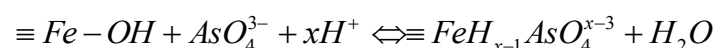
Example 1: Fig1a,b,c,d, thermo tuning effect on adsorption-desorption: shows the changing of temperature for the adsorption-desorption process.

Under 20°C, as time goes on, the adsorption is happened remarkably, The adsorption process obtains equilibrium at about 1h. After that, contact time has no effect in heavy metal removal percentage. Under 70°C, the desorption occurs as contact time increases. Very high adsorption rates were achieved at the beginning because of the great number of sites available for the sorption operation, desorption equilibrium were then gradually achieved as time goes on.

Example2: Fig2, thermo tuning effect: shows that in the bed mode, the temperature also has significant effect on arsenic adsorption, 10oC has better adsorption capability of the adsorbent than that under 20oC condition, the 70oC has the lowest adsorption capacity for arsenic removal. Which reveals, as temperature goes down, it will help the adsorbent to adsorb the arsenic, in opposite, as temperature rise up, it will prevent the adsorbent to adsorb the arsenic. The thermo tuning effect is very obvious. The effect of temperature could be explained in the thermodynamic aspect. The adsorption phenomenon is more efficient with the decrease in temperature. The process is controlled by the adsorbate-adsorbent interaction.

Example 3: Modeling of Arsenic Adsorption by a Ligand-Exchange Process.

A monodantate ligand-exchange mechanism, based on the Fe:As stoichiometry 1:1 previously discussed, is proposed for the adsorption of arsenic(V) on the SPION loaded in the sponge, as it has been considered for other iron-based materials. The corresponding reactions can be written as follows



With an equilibrium constant

$$K = \frac{[\overline{As}]}{[\overline{Fe}][H^+]^x[As]}$$

Where $[\overline{As}]$ indicates the amount of arsenic species adsorbed on the SPION in the sponge(mmol/g), $[\overline{Fe}]$ indicates the amount of iron adsorbed on the sponge and not complexed with As(mmol/g), $[H^+]$ indicates the concentration of free protons in solution(mmol/g), and $[As]$ indicates the free concentrations of the corresponding AsO_4^{3-} ions in solution(mmol/g) which have been calculated from the experimental values of total arsenic concentration and pH of the solution using the pKa values given before.

From equation 1 , defining Y(g/mmol)as

$$Y = \frac{[\overline{As}]}{[\overline{Fe}][As]} \quad (1)$$

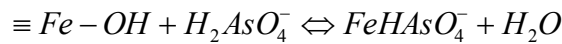
Then

$$\log Y = \log K - x pH$$

Y value at a given pH is estimated from the experimental data of arsenic adsorption by considering the formation of monodentate Fe-As complexes on the sponge. $[\overline{As}]$ is calculated from the differences in adsorption capacity between the SPION loaded and the blank sponge at each pH. $[\overline{Fe}]$ is calculated by subtracting the arsenic adsorption capacity and the iron desorbed from the initial amount of Fe(III) in the SPION-loaded sponge. $[As]$ in solution is determined as indicated in the experimental part.

A plot of logY vs pH for As(V) is given in Fig 3a,b. The values of x and logK obtained by the least squares fit are shown in table 1. The model indicates that $H_2AsO_4^-$ are the As(V) chemical forms adsorbed on the Fe(III) loaded in the sponge in the pH range studied.

When reaction is expressed as a function of the adsorbed species, the stability of the complexes can be accurately evaluated:



$$\log K = 0.50 \pm 0.02 (20^\circ C)$$

$$\log K = 0.12 \pm 0.03 (70^\circ C)$$

Table 1 Calculated Results from Fe-As Interaction Modeling Process Indicating the x and logK Values by the Least-Squares Fit

	pH range	X	logK	R
20°C	1-8	0.398	4.1975	0.8424
70°C	1-11	0.1061	1.0231	0.3791

Log K under 20oC is much higher than that under 70oC, which means the capability of adsorption under 20oC is much stronger than that under 70oC.

The thermo tuning of redox potential part:

Example 4: Fig 4 Changing the redox potential, therefore transforming between arsenite and arsenate, in order to control the adsorption-desorption: shows that the adsorbent has very good capacity for the As(V) adsorption and much lower capacity for the As(III). By changing the redox potential, the transform between As(V) and As(III) will lead the adsorption-desorption process and recycled use of the adsorbent. At the same time, the thermo tuning can help the adsorption-desorption to be much more significant and much quicker.

Redox potential part

Example5:

The potassium dichromate could oxidize the arsenite to arsenate by changing the redox potential.

Table 2 oxidation rate of As(III) to As(V) by potassium dichromate

Initial concentration of arsenite(ppm)	Concentration of potassium dichromate(mmol)	After oxidation, concentration of arsenate(ppm)	Conversion rate
94.913	1.33	87.192	91.87%
96.317	1.33	88.615	92.00%

The Zn powder could reduce the arsenate to arsenite by changing the redox potential.

Table 3 reduction rate of As(V) to As(III) by Zn powder

Arsenate loaded on the sponge(ppm)	After reduction, the arsenic left in the sponge(20oC)ppm	After reduction, the arsenic left in the sponge(70oC)ppm
18.569	4.119	1.239
18.931	3.780	1.827

The synergic thermo tuning of redox potential part:

Example 6: Fig 5 the synergic thermo tuning of redox potential part: shows that in the bed mode, both of the temperature and redox potential have significant effect on arsenic desorption. It could be combined the temperature effect with redox potential in order to get the better and stronger desorption process without adding reagents. It shows that in the bed mode, the adsorbent in the column could firstly adsorb the arsenic and then, the arsenic which are loaded in the adsorbent could be eluted by hot water with the help of Sn. After elution, the adsorbent could be reused to adsorb the arsenic again. Which means, the adsorption-desorption recycled process could be realized and the adsorbent could be reused for several times.

The real model of continuous mode for treating the real waste water

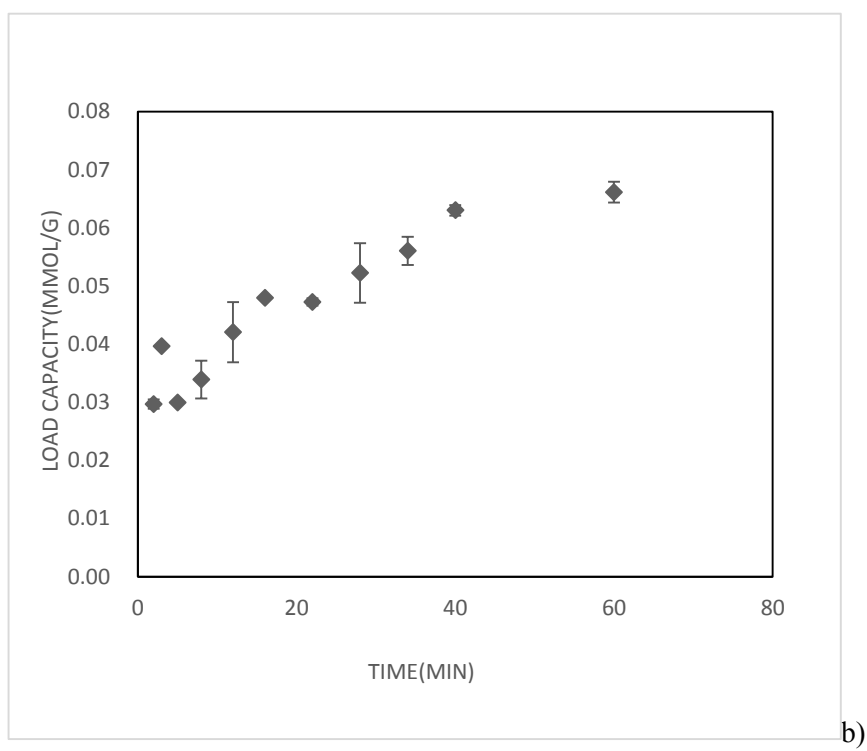
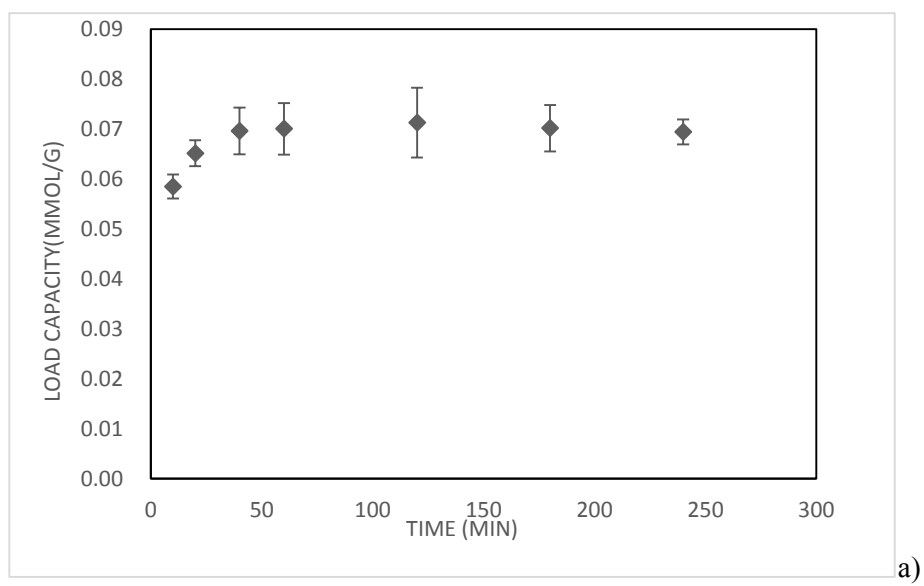
Example 7: Fig 6 the continuous waste water which contains 50ppm As(V) pass through the column. At the beginning, the arsenic is adsorbed on the adsorbent until the saturation is reached; Once the saturation reached, the waste water continue to pass through the column, but we change adsorption condition, for example, to change the temperature or redox potential, then the adsorption change to be desorption and the stripping solution is starting to be highly concentrated arsenic solution. Fig 6.1 shows that the adsorption-desorption process could be repeated, therefore the adsorbent could be used for several times by changing the temperature or redox potential. Fig 6.2 investigate the comparison of the effect of temperature and redox potential on desorption, it shows that temperature with redox potential has the best effect on the desorption process. Fig 6.3 shows that at the elution step, when we add 1 ml of As solution, we can have 0.13mg, 0.09mg, and 0.17mg of As eluted from the column material. So when we use Heating+Redox method, the elution will be the best.

Claims

- 1- The method for arsenic adsorption-desorption recycled process could be controlled by thermo tuning, or redox potential, or synergic of both. As the temperature goes up, The adsorption process can be changed to desorption process. And vice versa. In addition, the change of the redox potential can help the adsorption process transformed to be desorption process and vice versa.
- 2- If the claim 1 method is controlled by thermo tuning, the temperature could be between

10°C to 99°C.

- 3- According to claim 2, the adsorption can be done under room temperature and the desorption can be done under 70°C.
- 4- According to claim 1, the redox potential can be changed by reducing agent and oxidant.
- 5- According to claim 4, the reducing agent could be the one which has lower standard redox potential than that of arsenic, for example, Zn or Sn, and the oxidant could be the one which has higher standard redox potential than that of arsenic, for example, potassium dichromate or potassium permanganate.
- 6-According to claim 1, the redox potential could also be changed by external voltage.
- 7-According to claim 1, the synergic of lower temperature with higher redox potential could lead to very strong adsorption capacity. On the opposite, the synergic of higher temperature with lower redox potential could lead to desorption.
- 8-According to claim 7, the synergic of 10°C with oxidant make the adsorption process and the synergic of 70°C with reducing reagent make the desorption process.
- 9 – The adsorbent could be any kind of adsorbent which has the good capacity for arsenic adsorption.
- 10-The adsorbent could be made by sponge--a polymeric material having at least one functional group formed by carboxyl and thiol.
- 11- The adsorbent could be made by sponge loaded with the SPION which is loaded on the sponge by liquid spray method.
- 12 - The sponge of claim 10, wherein said sponge are an open-celled cellulose sponge which contains a water-insoluble polyamide chelating polymer, could be provided by cleanway company.
- 13 -The SPION according to claims 11, wherein said SPION has an average particle size between 15 nm and 100 nm.



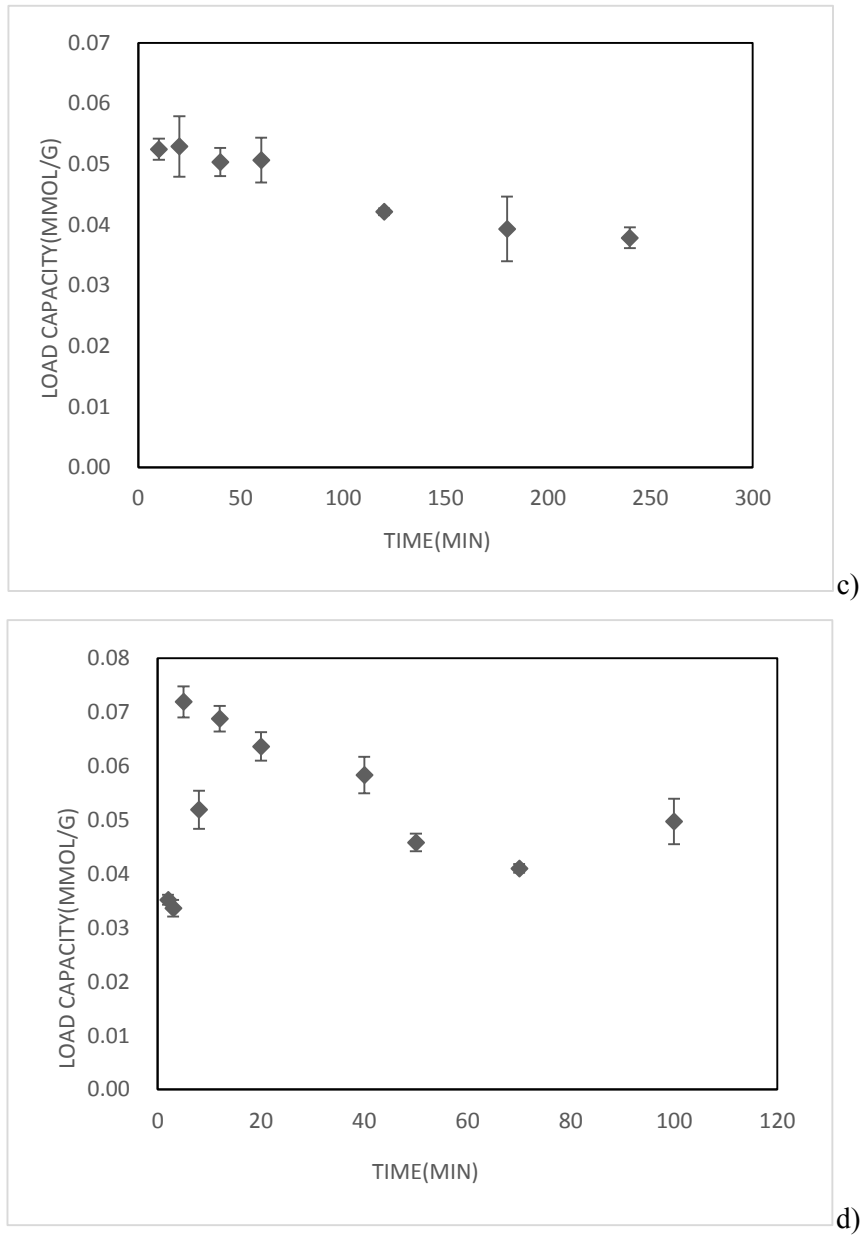


Fig 1 The effect of contact time on the adsorption capacity , a). from 10min to 240min, 20°C, b). from 2min to 60min, 20°C, c). from 10min to 240min, 70°C, d). from 2min to 60min, 70°C,

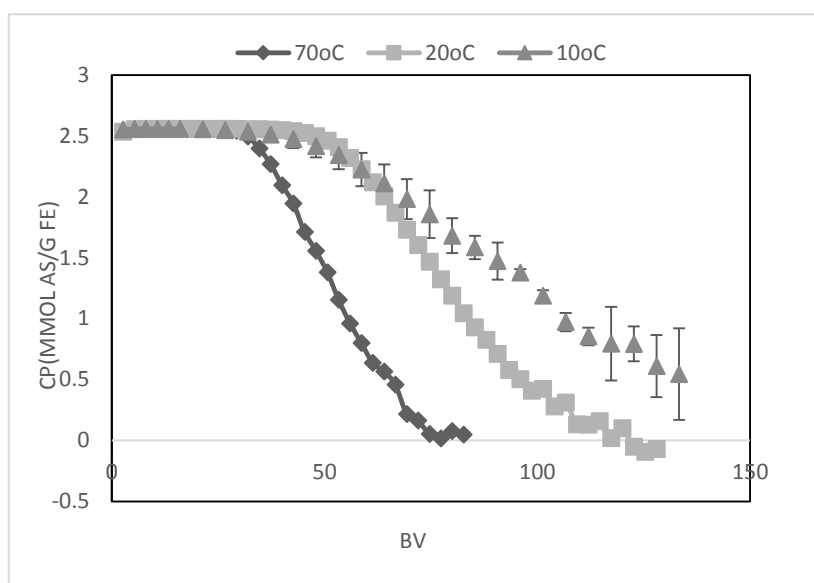


Fig 2 The thermo tunning effect on arsenic adsorption

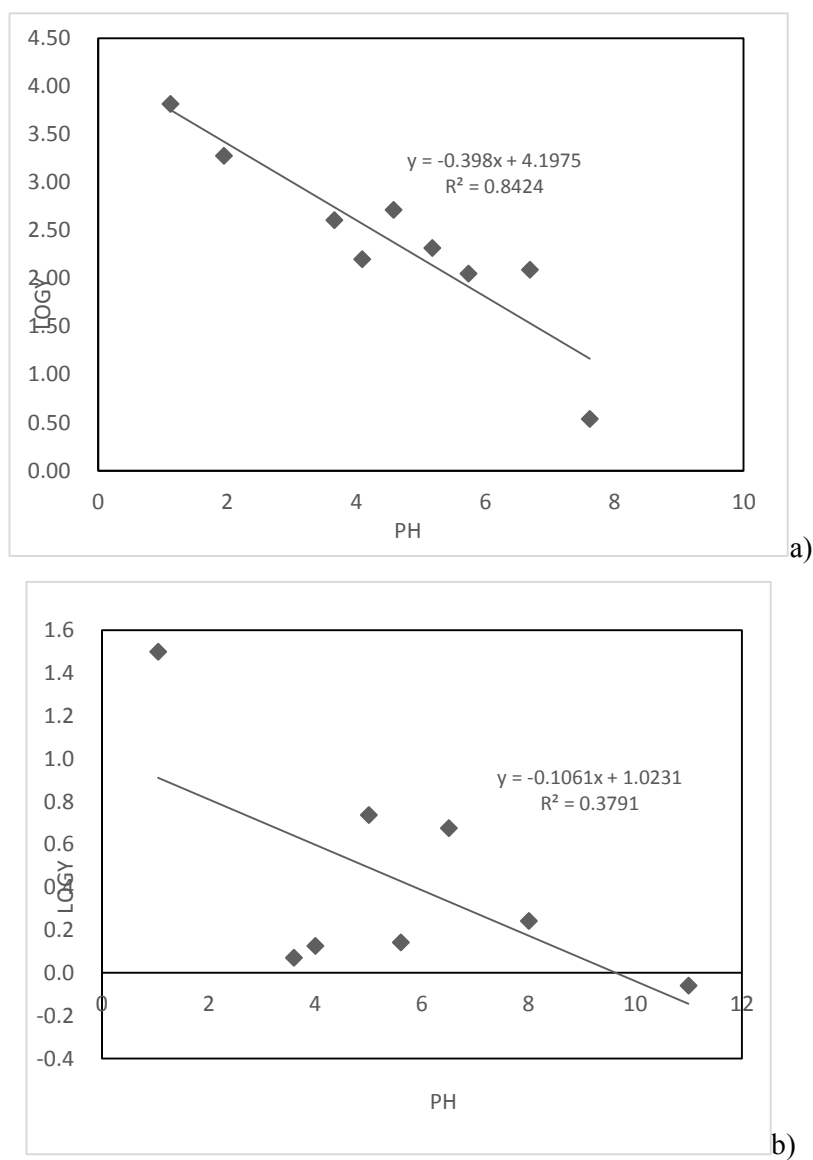


Fig 3 Modeling of arsenic species adsorption on the SPION-loaded in the sponge : linear

relationship between $\log Y$ and pH for As(V). a) 20°C, b) 70°C

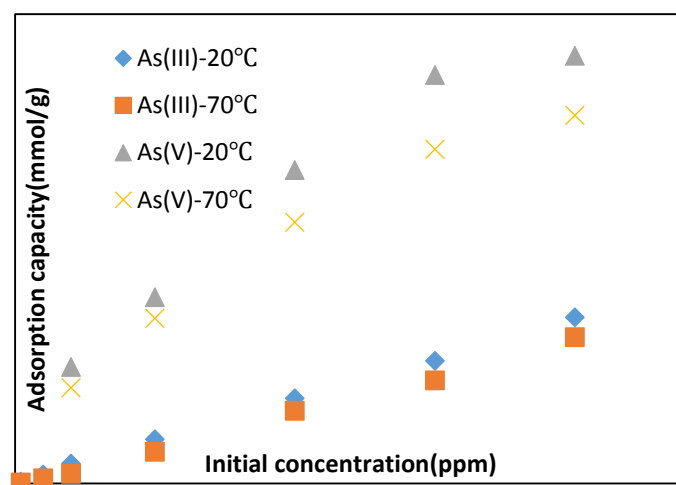


Fig 4 changing of redox potential, therefore transforming between the arsenite and arsenate, in order to control the adsorption-desorption.

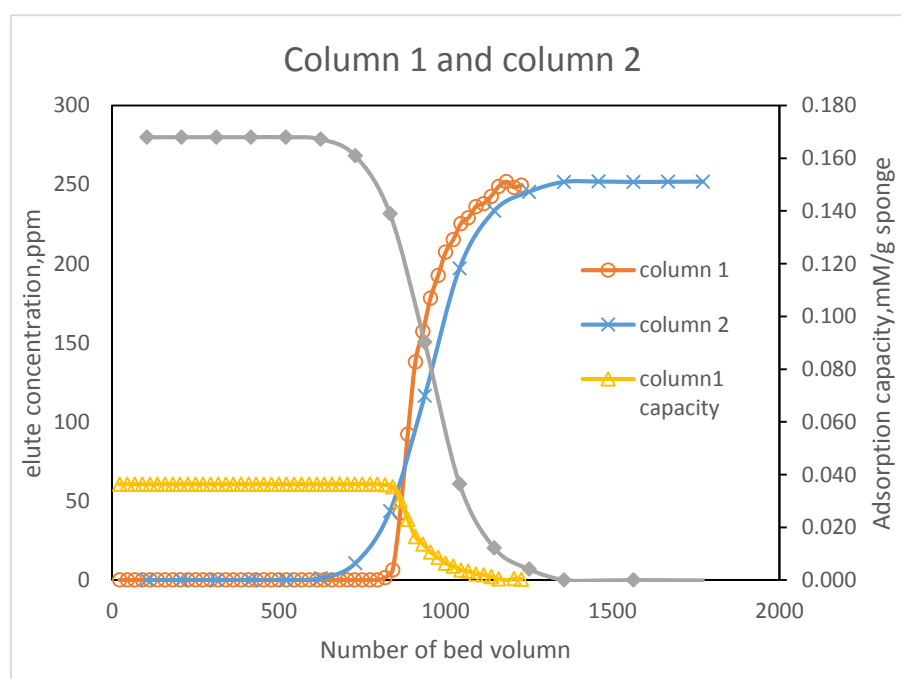


Fig 5 a column mode for adsorption-desorption, loading-elution

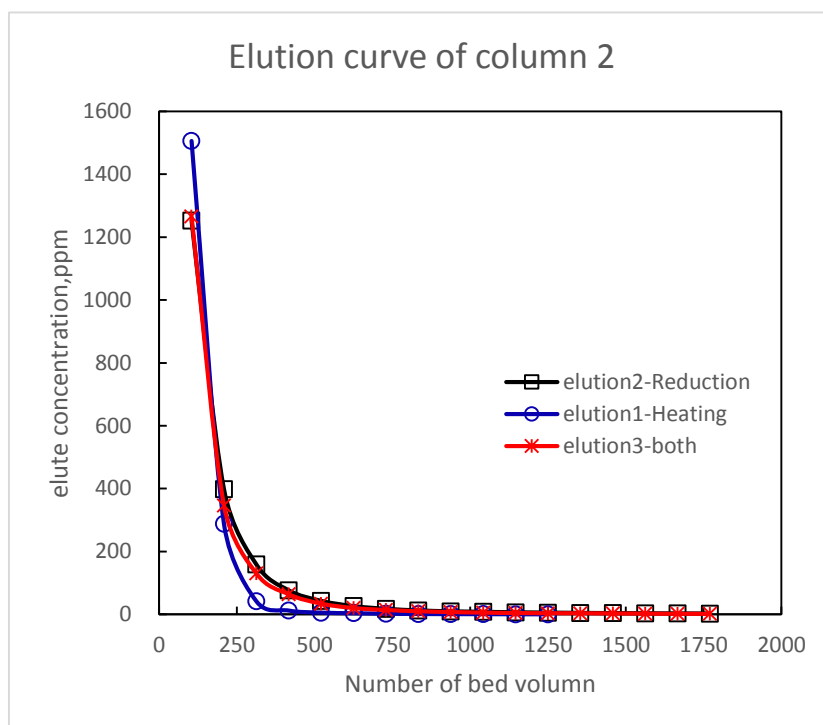


Fig 5b Temperature and reduction effect on elution

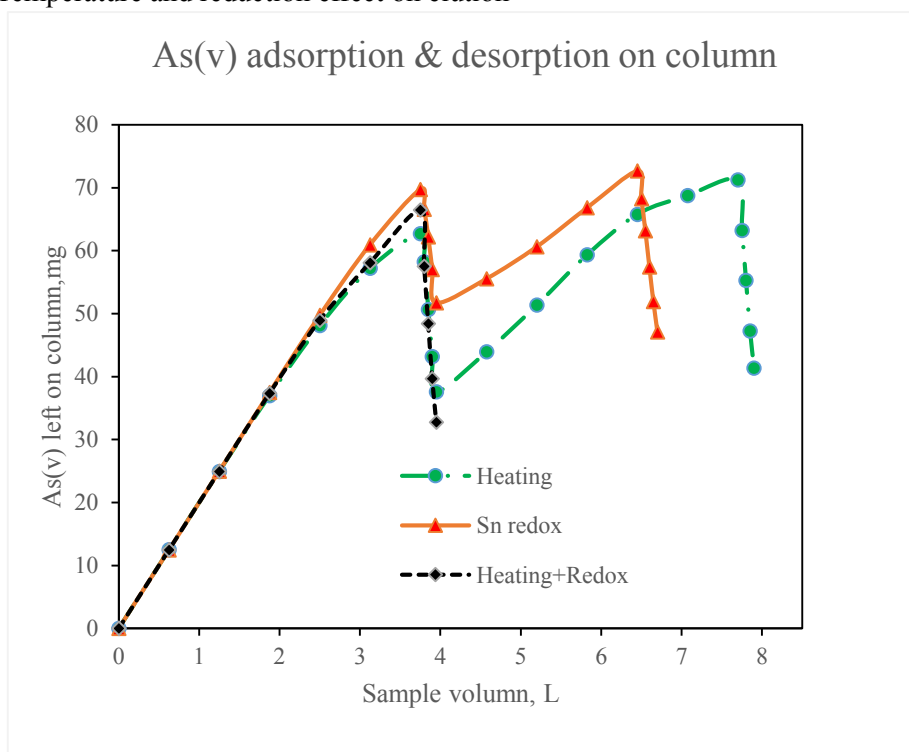


Fig.6.a means that the adsorption and desorption process can repeat.

As(v) adsorption & desorption on column

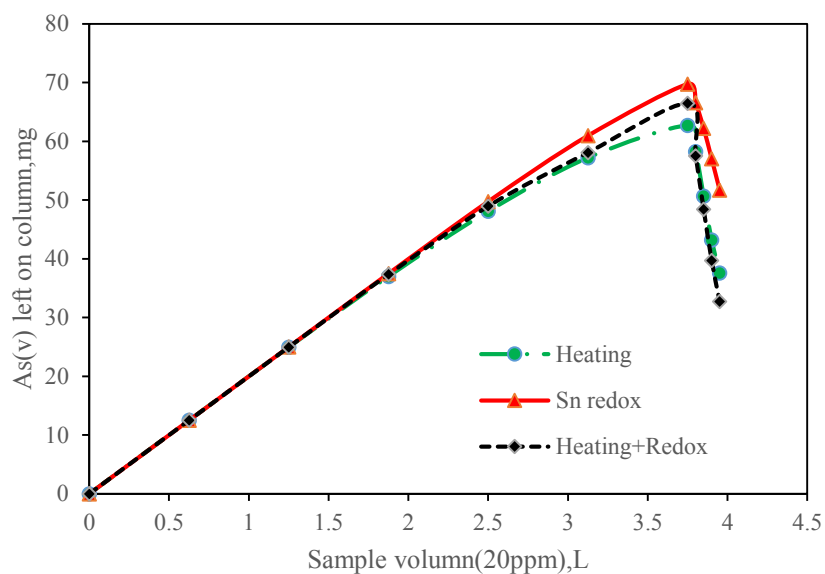


Fig.6.b means that the desorption effect of the three methods :

Heating+Redox > Heating > Sn-redox

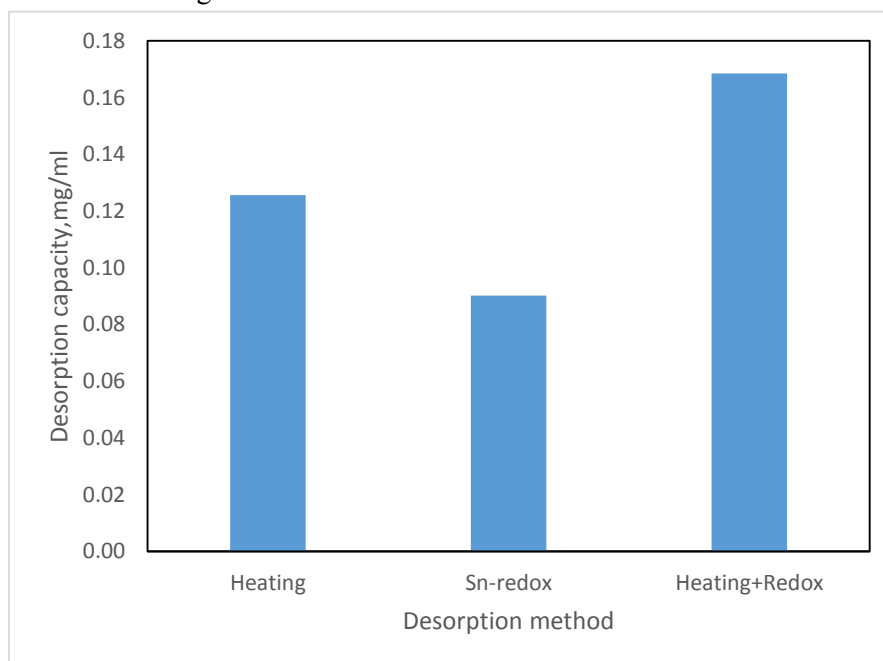


Fig.6.c means that at the elution step, when we add 1 ml of As solution, we can have 0.13mg, 0.09mg, and 0.17mg of As eluted from the column material. So when we use Heating+Redox method, the elution will be better.

